Diss. ETH No. 19615

Enhanced wastewater treatment by ozone and ferrate: Kinetics, transformation products and full-scale ozonation

A dissertation submitted to
ETH ZURICH
for the degree of
Doctor of Sciences

presented by

SASKIA GISELA ZIMMERMANN

Dipl.-Umweltwissenschaftlerin, Universität Trier
born on November 12, 1979
citizen of Germany

accepted on the recommendation of

Prof. Dr. Urs von Gunten, examiner
Prof. Dr. René P. Schwarzenbach, co-examiner
PD Dr. Thomas A. Ternes, co-examiner
Prof. Dr. Hansruedi Siegrist, co-examiner

2011

Danksagung

Ganz herzlich möchte ich mich bei Urs von Gunten für die ausgezeichnete Betreuung dieser Arbeit bedanken. Seine stets offene Tür und die grossartige Diskussionsbereitschaft, sowie ein grosser Freiraum für selbständige Arbeit aber auch Unterstützung in kritischen Momenten haben sehr zu dieser Arbeit beigetragen. Danke auch für die Möglichkeit der Aufenthalte an der Curtin University in Perth sowie an der BfG in Koblenz. René Schwarzenbach, Hansruedi Siegrist und Thomas Ternes danke ich herzlich für die Übernahme der Koreferate. Hansruedi Siegrist hat als Leiter des EU Projekts Neptune sowie bei der Ozonungsanlage in Regensdorf mit seinem Engagement und seiner Diskussionsfreude diese Diss sehr bereichert. Ein grosses Dankeschön möchte ich auch Thomas Ternes aussprechen, bei dem ich mich mehrere Monate mit der Strukturaufklärung von Oxidationsprodukten beschäftigen konnte.

In den verschiedenen Stadien dieser Diss waren sehr viele Personen beteiligt, die alle auf vielfältige Art und Weise zum Gelingen dieser Arbeit beigetragen haben.

Ich danke**...**

... Christoph Ort und Steve Brocker für das gemeinsame Durchleben und Beheben von Ozonalarmen, sowie allen weiteren Beteiligten des Projekts in Regensdorf

... Mathias Wittenwiler, der mit seinem Enthusiasmus und seiner ausgezeichneten Masterarbeit das Regensdorfprojekt unterstützt hat

... Lisa Salhi, die ihre Erfahrungen mit der Ozonmessung aus der Trinkwasseraufbereitung unermüdlich vor Ort mit mir teilte und als gute Seele des Laborbetriebs so einige Experimente gerettet hat

... Juliane Hollender, Stephan Koepke, Irene Steimen, Philipp Longrée, Martin Krauss, Ewa Gansner, Frederik Hammes, Hans-Peter Füchslin und Jacqueline Traber als Helfer und Unterstützer diversester Messkampagnen in Regensdorf

... Markus Gresch, Jakob Helbing und Christian Abegglen als Tracertest- und Modellierungsexperten

... allen Beteiligten des Neptune Projekts für die interessanten Diskussionen und schönen Projekttreffen in verschiedenen europäischen Ländern

... der CWQRC Gruppe an der Curtin University in Perth, Australien, für die äusserst nette Aufnahme, und vor allem Ina Kristiana und Caroline Taylor für erlebnisreiche Ausflüge rund um Perth

... der ganzen Abteilung G2 der BfG in Koblenz für die herzliche Atmosphäre, und im besonderen Manoj Schulz, Arne Wick, Michael Schlüsener und Jen Kormos als MS Experten - danke für die immense Messzeit!

... natürlich meinen Kollegen und Freunden aus der Gruppe von Urs von Gunten und der Eawag für die abwechslungs- und erfahrungsreiche Zeit während meiner Diss - sei es im Büro, im Labor, auf verschiedensten Apéros und Weihnachtsfeiern, am See oder auf dem Berg: Maaike Ramseier, Yunho Lee, Lisa Salhi, Andi Peter, Mike Dodd, Jannis Wenk, Mathias Wittenwiler, Jessica Benner, Merle Richter, Irene Wittmer, Anne Dietzel, Jakob Helbing, Ioannis Katsoyiannis, Marie Deborde, Hana Mestankova, Silvio Canonica, Hansueli Laubscher, Paul Borer, Barbara Sanchez, Holger Lutze, Anh Trung Kieu, Mathias Sturzenegger, Minju Lee, Melissa Huguet, Sébastian Allard, Sébastian Meylan, Carolina Garcia, Sabrina Bahnmüller, Matthias Rudolf von Rohr, Fabian Soltermann und Justine Criquet - Merci!

... meinem Bruder Lars Zimmermann (www.artworx3d.de) für das 1A Design des Umschlags und meiner ganzen Familie für die stete Unterstützung

... und ganz besonders Markus, der mich stets in allen Bereichen des Lebens unterstützt und dabei mit ans andere Ende der Welt reist

Table of Contents

List of frequently used abbreviations

AOC	assimilable organic carbon
AOP	advanced oxidation processes
DOC	dissolved organic carbon
DOM	dissolved organic matter
E. coli	*Escherichia coli*
EE2	17α-ethinylestradiol
ERM	electron-rich moieties
Fe(VI)	ferrate
GC-MS	gas chromatography - mass spectrometry
HPLC-MS/MS	high pressure liquid chromatography - tandem mass spectrometry
HRT	hydraulic retention time
LTQ-FT-MS	linear triple quadrupole ion trap Fourier transformation mass spectrometer
LOQ	limit of quantification
MRM	multiple reaction mode
NDMA	*N*-nitrosodimethylamine
NMOR	*N*-nitrosomorpholine
O_3	ozone
OH•	hydroxyl radicals
OP	oxidation product
*p*CBA	*para*-chlorobenzoic acid
PAC	powdered activated carbon
P.E.	population equivalents
PPCPs	pharmaceuticals and personal care products
Q	flow
Qq-LIT-MS	hybrid triple quadrupole-linear ion trap mass spectrometer
SMX	sulfamethoxazole
SPE	solid phase extraction
TCC	total cell counts
WWTP	wastewater treatment plant

Summary

This doctoral thesis investigated oxidative techniques as tertiary treatment options for municipal wastewater with a special focus on micropollutant transformation. Ozonation was assessed in a full-scale system whereas ferrate (Fe(VI)) experiments were carried out in laboratory-scale systems. For one micropollutant, tramadol, the Fe(VI) and ozone oxidation mechanisms were investigated.

A full-scale ozonation step at a municipal wastewater treatment plant (WWTP) was operated for 16 months (Chapter 1). Experiments at this step showed that ozonation efficiently oxidizes micropollutants in secondary wastewater effluent at the full-scale level, and confirmed results from previous laboratory and pilot-scale experiments (Chapter 2). At an ozone dose of 0.6 g O_3 g^{-1} DOC (~ 3 mg O_3 L^{-1}), micropollutants with second-order rate constants for the reaction with ozone > 10^4 M^1 s^{-1} (fast-reacting) were oxidized below their respective limit of quantification (LOQ). The LOQ was in the range of 1 - 118 ng L^{-1} for the analysis of ozonated secondary wastewater effluent samples based on tandem mass spectrometry. Micropollutants with rate constants for the reaction with ozone < 10^4 M^{-1} s^{-1} (slowly-reacting) were less eliminated but increasingly oxidized with increasing ozone doses. Atrazine and iopromide with rate constants < 10^2 M^{-1} s^{-1} for the reaction with ozone, which are also relatively slowly oxidized by hydroxyl radicals (< 5 x 10^9 M^{-1} s^{-1}), showed the lowest relative elimination. Altogether, a relative elimination < 95 % was only observed for a few triazine derivatives and X-ray contrast media (atrazine 49 %, iopromide 62 %) at the highest ozone dose of 1.16 g O_3 g^{-1} DOC (~ 5.3 mg O_3 L^{-1}).

Two modeling approaches slightly overestimated the measured micropollutants oxidation within a factor of 2.5. The first approach was based on an assumed plug flow behavior of the ozone reactor, and used the overall micropollutant elimination as assessed by 24h- or 48h- flow proportional composite samples (Chapter 2). The second modeling approach was a refined description of the ozone reactor based on coupling reactor hydraulics (described as series of continuously stirred tank reactors in Berkeley Madonna) with ozone chemistry and reaction kinetics. The corresponding samples were taken as grab samples from several points inside the ozone reactor (Chapter 3). Overall,

the slight overestimation of micropollutant oxidation in both model approaches may be caused by a certain protection of micropollutants from ozone attack by the interaction with aquatic colloids or sludge particles in the real wastewater system. This protection may be due to an ozone mass transfer limitation across the boundary layer of the sludge particles. However, this has not been experimentally confirmed yet.

A good overall disinfection capacity of the ozone reactor was proven as demonstrated by the fast decrease of total cell counts (TCC) and inactivation of *Escherichia coli (E. coli)* (Chapter 3). The receiving water (the Furtbach) at WWTP Wüeri even exhibited a microbiological water quality suitable for bathing, according to the amended bathing water directive of the European Union. However, predictions of *E. coli* inactivation based on the second modeling approach strongly deviated from full-scale measurements. This was attributed to the shielding of *E. coli* by activated sludge flocs (Chapter 3).

Bromate, a potential human carcinogen, and the carcinogenic *N*-nitrosamines were analyzed as known ozonation by-products which can be formed from wastewater matrix components (Chapter 3). Bromate formation was found to not be of concern since maximum concentrations were both below the drinking water standard of 10 μg L^{-1} and below the proposed ecotoxicologically relevant concentration of 3 mg L^{-1}. *N*-nitroso-dimethylamine (NDMA) was found to be the predominant *N*-nitrosamine compound formed during ozonation. In contrast to bromate, passage through the biologically active sand filter degraded NDMA by approximately 50 %. This resulted in NDMA concentrations < 10 ng L^{-1} in the sand filtration effluent which is below the action level of NDMA in drinking water in California. Other organic by-products can form from the oxidative breakdown of complex dissolved organic matter. They are usually biodegradable and can be measured as e.g. assimilable organic carbon (AOC). AOC is a sum parameter for carbon which can be used by microorganisms for their growth and may influence the quality of receiving waters after discharge of ozonated wastewater effluent. As shown in Chapter 3, AOC increased during ozonation, with no clear trend when correlated to the ozone dose. As for NDMA, the post-sand filtration degraded AOC by up to 50 %. These findings highlight the necessity of a biological post treatment step such as sand filtration after ozonation.

Ferrate (Fe(VI)) is a promising oxidant in wastewater treatment due to its dual function as an oxidant and coagulant, and was investigated in Chapter 4. A kinetic database for olefin-, phenol-, and amine-containing micropollutants and model compounds was developed, with second-order rate constants ranging from 1 M^{-1} s^{-1} (trimethylamine) to 9000 M^{-1} s^{-1} (aniline) in the pH range 7 to 8. When added to secondary wastewater effluent, Fe(VI) could efficiently oxidize micropollutants with the mentioned electron-rich functional groups, resulting in > 85 % oxidation for Fe(VI) doses of 5 mg Fe L^{-1} or higher. The micropollutants bezafibrate, iopromide, and ibuprofen without electron-rich functional groups were tested in the same wastewater matrix, and were only eliminated by less than 40 % even for Fe(VI) doses of 15 mg Fe L^{-1}. When comparing the second-order rate constants for the reaction of Fe(VI) and ozone with micropollutants, the ozone rate constant is usually three to four orders of magnitude higher than the respective Fe(VI) rate constant. Still, comparing the efficiency of both oxidants to oxidize micropollutants in a wastewater matrix revealed a similar or only slightly lower efficiency of micropollutant oxidation by Fe(VI) compared to ozone. This can be explained by the much longer lifetime of Fe(VI) in wastewater ($t_{1/2}$ ~ 10 minutes at pH 8) as compared to ozone ($t_{1/2}$ ~ several seconds at pH 8), leading to higher oxidant exposures. Fe(VI) doses required to achieve significant elimination of micropollutants in the tested wastewater (> 5 mg Fe L^{-1}) were lower than those needed for a significant phosphate removal (≥ 8 mg Fe L^{-1}) to achieve the regulatory limit for wastewater discharge in Switzerland of 0.8 mg PO_4-P L^{-1}, starting from 3.5 mg PO_4-P L^{-1}. Therefore, a combined use of Fe(VI) and Fe(III) as an additional coagulant could be an option, since Fe(VI) is significantly more expensive than Fe(III).

Oxidative treatment does not usually result in full mineralization but in the transformation of the target compounds. For a comprehensive environmental assessment of an oxidative technology, it is crucial to elucidate the transformation pathways of the critical micropollutants. Mechanistic information on ozonation products formed from micropollutants containing reactive functional groups such as olefins, phenols or amines is available, but much less is known about transformation mechanisms for Fe(VI) reactions. Tramadol, an environmentally relevant micropollutant containing a tertiary amine function, was chosen for a product study of a tertiary amine-containing compound, as presented in Chapter 5. Six main oxidation products (OPs) could be identified for both the oxidation by Fe(VI) and ozone using Qq-LIT-MS, LTQ-FT-MS, GC-MS, and moiety-specific chemical reactions. Together with kinetic information, OP identification confirmed that the lone electron pair of the amine-N is the predominant site of oxidant attack. An oxygen transfer mechanism can explain the formation of *N*-oxide-TRA, while a one-electron transfer may result in the formation of N-centered radical cation intermediates. These in turn could lead to the observed N-dealkylation, and to the identified formamide and aldehyde derivatives via several intermediate steps. The proposed radical intermediate mechanism is favored for Fe(VI) leading predominantly to *N*-desmethyl-TRA (≤ 40 %), whereas the proposed oxygen transfer prevails for O_3 attack resulting in *N*-oxide-TRA as the main OP (≤ 95 %).

In summary, the results obtained in this thesis showed that oxidative technologies such as ozonation or Fe(VI) application are effective means for the mitigation of micropollutants from municipal wastewater. Ozonation was shown to be feasible at the full-scale level, whereas experience for Fe(VI) application is currently only available in laboratory systems. Further positive effects of the respective oxidants such as disinfection (ozone) and phosphate removal (Fe(VI)) were investigated, and possible drawbacks such as by-product formation from wastewater matrix components were considered (mainly ozone). A kinetic and mechanistic study selecting tramadol as model micropollutant suggests that tertiary amines react via similar reaction mechanisms with ozone and Fe(VI), leading to the same OPs. However, significantly different yields were observed for the respective OPs.

Zusammenfassung

Im Rahmen dieser Arbeit wurden Ozon und Ferrat (Fe(VI)) als oxidative Verfahren der weitergehenden kommunalen Abwasserreinigung untersucht. Der Fokus lag dabei auf der Elimination von Mikroverunreinigungen. Die Ozonung wurde an einer Grossanlage getestet, während der Einsatz von Fe(VI) in Laborversuchen untersucht wurde. Die Reaktionsmechanismen beider Oxidationsmittel mit einem Spurenstoff, der ein tertiäres Amin enthält, konnten am Beispiel des umweltrelevanten Opioids Tramadol vorgeschlagen werden.

Der Einsatz der Ozonung wurde über 16 Monate an der Abwasserreinigunganlage (ARA) Wüeri in Regensdorf bei Zürich getestet (Kapitel 1). Die Ozonung konnte ein breites Spektrum an Mikroverunreinigungen entfernen, womit Resultate aus vorhergehenden Labor- und Pilotversuchen an einer Grossanlage bestätigt wurden (Kapitel 2). Mikroverunreinigungen, die hohe Reaktionskonstanten mit Ozon aufweisen ($> 10^4$ M^{-1} s^{-1}), wurden bereits bei einer mittleren Ozondosis von 0.6 g O_3 g^{-1} DOC (~ 3 mg O_3 L^{-1}) so stark oxidiert, dass ihre Konzentrationen unterhalb der Bestimmungsgrenze lagen. Die Bestimmungsgrenze der analytischen Methoden variierte dabei im ozonierten Ablauf der Nachklärung zwischen 1 und 118 ng L^{-1}. Mikroverunreinigungen mit Reaktionskonstanten $< 10^4$ M^{-1} s^{-1} mit Ozon wurden weniger gut entfernt. Die Elimination stieg jedoch mit zunehmender Ozondosis stark an. Atrazin und Iopromid, die sowohl mit Ozon ($< 10^2$ M^{-1} s^{-1}) als auch mit Hydroxylradikalen ($< 5 \times 10^9$ M^{-1} s^{-1}) relativ geringe Reaktionskonstanten aufweisen, wurden am wenigsten stark oxidiert. Bei der höchsten Ozondosis von 1.16 g O_3 g^{-1} DOC (~ 5.3 mg O_3 L^{-1}) wurden bis auf einige Triazinderivate und ausgewählte Röntgenkontrastmittel (z.B. Atrazin 49 %, Iopromid 62 %) alle untersuchten Mikroverunreinigungen zu mehr als 95 % eliminiert.

Im Rahmen dieser Arbeit wurde die Oxidation von Mikroverunreinigungen in der Grossanlage der Ozonung mit zwei verschiedenen Ansätzen modelliert. Das erste Modell basierte auf der Annahme, dass das hydraulische Verhalten des Ozonreaktors mit einer Pfropfenströmung beschrieben werden kann. Diese Modellergebnisse wurden mit Messwerten aus 24h- und 48h flussproportionalen Sammelproben verglichen (Kapitel 2). Das zweite Modell beschrieb die Spurenstoffoxidation innerhalb des Ozonreaktors mit

einer Kombination aus dem experimentell bestimmten hydraulischen Verhalten (Kaskade idealer Rührkessel), der Ozonchemie und der Reaktionskinetik deutlich detaillierter. Diese Ergebnisse wurden anschliessend mit Messwerten aus Proben verglichen, die als Punktproben aus dem Reaktor entnommen worden waren (Kapitel 3). Beide Ansätze überschätzten die tatsächlich gemessene Elimination in der Grossanlage um bis zu einen Faktor 2.5. Diese Abweichung wurde auf die Wechselwirkung der Mikroverunreinigungen mit der Oberfläche von Kolloiden oder Belebtschlammpartikeln zurückgeführt. Aufgrund dieser Wechselwirkungen und des begrenzten Ozonmassentransfers durch die Grenzschicht sind die Spurenstoffe an der Oberfläche dieser Partikel vor der Oxidation geschützt. Dies wurde jedoch in der vorliegenden Arbeit experimentell nicht untersucht und ist daher eine Hypothese.

Neben der effizienten Elimination der Spurenstoffe konnte eine sehr gute Desinfektion des Abwassers als eine Reduktion der Gesamtkeimzahl und Inaktivierung von *Escherichia coli (E. coli)* Bakterien durch die Ozonung bestimmt werden (Kapitel 3). Der Vorfluter wies nach der Badegewässerrichtlinie der EU sogar Badegewässerqualität auf. Der zweite, detailliertere Modellansatz überschätzte die Inaktivierung von *E. coli* Bakterien deutlich. Dies wurde auf eine Abschirmung der *E. coli* Bakterien in Belebtschlammflocken zurückgeführt (Kapitel 3).

Die Bildung schädlicher Ozonungsnebenprodukte wurde durch die Analyse des Abwassers hinsichtlich des potentiell kanzerogenen Bromats und der kanzerogenen *N*-Nitrosamine berücksichtigt (Kapitel 3). Dabei stellte die Bildung von Bromat kein Problem dar, da die erreichten Konzentrationen unterhalb des Trinkwassergrenzwerts von 10 $\mu g\ L^{-1}$ sowie unterhalb der ökotoxikologisch relevanten Konzentration von 3 $mg\ L^{-1}$ lagen. Während der Ozonung wurde an *N*-Nitrosaminen hauptsächlich das *N*-Nitrosodimethylamin (NDMA) gebildet. Im Gegensatz zum Bromat wurde die Konzentration des NDMA jedoch im nachgeschalteten Sandfilter um ca. 50 % reduziert. Die NDMA Konzentrationen im Ablauf der Sandfiltration lagen daraufhin unter 10 $ng\ L^{-1}$ und somit unterhalb des Wertes, ab dem in Kalifornien Massnahmen zur NDMA Reduzierung in der Trinkwasseraufbereitung ergriffen werden müssen. Weitere Oxidationsnebenprodukte können durch den oxidativen Abbau komplexer gelöster organischer

Substanz entstehen. Diese Produkte sind biologisch meist gut abbaubar und können daher als assimilierbarer organischer Kohlenstoff (AOC) analytisch erfasst werden. Erhöhte AOC Konzentrationen im ozonierten Abwasser können die Gewässerqualität des Vorfluters negativ beeinflussen. Im Rahmen dieser Studie konnte gezeigt werden, dass die AOC Konzentrationen im Abwasser durch die Ozonung anstiegen, dass dieser Anstieg jedoch nicht mit der Ozondosis korrelierte. Wie für NDMA führte auch hier der anschliessende Sandfilter zu einer Reduzierung der AOC Konzentration um bis zu 50 %. Diese Ergebnisse belegen eindeutig die Notwendigkeit einer biologischen Behandlungsstufe, wie z.B. eines Sandfilters, nach einer Ozonungsstufe.

Ferrat (Fe(VI)) ist aufgrund seiner Doppelfunktion als Oxidations- und Fällungsmittel vielversprechend für die weitergehende Abwasserbehandlung (Kapitel 4). In dieser Arbeit wurde eine Datenbank mit Reaktionskonstanten von Fe(VI) mit verschiedenen Mikroverunreinigungen und Modellsubstanzen, die funktionelle Gruppen wie Doppelbindungen, Phenole und Amine besitzen, aufgebaut. Diese Geschwindigkeitskonstanten lagen zwischen 1 M^{-1} s^{-1} (Trimethylamin) und 9000 M^{-1} s^{-1} (Anilin) für den pH Bereich 7 - 8. Mikroverunreinigungen mit den genannten elektronenreichen funktionellen Gruppen wurden in Laborversuchen bei einer Fe(VI)-Dosis von 5 mg Fe L^{-1} im Ablauf der Nachklärung zu über 85 % reduziert. Bezafibrat, Iopromid und Ibuprofen, die diese funktionellen Gruppen nicht aufweisen, wurden hingegen im gleichen Abwasser bei einer Fe(VI)-Dosis von 15 mg Fe L^{-1} nur zu 40 % eliminiert. Im Vergleich zu Ozon sind die Reaktionskonstanten von Mikroverunreinigungen mit Fe(VI) meist drei bis vier Grössenordnungen geringer. Trotzdem erreichte Fe(VI) eine ähnliche oder nur etwas geringere Elimination von Spurenstoffen im Abwasser. Dies wurde auf eine deutlich höhere Fe(VI)-Exposition aufgrund der sehr viel höheren Stabilität des Fe(VI) im Abwasser ($t_{1/2}$ ~ 10 Minuten bei pH 8) im Vergleich zu Ozon ($t_{1/2}$ ~ einige Sekunden bei pH 8) zurückgeführt. Fe(VI)-Dosen über 5 mg Fe L^{-1} wurden für eine weitestgehende Elimination von Mikroverunreinigungen benötigt, während über 8 mg Fe L^{-1} nötig waren, um die Phosphatkonzentration von 3.5 mg PO_4-P L^{-1} auf 0.8 mg PO_4-P L^{-1} zu senken, und somit den Phosphatgrenzwert für Abwasser in der Schweiz zu erreichen. Da Fe(VI) momentan noch sehr viel teurer ist als Fe(III), könnte man daher Fe(VI) in Kombination mit Fe(III) einsetzen.

Der Einsatz oxidativer Verfahren führt normalerweise nicht zur vollständigen Mineralisierung eines Spurenstoffs, sondern nur zu seiner Umwandlung. Für eine ausreichende Bewertung eines Oxidationsverfahrens ist es daher notwendig, die Umwandlungsprodukte und -mechanismen relevanter Spurenstoffe zu identifizieren. Die Mechanismen zur Bildung von Ozonungsprodukten sind grösstenteils bekannt, während die Umwandlung von Spurenstoffen durch Oxidation mit Fe(VI) bisher kaum untersucht wurde. Tramadol, ein umweltrelevanter Spurenstoff mit einer tertiären Aminfunktion, wurde daher für die Aufklärung der Reaktionsmechanismen mit dieser funktionellen Gruppe ausgewählt (Kapitel 5). Sechs Hauptoxidationsprodukte konnten mit Hilfe von Qq-LIT-MS, LTQ-FT-MS, GC-MS und spezifischer chemischer Reaktionen für die Reaktion mit Fe(VI) und Ozon identifiziert werden. In Kombination mit den pH-abhängigen Reaktionskonstanten wurde das freie Elektronenpaar des Amins als Hauptangriffspunkt des Oxidationsmittels identifiziert. Der Transfer eines Sauerstoffatoms erklärt dabei die Entstehung des *N*-Oxid-Tramadols, während die Übertragung eines Elektrons zur Bildung N-zentrierter radikalischer Kationen führen könnte. Diese könnten anschliessend zur beobachteten N-Dealkylierung und über mehrere Zwischenschritte zur Bildung der identifizierten Formamid- und Aldehydderivate führen. Der vorgeschlagene Radikalmechanismus läuft hauptsächlich bei der Oxidation durch Fe(VI) ab (Bildung von ≤ 40 % *N*-Desmethyl-Tramadol), während der Sauerstofftransfer für Ozon zu dominieren scheint (Bildung von ≤ 95 % *N*-Oxid-Tramadol).

Zusammengefasst zeigt die vorliegende Arbeit, dass oxidative Verfahren wie die Ozonung oder der Einsatz von Fe(VI) geeignete Mittel sind, um Mikroverunreinigungen effektiv aus dem kommunalen Abwasser zu entfernen. Die Machbarkeit des grosstechnischen Einsatzes der Ozonung wurde gezeigt, während für Fe(VI) grosstechnische Erfahrungen noch fehlen. Positive Nebeneffekte wie die Desinfektionswirkung des Ozons oder die Phosphatfällung durch Fe(VI) wurden ebenso untersucht wie die mögliche Bildung von Oxidationsnebenprodukten. Eine kinetische und mechanistische Studie mit Tramadol zeigte, dass ähnliche Mechanismen bei der Reaktion von tertiären Aminen mit Ozon und Fe(VI) ablaufen und zur Bildung der gleichen Oxidationsprodukte führen. Der Anteil der jeweiligen Oxidationsprodukte unterscheidet sich für die beiden Oxidationsmittel jedoch stark.

Chapter 1

General Introduction

1.1 Micropollutants in the aquatic environment

The increasing contamination of natural waters with synthetic compounds is becoming a major public concern. Approximately 300 million tons of synthetic compounds are used for agricultural, industrial and domestic purposes per year. After their applications, they can be released into natural waters. In the past 30 years, many of these compounds have been detected in the aquatic environment even in remote areas such as the Arctic or Antarctica. These areas are not the original places of use, indicating the persistence and long-range transport potential of some of these compounds *(1-3)*.

Classical analytical techniques such as gas chromatography with different kinds of detectors are mainly able to analyze volatile, thermostable and relatively non-polar organic compounds (e.g. polychlorinated biphenyls or polyaromatic hydrocarbons) in environmental samples. In the last 15 years, new techniques based on solid phase extraction (SPE) and high pressure liquid chromatography - mass or tandem mass spectrometry (HPLC-MS/MS) expanded the analytical capabilities towards the detection of non-volatile, thermolabile and polar organic compounds. Currently, the quantification of polar organic compounds down to the low ng L^{-1} or even pg L^{-1} range is possible. Due to these analytical developments, polar organic micropollutants such as pharmaceuticals and personal care products (PPCPs), household chemicals, biocides and pesticides have been ubiquitously discovered in a variety of water resources and technical systems causing great interest in their environmental fate, behavior and effects *(1,4-7)*. Impacted water resources include groundwater and surface waters often used for drinking water supply. As a result, this raises concerns about safe drinking water supply since groundwater is often distributed without any treatment or only with a single disinfection step such as UV treatment or the addition of chlorine or chlorine dioxide *(8,9)*. Even in the case of multi-barrier systems used for surface water treatment, some micropollutants can be detected in low concentrations in tap water *(6,10)*. With respect to ecosystem health, adverse effects on sensitive aquatic organisms by low concentrations of polar organic micropollutants cannot be excluded since many of them are designed to have a biological effect (e.g. antibiotics, biocides or pesticides). Additive and synergistic effects of complex micropollutant mixtures can be of special relevance *(1,11,12)*. In addition, chronic exposure to a single micropollutant can result in a collapse of wildlife

populations. This was shown in a 7-year whole lake study in Canada exposing fathead minnow to 5 - 6 ng L^{-1} 17α-ethinylestradiol (EE2), the active ingredient of the contraceptive pill *(13)*. Apart from these hints on adverse effects, the number and concentration of synthetic compounds in the aquatic environment should be minimized whenever possible based on the precautionary principle.

1.2 Micropollutants in conventional municipal wastewater treatment

Municipal wastewater has been identified as a major source of polar organic micropollutants, and in particular of human pharmaceuticals, entering the aquatic environment in countries with centralized wastewater collection and treatment systems *(14)*. Human pharmaceuticals are transformed in the human body to varying extents, and subsequently excreted in the urine or faeces as a mixture of altered and unaltered substances. Personal care products and household chemicals enter the sewer system via wash-off during showering, bathing and cleaning, whereas biocides can leach from facades and roof sealing membranes via run-off during stormy weather events into the sewer system *(14,15)*. Veterinary pharmaceuticals should reach municipal wastewater treatment plants (WWTPs) only to a minor extent *(14)*. This complex mixture of micropollutants from different sources is collected in the sewer system and transported to municipal WWTPs.

Historically, WWTPs have been constructed to protect the receiving water from adverse effects of waste- and stormwater collected from the urban drainage system. The first aim was to remove pathogenic organisms and to lower the organic load to the wastewater by activated sludge treatment because untreated wastewater caused hygienic problems and oxygen depletion in the receiving waters. Nitrification was implemented to convert ammonia into nitrate which is a much less toxic form of nitrogen. Nitrate in turn is a limiting factor for algal growth in coastal waters such as the North Sea, and accordingly, denitrification steps were introduced to transform nitrate into molecular nitrogen.

Phosphorus, the other main nutrient responsible for eutrophication in lakes (e.g. Switzerland), is either removed from wastewater by coagulants such as iron or aluminum salts, or by enhanced biological phosphorus removal *(14)*.

Accordingly, WWTPs have not specifically been designed to eliminate neither polar nor unpolar organic micropollutants; however, they are able to remove some of them at least partly via sorption, stripping, or biodegradation. Removal by sorption can proceed either via removal of particulate organic matter or via excess sludge withdrawal. Stripping by aeration is mainly relevant for volatile compounds *(16)*. With respect to biodegradation, organic micropollutants with biological degradation constants < 0.1 L g_{ss}^{-1} d^{-1} are not removed to a significant extent while biological degradation constants of > 10 L g_{ss}^{-1} d^{-1} lead to more than 90 % removal. In a study with 35 selected compounds, only four (ibuprofen, paracetamol, 17β-estradiol and estrone) belonged to the latter very biodegradable group whereas 17 compounds were removed by ~ 50 % *(17)*. Sludge age is one of the crucial parameters influencing organic micropollutant removal, and elevated sludge retention times can enhance the removal of some of them *(14)*. Overall, biodegradation was shown not to be efficient in removing polar organic micropollutants *(17)*. As a result, polar, non-volatile and persistent organic micropollutants are still constantly released from municipal WWTPs into the aquatic environment *(17,18)*. In order to appreciable remove them, enhanced wastewater treatment processes are needed and should be tested for their full-scale feasibility.

1.3 Enhanced wastewater treatment for micropollutant removal

Ozonation and powdered activated carbon (PAC) are currently considered the most promising enhanced treatment options for the removal of micropollutants from wastewater. Both have been shown to efficiently eliminate micropollutants during drinking water treatment *(19-21)*. Ozone has been used since the beginning of the 20th century in drinking water production for different purposes. The main objective in drinking water treatment is disinfection but ozone is also used for iron and manganese removal, decolorization, control of taste and odor compounds, removal of organic micropollutants, biological stabilization and the control of chlorination by-products *(22)*. Activated carbon has been applied in drinking water treatment in both powdered and granular form, and predominantly for odor and micropollutant control. In addition, the latter one is also used as a support medium for bacteria to biologically stabilize drinking water before distribution *(23)*.

In contrast to the two options for enhanced wastewater treatment, ferrate (Fe(VI)) is a relatively new promising chemical for (waste)water treatment. Its dual function as an oxidant and coagulant makes it suitable for wastewater treatment *(24,25)*.

1.3.1 Chemistry of oxidative water treatment

1.3.1.1 Ozone chemistry

Ozone is a very selective oxidant consisting of three oxygen atoms. The ozone structure can be described by four hybrid resonance structures *(26)* (Figure 1.1).

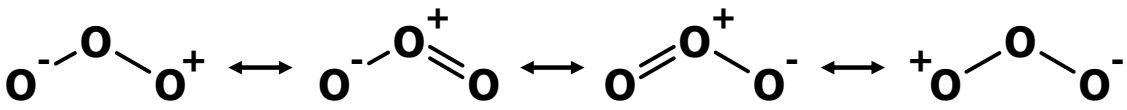

Figure 1.1. Hybrid resonance structures for ozone in aqueous solution *(26)*

Ozone reacts readily with electron-rich functional groups such as olefins, activated aromatic systems, deprotonated amines and sulfides by electrophilic addition reactions leading mainly to oxygen atom transfer and electron transfer *(27)*. Due to its selectivity, second-order rate constants for the reaction of inorganic and organic compounds with ozone cover a range of more than nine orders of magnitude *(27)*.

In aqueous solution, ozone decomposes into secondary oxidant species such as hydroxyl radicals by several initiation reactions via an autocatalytic chain reaction *(27-29)*. Hydroxyl radicals in turn are the strongest oxidants in water and in contrast to ozone, act more unspecifically. Second-order rate constants for hydroxyl radicals are hence generally higher and cover a range of only about three orders of magnitude *(27,30)*.

The decomposition of ozone in natural waters or wastewater can typically be divided into two phases: a rapid initial phase with half-lives in the order of < seconds, and a second phase with half-lives in the range of tens of minutes. The second phase can usually be described by an empirical first-order rate law whereas the initial phase is found to be of a higher order. When applied to municipal wastewater, ozone decomposes more rapidly than in natural waters due the higher organic matrix load *(31)*. Buffle et al. *(32)* suggested direct reactions of ozone with specific reactive moieties of dissolved organic matter (DOM) as the main decomposition mechanism during the initial phase of ozone decay in wastewater. An increasing ozone decomposition rate was observed with increasing pH. This was attributed to an increased deprotonation of reactive moieties at higher pH values, and not to the autocatalytic chain reaction. Hydroxyl radicals are

produced in higher amounts in wastewater compared to natural waters and yield oxidation conditions similar to ozone-based advanced oxidation processes (AOPs) in drinking water treatment *(27,32)*.

Accordingly, the combined action of both oxidants - especially during ozonation of wastewater - leads to a significant oxidation of micropollutants both with and without functional groups reactive towards ozone. However, oxidation does not usually lead to a full mineralization but to the transformation of micropollutants, resulting in the formation of oxidation products (OPs). The mechanisms and OPs formed from important functional groups such as olefins, activated aromatic systems, deprotonated amines and sulfides are summarized in von Gunten and von Sonntag (2011) *(33)*. In addition, some unexpected OPs have been formed as observed in the case of *N,N*-dimethylsulfamide that produced *N*-nitrosodimethylamine in the presence of bromide *(34)*.

By-products from the oxidation of wastewater matrix components may also be formed. Bromate, a potential human carcinogen, is a prominent example that forms from bromide during ozonation *(35)*.

Ozone is also known as an excellent disinfectant and can even inactivate protozoa (e.g. *Cryptosporidium parvum* oocysts and *Giardia lamblia* cysts). This is of advantage for a possible application in wastewater treatment with regard to the implementation of the EU Water Framework Directive. Hydroxyl radicals do not significantly contribute to disinfection *(35)*.

Altogether, the efficiency of an ozonation process with regard to micropollutant oxidation and disinfection largely depends on the ozone dose, the ozone stability, the hydroxyl radical yield and the second-order rate constants for the reaction of target compounds with ozone and hydroxyl radicals. Type and concentration of DOM, pH and alkalinity in turn influence the ozone stability considerably. Ozone is more stable at lower DOM concentrations, at lower pH values (protonated DOM slows down ozone decay) and at a higher alkalinity (carbonate is a hydroxyl radical scavenger and inhibitor of ozone decomposition).

1.3.1.2 Ferrate chemistry

Although iron is commonly found as metal or in the +2 and +3 oxidation state in the environment, hypervalent forms of iron such as Fe(IV), Fe(V) or Fe(VI) have been reported in numerous enzymes (e.g. oxygenases, horseradish peroxidase) *(36,37)* and Fe(IV) has been postulated as intermediate of the Fenton process *(38)*.

Ferrate (Fe(VI)) is the only hypervalent iron known to be stable in the form of salts such as K_2FeO_4 or $BaFeO_4$ *(39,40)*. According to an X-ray powder pattern study, Fe(VI) has a tetrahedral structure since it shows four equivalent oxygen atoms which are covalently bonded to an iron atom with a +6 oxidation state *(41)*. In addition, these four oxygen atoms are kinetically equivalent as confirmed by isotopic oxygen exchange *(42)*. In accordance with that, three hybrid resonance structures of Fe(VI) were proposed in aqueous solution *(43)* (Figure 1.2).

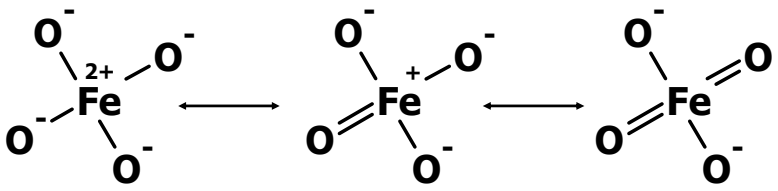

Figure 1.2. Hybrid resonance structures proposed for Fe(VI) in aqueous solution *(43)*

Fe(VI) undergoes an acid-base equilibrium and can exist as de-, mono-, di- or tri-protonated species in aqueous solution *(44)*. The experimentally determined pK_a values ($pK_{H_3FeO_4^+}$ = 1.5 *(44)*, $pK_{H_2FeO_4}$ = 3.5 *(44)* and $pK_{HFeO_4^-}$ = 7.2 *(45)*) were used to illustrate the speciation in Figure 1.3.

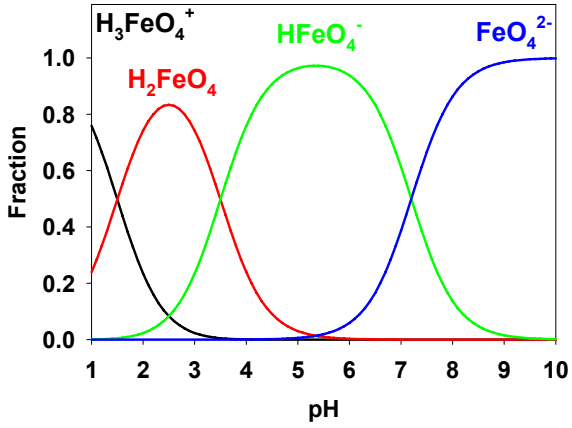

Figure 1.3. Speciation of Fe(VI) as a function of pH

Fe(VI) is a powerful selective oxidant and can oxidize a variety of organic and inorganic contaminants as reviewed in e.g. Lee et al. (2004) or Jiang and Lloyd (2002) *(24,46)*. Recently, some studies also focused on the ability of Fe(VI) to oxidize micropollutants such as ibuprofen, sulfamethoxazole, carbamazepine or EE2 *(47-50)*. The estrogenic activity of EE2 was effectively decreased during Fe(VI) treatment *(51)*, although Fe(VI) did not fully mineralize EE2. Other studies showed its ability to inactivate bacteria and viruses, and proved Fe(VI) to be a disinfectant *(52-55)*. Membrane damage of microorganisms was confirmed as cause of cell death *(56)*.

In addition to its function as an oxidant and disinfectant, Fe(VI) also acts as coagulant since ferric ion (Fe(III)) is a non-toxic decomposition product *(24)*. Coagulation of humic acid in model systems and raw water as well as removal of turbidity, chemical oxygen demand and suspended solids was shown for treated secondary wastewater exposed to doses of 15 mg Fe(VI) L^{-1} *(57,58)*. This feature of Fe(VI) may be of special interest during treatment of secondary wastewater since iron salts are commonly added to precipitate phosphate *(59)*. Accordingly, Fe(VI) has gained increasing attention as a potential water treatment chemical.

In aqueous solution, Fe(VI) is unstable even in the absence of reaction partners such as DOM or micropollutants due to self-decay. This self-decay can be described by second-order kinetics and increases with decreasing pH. The respective second-order self-decay rate constants were determined to be 450 M^{-1} s^{-1} at pH 5, 130 M^{-1} s^{-1} at pH 6, 52 M^{-1} s^{-1} at pH 7, and 6.2 M^{-1} s^{-1} at pH 8 *(60)*. It has been suggested that Fe(VI) forms

a dimer intermediate ($Fe_2O_7^{2-}$) as a first step, which is subsequently reduced to ferric ion and produces oxygen during the oxidation of water *(24)*. The self-decay can be minimized but not avoided by using low Fe(VI) concentrations and by keeping the pH as high as possible.

1.3.1.3 Prediction of micropollutant oxidation in water treatment

Typically, micropollutants react with oxidants according to a second-order rate law, and hence first-order with respect to the concentration of each reaction partner *(27,35,61,62)*:

$$-\frac{\mathrm{d}[\mathrm{P}]}{\mathrm{dt}} = k \cdot [\mathrm{Ox}] \cdot [\mathrm{P}] \tag{1.1}$$

with k as second-order rate constant for the reaction between the micropollutant P and the oxidant Ox.
In the integrated form, eq 1.1 rearranges to:

$$\ln \frac{[\mathrm{P}]}{[\mathrm{P}]_0} = -k \cdot \int [\mathrm{Ox}]\mathrm{dt} \tag{1.2}$$

In case the micropollutant undergoes an acid-base equilibrium, its speciation has to be taken into account:

$$\mathrm{PH^+} \leftrightarrow \mathrm{P} + \mathrm{H^+} \tag{1.3}$$

and eq 1.1 is rewritten to:

$$-\frac{\mathrm{d}[\mathrm{P}]_{\mathrm{tot}}}{\mathrm{dt}} = k_{\mathrm{app}} \cdot [\mathrm{Ox}] \cdot [\mathrm{P}]_{\mathrm{tot}} = k_1 \cdot [\mathrm{Ox}] \cdot [\mathrm{PH^+}] + k_2 \cdot [\mathrm{Ox}] \cdot [\mathrm{P}] \tag{1.4}$$

with k_{app} as apparent second-order rate constant at the respective pH, k_1 as species-specific rate constant of the oxidant with the protonated micropollutant and k_2 as species-specific rate constant of the oxidant with the deprotonated micropollutant.

The relative fraction of acid ($\alpha_{\mathrm{PH^+}}$) and conjugate base (α_{P}) can be calculated from the pH and the dissociation constant K *(63)*:

$$\alpha_{\mathrm{PH^+}} = \frac{[\mathrm{H^+}]}{K + [\mathrm{H^+}]} \tag{1.5}$$

$$\alpha_P = \frac{K}{K + [H^+]} \tag{1.6}$$

Therefore, for a non-dissociating oxidant such as ozone, k_{app} can be expressed as:

$$k_{app} = k_1 \cdot \alpha_{PH^+} + k_2 \cdot \alpha_P \tag{1.7}$$

During any ozonation process, but especially during wastewater ozonation, secondary oxidants such as hydroxyl radicals [OH•] are formed and contribute to the oxidation of a micropollutant:

$$-\frac{d[P]}{dt} = k_{O_3} \cdot [O_3] \cdot [P] + k_{OH\bullet} \cdot [OH\bullet] \cdot [P] \tag{1.8}$$

When integrated, eq 1.8 takes the form:

$$\ln \frac{[P]}{[P]_0} = -k_{O_3} \cdot \int [O_3]\,dt - k_{OH\bullet} \cdot \int [OH\bullet]\,dt \tag{1.9}$$

For oxidants such as ozone or Fe(VI), the oxidant exposure is determined by measuring the oxidant decay over time directly in the investigated wastewater. Concentrations of hydroxyl radicals are, however, so low that they cannot be measured directly but need to be determined indirectly with the help of e.g. a probe compound which is unreactive towards ozone. *p*-Chlorobenzoic acid (*p*CBA) can be used for this purpose *(64)*. The hydroxyl radical exposure can subsequently be determined from the relative decrease of *p*CBA and the known rate constant for the reaction of *p*CBA with hydroxyl radicals ($k_{pCBA,OH\bullet}$ = 5 x 10^9 M^{-1} s^{-1} *(65)*):

$$\ln \frac{[pCBA]}{[pCBA]_0} = -k_{pCBA,OH\bullet} \cdot \int [OH\bullet]\,dt \tag{1.10}$$

For Fe(VI) application, also the speciation of the oxidant itself needs to be considered (only the pK_a relevant for water treatment is mentioned here):

$$HFeO_4^- \leftrightarrow FeO_4^{2-} + H^+,\ pK_a = 7.2\ (45) \tag{1.11}$$

and eq 1.4 is completed to

$$\frac{-d[P]_{tot}}{dt} = k_{app} \cdot [Fe(VI)]_{tot} \cdot [P]_{tot}$$

$$= k_3 \cdot [HFeO_4^-] \cdot [PH^+] + k_4 \cdot [HFeO_4^-] \cdot [P] + k_5 \cdot [FeO_4^{2-}] \cdot [PH^+] + k_6 \cdot [FeO_4^{2-}] \cdot [P] \tag{1.12}$$

The apparent second-order rate constant k_{app} can therefore be described by eq 1.13:

$$k_{app} = k_3 \cdot \alpha_{PH^+} \cdot \beta_{HFeO_4^-} + k_4 \cdot \alpha_P \cdot \beta_{HFeO_4^-} + k_5 \cdot \alpha_{PH^+} \cdot \beta_{FeO_4^{2-}} + k_6 \cdot \alpha_P \cdot \beta_{FeO_4^{2-}} \quad (1.13)$$

with k_3, k_4, k_5 and k_6 being species-specific second-order rate constants, α_{PH}^+ and α_P representing the fraction of PH^+ and P, and β_{HFeO_4}- and β_{FeO_4}2- representing the fraction of $HFeO_4^-$ and FeO_4^{2-}, respectively.

1.3.2 Application of enhanced wastewater treatment options for micropollutant removal

1.3.2.1 Full-scale ozonation at WWTP Wüeri in Regensdorf

As part of the present doctoral thesis, a full-scale ozonation step was operated at WWTP Wüeri in Regensdorf from July 2007 to October 2008. WWTP Wüeri treats the wastewater of 25.000 population equivalents (P.E.) and consists of a grit chamber, a primary clarifier, activated sludge treatment with a denitrifying and nitrifying zone, and a secondary clarifier. Subsequently, an ozonation step treating the full wastewater stream was installed as a tertiary treatment, followed by the existing rapid sand filter.

Ozone gas is explosive at concentrations higher than 25 % [V V^{-1}] and can hence not be compacted and stored, but needs to be produced on-site from liquid oxygen or dried air. The ozone-containing oxygen gas was subsequently added to the wastewater stream via gas bubble diffusers in counter-current mode into a sealed contact reactor.

The full-scale ozonation step at WWTP Wüeri in Regensdorf consisted of the following components and equipment (Figure 1.4):

- Liquid oxygen tank including an evaporation station and pressure reduction valves
- Ozone generator combined with a cooling aggregate
- Diffusor elements for addition of the ozone/oxygen gas mixture to the wastewater stream
- Sealed ozone reactor with a sufficient hydraulic retention time
- Process measuring and control technology including online measurements for ozone dosing (flow (Q), dissolved organic carbon (DOC))
- Residual ozone destructor for the exhaust air
- Safety: ozone and oxygen gas detectors, dissolved ozone measurement devices to monitor the ozone decay and residual ozone at the effluent, ozone neutralization with bisulfite (optional)
- Rapid sand filter (recommended to degrade potentially toxic oxidation by-products)

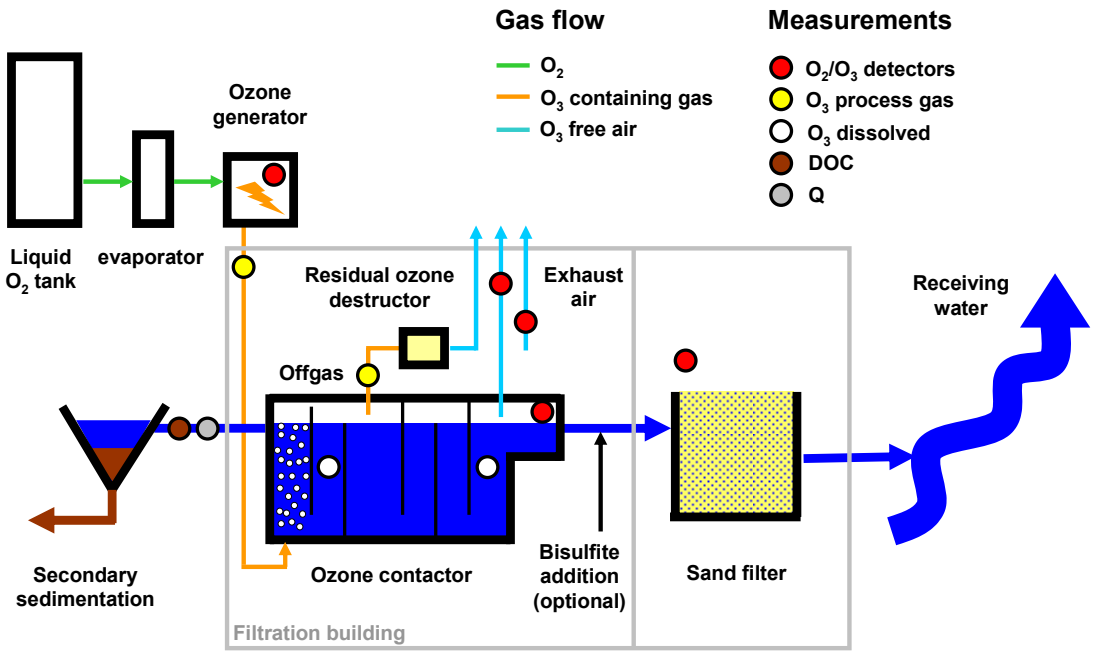

Figure 1.4. Scheme of the full-scale ozonation step at WWTP Wüeri in Regensdorf

Operation strategies for wastewater ozonation differ from those in drinking water ozonation (ozone residual measurement) since wastewater is not as critical in terms of immediate health impacts. In wastewater, DOC is the main constituent leading to ozone depletion. Hence, ozone was commonly dosed in the DOC-load proportional mode at the ozonation step of WWTP Wüeri in Regensdorf. Flow-proportional dosing was a further option. The DOC load was calculated online from two signals: the inflow and the DOC concentration. The flow to the reactor was measured by an ultrasonic device (Prosonic, Endress & Hauser, Germany) and the DOC was measured online by UV absorption using an S::can sensor (S::can, Austria), which was regularly calibrated by 0.45 µm filtered grab samples to using a total organic carbon analyzer (Shimadzu, Switzerland). Since the S::can sensors exhibited problems with the signal stability, an online total organic carbon analyzer with a preceding filtration step (pore size 0.45 µm) based on thermal digestion was tested as well. However, both techniques for online DOC measurements did not meet the requirements concerning maintenance, stability and simplicity. In addition, the ozone dosing according to the DOC load resulted in an ozone dose comparable to a theoretically calculated flow-proportional ozone dose (Figure 1.5).

This was due to the small variability of DOC concentration (5.0 ± 0.8 mg DOC L^{-1}) due to the high sludge age and well degradable influent organic load at WWTP Wüeri. For WWTPs with a comparable low variability in DOC concentration, the ozone dosing could accordingly be carried out by the flow-proportional mode. Ozone addition was finally achieved by holding a fixed ozone concentration in the process gas and varying the process gas flow or vice versa.

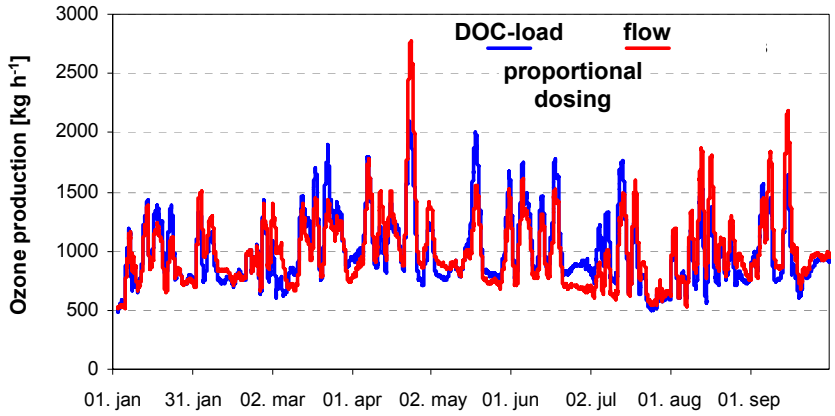

Figure 1.5. Ozone production for the DOC-load and flow-proportional operational mode (January to October 2008)

WWTPs undergo different flow regimes, with the strongest deviations from day to night and dry to stormy weather conditions. This can result in varying hydraulic retention times (HRT) within an ozone reactor. In any case, the HRT has to be sufficient to ensure complete ozone decay within the sealed ozone reactor which was not the case for stormy weather conditions at the ozone reactor at WWTP Wüeri. Hence, a more sophisticated attenuation of ozone dosing had to be implemented which was based on decreased ozone dosing for higher flow regimes (> 120 L s^{-1}) and for dissolved ozone detection in the last compartment of the reactor (> 0.3 mg L^{-1}), respectively.

In addition, a safety system was required to detect oxygen or ozone leakage to different working areas in the facilities since ozone is a toxic gas. Ozone concentrations > 200 µg m^{-3} in the indoor air of the building resulted in a complete shutdown of the ozone system.

Based on these experiences, it is recommended to operate ozone reactors either flow- or DOC- load proportional, and to design the reactor with a sufficient HRT for all flow regimes to avoid the need to attenuate the ozone dose. The time needed for complete ozone decay depends strongly on the wastewater quality parameters and is site-specific. In general, a HRT of 20 min for dry weather flow should be sufficient. During stormy weather conditions, the HRT should not be less than 5-10 minutes. In addition, a complete nitrification is recommended for the preceding biological treatment to prevent excessive ozone consumption since ozone reacts with nitrite in an equimolar ratio *(66)*.
Keeping the ozone concentration in the process gas between 160 - 180 g m^{-3} and minimizing the process gas flow resulted in the lowest energy consumption. The total energy consumption thereby consisted of two parts: first, 0.02 kWh m^{-3} wastewater were needed for pure oxygen production as calculated from the price for pure liquid oxygen (0.32 CHF kg^{-1} O_2) and electrical energy costs at WWTP Wüeri (0.086 CHF kWh^{-1}). Secondly, 0.04 kWh m^{-3} wastewater were used for ozone generation at an ozone dose of 0.6 g O_3 g^{-1} DOC (12 kWh kg^{-1} O_3, 4 - 6 mg DOC L^{-1}). In total, this corresponds to 15 - 20 % of the total energy consumption of a conventional wastewater treatment plant (0.3 - 0.4 kWh m^{-3}) *(67)*. When taking the investment costs into account as well, the overall cost for ozonation without sand filtration were calculated to be 0.087 CHF m^{-3} wastewater. These costs may vary between countries due to different energy and personnel costs. Further detailed information is available in the final report of the project *(68)*. Table 1.1 summarizes the advantages and disadvantages of ozone application during wastewater treatment.

Table 1.1. Advantages and disadvantages of ozone application during wastewater treatment

Advantages	Disadvantages
• fast oxidation of a broad spectrum of micropollutants • good disinfection of wastewater (*Escherichia coli*, total cell counts) • combination of ozonation and sand filtration lowers the DOC • effect-based measures of micropollutants reduced by ozonation (estrogenicity, inhibition of photosynthesis) • independent of preceding biological secondary treatment, however, nitrification should be achieved • easily integrated into an existing treatment plant, relatively small and only few components needed on-site • safe and reliable full-scale operation possible • energy requirement of a typical medium-sized nutrient removal WWTP is increased only by ~15%	• no removal of micropollutants from the wastewater stream, only transformation • limited transformation of some ozone-resistant micropollutants such as iodinated X-ray contrast media • formation of oxidation by-products such as bromate, *N*-Nitrosodimethyl-amine (NDMA) and assimilable organic carbon (AOC) • results from *in vivo* ecotoxicity tests are controversial • a subsequent biological treatment step (e.g. sand filtration) is recommended for the removal of NDMA, AOC and subtle ecotoxi-cological effects • prerequisite: efficient operation of the preceding biological treatment step (nitrification!) • installation only feasible at wastewater treatment plants > 10.000 P.E. • risk of ozone leakage into working areas • maintenance of monitoring and control components by external companies • use of ozone-resistant materials necessary

1.3.2.2 Fe(VI) application in wastewater treatment

Fe(VI) can be produced as a stable salt by the reaction of iron salts in alkaline solution with a strong oxidant (wet oxidation method) *(39)*:

$$2\ Fe^{3+} + 6\ NO_3^- + 13\ K^+ + 3\ ClO^- + 10\ OH^-$$

$$\rightarrow 2\ Fe(VI)O_4^{2-} + 6\ NO_3^- + 13\ K^+ + 3\ Cl^- + 5\ H_2O \qquad (1.14)$$

A second possibility is a dry oxidation step during which iron oxide is oxidized under high pressure and at high temperatures (> 300 °C) *(24,69)*:

$$Fe_2O_3 + 3\ Na_2O_2 \rightarrow 4\ Na^+ + 2\ FeO_4^{2-} + Na_2O \qquad (1.15)$$

For full-scale application in wastewater treatment, Fe(VI) could be produced off-site as solid salts in a relatively costly production process requiring several steps of separation and purification. As described before, contact with water must be strictly avoided due to its self-decay. After transport to the treatment plant, Fe(VI) salts would have to be stored safely and could then finally be added to the wastewater stream with the help of mixing devices, as already practiced at many WWTPs for phosphate precipitation by Fe(II) or Fe(III) salts. However, the chemical production of Fe(VI) either results in heavy use or production of chemicals (such as chlorine gas from hypochlorite) or high energy requirements. A more convenient approach is to generate Fe(VI) electrochemically in situ and to apply it rapidly to the wastewater stream. Accordingly, most of the research currently focuses on the development of optimum conditions for electrochemical methods of Fe(VI) production using a sacrificial iron anode according to eqs 1.16 - 1.18 *(70,71)*:

Anode reaction:

$$Fe + 8\ OH^- \rightarrow FeO_4^{2-} + 4\ H_2O + 6\ e^- \qquad (1.16)$$

Cathode reaction:

$$6\ H_2O + 6\ e^- \rightarrow 3\ H_2 + 6\ OH^- \qquad (1.17)$$

Overall reaction:

$$Fe + 2\ OH^- + 2\ H_2O \rightarrow FeO_4^{2-} + 3\ H_2 \qquad (1.18)$$

Electrochemical Fe(VI) production has already been tested in laboratory-scale experiments with secondary effluent and showed promising results for the removal of suspended solids, chemical oxygen demand, biochemical oxygen demand and phosphorus *(71-73)*.

For Fe(VI) application to wastewater, the consumption by the wastewater matrix should be minimized by applying Fe(VI) as a tertiary treatment. Figure 1.6 shows the relative stability of Fe(VI) in different wastewater matrices with and without activated sludge. At pH 8, Fe(VI) was consumed within > 30 min in secondary effluent without activated sludge, whereas it was completely consumed in < 3 min in the presence of activated sludge *(74)*.

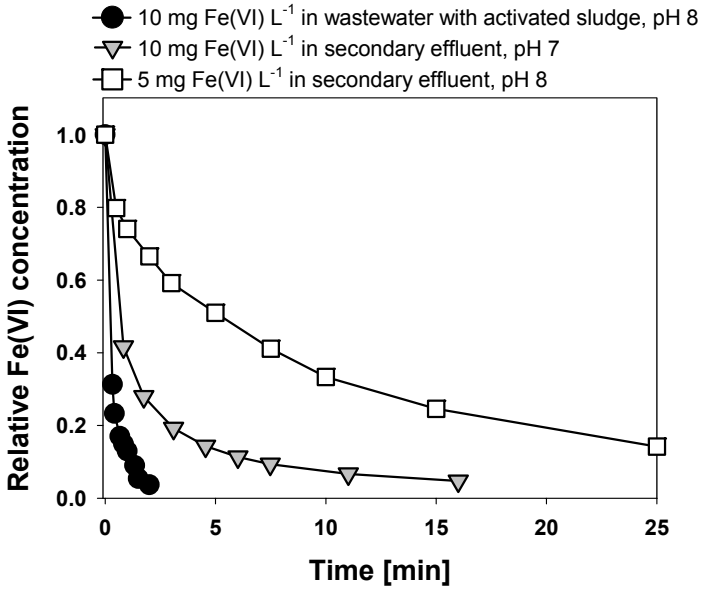

Figure 1.6. Comparison of the relative Fe(VI) consumption in different wastewater matrices with and without activated sludge. Wastewaters were taken from WWTP Dübendorf, Switzerland.

For full-scale application of Fe(VI), a subsequent sedimentation step after Fe(VI) addition will be necessary. This is comparable to sedimentation steps needed for chemical phosphorus removal by the addition of Fe(II) or Fe(III) salts.

1.3.2.3 Powdered activated carbon (PAC) for wastewater treatment

Apart from oxidative strategies, a wide range of micropollutants can also be removed from the wastewater stream by adsorbing on PAC, thereby not producing any by-products. Sorption was shown to be concentration dependent for many compounds and can be described by Freundlich isotherms rather than by a constant distribution coefficient K_d mostly used for sorption to activated sludge. However, complete retention of PAC by a final sedimentation and filtration step must be guaranteed. PAC addition does also not lead to disinfection of the wastewater stream.

Activated carbon can be produced from carbon-rich raw material such as black coal or charcoal, peat or coconut shells. A process called 'activation' can be carried out with the help of water vapor at 800 - 1000 °C, and therefore is very energy intense. Volatile constituents are stripped out and pores, breaks and cracks are generated that increase the surface of the activated carbon and lead to an increased sorption capacity. Highly activated carbon can have surface areas of up to 1500 $m^2 g^{-1}$ *(75)*.

The point of PAC addition to the wastewater stream is decisive for the efficiency of micropollutant removal. PAC addition to secondary effluent is advantageous since the DOC concentration competing with micropollutants for sorption sites is relatively low. In general, a broad spectrum of micropollutants is removed via sorption already by a single stage addition to secondary effluent. Still, the best overall micropollutants removal is achieved in a double stage treatment with PAC addition to secondary effluent and subsequent recycling of waste PAC into the preceding biology. This may be due to the additional sorption of micropollutants present in higher concentrations to the partly loaded PAC, as was observed for X-ray contrast media. For a DOC of 5 - 10 mg L^{-1} in secondary effluent, 10 - 20 mg PAC L^{-1} were sufficient to achieve micropollutant elimination between 50 - 100 % *(76)*.

Results from full-scale trials further demonstrated that an adequate mixing regime and adapted flocculants addition to the contact reactor achieved a good retention of the fine fraction of the PAC in the deep bed filter of a flocculation sand filtration *(77)*. Table 1.2 gives a brief overview on the advantages and disadvantages of PAC addition to wastewater.

Table 1.2. Advantages and disadvantages of powdered activated carbon (PAC) addition during wastewater treatment

Advantages	Disadvantages
• elimination of a broad spectrum of micropollutants from the wastewater stream by sorption to PAC • no formation of transformation products and by-products from wastewater matrix components • significant lowering of DOC concentration • most efficient elimination of micropollutants if loaded PAC sludge from the adsorption reactor is recycled into the preceding biological treatment step • single dosing into the adsorption reactor or into the biology is less efficient • no negative effect on nitrifiers observed in batch trials and during a one-year pilot trial with recycling of PAC sludge into the biology • addition of PAC improved the sludge index (settleability) of the activated sludge	• desorption of micropollutants possible • limited adsorption of some micropollutants such as iodinated X-ray contrast media • coagulants needed to enhance PAC sedimentation (no influence on micropollutants removal) • 5-10 % higher specific sludge production during operation mode with recycling of PAC sludge into the biology • space-consuming components • corrosive as a concentrated suspension since 2 % ash content increases the pH up to 12 • abrasive due to sharp PAC particles • complicated handling to prevent dust formation • complete retention of PAC by sedimentation and filtration necessary to avoid loss of loaded PAC into receiving waters

1.4 Thesis outline

This doctoral thesis was carried out within the framework of two projects: the ongoing Swiss project "Strategy MicroPoll" launched in 2006 by the Swiss Federal Office of the Environment, and the EU project NEPTUNE (2006 - 2010), which both focused on advancements in municipal wastewater treatment. The objective of the "Strategy MicroPoll" project is to minimize the release of micropollutants from wastewater discharge to receiving water bodies and includes the evaluation of the most promising options ozonation and PAC addition. The NEPTUNE project had a broader approach and focused on the development of new sustainable concepts and processes for the optimization and upgrading of municipal wastewater and sludge treatment. Within NEPTUNE, new technologies for micropollutant removal from wastewater were investigated, and included the use of ferrate (Fe(VI)) as a potential water treatment chemical.

This doctoral thesis investigates oxidative techniques as tertiary treatments of municipal wastewater with a special focus on micropollutant transformation. Ozonation was assessed in a full-scale system whereas ferrate (Fe(VI)) was investigated in laboratory-scale systems. The results are presented in the form of papers which were published in peer-reviewed journals (three papers), or which were submitted to a peer-reviewed journal (one paper).

Chapter 1 introduces the issue of (polar organic) micropollutants in the aquatic environment. The chemistry of oxidative technologies for micropollutant removal from municipal wastewater is presented, and the successful operation of a full-scale ozonation step for a 16 months period is reported. Fe(VI) is introduced as a new promising wastewater treatment chemical, and a brief overview on powdered activated carbon addition is given because it is another promising option for micropollutant removal from municipal wastewater.

Chapter 2 presents results on the removal of an extended selection of micropollutants along the treatment train of WWTP Wüeri in Regensdorf as assessed by 24h- or 48h-flow proportional composite samples. A simple model based on an assumed plug flow behavior of the ozone reactor was applied to predict overall micropollutant oxidation.

Chapter 3 focuses on the kinetic assessment and modeling of the full-scale ozone reactor in terms of micropollutant oxidation, disinfection and oxidation by-product formation. Measurements are based on grab samples from defined points inside the ozone reactor and hence accurately describe the kinetics within a full-scale ozone reactor for a given flow regime and ozone dose. The model was a refined approach based on the combination of reactor hydraulics determined in tracer tests, ozone chemistry, and micropollutant reactivity towards ozone and hydroxyl radicals as well as the rates of microorganism inactivation by ozone, respectively. Known oxidation by-products such as bromate, *N*-nitrosodimethylamine (NDMA) and assimilable organic carbon (AOC) were also determined.

Chapter 4 investigates Fe(VI) as a promising oxidant and coagulant for municipal wastewater treatment and includes (i) the development of a kinetic database for the oxidation of olefin-, phenol-, and amine-containing micropollutants, (ii) the oxidation of individually spiked micropollutants in a wastewater matrix including the prediction of oxidation efficiency, (iii) a comparison to the efficiency of ozone to oxidize micropollutants in wastewater, and (iv) the application of Fe(VI) to wastewater for simultaneous micropollutant oxidation and phosphate coagulation.

Chapter 5 identifies oxidation products formed during the oxidation of tramadol by Fe(VI) and ozone. Tramadol was chosen as environmentally relevant micropollutant containing an amine function. Based on kinetic data, the identified oxidation products, mass balances in buffered solutions and the available literature, reaction mechanisms for oxidation product formation are proposed for both oxidants.

In Chapter 6, general conclusions for a possible future application of ozone and Fe(VI) in municipal wastewater treatment are drawn.

1.5 References

(1) Schwarzenbach, R. P.; Escher, B. I.; Fenner, K.; Hofstetter, T. B.; Johnson, C. A.; von Gunten, U.; Wehrli, B. The challenge of micropollutants in aquatic systems. *Science* **2006**, *313*, 1072-1077.

(2) Bargagli, R. Environmental contamination in Antarctic ecosystems. *Sci. Total Environ.* **2008**, *400*, 212-226.

(3) Donaldson, S. G.; Van Oostdam, J.; Tikhonov, C.; Feeley, M.; Armstrong, B.; Ayotte, P.; Boucher, O.; Bowers, W.; Chan, L.; Dallaire, F.; Dallaire, R.; Dewailly, E.; Edwards, J.; Egeland, G. M.; Fontaine, J.; Furgal, C.; Leech, T.; Loring, E.; Muckle, G.; Nancarrow, T.; Pereg, D.; Plusquellec, P.; Potyrala, M.; Receveur, O.; Shearer, R. G. Environmental contaminants and human health in the Canadian Arctic. *Sci. Total Environ.* **2010**, *408*, 5165-5234.

(4) Halling-Sorensen, B.; Nielsen, S. N.; Lanzky, P. F.; Ingerslev, F.; Lutzhoft, H. C. H.; Jorgensen, S. E. Occurrence, fate and effects of pharmaceutical substances in the environment - A review. *Chemosphere* **1998**, *36*, 357-394.

(5) Daughton, C. G.; Ternes, T. A. Pharmaceuticals and personal care products in the environment: Agents of subtle change? *Environ. Health Perspect.* **1999**, *107*, 907-938.

(6) Heberer, T. Tracking persistent pharmaceutical residues from municipal sewage to drinking water. *Journal of Hydrology* **2002**, *266*, 175-189.

(7) Sacher, F.; Lang, F. T.; Brauch, H. J.; Blankenhorn, I. Pharmaceuticals in groundwaters - Analytical methods and results of a monitoring program in Baden-Wurttemberg, Germany. *J. Chromatogr. A* **2001**, *938*, 199-210.

(8) Gujer, W. *Siedlungswasserwirtschaft*. Springer: Berlin, 1999.

(9) Logsdon, G.; Hess, A.; Horsley, M.: Guide to selection of water treatment processes. In *Water quality and treatment: A handbook of community water supplies*; Letterman, R. D., Ed.; McGraw-Hill, Inc.: New York, 1999.

(10) Benotti, M. J.; Trenholm, R. A.; Vanderford, B. J.; Holady, J. C.; Stanford, B. D.; Snyder, S. A. Pharmaceuticals and Endocrine Disrupting Compounds in US Drinking Water. *Environ. Sci. Technol.* **2009**, *43*, 597-603.

(11) Kummerer, K. The presence of pharmaceuticals in the environment due to human use - present knowledge and future challenges. *Journal of Environmental Management* **2009**, *90*, 2354-2366.

(12) Brian, J. V.; Harris, C. A.; Scholze, M.; Backhaus, T.; Booy, P.; Lamoree, M.; Pojana, G.; Jonkers, N.; Runnalls, T.; Bonfa, A.; Marcomini, A.; Sumpter, J. P. Accurate prediction of the response of freshwater fish to a mixture of estrogenic chemicals. *Environ. Health Perspect.* **2005**, *113*, 721-728.

(13) Kidd, K. A.; Blanchfield, P. J.; Mills, K. H.; Palace, V. P.; Evans, R. E.; Lazorchak, J. M.; Flick, R. W. Collapse of a fish population after exposure to a synthetic estrogen. *Proc. Natl. Acad. Sci. U. S. A.* **2007**, *104*, 8897-8901.

(14) Ternes, T. A.; Joss, A. *Human Pharmaceuticals, Hormones and Fragrances. The Challenge of Micropollutants in Urban Water Management*. IWA Publishing: London, 2006.

(15) Burkhardt, M.; Kupper, T.; Hean, S.; Haag, R.; Schmid, P.; Kohler, M.; Boller, M. Biocides used in building materials and their leaching behavior to sewer systems. *Water Sci. Technol.* **2007**, *56*, 63-67.

(16) Joss, A.; Siegrist, H.; Ternes, T. A. Are we about to upgrade wastewater treatment for removing organic micropollutants? *Water Sci. Technol.* **2008**, *57*, 251-255.

(17) Joss, A.; Zabczynski, S.; Goebel, A.; Hoffmann, B.; Loeffler, D.; McArdell, C. S.; Ternes, T. A.; Thomsen, A.; Siegrist, H., 2006. Biological degradation of pharmaceuticals in municipal wastewater treatment: Proposing a classification scheme. *Water Res.* **2006**, *40*, 1686-1696.

(18) Joss, A.; Keller, E.; Alder, A. C.; Gobel, A.; McArdell, C. S.; Ternes, T.; Siegrist, H. Removal of pharmaceuticals and fragrances in biological wastewater treatment. *Water Res.* **2005**, *39*, 3139-3152.

(19) Ternes, T. A.; Meisenheimer, M.; McDowell, D.; Sacher, F.; Brauch, H. J.; Gulde, B. H.; Preuss, G.; Wilme, U.; Seibert, N. Z. Removal of pharmaceuticals during drinking water treatment. *Environ. Sci. Technol.* **2002**, *36*, 3855-3863.

(20) Huber, M. M.; Canonica, S.; Park, G. Y.; von Gunten, U. Oxidation of pharmaceuticals during ozonation and advanced oxidation processes. *Environ. Sci. Technol.* **2003**, *37*, 1016-1024.

(21) Westerhoff, P.; Yoon, Y.; Snyder, S.; Wert, E. Fate of endocrine-disruptor, pharmaceutical, and personal care product chemicals during simulated drinking water treatment processes. *Environ. Sci. Technol.* **2005**, *39*, 6649-6663.

(22) Legube, B.: Ozonation By-Products. In *The Handbook of Environmental Chemistry*; Springer-Verlag: Berlin, Heidelberg, 2003; Vol. 5, Part G, pp 95-116.

(23) Snoeyink, V. L.; Summers, R. S.: Adsorption of organic compounds. In *Water quality and treatment: A handbook of community water supplies*; Letterman, R. D., Ed.; McGraw-Hill, Inc.: New York, 1999.

(24) Lee, Y.; Cho, M.; Kim, J. Y.; Yoon, J. Chemistry of ferrate (Fe(VI)) in aqueous solution and its applications as a green chemical. *Journal of Industrial and Engineering Chemistry* **2004**, *10*, 161-171.

(25) Jiang, J. Q.; Panagouopoulos, A.; Bauer, M.; Pearce, P. The application of potassium ferrate for sewage treatment. *Journal of Environmental Management* **2006**, *79*, 215-220.

(26) Bailey, P. S. *Ozone reactions with organic compounds*. American Chemical Society: Washington, D.C., 1971.

(27) von Gunten, U. Ozonation of drinking water: Part I. Oxidation kinetics and product formation. *Water Res.* **2003**, *37*, 1443-1467.

(28) Staehelin, J.; Hoigne, J. Decomposition of Ozone in Water - Rate of Initiation by Hydroxide Ions and Hydrogen-Peroxide. *Environ. Sci. Technol.* **1982**, *16*, 676-681.

(29) Elliot, A. J.; McCracken, D. R. Effect of Temperature on O.- Reactions and Equilibria - a Pulse-Radiolysis Study. *Radiat. Phys. Chem.* **1989**, *33*, 69-74.

(30) Staehelin, J.; Hoigne, J. Decomposition of Ozone in Water in the Presence of Organic Solutes Acting as Promoters and Inhibitors of Radical Chain Reactions. *Environ. Sci. Technol.* **1985**, *19*, 1206-1213.

(31) Buffle, M. O. Mechanistic investigations of the initial phase of ozone decomposition in drinking water and wastewater. **2005**, ETH Zürich, Zürich.

(32) Buffle, M. O.; Schumacher, J.; Salhi, E.; Jekel, M.; von Gunten, U. Measurement of the initial phase of ozone decomposition in water and wastewater by means of a continuous quench-flow system: Application to disinfection and pharmaceutical oxidation. *Water Res.* **2006**, *40*, 1884-1894.

(33) von Gunten, U.; von Sonntag, C. *The Chemistry of Ozone in Water and Wastewater Treatment: From Basic Principles to Applications*. IWA Publishing, 2011, in preparation.

(34) von Gunten, U.; Salhi, E.; Schmidt, C. K.; Arnold, W. A. Kinetics and Mechanisms of *N*-Nitrosodimethylamine Formation upon Ozonation of *N,N*-Dimethylsulfamide-Containing Waters: Bromide Catalysis. *Environ. Sci. Technol.* **2010**, *44*, 5762-5768.

(35) von Gunten, U. Ozonation of drinking water: Part II. Disinfection and by-product formation in presence of bromide, iodide or chlorine. *Water Res.* **2003**, *37*, 1469-1487.

(36) Funabiki, T. *Oxygenases and model systems*. Kluwer Academic Publishers: Dordrecht, 1997.

(37) Silaghi-Dumitrescu, R. *Horseradish peroxidase - a versatile catalyst*. Trans-world Research Network: Kerala, India, 2006.

(38) von Sonntag, C. Advanced oxidation processes: mechanistic aspects. *Water Sci. Technol.* **2008**, *58*, 1015-1021.

(39) Thompson, G. W.; Ockerman, L. T.; Schreyer, J. M. Preparation and Purification of Potassium Ferrate. 6. *J. Am. Chem. Soc.* **1951**, *73*, 1379-1381.

(40) Bielski, B. H. J. Studies of Hypervalent Iron. *Free Radical Res. Commun.* **1991**, *12-3*, 469-477.

(41) Hoppe, M. L.; Schlemper, E. O.; Murmann, R. K. Structure of Dipotassium Ferrate(VI). *Acta Crystallographica Section B-Structural Science* **1982**, *38*, 2237-2239.

(42) Goff, H.; Murmann, R. K. Studies on Mechanism of Isotopic Oxygen Exchange and Reduction of Ferrate(VI) Ion (FeO42-). *J. Am. Chem. Soc.* **1971**, *93*, 6058-6065.

(43) Norcross, B. E.; Lewis, W. C.; Gai, H. F.; Noureldin, N. A.; Lee, D. G. The oxidation of secondary alcohols by potassium tetraoxoferrate(VI). *Canadian Journal of Chemistry-Revue Canadienne De Chimie* **1997**, *75*, 129-139.

(44) Rush, J. D.; Zhao, Z. W.; Bielski, B. H. J. Reaction of ferrate(VI)/ferrate(V) with hydrogen peroxide and superoxide anion - A stopped-flow and premix pulse radiolysis study. *Free Radic. Res.* **1996**, *24*, 187-198.

(45) Sharma, V. K.; Burnett, C. R.; Millero, F. J. Dissociation constants of the monoprotic ferrate(VI) ion in NaCl media. *Physical Chemistry Chemical Physics* **2001**, *3*, 2059-2062.

(46) Jiang, J. Q.; Lloyd, B. Progress in the development and use of ferrate(VI) salt as an oxidant and coagulant for water and wastewater treatment. *Water Res.* **2002**, *36*, 1397-1408.

(47) Sharma, V. K.; Mishra, S. K. Ferrate(VI) oxidation of ibuprofen: A kinetic study. *Environmental Chemistry Letters* **2006**, *3*, 182-185.

(48) Sharma, V. K.; Mishra, S. K.; Nesnas, N. Oxidation of sulfonamide antimicrobials by ferrate(VI) [Fe(VI)O42-]. *Environ. Sci. Technol.* **2006**, *40*, 7222-7227.

(49) Hu, L.; Martin, H. M.; Arcs-Bulted, O.; Sugihara, M. N.; Keatlng, K. A.; Strathmann, T. J. Oxidation of Carbamazepine by Mn(VII) and Fe(VI): Reaction Kinetics and Mechanism. *Environ. Sci. Technol.* **2009**, *43*, 509-515.

(50) Lee, Y.; Yoon, J.; Von Gunten, U. Kinetics of the oxidation of phenols and phenolic endocrine disruptors during water treatment with ferrate (Fe(VI)). *Environ. Sci. Technol.* **2005**, *39*, 8978-8984.

(51) Lee, Y.; Escher, B. I.; von Gunten, U. Efficient Removal of Estrogenic Activity during Oxidative Treatment of Waters Containing Steroid Estrogens. *Environ. Sci. Technol.* **2008**, *42*, 6333-6339.

(52) Cho, M.; Lee, Y.; Choi, W.; Chung, H. M.; Yoon, J. Study on Fe(VI) species as a disinfectant: Quantitative evaluation and modeling for inactivating Escherichia coli. *Water Res.* **2006**, *40*, 3580-3586.

(53) Schink, T.; Waite, T. D. Inactivation of F2 Virus with Ferrate(VI). *Water Res.* **1980**, *14*, 1705-1717.

(54) Kazama, F. Inactivation of Coliphage Q-Beta by Potassium Ferrate. *FEMS Microbiol. Lett.* **1994**, *118*, 345-349.

(55) Kazama, F. Viral Inactivation by Potassium Ferrate. *Water Sci. Technol.* **1995**, *31*, 165-168.

(56) Ramseier, M. K.; von Gunten, U.; Freihofer, P.; Hammes, F. Kinetics of membrane damage to high (HNA) and low (LNA) nucleic acid bacterial clusters in drinking water by ozone, chlorine, chlorine dioxide, monochloramine, ferrate(VI), and permanganate. *Water Res.* **2010**, *45*, 1490-1500.

(57) Graham, N. J. D.; Khoi, T. T.; Jiang, J. Q. Oxidation and coagulation of humic substances by potassium ferrate. *Water Sci. Technol.*, *62*, 929-936.

(58) Farooq, S.; Bari, A. Tertiary-Treatment with Ferrate and Ozone. *Journal of Environmental Engineering-Asce* **1986**, *112*, 301-310.

(59) Valsami-Jones, E. *Phosphorus in Environmental Technology: Principles and Applications*. IWA Publishing: London, 2004.

(60) Lee, Y.; Kieu, A. T.; Kissner, R.; von Gunten, U. Self-decomposition of ferrate (Fe(VI)) in water: kinetics, mechanism, and formation of hydrogen peroxide, in preparation.

(61) Hoigné, J.; Bader, H. Rate Constants of Reactions of Ozone with Organic and Inorganic-Compounds in Water. 1. Non-Dissociating Organic-Compounds. *Water Res.* **1983**, *17*, 173-183.

(62) Hoigné, J.; Bader, H. Rate Constants of Reactions of Ozone with Organic and Inorganic-Compounds in Water. 2. Dissociating Organic-Compounds. *Water Res.* **1983**, *17*, 185-194.

(63) Stumm, W.; Morgan, J. J. *Aquatic chemistry. Chemical equilibria and rates in natural waters*. 3rd ed. Wiley-Interscience: New York, 1996.

(64) Hoigné, J. Inter-calibration of OH radical sources and water quality parameters. *Water Sci. Technol.* **1997**, *35*, 1-8.

(65) Neta, P.; Dorfman, L. M. Pulse Radiolysis Studies .13. Rate Constants for Reaction of Hydroxyl Radicals with Aromatic Compounds in Aqueous Solutions. *Advances in Chemistry Series* **1968**, 222-230.

(66) Naumov, S.; Mark, G.; Jarocki, A.; von Sonntag, C. The Reactions of Nitrite Ion with Ozone in Aqueous Solution - New Experimental Data and Quantum-Chemical Considerations. *Ozone-Sci. Eng.* **2010**, *32*, 430-434.

(67) Müller, E. A.; Kobel, B. *Handbuch Energie in Kläranlagen*. Ministerium für Umwelt, Raumordnung und Landschaftwirtschaft des Landes Nordrhein-Westfalen: Düsseldorf, 1999.

(68) Abegglen, C.; Escher, B. I.; Hollender, J.; Koepke, S.; Ort, C.; Peter, A.; Siegrist, H.; von Gunten, U.; Zimmermann, S. G. *Ozonung von gereinigtem Abwasser, Schlussbericht Pilotversuch Regensdorf*. Eawag: Dübendorf, 2009.

(69) Martinez-Tamayo, E.; Beltran-Porter, A.; Beltran-Porter, D. Iron Compounds in High Oxidation-States. 2. Reaction between Na2O2 and FeSO4. *Thermochim. Acta* **1986**, *97*, 243-255.

(70) Alsheyab, M.; Jiang, J. Q.; Stanford, C. Electrochemical generation of ferrate (VI): Determination of optimum conditions. *Desalination* **2010**, *254*, 175-178.

(71) Alsheyab, M.; Jiang, J.-Q.; Stanford, C. Engineering Aspects of Electrochemical Generation of Ferrate: A Step Towards Its Full Scale Application for Water and Wastewater Treatment. *Water Air and Soil Pollution* **2010**, *210*, 203-210.

(72) Jiang, J. Q.; Stanford, C.; Alsheyab, M. The online generation and application of ferrate(VI) for sewage treatment - A pilot scale trial. *Separation and Purification Technology* **2009**, *68*, 227-231.

(73) Stanford, C.; Jiang, J. Q.; Alsheyab, M. Electrochemical Production of Ferrate (Iron VI): Application to the Wastewater Treatment on a Laboratory Scale and Comparison with Iron (III) Coagulant. *Water Air and Soil Pollution* **2010**, *209*, 483-488.

(74) Deliverable 5.4: Catalogue with criteria for evaluating technologies. *EU project Neptune* **2010**, http://www.eu-neptune.org/Publications%20and%20 Presentations/D25.24_Catalogue_with_front_page.pdf.

(75) Brendel, U. Einsatz von Aktivkohle in der kommunalen Abwasserreinigung. **1997**, RWTH Aachen, Aachen.

(76) Abegglen, C.; Böhler, M.; Hollender, J.; Zimmermann, S. G.; Zwickenpflug, B.; von Gunten, U.; Siegrist, H.; Thonney, D. Mikroverunreinigungen in Kläranlagen. Technische Verfahren zur Elimination von organischen Spurenstoffen. *GWA* **2010**, *7*, 587 - 594.

(77) Böhler, M. Department of Process Engineering, Eawag. personal communication. **2011**.

Chapter 2

Elimination of organic micropollutants in a municipal wastewater treatment plant upgraded with a full-scale post-ozonation followed by sand filtration

Reproduced with permission from Hollender, J.*; Zimmermann, S. G.*; Koepke, S.; Krauss, M.; McArdell, C. S.; Ort, C.; Singer, H.; von Gunten, U.; Siegrist, H. *Environmental Science and Technology* **2009**, *43*, 7862-7869.

http://pubs.acs.org/doi/abs/10.1021/es9014629

*Co-primary authors contributed equally to this work

Abstract

The removal efficiency for 220 micropollutants was studied at the scale of a municipal wastewater treatment plant (WWTP) upgraded with post-ozonation followed by sand filtration. During post-ozonation, compounds with activated aromatic moieties, amine functions, or double bonds such as sulfamethoxazole, diclofenac or carbamazepine with second-order rate constants for the reaction with ozone > 10^4 M^{-1} s^{-1} at pH 7 (fast-reacting) were eliminated to concentrations below the detection limit for an ozone dose of 0.47 g O_3 g^{-1} dissolved organic carbon (DOC). Compounds more resistant to oxidation by ozone such as atenolol and benzotriazole were increasingly eliminated with increasing ozone doses, resulting in > 85 % removal for a medium ozone dose (~ 0.6 g O_3 g^{-1} DOC). Only a few micropollutants such as some X-ray contrast media and triazine herbicides with second-order rate constants < 10^2 M^{-1} s^{-1} (slowly-reacting) persisted to a large extent. With a medium ozone dose, only 11 micropollutants of 55 detected in the secondary effluent were found at > 100 ng L^{-1}. The combination of reaction kinetics and reactor hydraulics, based on laboratory- and full-scale data, enabled a quantification of the results by model calculations. This conceptual approach allows a direct up-scaling from laboratory- to full-scale systems and can be applied to other similar systems. The carcinogenic by-products *N*-nitrosodimethylamine (NDMA) (≤ 14 ng L^{-1}) and bromate (< 10 μg L^{-1}) were produced during ozonation, however, their concentrations were below or in the range of the drinking water standards. Furthermore, it could be demonstrated that biological sand filtration is an efficient additional barrier for the elimination of biodegradable compounds formed during ozonation such as NDMA. The energy requirement for the additional post-ozonation step is about 0.035 kWh m^{-3}, which corresponds to 12 % of a typical medium-sized nutrient removal plant (5 g DOC m^{-3}).

2.1 Introduction

In recent decades, contamination of surface waters with organic micropollutants has received increasing scientific and public awareness. In industrialized countries, in which more than 90 % of the wastewater is treated in centralized WWTPs, they represent a major point source for micropollutants and are therefore the best location for mitigation. WWTPs are designed to reduce loads of C, N and P present in the influent in the mg L^{-1} range. Several pharmaceuticals with orders of magnitude lower concentration levels (ng L^{-1} to µg L^{-1}), such as paracetamol or ibuprofen, are also degraded in the activated sludge process of WWTPs by > 90 % *(1)*. Others, such as hydrophobic musk ketones or zwitterionic fluoroquinolone antimicrobials *(2)*, can be removed from the effluent by sorption to the sludge. However, many polar drugs and biocides, such as the antimicrobials clarithromycin and trimethoprim and the analgesic diclofenac are only partly degraded or sorbed while compounds such as several X-ray contrast media and the antiepileptic drug carbamazepine almost completely resist biological degradation *(1,3)*. To improve the removal efficiencies of micropollutants within WWTPs, discussion has focused on upgrading the overall treatment process with additional treatment steps *(4,5)*. Activated carbon and ozonation are processes bearing the potential to significantly lower the micropollutant load and are also feasible with regard to energy consumption and costs *(5)*. Doses of 10 - 20 mg L^{-1} of powdered activated carbon are expected to result in an advanced removal of a broad spectrum of micropollutants, but highly polar compounds need higher doses or can only be removed partly *(6,7)*. Ozonation of drinking and wastewater for disinfection purposes has a long tradition, but its benefits for micropollutant removal during wastewater treatment have only been discussed recently. First results from pilot plants utilizing post-ozonation revealed removal rates of > 95 % for many micropollutants *(8-11)*. Ozone is a selective oxidant with second-order rate constants for the reaction with organic compounds ranging over approximately 10 orders of magnitude, from no reaction up to almost 10^{10} M^{-1} s^{-1} *(12)*. It is particularly reactive towards functional groups with high electron density such as double bonds, activated aromatic systems, nonprotonated secondary and tertiary amines, and reduced sulfur species. Although ozonation results only in a partial oxidation, some studies indicate that the initial attack at the reactive functional groups destroys the

biological activity of compounds, as shown for estrogenic or antimicrobial compounds *(13-15)*. Simultaneously, ozone decomposes into hydroxyl radicals which react nonselectively with high rate constants of about 10^9 - 10^{10} M^{-1} s^{-1} with organic molecules *(12)*. Therefore, hydroxyl radicals can contribute to the oxidation of ozone-recalcitrant compounds. The major uncertainty of ozonation is related to the formation of oxidation by-products from matrix components and transformation products from micropollutants. The oxidation of organic matter results in a better biodegradable fraction which can be degraded during biological post-filtration *(16)*. Various studies revealed reaction products of micropollutants but their concentrations as well as the estrogenic and antimicrobial activity of the products was minor compared to the parent compounds *(13-15,17)*. The formation of bromate can be relevant if bromide occurs in high concentrations *(18)*. A recent study of Schmidt and Brauch *(19)* showed NDMA formation at high yields from the ozonation of dimethylsulfamide (a transformation product of the fungicide tolylfluanide), but also other compounds containing a dimethylamino moiety form NDMA with very low yields *(20,21)*. Furthermore, the formation of *N*-nitrosomorpholine was observed upon ozonation of a lake water sample *(22)*.

The main objectives of the present study were (a) assessment of ozonation as a treatment step for the removal of micropollutants (220 compounds) from a secondary effluent at the scale of a municipal WWTP, (b) quantification of the results based on a model which combined reaction kinetics determined in laboratory with reactor hydraulics, (c) assessment of the formation of toxic by-products such as bromate and nitrosamines, and (d) determination of the energy requirements for this enhanced wastewater treatment. The selected micropollutants with different functional groups have varying second-order rate constants with ozone ranging from < 1 M^{-1} s^{-1} up to > 10^8 M^{-1} s^{-1}, can be found in wastewaters in many countries including Switzerland *(23)*, and are known to partly persist during biological wastewater treatment.

2.2 Materials and Methods

2.2.1 Sampling at the wastewater treatment plant with ozonation

The WWTP Wüeri in Regensdorf, Switzerland with conventional activated sludge treatment was chosen as the study site and upgraded with a full-scale ozonation reactor followed by sand filtration (Figure S2.1 of the Supporting Information, Text S2.1). Eleven sampling campaigns were conducted with ozone doses in the range of 0.36 - 1.16 g O_3 g^{-1} DOC (Table 2.1). During these campaigns, 24 h-, 48 h- and in one case 72 h-volume proportional composite samples (70 - 160 mL every 50 m^3) were taken in the effluent of the primary and secondary clarifier, after the ozone reactor, and in the final effluent after sand filtration.

2.2.2 Determination of ozone and hydroxyl radical exposures and R_{ct} values

Due to the difficulty in determining the ozone and hydroxyl radical exposures in the reactor itself, they and the R_{ct} values were determined by means of a laboratory dispenser system *(24)*. The probe compound *p*-chlorobenzoic acid (*p*CBA), which is ozone-resistant, was used to determine the transient hydroxyl radical concentrations (Text S2.2).

2.2.3 Quantification of micropollutants

A set of 10 biocides and pesticides, 24 pharmaceuticals and 7 of their known transformation products, 6 X-ray contrast media, 2 corrosion inhibitors and 8 nitrosamines were analyzed by offline or online-SPE-HPLC-MS/MS methods using isotope dilution for quantification (Table S2.1, S2.3, Text S2.3). For two campaigns in May 2008 approximately 170 additional compounds were measured using LC-high-resolution tandem mass spectrometry (Table S2.2) and screening for known transformation products of ozonation of highly concentrated micropollutants was conducted (Text S2.3).

Table 2.1. Characterization of the measurement campaigns during the full-scale ozonation at the WWTP Wüeri

Sampling date	Averaged ozone dose	Transferred ozone dose		Ozone exposure[b]	OH radical exposure[b]	R_{ct}	DOC	Temperature	pH	Flow rate reactor	Hydraulic retention time reactor
	(g O_3 g^{-1} DOC)	(g O_3 g^{-1} DOC)	(mg O_3 L^{-1})	(M s)	(M s)	(-)	(mg L^{-1})	(°C)		(m^3 d^{-1})	(min:sec)
24.-26.09.2007		0.47[a]	2.8	2.17×10^{-03}	1.52×10^{-10}	4.1×10^{-08}	6.0	22.0	7.0	5600	9:20
06.-07.12.2007	0.40 ± 0.06	0.36	1.6	2.93×10^{-03}	6.51×10^{-11}	1.1×10^{-08}	4.7	11.5	7.0	14000	3:40
08.-10.01.2008		0.36	1.9	9.49×10^{-04}	5.04×10^{-11}	2.3×10^{-08}	5.4	10.3	7.0	7400	7:00
07.-08.02.2008		0.67	3.6	1.19×10^{-02}	1.82×10^{-10}	9.7×10^{-09}	5.4	11.8	7.0	5700	9:10
12.-13.02.2008		0.55	3.2	1.41×10^{-02}	1.36×10^{-10}	6.0×10^{-09}	5.8	12.2	7.0	5100	10:10
19.-21.05.2008	0.62 ± 0.05	0.62	3.2	5.86×10^{-03}	1.56×10^{-10}	1.6×10^{-08}	5.4	17.0	7.0	6200	8:20
21.-24.05.2008		0.65	3.3	5.86×10^{-03}	1.56×10^{-10}	1.6×10^{-08}	5.4	17.0	7.0	5400	9:40
24.-26.05.2008		0.60	3.2	5.86×10^{-03}	1.56×10^{-10}	1.6×10^{-08}	5.4	17.0	7.0	5500	9:30
18.-19.06.2008	1.16	1.16	5.3	3.37×10^{-02}	6.86×10^{-10}	1.5×10^{-08}	4.6	18.8	7.0	5300	9:50
26.-28.08.2008	0.79 ± 0.02	0.77	3.2	9.74×10^{-03}	1.57×10^{-10}	1.0×10^{-08}	4.2	20.5	7.0	5200	10:00
23.- 25.09.2008		0.81	3.7	1.09×10^{-02}	1.74×10^{-10}	1.0×10^{-08}	4.6	20.0	7.0	5300	9:50

[a] flowproportional dosing before installation of DOC sensor, calculation by retrospective calibration of the spectra
[b] from batch experiments

Removal efficiencies during secondary treatment and ozonation were calculated from the concentrations in primary, secondary, and ozonation effluent. For these calculations, concentrations below the limit of quantification (LOQ) were set to half of the LOQ value. Standard deviations of the removal efficiency were calculated using Gaussian error propagation from the standard deviations of the effluent samples. For samples which were analyzed in replicates, the actual standard deviations were used. For samples analyzed without replicates, a standard deviation corresponding to a coefficient of variation of 20 % was assumed.

2.2.4 Prediction of relative elimination of micropollutants

The predicted relative elimination of micropollutants during ozonation was calculated from the ozone and hydroxyl radical exposures determined in laboratory experiments, and the second-order rate constants using eq 2.1:

$$\frac{[P]}{[P_0]} = e^{-k_{O_3}\int[O_3]dt - k_{OH\bullet}\int[OH\bullet]dt} \qquad (2.1)$$

with [P] as micropollutant concentration, $\int[O_3]dt$ as ozone exposure, and $\int[OH\bullet]dt$ as hydroxyl radical exposure *(12)*. The second-order rate constants for the reaction with ozone (k_{O_3}) and hydroxyl radicals ($k_{OH\bullet}$) were taken from literature and corrected for the pH and temperature measured during the campaigns (Table S2.4, Text S2.4). The ozone consumption along the ozone reactor was measured for three different ozone doses ranging from 0.41 to 1.24 g O_3 g^{-1} DOC and was found to be similar to the ozone decrease in a batch system with the same effluent sample and ozone dose *(25)*. Tracer tests with the conservative tracer fluoresceine confirmed further that the hydraulic behavior of the ozone reactor is close to that of a plug flow reactor *(25)*. Based on these findings, eq 2.1 can be applied for comparison between full-scale and laboratory-scale experiments.

2.3 Results and Discussion

2.3.1 Elimination of micropollutants in the WWTP with post-ozonation

The studied WWTP receives a typical Swiss municipal wastewater with micropollutants detected in the ng L^{-1} range up to several µg L^{-1} after the primary clarifier (Table S2.5). The secondary biological treatment process was very effective as indicated by DOC concentrations of only 5.2 ± 0.6 mg L^{-1} in the effluent and eliminations of > 85 % for the easily biodegradable compounds ibuprofen, paracetamol, N_4-acetylsulfamethoxazole, and mefenamic acid. Compounds known to be moderately persistent such as diclofenac, naproxen, bezafibrate, sulfonamide antibiotics, macrolide antibiotics, several beta blockers, and the anticorrosive agents benzotriazole and 5-methylbenzotriazole showed eliminations between 20 and 80 %. As expected, carbamazepine and a few triazine derivatives almost completely persisted during activated sludge treatment. During a weekly sampling campaign in June 2007 prior to implementation of the ozonation process, the biological sand filter further eliminated a few compounds: diclofenac 20 %, atenolol 15 %, sotalol 15 %, naproxen 30 %, carbendazim 15 %, and trimethoprim 15 % (data not shown).

A medium level ozone dose of 0.62 ± 0.05 g O_3 g^{-1} DOC was studied most intensively in five campaigns and the relative concentration profiles throughout the treatment process are depicted for selected compounds in Figure 2.1. For the compounds with relatively high concentrations in the secondary effluent, ozonation contributes 40-50 % (naproxen, benzotriazole, atenolol, clarithromycin), 60-70 % (metoprolol, 5-methylbenzotriazole, sulfamethoxazole), > 80 % (diclofenac, carbamazepine, trimethoprim) to the elimination of the whole treatment process (relative to the influent concentration). In contrast, mefenamic acid is nearly fully degraded during biological treatment, so that ozonation only accounts for 6 % of the total elimination. The concentrations of the iodinated X-ray contrast media in the primary and secondary effluent showed high fluctuations even in composite samples of two days most probably due to varying input loads. However, if these compounds were present in the secondary effluent, only a minor part was oxidized during ozonation. Overall, only compounds with second order rate constants

< 10^4 M^{-1} s^{-1} such as benzotriazole, betablockers, the biocide mecoprop, and the X-ray contrast medium iopromide were still found after ozonation. Compounds with rate constants > 10^4 M^{-1} s^{-1} such as carbamazepine, diclofenac, macrolide antibiotics, and sulfonamide antibiotics with activated aromatic systems, amine moieties, or double bonds were oxidized to concentrations below the LOQ. In contrast to Nakada et al. *(11)*, we observed complete oxidation of carbamazepine which is in agreement with the rate constant reported in the literature and other studies *(10,26,27)*.

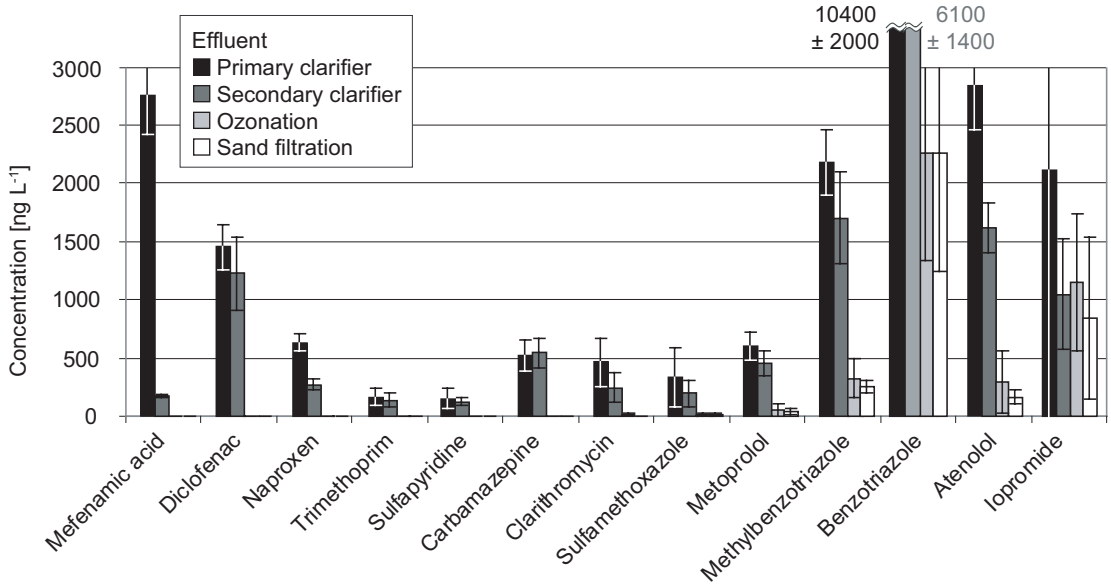

Figure 2.1. Average concentrations with standard deviations of selected micropollutants along the treatment process at WWTP Wüeri for an ozone dose of 0.62 ± 0.05 g O_3 g^{-1} DOC (n = 5, Table 2.1)

For two out of three campaigns in May 2008 (0.60 and 0.62 g O_3 g^{-1} DOC), approximately 170 further polar compounds (Table S2.2) with diverse functional groups were analyzed, among them additional pharmaceuticals, pesticides, biocides, food additives, corrosion inhibitors and personal care products including known transformation products. Besides the 14 compounds shown in Figure 2.2, 42 further compounds were detected in the secondary effluents during those two campaigns with concentrations > 15 ng L^{-1} (Table 2.2). Most of them such as the pharmaceutical metabolites 4-acetamidoantipyrine and the antidepressant venlafaxine (both amines) were efficiently eliminated during ozonation. Similar to Nakada et al. *(11)* we observed

for the group of analgesics that the napthylderivate naproxen was better removed than the benzophenone derivate ketoprofen and compounds with an amide function such as *N,N*-diethyl-3-methylbenzamide and 2,6-dichlorobenzamide. This is due to the lack of electron-donating substituents of the latter compounds. The antiepileptic drug levetiracetame with two amide functions showed relatively high persistence against oxidation. This can be expected due to the low reactivity of amide functional groups *(28)*. The chlorinated disaccharide sucralose, an artificial sweetener, was detected at several μg L^{-1} in the secondary effluent and, as expected, the electron-withdrawing chloro-substituent led to low ozonation elimination of about 30 % *(12)*. This compound only reacts with the secondarily formed hydroxyl radicals.

Screening for known ozonation transformation products of diclofenac, carbamazepine, and sulfamethoxazole as well as possible oxidation products of benzotriazole and atenolol was conducted by HPLC coupled with high resolution mass spectrometry (Text S2.3). No transformation products of those compounds could clearly be identified. This was expected based on their often low stability and only partial formation with minor rates *(13,15,17)*. A study run in parallel showed that the specific and unspecific toxicity of wastewater effluent (tested by a battery of toxicity tests including different toxicological end points such as baseline toxicity, algae inhibition, and endocrine disruption) was reduced significantly by ozonation, indicating that not only compounds are oxidized but also no toxic by-products are formed in higher concentrations *(29)*.

Altogether, for an ozone dose of about 0.6 O_3 g^{-1} DOC, 11 (atenolol, diatrizoate, iopromide, mecoprop, benzotriazole, 5-methylbenzotriazole, sucralose, DEET, diazinon, galaxolidone and benzothiazole) of approximately 220 measured compounds were found in at least one campaign above 100 ng L^{-1} after ozonation. No additional elimination in the subsequent sand filtration could be observed for these few remaining compounds. A comparison of the micropollutant concentrations under dry weather conditions in the creek before (June 2007) and after implementation of the ozonation step (May 2008) illustrates the improvement of the water quality (Figure S2.2).

Table 2.2. Detected compounds (> 15 ng L^{-1}) in the secondary effluent except those shown in Figure 2.1 and their average elimination during ozonation (± standard deviation) at about 0.6 g O_3 g^{-1} DOC

Compound	Compound group	0.62 g O_3 g^{-1} DOC (May 19-21, 2008)		0.60 g O_3 g^{-1} DOC (May 24-26, 2008)		Elimination (%)
		Secondary clarifier (ng L^{-1})	Ozonation (ng L^{-1})	Secondary clarifier (ng L^{-1})	Ozonation (ng L^{-1})	
4-acetamidoantipyrine	analgesic TP	1500	25	1180	2	99 ± 1
aminopyrine = 4-dimethylaminoantipyrine	analgesic	4200	< 1	150	< 1	> 99
antipyrene = phenazone	analgesic	346	< 13	34	< 13	> 90
atenolic acid	beta blocking agents TP	1000	85	1200	84	93 ± 1
azithromycin	macrolide antibacterial	55	< 1	150	< 0.1	> 99
bezafibrate	lipid modifying agent	55	< 14	67	< 14	> 89
clindamycin	lincosamide antibacterial	18	< 3	64	< 3	> 95
clofibric acid	lipid modifying agent	44	15	n.d.	n.d.	66
O-desvenlafaxin	psychoanaleptic TP	86	5	110	4	96 ± 1
erythromycin + erythromycin-H_2O	macrolide antibacterial	19	< 20	49	< 20	> 64
fluconazole	antifungal	58	< 10	n.d.	n.d.	> 91
hydrochlorothiazide	diuretic	140	< 100	200	< 100	n.c.
iohexole	X-ray contrast medium	31	44	n.m.	n.m.	n.c.
iopamidol	X-ray contrast medium	31	26	n.m.	n.m.	16
ketoprofen	antiinflammatory, antirheumatic product	98	43	160	28	69 ± 14
levetiracetame	antiepileptic	170	76	110	97	33 ± 22
lidocaine	anesthetic	19	1	38	1	98 ± 1
primidone	antiepileptic	29	10	58	27	59 ± 7
propranolol	beta blocking agent	n.d.	n.d.	67	< 5	> 96
sotalol	beta blocking agent	331	< 16	492	< 16	> 98
trimethoprim	antibacterial	76	< 5	111	< 5	> 98
venlafaxine	psychoanaleptic	150	3	270	3	99 ± 1
2-aminobenzimidazole	benzimidazole fungicide	n.d.	n.d.	28	< 1	> 98
diuron	urea herbicide	n.d.	n.d.	70	18	74
mecoprop	phenoxy herbicide	3488	564	163	40	79 ± 5
2-methylisothiazolin-3-one	isothiazolone biocide	170	< 150	270	< 150	n.c.
terbutryn	triazine herbicide	28	< 6	26	< 6	> 89
atrazine-desethyl	triazine herbicide TP	50	49	36	31	8 ± 6
diazinon	organophosphorus insecticide	59	13	492	160	72 ± 6
2,6-dichlorobenzamide	nitrile herbicide	88	28	32	15	61 ± 8
chloridazone	pyridazinone herbicide	n.d.	n.d.	34	4	88
isoproturon	urea herbicide	159	< 3	38	< 3	> 99
linuron	urea herbicide	21	5	110	55	63 ± 12
metalaxyl	pesticide	180	15	n.d.	n.d.	92
metamitrone	triazinone herbicide	67	< 1	n.d.	n.d.	> 99
2-methyl-4-chlorophenoxy-acetic acid (MCPA)	phenoxy herbicide	22	8	n.d.	n.d.	75
terbuthylazine-desethyl-2-hydroxy	triazine herbicide TP	26	47	10	21	n.c.
galaxolidone	personal care product TP	410	240	1200	190	63 ± 22
benzothiazole	industrial product	20000	5900	n.d.	n.d.	70
sucralose	food additive	3000	2200	4700	3000	31 ± 6
N,N-diethyl-3-methylbenzamide (DEET)	insect repellent	360	130	600	240	62 ± 2
2-hydroxy-4-methoxybenzophenone	UV-filter	46	< 10	24	< 5	> 84

[a] n.d., not detected; n.m., not measured; n.c., not calculated because of fluctuating concentrations or values near to the LOQ; TP, transformation product. If the value after ozonation was < LOQ, 0.5 x LOQ was used for calculating the elimination efficiency.

Most campaigns were conducted under dry weather conditions (Table 2.1), apart from the campaign in December 2007 which was carried out at the low ozone dose of 0.36 g O_3 g^{-1} DOC. The 2-fold increased flow rate compared to the campaign in January 2008, carried out at the same low ozone dose, resulted in significantly lower influent concentrations for most compounds due to the dilution with rain water (Table S2.5). Despite a hydraulic retention time (HRT) in the reactor of only about 4 min under these conditions, the elimination efficiency by the secondary treatment and by ozonation was not clearly different for these two campaigns.

2.3.2 Effect of ozone dose on the elimination of selected micropollutants

In Figure 2.2, the effect of the ozone dose on selected compounds with different functional moieties is depicted. All compounds with tertiary amino groups or aniline moieties such as diclofenac, the macrolide and sulfonamide antibiotics, as well as compounds with activated aromatic systems and double bonds such as trimethoprim and carbamazepine, were eliminated significantly with even a relatively low ozone dose of 0.36 g O_3 g^{-1} DOC (approx. 2.1 mg L^{-1} O_3). The high efficiency at such low ozone doses can be attributed to the high second-order rate constants for the reaction of those compounds with ozone (> 10^4 M^{-1} s^{-1}), the low average DOC effluent concentration of 5.2 mg L^{-1}, the nearly complete absence of competitors for ozone consumption such as nitrite (~ 0.05 mg L^{-1}), and the circumneutral pH which leads to a relatively high ozone stability. During ozonation 100 - 500 µg L^{-1} assimilable organic carbon was produced and eliminated by about 10-50 % in the following obviously biologically active sand filter *(25)*. Correspondingly, the DOC was not reduced by the ozonation but by 0.7 ± 0.4 mg L^{-1} during sand filtration. Compounds with rate constants < 10^4 M^{-1} s^{-1} were increasingly oxidized with increasing ozone doses. Atrazine and iopromide with rate constants < 10^2 $M^{-1}s^{-1}$, which are also relatively slowly attacked by hydroxyl radicals (k_{OH}. < 5 x 10^9 $M^{-1}s^{-1}$) *(26,28)* showed the lowest oxidative transformation. Only for a few triazine derivatives and X-ray contrast media was the relative elimination < 95 % at the highest ozone dose of 1.16 g O_3 g^{-1} DOC (atrazine 49 % elimination, iopromide

62 % elimination). This resulted in effluent concentrations < 100 ng L^{-1} for all contaminants except two X-ray contrast media, namely iopromide and ioxitalamic acid.

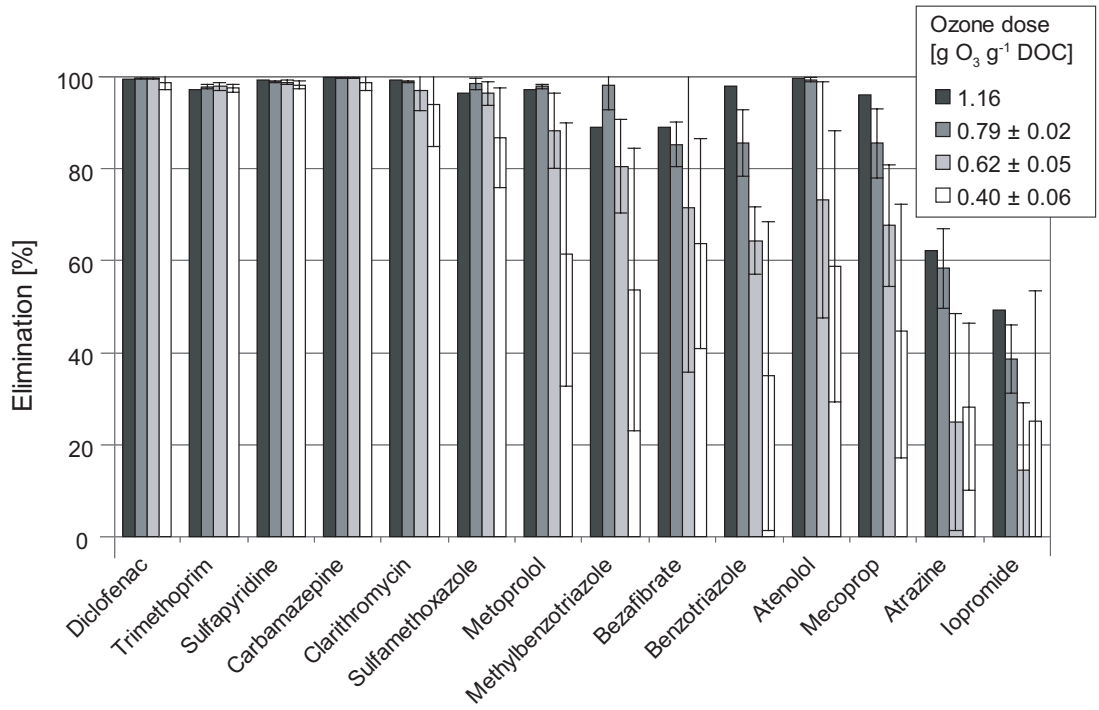

Figure 2.2. Effect of the ozone dose on the relative elimination of selected micropollutants in the ozone reactor. Results of campaigns with similar ozone doses (Table 2.1) were averaged (± standard deviation).

2.3.3 Formation of oxidation by-products during ozonation

Bromate formation during ozonation of bromide-containing waters occurs through a complicated mechanism involving ozone and hydroxyl radicals *(18)*. Since the bromide levels in the secondary effluent were relatively low (16 - 31 μg L^{-1}), bromate concentrations in the final effluent (7.5 μg L^{-1}) were below the drinking water standard of 10 μg L^{-1} even for a very high ozone dose of 1.16 g O_3 g^{-1} DOC *(25)*. Compared with a proposed ecotoxicologically relevant concentration of 3 mg L^{-1} *(30)*, these levels are not problematic. The fate of eight nitrosamines was also studied during the treatment process. The concentrations of the nitrosamines, which were found above the LOQ of about 1 ng L^{-1} are shown in Figure 2.3. The concentrations are generally in the low ng L^{-1} range with NDMA being the predominant compound. This is in accordance with our recent study on the fate of nitrosamines in 20 WWTPs in Switzerland *(31)*. *N*-nitrosodi-n-butylamine, *N*-nitrosodiethylamine, and *N*-nitrosopiperidine were efficiently removed during secondary treatment and were not produced during ozonation. *N*-nitrosomorpholine was relatively persistent against biological degradation (40 ± 29 % removal) as well as ozonation (13 ± 11 % removal). Even with the highest ozone dose of 1.16 g O_3 g^{-1} DOC, the elimination was only 36 %. NDMA was biologically removed by 66 ± 35 %, but significantly formed in concentrations of up to 14 ng L^{-1} during ozonation (*t*-test, p =0.05, one campaign with peak concentration as outlier excluded from averaging). This resulted in concentrations after ozonation of up to 21 ng L^{-1}. However, the formation of NDMA did not correlate with the ozone dose. Thus, the secondary clarifier effluent composition with likely changing concentrations of different NDMA precursors and varying NDMA formation rates affected the formation rate more than the ozone dose. The low reactivity of NDMA with ozone (0.052 ± 0.0016 M^{-1} s^{-1}) and hydroxyl radicals (4.5 x 10^8 ± 0.21 x 10^8 M^{-1} s^{-1}) *(32)* leads to an only insignificant removal under typical ozonation conditions of the secondary effluent. Only at the highest ozone dose, the elevated hydroxyl radical exposure (Table 2.1) could result in about 25 % NDMA removal. During passage through the biological sand filter, 50 ± 17 % of NDMA was removed. This is consistent with observations in other plants and probably caused by biodegradation *(31)*. The resulting concentrations in the sand filtration effluent were < 10 ng L^{-1} which is the action level of NDMA in drinking water

in California. Therefore, biological sand filtration is a useful additional barrier for elimination of biodegradable compounds formed during ozonation such as NDMA while also improving suspended solids and phosphate removal.

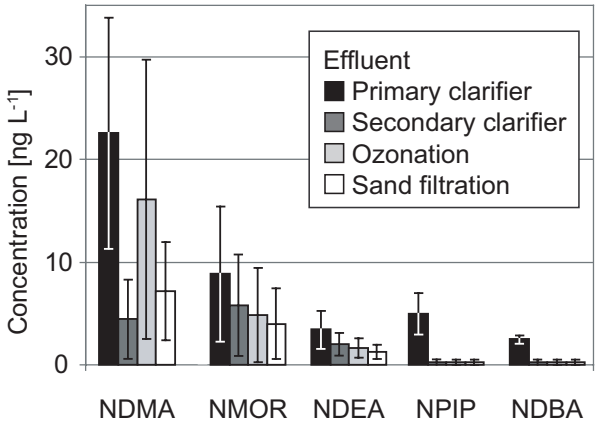

Figure 2.3. Median concentrations with 25th and 75th percentile for *N*-nitroso-dimethylamine (NDMA), *N*-nitrosomorpholine (NMOR), *N*-nitrosodiethylamine (NDEA), *N*-nitrosopiperidine (NPIP) and *N*-nitrosodi-n-butylamine (NDBA) along the treatment process at WWTP Wüeri for all campaigns listed in Table 2.1

2.3.4 Correlation of measured and predicted relative elimination of micropollutants during ozonation

The relative eliminations for 15 compounds with known rate constants for the reaction with ozone and hydroxyl radicals were predicted according to eq 2.1 and compared to the measured values. Figure 2.4 shows the comparison for selected compounds covering a broad range of reaction rate constants with the two oxidants. The predicted relative elimination is subdivided into the oxidation by ozone and hydroxyl radicals. The percentage of the elimination which can be attributed to hydroxyl radicals is negligible for compounds reacting fast with ozone but its contribution increases for contaminants with low second-order rate constants for the reaction with ozone. Hence, the relevance of hydroxyl radicals increases in the order diclofenac < atenolol < benzotriazole, mecoprop < atrazine < iopromide which is in accordance with decreasing second-order rate constants of their reaction with ozone. For all compounds reacting fast with ozone (carbamazepine, clarithromycin, diclofenac, naproxen, sulfamethoxazole, sulfapyridine),

the measured and predicted elimination were in excellent agreement (data only shown for diclofenac). However, deviations between the measured and predicted degree of oxidation were observed for the more persistent compounds that are oxidized to a certain extent by hydroxyl radicals. Apart from mecoprop, the measured eliminations were lower than the predicted ones. This may have been caused by (i) sorption of some compounds to sludge particles and/or interaction with colloids which may have partially prevented oxidation as suggested in a pilot study *(8)*, as well as (ii) a short circuit from the first into the second compartment of the reactor observed in tracer tests (data not shown). Due to the short-circuit, ~ 15 % of the water circulating into the second compartment did not contact the process gas at this point of the reactor but may subsequently mix with ozone-containing water fractions depending on the remaining dissolved ozone concentration. This nonideal hydraulic behavior leads to lower ozone and hydroxyl radical exposures for the short-circuiting fraction of the treated wastewater and to higher exposures for the remaining fraction, resulting in lower measured eliminations. The predictions deviated most strongly for the highest ozone dose for atrazine (29 %) and iopromide (44 %), both compounds almost solely reacting with hydroxyl radicals. One reason may be the dependence of the hydroxyl radical formation rate and yield on the ozone dose *(33)*. This in turn varies for different wastewater fractions due to the observed short-circuit and may increase the deviations with increasing applied ozone dose. Overall, the results prove that oxidation rates in a full-scale ozonation plant can be adequately predicted for fast reacting compounds and can be predicted within acceptable error margins for compounds reacting slowly with ozone.

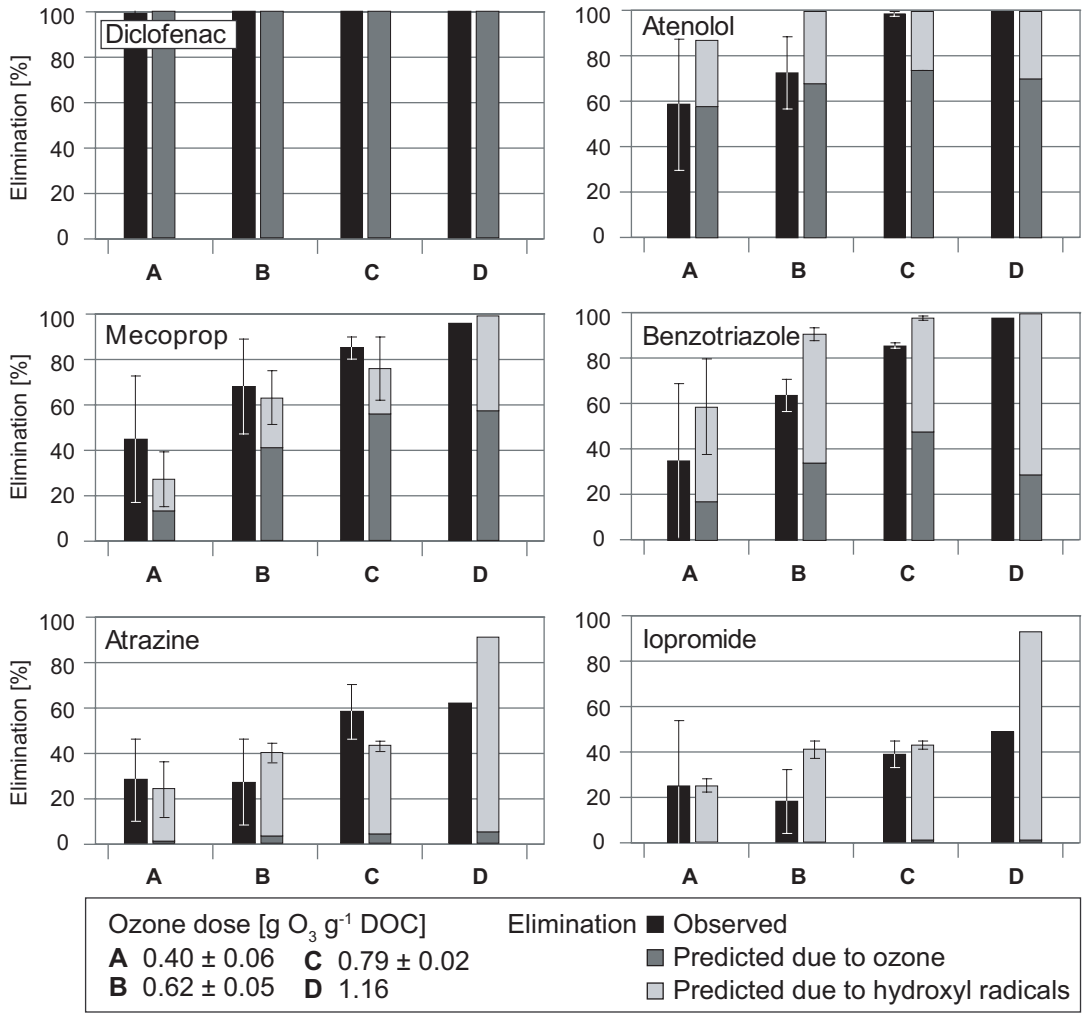

Figure 2.4. Comparison of the observed and predicted relative elimination for the oxidation of selected micropollutants with ozone and hydroxyl radicals at four different ozone doses. Observed and predicted results of campaigns with similar ozone doses (Table 2.1) were averaged (± standard deviation). k_{O_3} and k_{OH}**.** are listed in Table S2.4.

2.3.5 Energy consumption

The full life-cycle of energy costs of the ozonation step was optimized during the study by taking into account energy consumption at the plant (ozone production, ozone sensors, ozone destroyer, etc.) along with the energy-intensive oxygen production and transport. Energy consumption at the plant (12 kWh kg^{-1} O_3) remained constant in the range of 100 - 170 g O_3 m^{-3} process gas (Figure S2.3). For an ozone dose of 0.6 g O_3 g^{-1} DOC

(effluent DOC ~ 5 g m^{-3}), 0.035 kWh m^{-3} wastewater was consumed which is 12 % of the total energy consumption of a typical nutrient removal plant (0.3 kWh m^{-3} wastewater). Additionally, 0.01 - 0.015 kWh m^{-3} is needed for pure oxygen production (Figure S2.3).

2.3.6 Implications for wastewater treatment

This study shows that ozonation is a promising technology to significantly reduce the micropollutant load of full-scale WWTPs. The removal efficiency by ozonation can be predicted with acceptable accuracy by combination of reactor hydraulics, reaction kinetics, and measurement of ozone and hydroxyl radical exposures in laboratory-scale experiments. Additional tests for the formation of the potentially carcinogenic bromate and carcinogenic NDMA have to be made to assess the overall resulting water quality. For NDMA, a significant reduction, while for bromate no reduction can be expected for the recommended post-treatment with biological sand filtration. Therefore, design and operation of new treatment steps for wastewater ozonation can be based on laboratory experiments and allow a direct upscaling to full-scale, without costly and labor intensive piloting. Furthermore, the operational costs can be estimated based on the required ozone doses determined in laboratory experiments.

Acknowledgements

Authors J.H. and S.G.Z. contributed equally to this work. We thank Manuel Dahinden, Falk Dorusch, and Philipp Longrée for technical assistance and BMG Engineering AG (Schlieren, Switzerland) for sampling. Installation and support with maintenance of the ozonation plant by Daniel Rensch and Steve Brocker from Hunziker-Betatech AG as well as characterization of standard wastewater parameters by Markus Koch and Eva Gansner from AWEL Zürich is highly appreciated. The study was financially supported by the Swiss Federal Offices for the Environment (FOEN) within the project MicroPoll and the EU NEPTUNE project (Contract No 036845, SUSTDEV-2005-3.II.3.2). We especially appreciate the support by and discussions with Michael Schärer from FOEN and Beate Escher from Eawag.

2.4 References

(1) Joss, A.; Keller, E.; Alder, A. C.; Göbel, A.; McArdell, C. S.; Ternes, T.; Siegrist, H. Removal of pharmaceuticals and fragrances in biological wastewater treatment. *Water Res.* **2005**, *39*, 3139-3152.

(2) Golet, E. M. X., I.; Siegrist, H.; Alder, A.C.; Giger, W. Environmental exposure assessment of fluoroquinolone antibacterial agents from sewage to soil. *Environ. Sci. Technol.* **2003**, *37*, 3243-3249.

(3) Ternes, T. A.; Joss, A.; Siegrist, H. Scrutinizing pharmaceuticals and personal care products in wastewater treatment. *Environ. Sci. Technol.* **2004**, *38*, 392A - 399A.

(4) Jones, O. A. H.; Green, P. G.; Voulvoulis, N.; Lester, J. N. Questioning the excessive use of advanced treatment to remove organic micropollutants from wastewater. *Environ. Sci. Technol.* **2007**.

(5) Joss, A.; Siegrist, H.; Ternes, T. A. Are we about to upgrade wastewater treatment for removing organic micropollutants? *Wat. Sci. Technol.* **2008**, *57*, 251-255.

(6) Snyder, S. A.; Adham, S.; Redding, A. M.; Cannon, F. S.; DeCarolis, J.; Oppenheimer, J.; Wert, E. C.; Yoon, Y. Role of membranes and activated carbon in the removal of endocrine disruptors and pharmaceuticals. *Desalination* **2007**, *202*, 156-181.

(7) Nowotny, N.; Epp, B.; Von Sonntag, C.; Fahlenkamp, H. Quantification and modeling of the elimination behavior of ecologically problematic wastewater micropollutants by adsorption on powdered and granulated activated carbon. *Environ. Sci. Technol.* **2007**, *41*, 2050-2055.

(8) Huber, M. M.; Göbel, A.; Joss, A.; Hermann, N.; Löffler, D.; McArdell, C. S.; Ried, A.; Siegrist, H.; Ternes, T. A.; von Gunten, U. Oxidation of pharmaceuticals during ozonation of municipal wastewater effluents: A pilot study. *Environ. Sci. Technol.* **2005**, *39*, 4290-4299.

(9) Ternes, T. A.; Stuber, J.; Herrmann, N.; McDowell, D.; Ried, A.; Kampmann, M.; Teiser, B. Ozonation: A tool for removal of pharmaceuticals, contrast media and musk fragrances from wastewater? *Water Res.* **2003**, *37*, 1976-1982.

(10) Wert, E. C., Rosario-Ortiz, F.L. and Snyder, S.A. Effect of ozone exposure on the oxidation of trace organic contaminants in wastewater. *Water Res.* **2009**, *43*, 1005-1014.

(11) Nakada, N.; Shinohara, H.; Murata, A.; Kiri, K.; Managaki, S.; Sato, N.; Takada, H. Removal of selected pharmaceuticals and personal care products (PPCPs) and endocrine-disrupting chemicals (EDCs) during sand filtration and ozonation at a municipal sewage treatment plant. *Water Res.* **2007**, *41*, 4373-4382.

(12) von Gunten, U. Ozonation of drinking water: Part I. Oxidation kinetics and product formation. *Water Res.* **2003**, *37*, 1443-1467.

(13) Huber, M. M.; Ternes, T. A.; von Gunten, U. Removal of estrogenic activity and formation of oxidation products during ozonation of 17-alpha-ethinylestradiol. *Environ. Sci. Technol.* **2004**, *38*, 5177-5186.

(14) Dodd, M. C.; E., K. H.-P.; von Gunten, U. Oxidation of antimicrobial compounds by ozone and hydroxyl radical: elimination of biological activity during aqueous ozonation processes. *Environ. Sci. Technol.* **2009**, *43*, 2498-2504.

(15) Suarez, S.; Dodd, M. C.; Omil, F.; von Gunten, U. Kinetics of triclosan oxidation by aqueous ozone and consequent loss of antibacterial activity: Relevance to municipal wastewater ozonation. *Water Res.* **2007**, *41*, 2481-2490.

(16) Hammes, F.; Salhi, E.; Köster, O.; Kaiser, H. P.; Egli, T.; von Gunten, U. Mechanistic and kinetic evaluation of organic disinfection by-product and assimilable organic carbon (AOC) formation during the ozonation of drinking water. *Water Res.* **2006**, *40*, 2275-2286.

(17) Dewitte, B.; Dewulf, J.; Demeestere, K.; Van De Vyvere, V.; De Wispelaere, P.; Van Langenhove, H. Ozonation of ciprofloxacin in water: HRMS identification of reaction products and pathways. *Environ. Sci. Technol.* **2008**, *42*, 4889-4895.

(18) von Gunten, U. Ozonation of drinking water: Part II. Disinfection and by-product formation in presence of bromide, iodide or chlorine. *Water Res.* **2003**, *37*, 1469-1487.

(19) Schmidt, C. K.; Brauch, H. J. *N,N*-dimethylsulfamide as precursor for *N*-nitrosodimethylamine (NDMA) formation upon ozonation and its fate during drinking water treatment. *Environ. Sci. Technol.* **2008**, *42*, 6340-6346.

(20) Andrzejewski, P.; Kasprzyk-Hordern, B.; Nawrocki, J. *N*-nitrosodimethylamine (NDMA) formation during ozonation of dimethylamine-containing waters. *Water Res.* **2008**, *42*, 863-870.

(21) Oya, M.; Kosaka, K.; Asami, M.; Kunikane, S. Formation of *N*-nitrosodimethylamine (NDMA) by ozonation of dyes and related compounds. *Chemosphere* **2008**, *73*, 1724-1730.

(22) Zhao, Y. Y.; Boyd, J. M.; Woodbeck, M.; Andrews, R. C.; Qin, F.; Hrudey, S. E.; Li, X. F. Formation of N-nitrosamines from eleven disinfection treatments of seven different surface waters. *Environ. Sci. Technol.* **2008**, *42*, 4857-4862.

(23) Ort, C.; Hollender, J.; Schärer, M.; Siegrist, H. Model based evaluation of reduction strategies for micropollutants from wastewater treatment plants in complex river networks. *Environ. Sci. Technol.* **2009**, *43*, 3214-3220.

(24) Hoigné, J. B., H. Characterization of water quality criteria for ozonation processes. Part II: lifetime of added ozone *Ozone Sci. Eng.* **1994**, *16*, 121-134.

(25) Zimmermann, S. G.; Wittenwiler, M.; Hollender, J.; Krauss, M.; Ort, C.; Siegrist, H.; von Gunten, U. Kinetic assessment and modeling of an ozonation stepfor full-scale municipal wastewater treatment: Micropollutant oxidation, by-product formation and disinfection. *Water Res.* **2011**, *45*, 605-617.

(26) Huber, M. M.; Canonica, S.; Park, G. Y.; von Gunten, U. Oxidation of pharmaceuticals during ozonation and advanced oxidation processes. *Environ. Sci. Technol.* **2003**, *37*, 1016-1024.

(27) McDowell, D. C.; Huber, M. M.; Wagner, M.; von Gunten, U.; Ternes, T. A. Ozonation of carbamazepine in drinking water: Identification and kinetic study of major oxidation products. *Environ. Sci. Technol.* **2005**, *39*, 8014-8022.

(28) Acero, J. L.; Stemmler, K.; von Gunten, U. Degradation kinetics of atrazine and its degradation products with ozone and OH radicals: A predictive tool for drinking water treatment. *Environ. Sci. Technol.* **2000**, *34*, 591-597.

(29) Escher, B. I.; Bramaz, N.; Ort, C. Monitoring the treatment efficiency of a full scale ozonation on a sewage treatment plant with a mode-of-action based test battery. *J. Environ. Monitor.* **2009**, *11*, 1836-1846.

(30) Hutchinson, T. H., Hutchings, H.J., Moore, K.W. A review of the effects of bromate on aquatic organisms and toxicity of bromate to oyster (Crassostrea gigas) embryos. *Ecotoxicol. Environ. Saf.* **1997**, *38*, 238-243.

(31) Krauss, M.; Longrée, P.; Dorusch, F.; C., O.; Hollender, J. Occurrence and removal of *N*-nitrosamines in wastewater treatment plants. *Water Res.* **2009**, *43*, 4381-4391.

(32) Lee, C.; Yoon, J.; von Gunten, U. Oxidative degradation of *N*-nitrosodimethylamine by conventional ozonation and the advanced oxidation process ozone/hydrogen peroxide. *Water Res.* **2007**, *41*, 581-590.

(33) Buffle, M. O.; Schumacher, J.; Meylan, S.; Jekel, M.; von Gunten, U. Ozonation and advanced oxidation of wastewater: Effect of O3 dose, pH, DOM and HO.-scavengers on ozone decomposition and HO . generation. *Ozone Sci. Eng.* **2006**, *28*, 247-259.

Supporting Information for Chapter 2

Elimination of organic micropollutants in a municipal wastewater treatment plant upgraded with a full-scale post-ozonation followed by sand filtration

5 tables, 3 figures and 4 texts

http://pubs.acs.org/doi/abs/10.1021/es9014629

*Co-primary authors contributed equally to this work

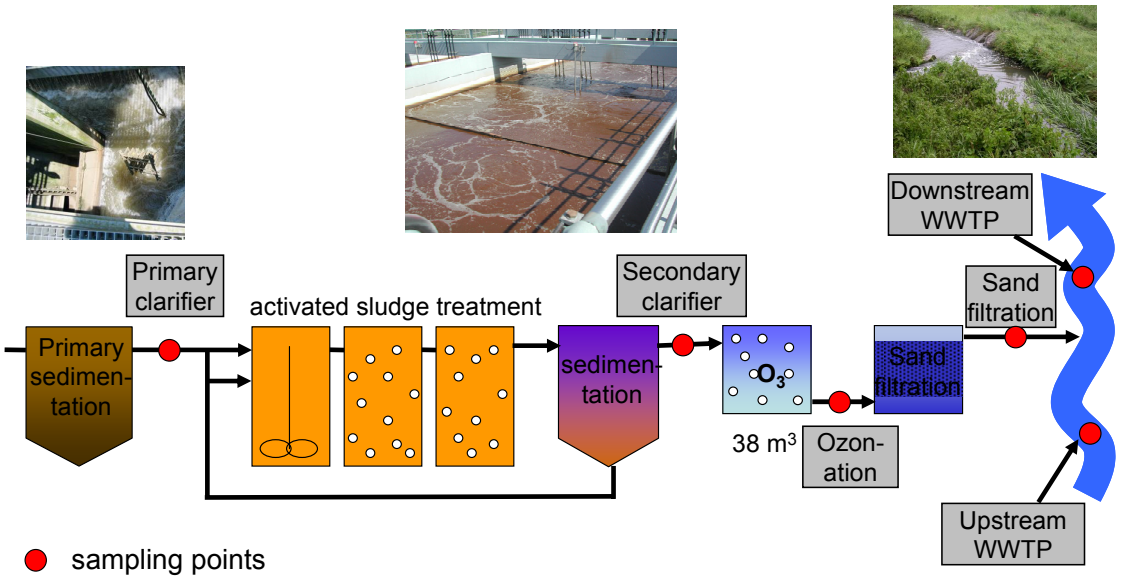

Figure S2.1. Scheme of the WWTP Wüeri in Regensdorf with sampling points

Text S2.1. Description of the WWTP and adjustment of ozone dose

The WWTP Wüeri in Regensdorf, Switzerland treats under dry weather conditions on average 5500 m^3 wastewater per day (~ 25,000 population equivalents) with a flow of 30-40 L s^{-1} at night to 100-120 L s^{-1} during the day. The hydraulic retention time is 16-18 h and the sludge retention time 16-17 d. The plant consists of a grit chamber, a primary clarifier, activated sludge treatment with a denitrifying and nitrifying zone, a secondary clarifier, and sand filtration (Figure S2.1). The sand filter has a thickness of ca. 1 m and a filter velocity of 14.4 m h^{-1}. After sand filtration, the effluent is discharged into the creek Furtbach. Under dry weather conditions the average percentage of wastewater in the creek downstream from the WWTP is approximately 60 %. Between August 2007 and October 2008, the 36 m^3 (4.5 x 2.55 x 3.15 m) flocculation tank was operated as an ozone reactor. Inside the reactor, 5 baffles were installed resulting in a six compartment reactor with a retention time of 8 to 15 min (during day and night, respectively) during dry weather conditions and 3 min during heavy storm conditions. Ozone was generated from oxygen and the oxygen/ozone mixture was injected in counter-current mode through a series of disc diffusers at the bottom of the first

compartment. The inflow to the reactor was measured by an ultrasonic device (Prosonic, Endress & Hauser, Germany), ozone was determined by an amperometric electrode (Aquatector, Mesin AG, Switzerland), and DOC was measured online by UV absorption using a S::can sensor (S::can, Austria), which was regularly calibrated by grab samples filtered to 0.45 μm using a total organic carbon analyzer (Shimadzu, Switzerland).

Ozone dose was automatically adjusted according to the DOC load. In case of stormwater conditions, the ozone dose was attenuated to avoid ozone residual in the effluent of the reactor. Above 120, 150, 180 L s^{-1}, the ozone dose was diminished to the 0.9, 0.8, 0.7 fold ozone dose. For safety reasons, the ozone dose was reduced to the 0.7 and 0.5 fold ozone dose in case ozone concentrations > 0.3 and 0.4 mg L^{-1} were found in the last compartment of the reactor, respectively. Ozone concentrations above 200 μg m^{-3} in the indoor air of the building resulted in a complete shutdown of the ozonation system. The size of the ozonation tank was given by the flocculation tank and was not sufficient under stormwater conditions. It is recommended to have a minimum HRT of 5-10 min, corresponding to about 20 min for dry weather conditions to prevent ozone loss during storm water and to simplify control of ozone dosage.

Text S2.2. Determination of ozone and hydroxyl radical exposures and R_{ct} values

Secondary effluent from the sampling campaigns was filtered to < 0.45 μm and stored at 4 °C. Samples were buffered to the pH of the respective campaign (Table 2.1). The probe compound *p*-chlorobenzoic acid (*p*CBA), which is ozone-resistant, was spiked to determine the transient hydroxyl radical concentrations *(1)*. Experiments were carried out at the temperature of the respective campaign and started by the same ozone dose as in the full-scale campaign. After ozone addition, samples were withdrawn in regular time intervals starting from 10 s until complete ozone consumption. Ozone was quenched with indigo for residual ozone measurements, while *p*CBA was determined by a HPLC-UV-system. Ozone exposures were calculated by integrating the respective decay curves over time *(2)*. The hydroxyl radical exposures were determined from the relative decrease of *p*CBA while the R_{ct} value was derived from the slope of the $\ln(pCBA/pCBA_0)$ vs. ozone exposure plot *(1,2)*.

Text S2.3. Description of the analytical methods for micropollutants

The composite water samples were filtered onsite the WWTP the same day using 1 μm glass fibre filters and cooled to 4 °C. They were analyzed after transfer to the laboratory within a few days or frozen until analysis. All details of the applied analytical methods are summarized in Table S2.3. In the case of HPLC combined with tandem mass spectrometry, identification of compounds was carried out by comparison of two selective mass transitions and the retention time with reference standards. In the case of HPLC coupled with high resolution mass spectrometry, the identification was performed by comparison of the accurate mass (mass error < 5 ppm), the occurrence of stable isotopes (^{37}Cl, ^{13}C, ^{34}S), characteristic MS-MS-fragments and the retention time with reference standards. Internal standards were used for quantification and, if available, isotope labeled compounds were used (Table S2.1). For sucralose (Dr. Ehrenstorfer), sucralose-d6 (Toronto Research Chemicals Inc.) was applied as internal standard. In the case no isotope labeled compound could be purchased, one of another compound with a similar retention time was used as an internal standard. Spiked wastewater samples were routinely analyzed for all matrices to check method performance and the mean recoveries are listed in Table S2.1. Recoveries of 80-100 % were accepted for compounds with isotope-labeled internal standards. For all other compounds, recoveries between 70-130 % were defined as acceptable. Blank samples consisting of nanopure water were analyzed with each batch of samples, and blanks were subtracted from the measured values. Limits of detection (LOD) and limits of quantification (LOQ) were determined by a signal-to-noise ratio of 3 (LOD) and 10 (LOQ) in each sample matrix. LOQs for all analytes are listed in Table S2.1 and S2.2.

For screening of known ozonation transformation products, HPLC coupled with high resolution mass spectrometry after enrichment by the mixed cartridge was used (Table S2.3). We screened (i) for the accurate mass (mass error < 5 ppm), (ii) for the occurrence of stable isotopes (^{37}Cl, ^{13}C, ^{34}S), and (iii) for characteristic MS-MS-fragments. Screening was conducted for the known oxidation products of diclofenac *(3,4)*, carbamazepine *(5)*, sulfamethoxazole *(5)* as well as for possible transformation products of benzotriazol and atenolol because these parent compounds were found in the highest concentrations in the effluent. In case of atenolol we screened for accurate masses of products with oxidized substituents (3-[4-(2-amino-2-oxoethyl)phenoxy]-2-hydroxy-

propanoic acid, $C_{11}H_{13}NO_5$; 2-[4-[2-oxo-3-(propan-2-ylamino)propoxy]phenyl]-acetamide, $C_{14}H_2ON_2O_3$; 3-[4-(carboxy-methyl)phenoxy]-2-hydroxypropanoic acid, $C_{11}H_{12}O_6$). In case of benzotriazol we screened for products with a mono- or dihydroxylated aromatic ring system ($C_6H_5N_3O$; $C_6H_5N_3O_2$).

Table S2.1. Compounds analyzed with CAS, structure, supplier, internal standards, LOQs and recoveries of the analytical method

Substance *internal standard*	CAS-Nr.	Structure	Supplier	Class	Subclass	primary clarifier		secondary clarifier		ozonation		sand filter / Furtbach		Method
						LOQ ng/L	Recovery [n=10] %	LOQ ng/L	Recovery [n=10] %	LOQ ng/L	Recovery [n=10] %	LOQ ng/L	Recovery [n=10] %	
N4-Acetylsulfamethoxazole *Acetylsulfamethoxazole-d4*	21312-10-7		Eawag synthesis (6)	pharmaceutical	antibiotic metabolite	42	99 ±6	28	103 ±7	8	100 ±8	6	96 ±6	online-SPE, LC-MS-MS
Atenolol *Atenolol-d7*	29122-68-7		Sigma-Aldrich *Toronto Research Chemicals Inc.*	pharmaceutical	β-blocker	55	94 ±10	35	94 ±12	10	97 ±13	9	98 ±13	online-SPE, LC-MS-MS
Atrazine *Atrazine-d5*	1912-24-9		Riedel-de-Haën *Dr. Ehrenstorfer*	pesticide	herbicide	31	101 ±9	27	98 ±8	6	97 ±7	6	95 ±10	online-SPE, LC-MS-MS
Atrazine-Desethyl *Atrazine-Desethyl-d6*	6190-65-4		Dr. Ehrenstorfer *Dr. Ehrenstorfer*	pesticide	transformation product	40	97 ±7	30	102 ±10	6	99 ±5	6	100 ±11	online-SPE, LC-MS-MS
Atrazine-Desisopropyl *Atrazin-Desisopropyl-d5*	1007-28-9		Dr. Ehrenstorfer *Dr. Ehrenstorfer*	pesticide	transformation product	127	100 ±10	117	106 ±5	23	102 ±6	23	103 ±6	online-SPE, LC-MS-MS
Atrazine-2-Hydroxy *Atrazine-2-Hydroxy-d5*	2163-68-0		Riedel-de-Haën *Dr. Ehrenstorfer*	pesticide	transformation product	30	100 ±10	30	101 ±7	5	98 ±3	5	96 ±10	online-SPE, LC-MS-MS
Benzotriazole *Benzotriazol-d4*	95-14-7		Sigma-Aldrich *Toronto Research Chemicals Inc.*	anticorrosive		200	100 ±12	165	95 ±12	37	104 ±22	36	99 ±10	online-SPE, LC-MS-MS
Bezafibrate *Bezafibrat-d4*	41859-67-0		Sigma-Aldrich *Toronto Research Chemicals Inc.*	pharmaceutical	lipid regulator	70	100 ±7	65	101 ±8	14	100 ±7	13	100 ±10	online-SPE, LC-MS-MS
Carbamazepine *Carbamazepin-13C,d2*	298-46-4		Sigma-Aldrich *Toronto Research Chemicals Inc.*	pharmaceutical	antiepileptic	20	99 ±5	15	98 ±6	3	100 ±5	3	100 ±6	online-SPE, LC-MS-MS
Carbendazim *Carbendazim-d4*	10605-21-7		Dr. Ehrenstorfer *Dr. Ehrenstorfer*	biocide		118	92 ±10	87	94 ±7	22	93 ±8	22	92 ±10	online-SPE, LC-MS-MS
Clarithromycin *Clarithromycin-d3*	81103-11-9		Abbott Laboratories LTD *Toronto Research Chemicals Inc.*	pharmaceutical	macrolide antibiotic	10	102 ±7	5	100 ±10	3	99 ±6	3	101 ±8	online-SPE, LC-MS-MS
Clindamycin *Erythromycin- ^{13}C3*	18323-44-9		Sigma-Aldrich *Cambridge Isotope Laboratories Inc.*	pharmaceutical	antibiotic	25	113 ±3	5	97 ±9	3	94 ±12	3	97 ±12	online-SPE, LC-MS-MS
Clofibric acid *Clofibric acid-d4*	882-09-7		Sigma-Aldrich *Dr. Ehrenstorfer*	pharmaceutical	lipid regulator	10	99 ±8	5	98 ±9	3	99 ±9	3	102 ±11	online-SPE, LC-MS-MS

Substance *internal standard*	CAS-Nr.	Structure	Supplier	Class	Subclass	primary clarifier		secondary clarifier		ozonation		sand filter / Furtbach		Method
						LOQ ng/L	Recovery [n=10] %	LOQ ng/L	Recovery [n=10] %	LOQ ng/L	Recovery [n=10] %	LOQ ng/L	Recovery [n=10] %	
Diatrizoate *Diatrizoate-d6*	117-96-4	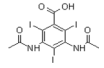	Dr. Ehrenstorfer *Toronto Research Chemicals Inc.*	pharmaceutical	contrast media	25	104 ±5 [n=2]	25	103 ±4 [n=2]	25	128 ±0 [n=2]	25	103 ±5 [n=4]	offline-SPE, LC-MS-MS
Diazinon *Diazinion-d10*	333-41-5	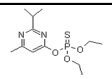	Dr. Ehrenstorfer *Dr. Ehrenstorfer*	pesticide	insecticide	10	107 ±5	10	102 ±7	2	102 ±6	2	103 ±6	online-SPE, LC-MS-MS
Diclofenac *Diclofenac-d4*	15307-86-5	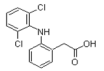	Sigma-Aldrich *Dr. Ehrentorfer*	pharmaceutical	anti inflammatory	50	102 ±7	50	100 ±7	10	98 ±8	10	101 ±7	online-SPE, LC-MS-MS
Diuron *Diuron-d6*	330-54-1		Dr. Ehrenstorfer *Dr. Ehrenstorfer*	biocide	herbicide	105	102 ±6	88	98 ±7	21	102 ±5	21	99 ±6	online-SPE, LC-MS-MS
N,N-dimethylaminosulfanilid (DMSA) *Atrazine-Desethyl-d6*	4710-17-2		Dr. Ehrenstorfer *Dr. Ehrenstorfer*	pesticide	transformation product	500	89 ±19	500	96 ±23	100	86 ±26	100	87 ±26	online-SPE, LC-MS-MS
Dimethyltolylsulfamid *Atrazine-d5*	66840-71-9		Dr. Ehrenstorfer *Dr. Ehrenstorfer*	pesticide	transformation product	500	81 ±17	500	86 ±23	100	81 ±25	100	82 ±27	online-SPE, LC-MS-MS
Erythromycin *Erythromycin-^{13} C3*	114-07-8	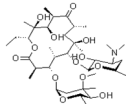	Sigma-Aldrich *Cambridge Isotope Laboratories Inc.*	pharmaceutical	antibiotic	150	105 ±8	75	102 ±9	20	106 ±9	20	102 ±8	online-SPE, LC-MS-MS
Ibuprofen *Ibuprofen-d3*	15687-27-1	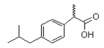	Sigma-Aldrich *Dr. Ehrenstorfer*	pharmaceutical	anti inflammatory	100	107 ±11	80	104 ±8	20	103 ±10	20	105 ±11	online-SPE, LC-MS-MS
Iohexol *Iohexol-d5*	66108-95-0	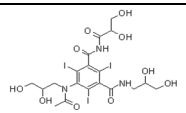	Dr. Ehrenstorfer *Toronto Research Chemicals Inc.*	pharmaceutical	contrast media	50	84 ±14 [n=2]	25	75 ±0 [n=2]	3	60 ±0 [n=2]	25	75 ±6 [n=4]	offline-SPE, LC-MS-MS
Iomeprol *Iomeprol-d3*	78649-41-9	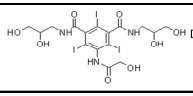	Dr. Ehrenstorfer *Toronto Research Chemicals Inc.*	pharmaceutical	contrast media	50	103 ±1 [n=2]	25	100 ±1 [n=2]	25	105 ±0 [n=2]	25	110 ±6 [n=4]	offline-SPE, LC-MS-MS
Iopamidol *Iopamidol-d3*	62883-00-5	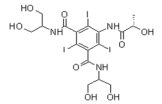	Dr. Ehrenstorfer *Toronto Research Chemicals Inc.*	pharmaceutical	contrast media	50	98 ±5 [n=2]	25	95 ±11 [n=2]	25	122 ±0 [n=2]	25	103 ±10 [n=4]	offline-SPE, LC-MS-MS
Iopromide *Desmethoxy-Iopromide*	73334-07-3	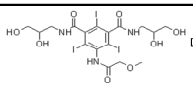	Dr. Ehrenstorfer *Toronto Research Chemicals Inc.*	pharmaceutical	contrast media	50	118 ±39 [n=2]	25	95 ±15 [n=2]	25	170 ±0 [n=2]	25	145 ±40 [n=4]	offline-SPE, LC-MS-MS
Ioxitalamic acid *Ioxitalamic acid-d4*	28179-44-4	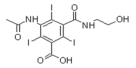	Dr. Ehrenstorfer *Toronto Research Chemicals Inc.*	pharmaceutical	contrast media	50	94 ±11 [n=2]	25	109 ±3 [n=2]	25	109 ±10 [n=2]	25	90 ±10 [n=4]	offline-SPE, LC-MS-MS

Substance *internal standard*	CAS-Nr.	Structure	Supplier	Class	Subclass	primary clarifier		secondary clarifier		ozonation		sand filter / Furtbach		Method
						LOQ ng/L	Recovery [n=10] %	LOQ ng/L	Recovery [n=10] %	LOQ ng/L	Recovery [n=10] %	LOQ ng/L	Recovery [n=10] %	
Irgarol *Irgarol-d9*	28159-98-0	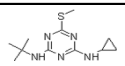	Dr. Ehrenstorfer *Toronto Research Chemicals Inc.*	biocide	herbicide	18	104 ±11	12	106 ±4	3	109 ±4	3	107 ±8	online-SPE, LC-MS-MS
Irgarol-Descyclopropyl *Terbutryn-d5*	30125-65-6	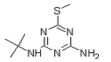	*Dr. Ehrenstorfer*	biocide	transformation product	25	75 ±23	25	65 ±16	5	68 ±17	5	76 ±15	online-SPE, LC-MS-MS
Isoproturon *Isoproturon-d6*	34123-59-6	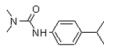	Riedel-de-Haën *Dr. Ehrenstorfer*	biocide	herbicide	20	105 ±13	10	100 ±6	3	102 ±6	3	99 ±10	online-SPE, LC-MS-MS
Mecoprop *Mecoprop-d6*	93-65-2	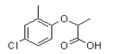	Riedel-de-Haën *Dr. Ehrenstorfer*	pesticide	herbicide	100	103 ±11	100	98 ±5	20	84 ±17	20	85 ±26	online-SPE, LC-MS-MS
Mefenamic acid *Mefenamic acid-d3*	61-68-7	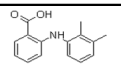	Sigma-Aldrich *Toronto Research Chemicals Inc.*	pharmaceutical	anti inflammatory	15	101 ±10	15	106 ±12	6	105 ±7	6	104 ±10	online-SPE, LC-MS-MS
5-Methylbenzotriazole *Benzotriazol-d4*	29385-43-1		Sigma-Aldrich *Toronto Research Chemicals Inc.*	anticorrosive		70	89 ±16	55	91 ±13	12	90 ±15	12	96 ±16	online-SPE, LC-MS-MS
Metoprolol *Metoprolol-d7*	37350-58-6	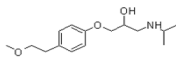	CDN Isotopes *Toronto Research Chemicals Inc.*	pharmaceutical	β-blocker	120	102 ±6	85	100 ±6	19	102 ±6	17	101 ±6	online-SPE, LC-MS-MS
Naproxen *Naproxen-13C,d3*	22204-53-1	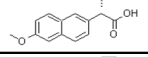	Sigma-Aldrich *Cambridge Isotope Laboratories Inc.*	pharmaceutical	anti inflammatory	200	99 ±7	175	99 ±6	10	99 ±7	10	99 ±8	online-SPE, LC-MS-MS
N-Nitrosodi-n-butylamine *N-Nitrosodi-n-propylamin-d14*	924-16-3	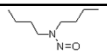	Sigma-Aldrich *Cambridge Isotope Laboratories Inc.*	nitrosamine		4	75 [n=1]	3	98 ±6 [n=4]	3	89 ±20 [n=2]	3	102 ±12 [n=3]	LC-LTQ-Orbitrap-MS
N-Nitrosodiethylamine *N-Nitrosopyrrolidine-d8*	55-18-5		Sigma-Aldrich *Dr. Ehrenstorfer*	nitrosamine		4	78 ±12 [n=2]	1	90 ±18 [n=4]	1	115 ±36 [n=2]	1	84 ±9 [n=3]	LC-LTQ-Orbitrap-MS
N-Nitrosodimethylamine *N-Nitrosodimethylamine-d6*	62-75-9		Sigma-Aldrich *Cambridge Isotope Laboratories Inc.*	nitrosamine		2	127 ±6 [n=2]	2	113 ±8 [n=4]	2	107 ±22 [n=2]	2	118 ±5 [n=3]	LC-LTQ-Orbitrap-MS
N-Nitrosodi-n-propylamine *N-Nitrosodi-n-propylamine-d14*	621-64-7		Sigma-Aldrich *Cambridge Isotope Laboratories Inc.*	nitrosamine		1	84 ±5 [n=2]	1	103 ±6 [n=4]	1	100 ±7 [n=2]	1	103 ±9 [n=3]	LC-LTQ-Orbitrap-MS
N-Nitrosomethylethylamine *N-Nitrosomorpholine-d8*	10595-95-6	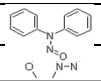	Sigma-Aldrich *Dr. Ehrenstorfer*	nitrosamine		n.d.	58 ±30 [n=2]	2	95 ±3 [n=4]	2	102 ±2 [n=2]	2	98 ±3 [n=3]	LC-LTQ-Orbitrap-MS
N-Nitrosomorpholine *N-Nitrosomorpholine-d8*	59-89-2		Sigma-Aldrich *Dr. Ehrenstorfer*	nitrosamine		2	95 ±24 [n=2]	1	109 ±7 [n=2]	1	109 ±4 [n=2]	1	113 ±6 [n=3]	LC-LTQ-Orbitrap-MS
N-Nitrosopiperidine *N-Nitrosopyrrolidine-d8*	100-75-4		Sigma-Aldrich *Dr. Ehrenstorfer*	nitrosamine		2	87 ±2 [n=2]	2	103 ±2 [n=4]	2	106 ±4 [n=2]	2	100 ±1 [n=3]	LC-LTQ-Orbitrap-MS
N-Nitrosopyrrolidine *N-Nitrosopyrrolidine-d8*	930-55-2		Sigma-Aldrich *Dr. Ehrenstorfer*	nitrosamine		n.d.	w/o primary effluent	3	104 ±3 [n=4]	3	91 ±24 [n=2]	3	103 ±4 [n=3]	LC-LTQ-Orbitrap-MS
Paracetamol *Paracetamol-d4*	103-90-2	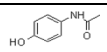	Sigma-Aldrich *Dr. Ehrenstorfer*	pharmaceutical	analgetic	855	100 ±12	590	100 ±7	118	98 ±6	106	99 ±9	online-SPE, LC-MS-MS

Substance *internal standard*	CAS-Nr.	Structure	Supplier	Class	Subclass	primary clarifier		secondary clarifier		ozonation		sand filter / Furtbach		Method
						LOQ ng/L	Recovery [n=10] %	LOQ ng/L	Recovery [n=10] %	LOQ ng/L	Recovery [n=10] %	LOQ ng/L	Recovery [n=10] %	
Phenazone *Phenazon-d3*	60-80-0		Dr. Ehrenstorfer *Toronto Research Chemicals Inc.*	pharmaceutical	analgetic	85	92 ±8	55	97 ±8	13	100 ±8	12	100 ±10	online-SPE, LC-MS-MS
Primidone *Primidon-d5*	125-33-7		Sigma-Aldrich *Toronto Research Chemicals Inc.*	pharmaceutical	antiepileptic	20	102 ±8	20	104 ±8	10	106 ±5	10	103 ±6	online-SPE, LC-MS-MS
Propranolol *Propranolol-d7*	525-66-6	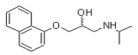	Sigma-Aldrich *Dr. Ehrenstorfer*	pharmaceutical	β-blocker	45	94 ±10	10	107 ±5	5	107 ±6	5	106 ±7	online-SPE, LC-MS-MS
Roxithromycin *Clarithromycin-d3*	80214-83-1	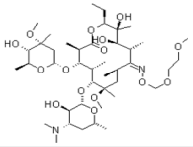	Sigma-Aldrich *Toronto Research Chemicals Inc.*	pharmaceutical	antibiotic	15	88 ±16	3	104 ±13	3	110 ±16	3	106 ±10	online-SPE, LC-MS-MS
Sotalol *Sotalol-d6*	3930-20-9	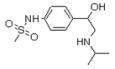	Sigma-Aldrich *Dr. Ehrenstorfer*	pharmaceutical	β-blocker	125	97 ±15	45	96 ±9	16	93 ±6	13	97 ±6	online-SPE, LC-MS-MS
Sulcotrione *Sulcotrione-d3*	99105-77-8	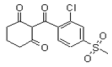	AstraZeneca *Solvias AG Basel*	pesticide	herbicide	98	98 ±9	77	99 ±4	28	99 ±9	25	106 ±12	online-SPE, LC-MS-MS
Sulfadiazine *Sulfadiazin-d4*	68-35-9	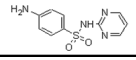	Sigma-Aldrich *Toronto Research Chemicals Inc.*	pharmaceutical	sulfonamide antibiotic	175	102 ±12	100	99 ±9	35	101 ±6	35	102 ±6	online-SPE, LC-MS-MS
Sulfadimethoxine *Sulfadimethoxine-d4*	122-11-2	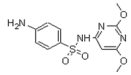	Sigma-Aldrich *Toronto Research Chemicals Inc.*	pharmaceutical	sulfonamide antibiotic	95	99 ±6	60	99 ±5	13	99 ±8	12	98 ±6	online-SPE, LC-MS-MS
Sulfamethazine *Sulfamethazine-^{13}C6*	57-68-1	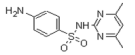	Sigma-Aldrich *Cambridge Isotope Laboratories Inc.*	pharmaceutical	sulfonamide antibiotic	7	99 ±6	5	99 ±8	5	100 ±7	5	100 ±9	online-SPE, LC-MS-MS
Sulfamethoxazole *Sulfamethoxazole-d4*	723-46-6	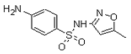	Sigma-Aldrich *Toronto Research Chemicals Inc.*	pharmaceutical	sulfonamide antibiotic	40	101 ±7	25	104 ±9	7	104 ±10	6	103 ±9	online-SPE, LC-MS-MS
Sulfapyridine *Sulfadimethoxine-d4*	144-83-2	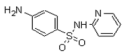	Riedel-de-Haën *Toronto Research Chemicals Inc.*	pharmaceutical	sulfonamide antibiotic	25	92 ±19	15	105 ±22	3	102 ±20	3	107 ±23	online-SPE, LC-MS-MS
Terbutryn *Terbutryn-d5*	886-50-0		Dr. Ehrenstorfer *Dr. Ehrenstorfer*	biozide	herbicide	30	104 ±10	25	99 ±5	6	103 ±2	5	99 ±3	online-SPE, LC-MS-MS
Terbuthylazine *Terbuthylazin-d5*	5915-41-3	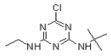	Dr. Ehrenstorfer *Dr. Ehrenstorfer*	pesticide	herbicide	38	102 ±11	28	99 ±5	6	102 ±5	6	99 ±6	online-SPE, LC-MS-MS
Trimethoprim *Trimethoprim-d9*	738-70-5	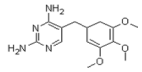	Sigma-Aldrich *Toronto Research Chemicals Inc.*	pharmaceutical	analgetic	45	93 ±11	30	88 ±11	5	93 ±13	5	96 ±14	online-SPE, LC-MS-MS

Table S2.2. Compounds of the targeted screening of the secondary effluent and ozonation effluent by SPE followed by LTQ-Orbitrap high resolution mass spectrometry

Compound group	Compound	CAS	Transformation product of	Chemical formula	Ionization	LOQ (ng/L)
Pharmaceutical	2',2'-Difluoro-2'-deoxyuridine	114248-23-6	Gemcitabine	C9H10F2N2O5	ESI+	100
Pesticide	2,4-D	94-75-7		C8H6Cl2O3	ESI-	10
Pesticide	2,6-Dichlorbenzamide	2008-58-4	Dichlobenil	C7H5Cl2NO	ESI+	1
Industry chemical	2,7-Naphthalenedisulfonic acid	92-41-1		C10H8O6S2	ESI-	390
Biocide	2-Aminobenzimidazole	934-32-7	Carbendazim	C7H7N3	ESI+	1
Pesticide	2-Methyl-4-amino-6-methoxy-s-triazine	1668-54-8	Thifensulfuron-methyl /Metsulfuron-methyl	C5H8N4O	ESI+	78
Biocide	2-Methylisothiazolin-3-one (MI)	2682-20-4		C4H5N1O1S1	ESI+	150
Industry chemical	2-Naphthalenesulfonic acid	120-18-3		C10H8O3S	ESI-	5
Biocide	2-n-Octyl-4-isothiazolin-3-one (OI)	26530-20-1		C11H19NOS	ESI+	15
Pesticide	3-Phenoxybenzoic acid	3739-38-6	Permethrin	C13H10O3	ESI-	620
Biocide	4,5-Dichloro-2-n-octyl-3(2H)-isothiazolo	64359-81-5		C11H17Cl2NOS	ESI+	800
Pharmaceutical	4-Acetamidoantipyrine	83-15-8	Metamizol	C13H15N3O2	ESI+	0.1
Pharmaceutical	4-Aminoantipyrine	83-07-8	Aminopyrine	C11H13N3O1	ESI+	n.d
Industry chemical	4-Amino-N-acetyl-N-methylaniline	119-63-1		C9H12N2O	ESI+	68
Pesticide	4-Chloro-2-methylphenol	1570-64-5	Mecoprop	C7H7ClO	ESI-	1
Pharmaceutical	4-Formylaminoantipyrine	1672-58-8	Aminopyrine	C12H13N3O2	ESI+	50
Biocide	5-Chloro-2-methyl-4-isothiazolin-3-one (	26172-55-4		C4H4ClNOS	ESI+	66
Corrosion inhibitor	5-Methyl-1H-benzotriazole	136-85-6		C7H7N3	ESI+	50
Pesticide	Acetochlor	34256-82-1		C14H20ClNO2	ESI+	22
Pesticide	Acetochlor ESA	187022-11-3	Acetochlor	C14H21NO5S	ESI-	15
Pesticide	Acetochlor OXA	194992-44-4	Acetochlor	C14H19NO4	ESI-	15
Pesticide	Alachlor	15972-60-8		C14H20ClNO2	ESI+	22
Pesticide	Alachlor ESA	142363-53-9	Alachlor	C14H21NO5S	ESI-	15
Pesticide	Alachlor OXA	171262-17-2	Alachlor	C14H19NO4	ESI-	20
Pesticide	Aldicarb	116-06-3		C7H14O2N2S1	ESI+	360
Pharmaceutical	Aminopyrine	58-15-1		C13H17N3O	ESI+	10
Pharmaceutical	Antipyrene (Phenazone)	60-80-0		C11H12N2O	ESI+	0.1
Pesticide	Asulam	3337-71-1		C8H10N2O4S1	ESI+	30
Pharmaceutical	Atenolol	29122-68-7		C14H22N2O3	ESI+	1
Pharmaceutical	Atenolol acid (Metoprolol acid)	56392-14-4	Atenolol/Metoprolol	C14H21N1O4	ESI+	0.1
Pharmaceutical	Atenolol-desisopropyl	81346-71-6	Atenolol	C11H16N2O3	ESI+	100
Pesticide	Atraton	1610-17-9		C9H17N5O	ESI+	1.7
Pesticide	Atrazine	1912-24-9		C8H14Cl1N5	ESI+	1
Pesticide	Atrazine-2-hydroxy	2163-68-0	Atrazine	C8H15N5O	ESI+	1
Pesticide	Atrazine-6-deisopropyl	1007-28-9	Atrazine	C5H8ClN5	ESI+	83
Pesticide	Atrazine-desethyl	6190-65-4	Atrazine	C6H10ClN5	ESI+	56
Pesticide	Atrazine-desethyl-2-hydroxy	19988-24-0	Prometon/Atrazin	C6H11N5O	ESI+	0.1
Pharmaceutical	Azithromycin	83905-01-5		C38H72N2O12	ESI+	0.1
Pesticide	Azoxystrobin	131860-33-8		C22H17N3O5	ESI+	12
Pesticide	Bentazon	25057-89-0		C10H12N2O3S	ESI-	2.5
Biocide	Benzisothiazolone (BIT)	2634-33-5		C7H5NOS	ESI+	470
Pesticide	Benzoic acid, 2-(aminosulfonyl)-, methy	57683-71-3	Metsulfuron-methyl / Tril	C8H9NO4S	ESI+	500
Pesticide	Benzoic acid, 3,5-dibromo-4-hydroxy-	3337-62-0	Bromoxynil	C7H4Br2O3	ESI-	630
Personal care product	Benzophenone-3	131-57-7		C14H12O3	ESI+	10
Industry chemical	Benzothiazole	95-16-9		C7H5NS	ESI+	300
Corrosion inhibitor	Benzotriazole	95-14-7		C6H5N3	ESI+	1
Pharmaceutical	Bezafibrate	41859-67-0		C19H20ClNO4	ESI+	5
Pesticide	Bifenox	53774-07-5	Bifenox	C13H7Cl2NO5	ESI-	200
Pesticide	Bromazil	314-40-9		C9H13BrN2O2	ESI+	210
Pesticide	Bromoxynil	1689-84-5		C7H3Br2N1O1	ESI-	1.5
Food additive	Caffeine	58-08-2		C8H10N4O2	ESI+	33
Pharmaceutical	Carbamazepine	298-46-4		C15H12N2O	ESI+	0.1
Pharmaceutical	Carbamazepine epoxide	36507-30-9	Carbamazepine	C15H12N2O2	ESI+	20
Biocide	Carbendazim	10605-21-7		C9H9N3O2	ESI+	48
Pesticide	Carbetamide	16118-49-3		C12H16N2O3	ESI-	1
Pesticide	Chloridazon	1698-60-8		C10H8Cl1N3O1	ESI+	1
Pesticide	Chloridazone-desphenyl	6339-19-1	Chloridazon	C4H4ClN3O	ESI+	200
Pesticide	Chloridazone-methyl-desphenyl	17254-80-7	Chloridazon	C5H6ClN3O	ESI+	n.d
Pesticide	Chlortoluron	15545-48-9		C10H13ClN2O	ESI+	19
Pharmaceutical	Cilastatin	82009-34-5		C16H26N2O5S	ESI+	100
Pharmaceutical	Clarithromycin	81103-11-9		C38H69NO13	ESI+	0.1
Pharmaceutical	Clindamycin	18323-44-9		C18H33ClN2O5S1	ESI+	13
Pharmaceutical	Clofibric acid	882-09-7	Clofibrate	C10H11ClO3	ESI-	1
Pesticide	Clomazone	81777-89-1		C12H14ClNO2	ESI+	22
Pharmaceutical	Clotrimazole	23593-75-1		C22H17ClN2	ESI+	n.d
Pharmaceutical	Cyclophosphamide	50-18-0		C7H15Cl2N2O2P	ESI+	10
Pesticide	Cymoxanil	57966-95-7		C7H10N4O3	ESI+	100
Pesticide	Cyproconazole	94361-06-5		C15H18ClN3O	ESI+	140

Compound group	Compound	CAS	Transformation product of	Chemical formula	Ionization	LOQ (ng/L)
Pesticide	Cyprodinil	121552-61-2		C14H15N3	ESI+	1
Pharmaceutical	D617	34245-14-2	Verapamil	C17H26N2O2	ESI+	10
Pesticide	Desmedipham	13684-56-5		C16H16N2O4	ESI+	64
Pharmaceutical	Desvenlafaxine	93413-62-8	Venlafaxin	C16H25N1O2	ESI+	10
Pharmaceutical	Dexamethasone	50-02-2		C22H29FO5	ESI+	10
Pharmaceutical	Diazepam	439-14-5		C16H13ClN2O	ESI+	10
Pesticide	Diazinon	333-41-5		C12H21N2O3P1S1	ESI+	1
Pesticide	Dichlorprop	120-36-5		C9H8O3Cl2	ESI-	140
Pharmaceutical	Diclofenac	15307-86-5		C14H11Cl2N1O2	ESI+	1
Pesticide	Diethyltoluamide (DEET)	134-62-3		C12H17NO	ESI+	0.1
Industry chemical	Diglyme	111-96-6		C6H14O3	ESI+	n.d
Pesticide	Dimethachlor	50563-36-5		C13H18ClNO2	ESI+	2
Pesticide	Dimethachlor ESA		Dimethachlor	C13H19NO5S	ESI-	n.d
Pesticide	Dimethachlor OXA	1086384-49-7	Dimethachlor	C13H17NO4	ESI-	n.d
Pesticide	Dimethenamid	87674-68-8		C12H18ClNO2S	ESI+	0.1
Pesticide	Dimethenamid ESA	205939-58-8	Dimethenamid	C12H19N1O5S2	ESI-	11
Pesticide	Dimethenamid OXA	380412-59-9	Dimethenamid	C12H17N1O4S1	ESI-	11
Pesticide	Dinoseb	88-85-7		C10H12N2O5	ESI-	29
Biocide	Diuron	330-54-1		C9H10Cl2N2O1	ESI+	1
Pesticide	Diuron-desdimethyl	2327-02-8	Diuron	C7H6Cl2N2O	ESI+	330
Pesticide	Diuron-monomethyl (DCPMU)	3567-62-2	Diuron	C8H8Cl2N2O	ESI+	120
Pesticide	Epoxiconazole	133855-98-8		C17H13ClFN3O	ESI+	390
Pharmaceutical	Erythromycin	114-07-8		C37H67NO13	ESI+	21
Pesticide	Ethofumesate	26225-79-6		C13H18O5S1	ESI+	180
Pesticide	Ethylenethiourea (ETU)	96-45-7	Mancozeb	C3H6N2S	ESI+	n.d
Pharmaceutical	Exemestane	107868-30-4		C20H24O2	ESI+	1
Pharmaceutical	Fenofibric acid	42017-89-0	Fenofibrate	C17H15ClO4	ESI-	5
Pesticide	Fenpropimorph	67306-03-0		C20H33NO	ESI+	13
Pesticide	Fluazifop	69335-91-7		C15H12F3NO4	ESI-	100
Pharmaceutical	Fluconazole	86386-73-4		C13H12F2N6O	ESI+	10
Pesticide	Fludioxonil	131341-86-1		C12H6F2N2O2	ESI-	110
Pesticide	Flufenacet	142459-58-3		C14H13F4N3O2S	ESI+	n.d
Pesticide	Flufenacet ESA	201668-32-8	Flufenacet	C11H14F1NO4S1	ESI-	13
Pesticide	Flufenacet OXA	201668-31-7	Flufenacet	C11H12F1N1O3	ESI-	23
Pharmaceutical	Fluoxetine	54910-89-3		C17H18F3NO	ESI+	28
Pesticide	Fluroxypyr	69377-81-7		C7H5Cl2FN2O3	ESI-	830
Pesticide	Formamide, N-(2,4-dimethylphenyl)-	60397-77-5	Amitraz	C9H11NO	ESI+	3
Pharmaceutical	Gabapentin	60142-96-3		C9H17NO2	ESI+	100
Personal care product	Galaxolidon	256393-37-0	Galaxolid	C18H24O2	ESI+	0.1
Pharmaceutical	Gemcitabine	95058-81-4		C9H11F2N3O4	ESI+	100
Pharmaceutical	Gentamicins	1403-66-3		C21H43N5O7	ESI+	200
Pesticide	Hexazinone	51235-04-2		C12H20N4O2	ESI+	17
Pharmaceutical	Hydrochlorothiazide	58-93-5		C7H8ClN3O4S2	ESI-	n.d
Pharmaceutical	Ibuprofen	15687-27-1		C13H18O2	ESI+	5
Pharmaceutical	Indomethacin	53-86-1		C19H16ClNO4	ESI+	10
Biocide	Iodopropynyl butylcarbamate (IPBC)	55406-53-6		C8H12I1N1O2	ESI+	220
Pharmaceutical	Iomeprol	78649-41-9		C17H22I3N3O8	ESI+	900
Pharmaceutical	Iopamidol	62883-00-5		C17H22I3N3O8	ESI+	900
Pharmaceutical	Iopromide	73334-07-3		C18H24I3N3O8	ESI+	15
Pharmaceutical	Ioxitalamic acid	28179-44-4		C12H11I3N2O5	ESI+	n.d
Pesticide	Ioxynil	1689-83-4		C7H3I2NO	ESI-	0.1
Biocide	Irgarol 1051	28159-98-0		C11H19N5S1	ESI+	20
Biocide	Irgarol-descyclopropyl	30125-65-6	Irgarol	C8H15N5S	ESI+	18
Pesticide	Isoproturon	34123-59-6		C12H18N2O1	ESI+	0.1
Pesticide	Isoproturon-desmethyl	56046-17-4	Isoproturon	C10H14N2O	ESI+	1
Pesticide	Isoproturon-N-monodemethyl	34123-57-4	Isoproturon	C11H16N2O	ESI+	1
Pharmaceutical	Ketoprofen	22071-15-4		C16H14O3	ESI+	5
Pesticide	Kresoxim-methyl	143390-89-0		C18H19NO4	ESI+	110
Pharmaceutical	Levetiracetam	102767-28-2		C8H14N2O2	ESI+	10
Pharmaceutical	Lidocaine	137-58-6		C14H22N2O	ESI+	10
Pesticide	Linuron	330-55-2		C9H10Cl2N2O2	ESI+	1
Pesticide	MCPA	94-74-6		C9H9ClO3	ESI-	1
Pesticide	Mecoprop	93-65-2		C10H11ClO3	ESI-	5
Pharmaceutical	Mefenamic acid	61-68-7		C15H15N1O2	ESI+	5
Pesticide	Mesotrione	104206-82-8		C14H13NO7S	ESI+	750
Pesticide	Mesotrione MNBA	110964-79-9	Mesotrion	C8H7NO6S	ESI-	550
Pesticide	Metamitron	41394-05-2		C10H10N4O1	ESI+	62
Pesticide	Metamitron-desamino	36993-94-9	Metamitron	C10H9N3O1	ESI+	5
Pesticide	Metazachlor	67129-08-2		C14H16ClN3O	ESI+	0.1
Pesticide	Metazachlor ESA	172960-62-2	Metazachlor	C14H17N3O4S	ESI-	n.d
Pesticide	Metazachlor OXA		Metazachlor	C14H15N3O3	ESI-	n.d
Pharmaceutical	Metformin	657-24-9		C4H11N5	ESI+	20
Pharmaceutical	Methylprednisolone	83-43-2		C22H30O5	ESI+	20
Pesticide	Metolachlor	51218-45-2		C15H22ClNO2	ESI+	3.3
Pesticide	Metolachlor ESA	171118-09-5	Metolachlor	C15H23N1O5S1	ESI-	20
Pesticide	Metolachlor OXA	152019-73-3	Metolachlor	C15H21N1O4	ESI-	9.7
Pesticide	Metolachlor-Morpholinon	120375-14-6	Metolachlor	C14H19N1O2	ESI+	10
Pharmaceutical	Metoprolol	37350-58-6		C15H25NO3	ESI+	1

Compound group	Compound	CAS	Transformation product of	Chemical formula	Ionization	LOQ (ng/L)
Pesticide	Metribuzin	21087-64-9		C8H14N4O1S1	ESI+	28
Pharmaceutical	Metronidazole	443-48-1		C6H9N3O3	ESI+	5
Pesticide	Metsulfuron-methyl	74223-64-6		C14H15N5O6S	ESI+	390
Pesticide	Monuron	150-68-5		C9H11ClN2O	ESI+	21
Pesticide	N'-(2,4-Dimethylphenyl)-N-methylforma	33089-74-6	Amitraz	C10H14N2	ESI+	20
Pharmaceutical	N,N-Didesmethylvenlafaxine	93413-77-5	Venlafaxin	C15H23N1O2	ESI+	100
Pesticide	N,N-Dimethyl-N'-phenylsulphamide (DM	4710-17-2	Dichlofluanid	C8H12N2O2S	ESI+	8.8
Pesticide	N,N-Dimethyl-N'-p-tolylsulphamide	66840-71-9	Tolyfluanid	C9H14N2O2S	ESI+	8
Pharmaceutical	N,O-Didesmethylvenlafaxine	135308-74-6	Venlafaxin	C15H23N1O2	ESI+	20
Pharmaceutical	N4-Acetylsulfadiazine	127-74-2	Sulfadiazin	C12H12N4O3S	ESI+	320
Pharmaceutical	N4-Acetylsulfadimethoxine	24341-30-8	Sulfadimethoxin	C14H16N4O5S	ESI+	48
Pharmaceutical	N4-Acetylsulfamethazine	100-90-3	Sulfamethazin	C14H16N4O3S	ESI+	110
Pharmaceutical	N4-Acetylsulfamethoxazole	21312-10-7	Sulfamethoxazole	C12H13N3O4S	ESI+	29
Pharmaceutical	N4-Acetylsulfathiazole	127-76-4	Sulfathiazol	C11H11N3O3S2	ESI+	360
Pesticide	Napropamide	15299-99-7		C17H21NO2	ESI+	11
Pharmaceutical	Naproxen	22204-53-1		C14H14O3	ESI+	5
Pharmaceutical	N-Desmethylvenlafaxine	149289-30-5	Venlafaxin	C16H25N1O2	ESI+	20
Pesticide	Nicosulfuron	111991-09-4		C15H18N6O6S	ESI+	200
Industry chemical	N-Methylacetanilide	579-10-2		C9H11NO	ESI+	n.d
Personal care product	Octocrylene	6197-30-4		C24H27NO2	ESI+	n.d
Pesticide	Orbencarb	34622-58-7		C12H16ClNOS	ESI+	1
Pharmaceutical	Oseltamivir	196618-13-0		C16H28N2O4	ESI+	7.7
Pharmaceutical	Oseltamivir carboxylate	187227-45-8	Oseltamivir	C14H24N2O4	ESI+	35
Pharmaceutical	Paracetamol	103-90-2		C8H9N1O2	ESI+	160
Pesticide	Pethoxamid	106700-29-2		C16H22ClNO2	ESI+	8.4
Pesticide	Phenmedipham	13684-63-4		C16H16N2O4	ESI+	64
Pesticide	Pinoxaden	243973-20-8		C23H32N2O4	ESI+	n.d
Pharmaceutical	Primidone	125-33-7		C12H14N2O2	ESI+	5
Pesticide	Prometon	1610-18-0		C10H19N5O	ESI+	0.5
Pesticide	Prometryn	7287-19-6		C10H19N5S	ESI+	16
Pesticide	Propachlor	1918-16-7		C11H14ClNO	ESI+	10
Pesticide	Propachlor ESA	123732-85-4	Propachlor	C11H15N1O4S1	ESI-	19
Pesticide	Propachlor OXA	70628-36-3	Propachlor	C11H13N1O3	ESI-	33
Pharmaceutical	Propanolol	525-66-6		C16H21NO2	ESI+	0.1
Pesticide	Propazine-2-hydroxy	7371-53-0	Prometon	C9H17N5O	ESI+	0.1
Biocide	Propiconazole	60207-90-1		C15H17Cl2N3O2	ESI+	400
Pesticide	Prosulfocarb	52888-80-9		C14H21NOS	ESI+	150
Pharmaceutical	Ranitidine	66357-35-5		C13H22N4O3S	ESI+	50
Pharmaceutical	Ritalinic acid	19395-41-6	Methylphenidate	C13H17NO2	ESI+	10
Pharmaceutical	Ritonavir	155213-67-5		C37H48N6O5S2	ESI+	100
Pharmaceutical	Roxithromycin	80214-83-1		C41H76N2O15	ESI+	26
Pesticide	Sebuthylazine	7286-69-3		C9H16Cl1N5	ESI+	0.1
Pesticide	Secbumeton	26259-45-0		C10H19N5O1	ESI+	0.5
Pesticide	Simazine	122-34-9		C7H12ClN5	ESI+	1
Pesticide	Simazine-2-hydroxy	2599-11-3	Simazin	C7H13N5O1	ESI+	16
Pesticide	Simeton	673-04-1		C8H15N5O1	ESI+	0.1
Pharmaceutical	Sotalol	3930-20-9		C12H20N2O3S	ESI+	0.1
Food additive	Sucralose	56038-13-2		C12H19Cl3O8	ESI-	50
Pesticide	Sulcotrione CMBA	53250-83-2	Sulcotrione	C8H7Cl1O4S1	ESI-	80
Pharmaceutical	Sulfadiazine	68-35-9		C10H10N4O2S	ESI+	65
Pharmaceutical	Sulfadimethoxine	122-11-2		C12H14N4O4S	ESI+	67
Pharmaceutical	Sulfamethazine	57-68-1		C12H14N4O2S	ESI+	120
Pharmaceutical	Sulfamethoxazole	723-46-6		C10H11N3O3S1	ESI+	1
Pharmaceutical	Sulfapyridine	144-83-2		C11H11N3O2S1	ESI+	1
Pharmaceutical	Sulfathiazole	72-14-0		C9H9N3O2S2	ESI+	120
Industry chemical	Surfynol 104A	126-86-3		C14H26O2	ESI+	n.d
Pesticide	Tebuconazole	107534-96-3		C16H23ClN3O	ESI+	400
Pesticide	Tebutam	35256-85-0		C15H23NO	ESI+	1
Pesticide	Terbumeton	33693-04-8		C10H19N5O	ESI+	0.5
Biocide	Terbutryn	886-50-0		C10H19N5S1	ESI+	16
Pesticide	Terbutylazine	5915-41-3		C9H16ClN5	ESI+	0.1
Pesticide	Terbutylazine-2-hydroxy	66753-07-9	Terbutylazin	C9H17N5O	ESI+	34
Pesticide	Terbutylazine-desethyl	30125-63-4	Terbutylazine	C7H12Cl1N5	ESI+	1
Pesticide	Terbutylazine-desethyl-2-hydroxy	66753-06-8	Terbutylazine	C7H13N5O1	ESI+	0.1
Pesticide	Thifensulfuron-methyl	79277-27-3		C12H13N5O6S2	ESI-	300
Pharmaceutical	Tramadol	27203-92-5		C16H25NO2	ESI+	10
Pharmaceutical	Trimethoprim	738-70-5		C14H18N4O3	ESI+	0.1
Pesticide	Trinexapac-ethyl	95266-40-3		C13H16O5	ESI+	180
Pharmaceutical	Valsartan	137862-53-4		C24H29N5O3	ESI+	20
Pharmaceutical	Venlafaxine	93413-69-5		C17H27NO2	ESI+	0.1
Pharmaceutical	Verapamil	152-11-4		C27H38N2O4	ESI+	2.8

n.d. not determined

Table S2.3. Description of the analytical methods

Method	Substances	Preparation	SPE-Cartridges	Workup	Measurement		
					Instrument	Column	HPLC
LC-LTQ-Orbitrap-MS (7)	Nitrosamines	thawing; filtration; internal standard addition	cartridge 1: Waters - Oasis HLB 200mg; cartridge 2: Mallinckrodt Baker - Bakerbond Carbon 1000mg	conditioning with pentane, acetone, methanol, tap-water; solid phase extraction; washing with HPLC-water; drying (N_2 stream); elution with dichloromethane; evaporation of dichloromethane with rotary evaporator	autosampler: CTC Analytics - HTS PAL; pump: Flux Instruments AG - Rheos 2000 with solvent degasser; mass spectrometer: Thermo Electron - LTQ Orbitrap	Waters - X-BridgeC18, 3 µm,100x2.1mm with pre-column; Phenomenex Synergi 2.5µm polar RP 100A (100x 3mm, 2.5µm)	Eluent A:HPLC water with 0.4% acetic acid: Eluent B: methanol with 0.4% acetic acid; Eluent A: 95% → 5%
online-SPE, LC-MS-MS (8)	biocides, pesticides, pharmaceutics	thawing; filtration; internal standard addition	cartridge 1:Waters - Oasis HLB; cartridge 2: Mix of Phenomenex - Strata XCW, Phenomenex - Strata XAW, Separtis GmbH Isolute - ENV+	online	autosampler: CTC Analytics - HTS PAL; pump: Flux Instruments AG - Rheos 2000 & Co. KG - Gravity with solvent degasser; Flux Instruments AG - Rheos 2200 with solvent degasser; Thermo Finnagan - Surveyor; mass spectrometer: Thermo Electron TSQ Quantum Ultra	Macherey Nagel GmbH Nucleodur C-18, 5µm, 2x50mm	Eluent A: HPLC-Water with 5mM Ammoniumacetat (pH5); Eluent B: methanol with 0.5% ammonia; Eluent A: 90% → 5%
offline-SPE, LC-MS-MS (9)	x-ray contrast medium	thawing; filtration; adjust to pH 2.8; internal standard addition	cartridge 1: Waters - Oasis MCX 3cc 60mg; cartridge 2: Separtis GmbH Isolute - ENV+ 200mg	conditioning with n-heptane, acetone, methanol, tap-water(pH 2.8);SPE; drying of Isolute ENV+ 200mg (N_2 stream); elution (Methanol); evaporation (N_2 stream), fill up with Eluent A	autosampler: Gastorr 152, Agilent 1100 ALS (G1329A) with Agilent 1100 ALSTherm (G1330B); pump: Agilent 1100 BinPump (G1312A); mass spectrometer: Applied Biosystems API 4000	Phenomenex - Polar-RP, 4µm, 150x3mm, 80Å	Eluent A: HPLC-water (89.4%), acetonitril (10%), 0.5% formic acid, 0.1% ammoniumformiat; Eluent B: acetonitril; Eluent A: 95% → 85%
LC-LTQ-Orbitrap-Screening (10)	substances Table S2	thawing; adjust to pH 6.7; filtration; internal standard addition	cartridge 1:Waters - Oasis HLB; cartridge 2: Mix of Phenomenex - Strata XCW, Phenomenex - Strata XAW, Separtis GmbH Isolute - ENV+	conditioning; SPE; drying; elution with methanol / ethylacetate (v:v 50:50) with 2% ammonia and methanol / ethylacetate (v:v 50:50) with 1.7% formic acid; evaporation (N_2 stream); fill up with HPLC-water	autosampler: CTC Analytics - HTS PAL; pump: Flux Instruments AG - Rheos 2000 with solvent degasser; mass spectrometer: Thermo Electron - LTQ Orbitrap	Waters - X-BridgeC18, 3.5µm, 50x2.1mm with pre-column	HPLC-water with 0.1% formic acid; Eluent B: methanol with 0.1% formic acid; Eluent A: 90% → 5%

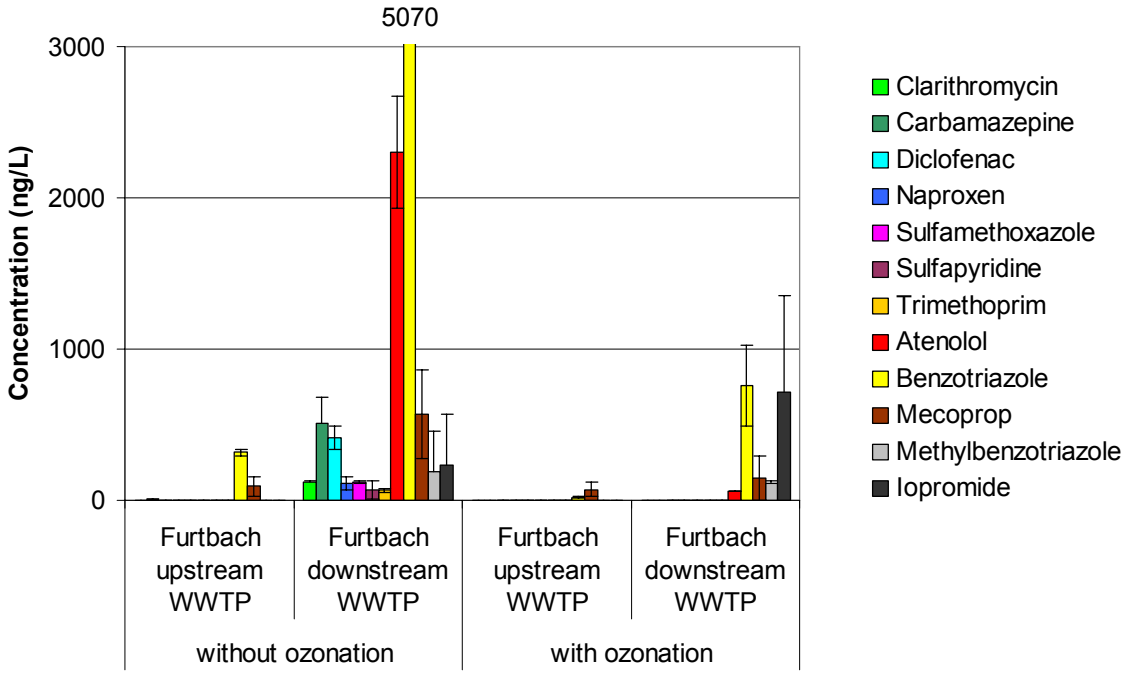

Figure S2.2. Micropollutants concentrations under dry weather conditions in the creek Furtbach upstream and downstream the WWTP before (campaign in June 2007, two 48h-samples) and after (campaign Mai 2008, three 48-72h-samples) implementation of the ozonation step. Sampling of the creek was carried out time-proportionally (40 mL every 12 min).

Text S2.4 Correction of second-order reaction rate constants

The second-order reaction rate constants (Table S2.4) were corrected for pH by taking the acid-base ionization of the respective micropollutant into account and by using the species-specific reaction rate constants with ozone. The correction for temperature was carried out according to the Arrhenius equation. An activation energy of 50 kJ mol^{-1} was used for temperature correction because typical activation energies for the reaction with ozone range from 35 to 50 kJ mol^{-1} *(11)* and the activation energies for ibuprofen and bezafibrate were determined to be 57 and 39 kJ mol^{-1}, respectively *(12)*.

Table S2.4. k_{O_3} and k_{OH}. values of the compounds shown in Figure 2.4

Compound	k_{O_3} in $M^{-1}s^{-1}$	k_{OH}. in $M^{-1}s^{-1}$	References
Diclofenac	6.8×10^5	7.5×10^9	*(3,13)*
Atenolol	1.7×10^3	8.0×10^9	*(14)*
Mecoprop	1.05×10^2	1.9×10^9	*(15)*
Benzotriazole	2.3×10^2	7.6×10^9	*(16,17)*
Atrazine	6.0	3.0×10^9	*(18)*
Iopromide	< 0.8	3.3×10^9	*(12)*

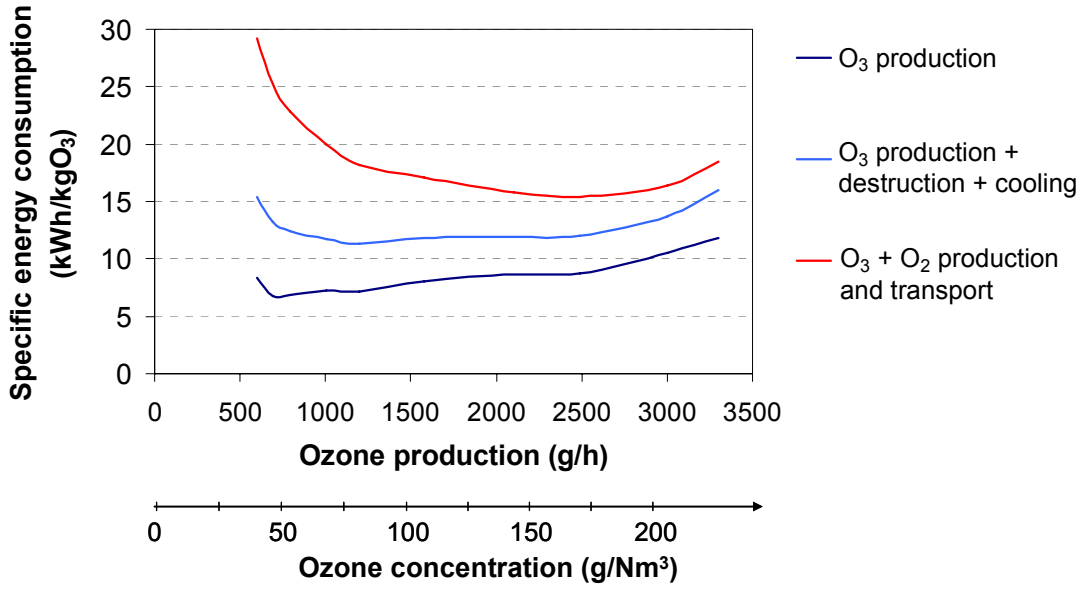

Figure S2.3. Specific energy consumption against ozone production/ozone concentration in the gas mixture at a constant gas flow of 15 $Nm^3 h^{-1}$

Table S2.5. Concentrations of analyzed compounds during the 11 sampling campaigns

Sampling: 24.09, 8:00 - 26.09.2007, 8:00
Ozone dose: 0.47 g O_3/g DOC

Compounds	Primary effluent (ng/L)	Secondary effluent (ng/L)	Ozonation effluent (ng/L)	Sand filtration effluent (ng/L)	Elimination in secondary treatment (%)	Elimination by ozone (%)	Elimination of the whole treatment process (%)
N4-Acetylsulfamethoxazole	667	<LOQ	<LOQ	<LOQ	98	not detected	100
Atenolol	2873	1760	171	129	39	90	96
Atrazine	11	16	9	10	-45	41	5
Atrazine-Desethyl	33	29	25	27	11	16	19
Atrazine-Desisopropyl	<LOQ	<LOQ	<LOQ	<LOQ	not detected	not detected	not detected
Atrazine-Hydroxy	<LOQ	<LOQ	<LOQ	<LOQ	not detected	not detected	not detected
Benzotriazole	12268	5852	1785	2287	52	69	81
Bezafibrate	624	48	9	6	92	82	99
Carbamazepine	660	687	<LOQ	<LOQ	-4	100	100
Carbendazim	78	71	<LOQ	<LOQ	9	85	86
Clarithromycin	242	99	<LOQ	<LOQ	59	98	99
Clindamycin	124	70	<LOQ	<LOQ	44	98	99
Clofibric acid	<LOQ	<LOQ	<LOQ	<LOQ	not detected	not detected	not detected
Diatrizoate	<LOQ	19	13	11	not detected	31	not detected
Diazinion	9	15	1	8	-66	90	12
Diclofenac	1990	1365	<LOQ	<LOQ	31	100	100
Diuron	<LOQ	<LOQ	<LOQ	<LOQ	not detected	not detected	not detected
N,N-Dimethylaminosulfanilid	<LOQ	<LOQ	<LOQ	<LOQ	not detected	not detected	not detected
Dimethyltolylsulfamid	<LOQ	<LOQ	<LOQ	<LOQ	not detected	not detected	not detected
Erythromycin z.T. mit Metabolit	29	17	<LOQ	<LOQ	41	41	66
Ibuprofen	4148	<LOQ	<LOQ	<LOQ	99	not detected	100
Iohexol	2561	75	86	70	97	-15	97
Iomeprol	<LOQ	<LOQ	<LOQ	<LOQ	not detected	not detected	not detected
Iopamidol	48	42	62	60	13	-48	-25
Iopromide	7090	1180	958	875	83	19	88
Ioxitalamic acid	91	33	32	26	63	2	72
Irgarol	<LOQ	<LOQ	<LOQ	<LOQ	not detected	not detected	not detected
Irgarol-Descyclopropyl	<LOQ	<LOQ	<LOQ	<LOQ	not detected	not detected	not detected
Isoproturon	<LOQ	<LOQ	<LOQ	<LOQ	not detected	not detected	not detected
Mecoprop	214	125	30	42	42	76	81
Mefenamic acid	2509	116	<LOQ	<LOQ	95	97	100
Methylbenzotriazole	743	543	63	80	27	88	89
Metoprolol	445	354	21	27	20	94	94
Naproxen	526	223	<LOQ	<LOQ	58	98	99
N-Nitrosodi-n-butylamine	3	<LOQ	<LOQ	<LOQ	48	not detected	48
N-Nitrosodiethylamine	2	8	<LOQ	21	-311	96	-995
N-Nitrosodimethylamine	2	2	10	7	-9	-308	-227
N-Nitrosomorpholine	6	4	3	3	40	14	43
N-Nitrosopiperidine	2	<LOQ	<LOQ	<LOQ	48	not detected	48
N-Nitrosodiphenylamine	<LOQ	<LOQ	<LOQ	<LOQ	not detected	not detected	not detected
N-Nitrosodipropoylamine	<LOQ	<LOQ	<LOQ	<LOQ	not detected	not detected	not detected
N-Nitrisodipyrrolidine	<LOQ	<LOQ	<LOQ	<LOQ	not detected	not detected	not detected
N-Nitrosomethylethylamine	<LOQ	<LOQ	<LOQ	<LOQ	not detected	not detected	not detected
Paracetamol	22100	<LOQ	<LOQ	<LOQ	99	not detected	100
Phenazone	<LOQ	50	5	<LOQ	not detected	90	not detected
Primidone	82	78	35	35	5	55	57
Propanolol	204	131	11	44	36	92	78
Roxithromycin	<LOQ	7	<LOQ	<LOQ	not detected	79	not detected
Sotalol	665	484			27	100	100
Sulcotrione	<LOQ	<LOQ	<LOQ	<LOQ	not detected	not detected	not detected
Sulfadiazine	152	127	50	<LOQ	16	61	88
Sulfadimethoxine	<LOQ	<LOQ	<LOQ	<LOQ	not detected	not detected	not detected
Sulfamethazine	<LOQ	<LOQ	<LOQ	<LOQ	not detected	not detected	not detected
Sulfamethoxazole	447	434	<LOQ	<LOQ	3	99	99
Sulfapyridine	155	148	<LOQ	<LOQ	5	99	99
Terbutryn	36	34	<LOQ	<LOQ	4	91	93
Terbutylazine	<LOQ	<LOQ	<LOQ	<LOQ	not detected	not detected	not detected
Trimethoprim	192	135	<LOQ	<LOQ	30	98	99

Sampling: 6.12., 8:00 - 7.12.2007, 8:00
Ozone dose: 0.36g O_3/g DOC

Compounds	Primary effluent (ng/L)	Secondary effluent (ng/L)	Ozonation effluent (ng/L)	Sand filtration effluent (ng/L)	Elimination in secondary treatment (%)	Elimination by ozone (%)	Elimination of the whole treatment process (%)
N4-Acetylsulfamethoxazole	395.0	<LOQ	<LOQ	<LOQ	96	not detected	99
Atenolol	1539	1153	785	957	25	32	38
Atrazine	19.0	13.0	11.0	11.0	32	15	42
Atrazine-Desethyl	<LOQ	<LOQ	<LOQ	<LOQ	not detected	not detected	not detected
Atrazine-Desisopropyl	<LOQ	<LOQ	<LOQ	<LOQ	not detected	not detected	not detected
Atrazine-Hydroxy	<LOQ	<LOQ	<LOQ	<LOQ	not detected	not detected	not detected
Benzotriazole	3696	3732	2507	3083	-1	33	17
Bezafibrate	202	102	63	79	50	38	61
Carbamazepine	228	186	6	11	18	97	95
Carbendazim	91	43	21	32	53	51	65
Clarithromycin	186	139	23	110	25	83	41
Clindamycin	22	<LOQ	<LOQ	<LOQ	89	not detected	93
Clofibric acid	<LOQ	<LOQ	<LOQ	<LOQ	not detected	not detected	not detected
Diatrizoate	196	189	328	333	4	-74	-70
Diazinion	6	7	4	8	-17	43	-33
Diclofenac	591	501	15	346	15	97	41
Diuron	95	55	41	54	42	25	43
N,N-Dimethylaminosulfanilid	<LOQ	<LOQ	<LOQ	<LOQ	not detected	not detected	not detected
Dimethyltolylsulfamid	<LOQ	<LOQ	<LOQ	<LOQ	not detected	not detected	not detected
Erythromycin z.T. mit Metabolit	65	15	73	19	77	-387	71
Ibuprofen	1697	<LOQ	<LOQ	<LOQ	98	not detected	99
Iohexol	42	<LOQ	49	<LOQ	70	not detected	70
Iomeprol	<LOQ	<LOQ	<LOQ	<LOQ	not detected	not detected	not detected
Iopamidol	55	83	45	39	-51	46	29
Iopromide	437	448	197	244	-3	56	44
Ioxitalamic acid	394	87	153	221	78	-76	44
Irgarol	<LOQ	<LOQ	<LOQ	<LOQ	not detected	not detected	not detected
Irgarol-Descyclopropyl	17	3	3	5	82	0	71
Isoproturon	63	38	12	30	40	68	52
Mecoprop	167	148	112	137	12	24	18
Mefenamic acid	914	118	<LOQ	53	87	97	94
Methylbenzotriazole	534	715	415	564	-34	42	-6
Metoprolol	232	228	134	200	2	41	14
Naproxen	445	194	<LOQ	79	56	97	82
N-Nitrosodi-n-butylamine	2.3	<LOQ	<LOQ	<LOQ	36	not detected	36
N-Nitrosodiethylamine	4.9	8.1	1.7	8.5	-66	79	-74
N-Nitrosodimethylamine	14.1	4.0	8.8	4.8	72	-124	66
N-Nitrosomorpholine	6.7	8.0	8.2	8.0	-20	-2	-20
N-Nitrosopiperidine	4.6	<LOQ	<LOQ	<LOQ	76	not detected	76
N-Nitrosodiphenylamine	<LOQ	<LOQ	<LOQ	<LOQ	not detected	not detected	not detected
N-Nitrosodipropoylamine	<LOQ	<LOQ	<LOQ	<LOQ	not detected	not detected	not detected
N-Nitrisodipyrrolidine	<LOQ	<LOQ	<LOQ	<LOQ	not detected	not detected	not detected
N-Nitrosomethylethylamine	<LOQ	<LOQ	<LOQ	<LOQ	not detected	not detected	not detected
Paracetamol	13926	<LOQ	<LOQ	<LOQ	98	not detected	100
Phenazone	<LOQ	33	<LOQ	<LOQ	not detected	80	not detected
Primidone	67	80	32	40	-19	60	40
Propanolol	60	55	<LOQ	24	9	95	59
Roxithromycin	21	<LOQ	<LOQ	<LOQ	93	not detected	93
Sotalol	212	199	<LOQ	106	6	96	50
Sulcotrione	<LOQ	<LOQ	<LOQ	<LOQ	not detected	not detected	not detected
Sulfadiazine	<LOQ	<LOQ	<LOQ	<LOQ	not detected	not detected	not detected
Sulfadimethoxine	<LOQ	<LOQ	<LOQ	<LOQ	not detected	not detected	not detected
Sulfamethazine	<LOQ	<LOQ	<LOQ	<LOQ	not detected	not detected	not detected
Sulfamethoxazole	122	84	16	45	31	81	63
Sulfapyridine	56	55	<LOQ	18	2	97	68
Terbutryn	87	18	8	12	79	56	86
Terbutylazine	<LOQ	<LOQ	<LOQ	<LOQ	not detected	not detected	not detected
Trimethoprim	124	71	<LOQ	31	43	96	75

Sampling: 08.01.2008, 8:00 - 10.01.2008, 8:00
Ozone dose: 0.36 g O3/g DOC

Compounds	Primary effluent (ng/L)	Secondary effluent (ng/L)	Ozonation effluent (ng/L)	Sand filtration effluent (ng/L)	Elimination in secondary treatment (%)	Elimination by ozone (%)	Elimination of the whole treatment process (%)
N4-Acetylsulfamethoxazole	560	<LOQ	<LOQ	<LOQ	98	not detected	
Atenolol	2313	1211	558	560	48	54	76
Atrazine	<LOQ	<LOQ	10	10	not detected	not detected	not detected
Atrazine-Desethyl	<LOQ	23	25	22	not detected	-6	not detected
Atrazine-Desisopropyl	<LOQ	<LOQ	<LOQ	<LOQ	not detected	not detected	not detected
Atrazine-Hydroxy	<LOQ	<LOQ	8	8	not detected	not detected	not detected
Benzotriazole	8406	4235	4133	2622	50	2	69
Bezafibrate	346	133	39	75	62	71	78
Carbamazepine	330	271	<LOQ	11	18	99	97
Carbendazim	<LOQ	<LOQ	<LOQ	<LOQ	not detected	not detected	not detected
Clarithromycin	650	357	<LOQ	35	45	100	95
Clindamycin	31	21	2	<LOQ	32	93	95
Clofibric acid	<LOQ	<LOQ	<LOQ	<LOQ	not detected	not detected	not detected
Diatrizoate	<LOQ	<LOQ	<LOQ	<LOQ	not detected	not detected	not detected
Diazinion	12	13	9	9	-12	32	23
Diclofenac	1228	856	<LOQ	<LOQ	30	99	100
Diuron	<LOQ	<LOQ	<LOQ	<LOQ	not detected	not detected	not detected
N,N-Dimethylaminosulfanilid	<LOQ	<LOQ	<LOQ	<LOQ	not detected	not detected	not detected
Dimethyltolylsulfamid	<LOQ	<LOQ	<LOQ	<LOQ	not detected	not detected	not detected
Erythromycin z.T. mit Metabolit	<LOQ	<LOQ	<LOQ	<LOQ	not detected	not detected	not detected
Ibuprofen	3186	86	<LOQ	<LOQ	97	88	100
Iohexol	<LOQ	<LOQ	<LOQ	<LOQ	not detected	not detected	not detected
Iomeprol	<LOQ	<LOQ	<LOQ	<LOQ	not detected	not detected	not detected
Iopamidol	65	55	48	68	15	13	-5
Iopromide	4750	1450	1445	1233	69	0	74
Ioxitalamic acid	<LOQ	28	95	85	not detected	-239	not detected
Irgarol	<LOQ	<LOQ	<LOQ	<LOQ	not detected	not detected	not detected
Irgarol-Descyclopropyl	<LOQ	<LOQ	<LOQ	<LOQ	not detected	not detected	not detected
Isoproturon	<LOQ	<LOQ	<LOQ	<LOQ	not detected	not detected	not detected
Mecoprop	143	225	150	126	-57	33	12
Mefenamic acid	1715	196	<LOQ	<LOQ	89	98	100
Methylbenzotriazole	1211	1073	746	462	11	30	62
Metoprolol	445	306	157	138	31	49	69
Naproxen	548	286	<LOQ	<LOQ	48	98	99
N-Nitrosodi-n-butylamine	2.8	0.7	0.9	1.0	74	-27	65
N-Nitrosodiethylamine	8.1	0.8	1.6	1.4	90	-100	83
N-Nitrosodimethylamine	110.2	6.2	18.6	13.2	94	-200	88
N-Nitrosomorpholine	15.0	8.3	8.2	7.5	44	2	50
N-Nitrosopiperidine	12.1	0.2	0.2	0.3	98	-24	98
N-Nitrosodiphenylamine	<LOQ	<LOQ	<LOQ	<LOQ	not detected	not detected	not detected
N-Nitrosodipropoylamine	<LOQ	<LOQ	<LOQ	<LOQ	not detected	not detected	not detected
N-Nitrisodipyrrolidine	<LOQ	<LOQ	<LOQ	<LOQ	not detected	not detected	not detected
N-Nitrosomethylethylamine	<LOQ	<LOQ	<LOQ	<LOQ	not detected	not detected	not detected
Paracetamol	34897	<LOQ	<LOQ	<LOQ	99	not detected	100
Phenazone	<LOQ	<LOQ	<LOQ	<LOQ	not detected	not detected	not detected
Primidone	57	<LOQ	48	27	82	not detected	52
Propanolol	88	92	<LOQ	<LOQ	-4	97	97
Roxithromycin	10	6	<LOQ	<LOQ	38	76	85
Sotalol	302	313	<LOQ	<LOQ	-4	97	98
Sulcotrione	<LOQ	<LOQ	<LOQ	<LOQ	not detected	not detected	not detected
Sulfadiazine	76	<LOQ	<LOQ	<LOQ	34	not detected	77
Sulfadimethoxine	<LOQ	<LOQ	<LOQ	<LOQ	not detected	not detected	not detected
Sulfamethazine	<LOQ	<LOQ	<LOQ	<LOQ	not detected	not detected	not detected
Sulfamethoxazole	124	88	18	11	29	80	91
Sulfapyridine	69	83	<LOQ	<LOQ	-21	98	98
Terbutryn	<LOQ	<LOQ	<LOQ	<LOQ	not detected	not detected	not detected
Terbutylazine	<LOQ	<LOQ	<LOQ	<LOQ	not detected	not detected	not detected
Trimethoprim	103	108	<LOQ	<LOQ	-5	98	98

Sampling: 7.2.2008, 8:00 - 8.2.2008, 8:00
Ozone dose: 0.67 g O_3/g DOC

Compounds	Primary effluent (ng/L)	Secondary effluent (ng/L)	Ozonation effluent (ng/L)	Sand filtration effluent (ng/L)	Elimination in secondary treatment (%)	Elimination by ozone (%)	Elimination of the whole treatment process (%)
N4-Acetylsulfamethoxazole	1073	<LOQ	<LOQ	<LOQ	99	not detected	
Atenolol	3103	1444	299	248	53	79	92
Atrazine	<LOQ	<LOQ	11	11		not detected	not detected
Atrazine-Desethyl	<LOQ	25	30	26		-17	not detected
Atrazine-Desisopropyl	<LOQ	<LOQ	<LOQ	<LOQ		not detected	not detected
Atrazine-Hydroxy	<LOQ	<LOQ	4	3		not detected	not detected
Benzotriazole	10329	7625	3225	3192	26	58	69
Bezafibrate	379	108	21	24	71	81	94
Carbamazepine	337	356	<LOQ	<LOQ	-6	98	100
Carbendazim	<LOQ	<LOQ	<LOQ	<LOQ		not detected	not detected
Clarithromycin	588	356	<LOQ	<LOQ	40	99	100
Clindamycin	43	26	<LOQ	<LOQ	40	90	97
Clofibric acid	<LOQ	12	<LOQ	7		79	not detected
Diatrizoate	123	125	62	0	-2	50	100
Diazinion	<LOQ	9	2	6		74	not detected
Diclofenac	1467	1200	<LOQ	<LOQ		98	100
Diuron	<LOQ	<LOQ	<LOQ	<LOQ		not detected	not detected
N,N-Dimethylaminosulfanilid	<LOQ	<LOQ	<LOQ	<LOQ		not detected	not detected
Dimethyltolylsulfamid	<LOQ	<LOQ	<LOQ	<LOQ		not detected	not detected
Erythromycin z.T. mit Metabolit	<LOQ	<LOQ	<LOQ	<LOQ		not detected	not detected
Ibuprofen	3816	80	<LOQ	<LOQ	98	50	100
Iohexol	<LOQ	<LOQ	<LOQ	96		not detected	not detected
Iomeprol	<LOQ	<LOQ	<LOQ	<LOQ	not detected	not detected	not detected
Iopamidol	<LOQ	34	<LOQ	<LOQ	not detected	63	not detected
Iopromide	689	792	632	636	-15	20	8
Ioxitalamic acid	147	143	48	<LOQ	3	66	91
Irgarol	<LOQ	<LOQ	<LOQ	<LOQ		not detected	not detected
Irgarol-Descyclopropyl	<LOQ	<LOQ	<LOQ	<LOQ		not detected	not detected
Isoproturon	<LOQ	<LOQ	<LOQ	<LOQ		not detected	not detected
Mecoprop	97	123	53	45	-27	57	53
Mefenamic acid	2694	193	<LOQ	<LOQ	93	96	100
Methylbenzotriazole	1844	1459	330	306	21	77	83
Metoprolol	554	448	62	69	19	86	88
Naproxen	506	215	<LOQ	<LOQ	57	59	99
N-Nitrosodi-n-butylamine	0.4	0.7	0.7	0.5	-97	3	-38
N-Nitrosodiethylamine	<LOQ	2.7	2.1	1.3		22	not detected
N-Nitrosodimethylamine	6.4	5.3	13.5	4.8	18	-157	25
N-Nitrosomorpholine	7.6	24.1	19.5	19.6	-217	19	-158
N-Nitrosopiperidine	<LOQ	0.2	<LOQ	<LOQ		-505	not detected
N-Nitrosodiphenylamine	<LOQ	<LOQ	<LOQ	<LOQ	not detected	not detected	not detected
N-Nitrosodipropoylamine	<LOQ	<LOQ	<LOQ	<LOQ	not detected	not detected	not detected
N-Nitrisodipyrrolidine	<LOQ	<LOQ	<LOQ	<LOQ	not detected	not detected	not detected
N-Nitrosomethylethylamine	<LOQ	<LOQ	<LOQ	<LOQ	not detected	not detected	not detected
Paracetamol	46606	<LOQ	<LOQ	<LOQ	99	not detected	100
Phenazone	<LOQ	<LOQ	<LOQ	<LOQ		not detected	not detected
Primidone	78	61	22	30	22	64	61
Propanolol	134	122	<LOQ	<LOQ	9	96	98
Roxithromycin	23	7	<LOQ	<LOQ	67	80	93
Sotalol	410	456	<LOQ	<LOQ	-11	95	98
Sulcotrione	<LOQ	<LOQ	<LOQ	<LOQ		not detected	not detected
Sulfadiazine	53	<LOQ	<LOQ	<LOQ	6	not detected	67
Sulfadimethoxine	<LOQ	<LOQ	<LOQ	<LOQ		not detected	not detected
Sulfamethazine	<LOQ	20	<LOQ	<LOQ		88	not detected
Sulfamethoxazole	490	274	<LOQ	<LOQ	44	95	99
Sulfapyridine	135	128	<LOQ	<LOQ	5	94	99
Terbutryn	<LOQ	<LOQ	<LOQ	<LOQ		not detected	not detected
Terbutylazine	<LOQ	<LOQ	<LOQ	<LOQ		not detected	not detected
Trimethoprim	228	165	<LOQ	<LOQ	28	91	99

Sampling: 12.2.2008, 8:00 - 13.2.2008, 8:00
Ozone dose: 0.55 O_3/g DOC

Compounds	Primary effluent (ng/L)	Secondary effluent (ng/L)	Ozonation effluent (ng/L)	Sand filtration effluent (ng/L)	Elimination in secondary treatment (%)	Elimination by ozone (%)	Elimination of the whole treatment process (%)
N4-Acetylsulfamethoxazole	1249	<LOQ	<LOQ	<LOQ	99	not detected	100
Atenolol	3333	1676	751	209	50	55	94
Atrazine	<LOQ	14	15	16		-10	not detected
Atrazine-Desethyl	34	33	37	38	3	-13	-12
Atrazine-Desisopropyl	<LOQ	<LOQ	<LOQ	<LOQ		not detected	not detected
Atrazine-Hydroxy	<LOQ	<LOQ	<LOQ	<LOQ		not detected	not detected
Benzotriazole	13464	7255	3154	3404	46	57	75
Bezafibrate	599	83	76	15	86	8	98
Carbamazepine	623	498	<LOQ	<LOQ	20	98	100
Carbendazim	96	49	<LOQ	<LOQ	49	11	89
Clarithromycin	740	350	37	<LOQ	53	89	100
Clindamycin	58	45	<LOQ	<LOQ	22	94	97
Clofibric acid	<LOQ	<LOQ	<LOQ	<LOQ		not detected	not detected
Diatrizoate	1080	257	380	348	76	-48	68
Diazinion	<LOQ	9	4	9		52	not detected
Diclofenac	1774	1731	<LOQ	<LOQ	2	99	100
Diuron	<LOQ	<LOQ	<LOQ	<LOQ		not detected	not detected
N,N-Dimethylaminosulfanilid	<LOQ	<LOQ	<LOQ	<LOQ		not detected	not detected
Dimethyltolylsulfamid	<LOQ	<LOQ	<LOQ	<LOQ		not detected	not detected
Erythromycin z.T. mit Metabolit	<LOQ	<LOQ	<LOQ	<LOQ		not detected	not detected
Ibuprofen	4618	56	80	<LOQ	99	-43	100
Iohexol	73	21	87	103	71	-314	-41
Iomeprol	12	47	26	22	-292	45	-83
Iopamidol	59	152	105	99	-158	31	-68
Iopromide	3020	1690	1400	1613	44	17	47
Ioxitalamic acid	2020	104	242	170	95	-133	92
Irgarol	<LOQ	<LOQ	<LOQ	<LOQ		not detected	not detected
Irgarol-Descyclopropyl	<LOQ	<LOQ	<LOQ	<LOQ		not detected	not detected
Isoproturon	280	<LOQ	<LOQ	<LOQ	98	not detected	99
Mecoprop	102	57	28	27	44	52	73
Mefenamic acid	3086	173	<LOQ	<LOQ	94	96	100
Methylbenzotriazole	2298	1654	595	269	28	64	88
Metoprolol	803	583	147	68	27	75	91
Naproxen	629	292	<LOQ	<LOQ	54	70	99
N-Nitrosodi-n-butylamine	<LOQ	0.3	0.4	0.6		-61	not detected
N-Nitrosodiethylamine	3.4	1.1	0.9	0.7	68	22	78
N-Nitrosodimethylamine	22.6	4.5	15.3	7.2	80	-241	68
N-Nitrosomorpholine	29.1	9.0	7.4	6.0	69	17	79
N-Nitrosopiperidine	12.3	0.4	0.7	0.4	97	-66	97
N-Nitrosodiphenylamine	<LOQ	<LOQ	<LOQ	<LOQ	not detected	not detected	not detected
N-Nitrosodipropoylamine	<LOQ	<LOQ	<LOQ	<LOQ	not detected	not detected	not detected
N-Nitrisodipyrrolidine	<LOQ	<LOQ	<LOQ	<LOQ	not detected	not detected	not detected
N-Nitrosomethylethylamine	<LOQ	<LOQ	<LOQ	<LOQ	not detected	not detected	not detected
Paracetamol	54102	<LOQ	<LOQ	<LOQ	99	not detected	100
Phenazone	<LOQ	33	<LOQ	<LOQ		16	not detected
Primidone	70	84	27	21	-19	68	70
Propanolol	246	159	<LOQ	<LOQ	35	97	99
Roxithromycin	42	26	<LOQ	<LOQ	38	94	96
Sotalol	590	555	<LOQ	<LOQ	6	96	99
Sulcotrione	<LOQ	<LOQ	<LOQ	<LOQ		not detected	not detected
Sulfadiazine	60	<LOQ	<LOQ	<LOQ	16	not detected	71
Sulfadimethoxine	<LOQ	<LOQ	<LOQ	<LOQ		not detected	not detected
Sulfamethazine	<LOQ	<LOQ	<LOQ	<LOQ		not detected	not detected
Sulfamethoxazole	709	358	29	28	50	92	96
Sulfapyridine	178	140	<LOQ	<LOQ	21	95	99
Terbutryn	<LOQ	<LOQ	<LOQ	<LOQ		not detected	not detected
Terbutylazine	<LOQ	<LOQ	<LOQ	<LOQ		not detected	not detected
Trimethoprim	241	234	<LOQ	<LOQ	3	94	99

Sampling: 19.5.2008, 8:00 - 21.5.2008, 8:00
Ozone dose: 0.62 O_3/g DOC

Compounds	Primary effluent (ng/L)	Secondary effluent (ng/L)	Ozonation effluent (ng/L)	Sand filtration effluent (ng/L)	Furtbach upstream (ng(L)	Furtbach downstream (ng(L)	Elimination in secondary treatment (%)	Elimination by ozone (%)	Elimination of the whole treatment process (%)
N4-Acetylsulfamethoxazole	304	<LOQ	<LOQ	<LOQ	<LOQ	<LOQ	95	not detected	99
Atenolol	2403	1365	108	132	<LOQ	62	43	92	95
Atrazine	107	131	78	81	21	52	-22	40	24
Atrazine-Desethyl	50	50	49	47	37	52	0	2	6
Atrazine-Desisopropyl	<LOQ	<LOQ	<LOQ	<LOQ	<LOQ	<LOQ		not detected	not detected
Atrazine-Hydroxy	<LOQ	<LOQ	<LOQ	7	15	13		not detected	not detected
Benzotriazole	7856	4347	1121	1030	22	468	45	74	87
Bezafibrate	267	55	<LOQ	<LOQ	<LOQ	<LOQ	79	87	98
Carbamazepine	568	570	<LOQ	<LOQ	<LOQ	1	0	100	100
Carbendazim	<LOQ	<LOQ	<LOQ	<LOQ	<LOQ	<LOQ		not detected	not detected
Clarithromycin	195	67	<LOQ	<LOQ	<LOQ	<LOQ	66	98	99
Clindamycin	40	18	<LOQ	<LOQ	<LOQ	<LOQ	55	92	96
Clofibric acid	37	44	15	20	<LOQ	5	-19	66	46
Diatrizoate	23	<LOQ	<LOQ	<LOQ	<LOQ	<LOQ	46	not detected	46
Diazinion	40	59	13	15	<LOQ	6	-48	78	63
Diclofenac	1372	855	<LOQ	<LOQ	<LOQ	<LOQ	38	99	100
Diuron	<LOQ	<LOQ	<LOQ	<LOQ	<LOQ	<LOQ		not detected	not detected
N,N-Dimethylaminosulfanilid	<LOQ	<LOQ	<LOQ	<LOQ	<LOQ	<LOQ		not detected	not detected
Dimethyltolylsulfamid	<LOQ	<LOQ	<LOQ	<LOQ	<LOQ	<LOQ		not detected	not detected
Erythromycin z.T. mit Metabolit	41	19	<LOQ	<LOQ	<LOQ	<LOQ	54	47	76
Ibuprofen	3674	<LOQ	<LOQ	<LOQ	<LOQ	<LOQ	99	not detected	100
Iohexol	<LOQ	31	44		<LOQ	58	not detected	-42	not detected
Iomeprol	<LOQ	<LOQ	<LOQ		<LOQ	3	not detected	not detected	not detected
Iopamidol	<LOQ	31	26		<LOQ	19	not detected	16	not detected
Iopromide	211	1090	713		<LOQ	511	-417	35	100
Ioxitalamic acid	38	<LOQ	<LOQ		<LOQ	<LOQ	67	not detected	100
Irgarol	28	12	<LOQ	<LOQ	<LOQ	<LOQ	57	88	95
Irgarol-Descyclopropyl	<LOQ	<LOQ	<LOQ	<LOQ	<LOQ	<LOQ		not detected	not detected
Isoproturon	155	159	<LOQ	<LOQ	<LOQ	26	-3	99	99
Mecoprop	695	3488	564	550	119	309	-402	84	21
Mefenamic acid	2240	165	<LOQ	<LOQ	<LOQ	<LOQ	93	98	100
Methylbenzotriazole	2054	1541	168	183	10	89	25	89	91
Metoprolol	500	281	16	20	<LOQ	<LOQ	44	94	96
Naproxen	700	223	5	<LOQ	<LOQ	<LOQ	68	98	99
N-Nitrosodi-n-butylamine	7	<LOQ	<LOQ	<LOQ			78	not detected	78
N-Nitrosodiethylamine	6.6	2.0	0.9	<LOQ			69	54	95
N-Nitrosodimethylamine	989.3	188.1	85.4	32.1			81	55	97
N-Nitrosomorpholine	18.5	5.8	4.8	4.0			69	17	78
N-Nitrosopiperidine	2	<LOQ	<LOQ	<LOQ			42	not detected	42
N-Nitrosodiphenylamine	<LOQ	<LOQ	<LOQ	<LOQ	<LOQ	<LOQ	not detected	not detected	not detected
N-Nitrosodipropoylamine	<LOQ	<LOQ	<LOQ	<LOQ	<LOQ	<LOQ	not detected	not detected	not detected
N-Nitrisodipyrrolidine	<LOQ	<LOQ	<LOQ	<LOQ	<LOQ	<LOQ	not detected	not detected	not detected
N-Nitrosomethylethylamine	<LOQ	<LOQ	<LOQ	<LOQ	<LOQ	<LOQ	not detected	not detected	not detected
Paracetamol	26053	<LOQ	<LOQ	<LOQ	<LOQ	<LOQ	99	not detected	100
Phenazone	nicht auswertbar	346	<LOQ	<LOQ	<LOQ	<LOQ		98	#VALUE!
Primidone	48	29	10	10	<LOQ	4	40	66	79
Propanolol	50	10	<LOQ	<LOQ	<LOQ	<LOQ	80	75	95
Roxithromycin	<LOQ	4	1	0	<LOQ	<LOQ		75	not detected
Sotalol	566	331	<LOQ	<LOQ	<LOQ	<LOQ	42	98	99
Sulcotrione	<LOQ	<LOQ	<LOQ	<LOQ	<LOQ	<LOQ		not detected	not detected
Sulfadiazine	<LOQ	<LOQ	<LOQ	<LOQ	<LOQ	<LOQ		not detected	not detected
Sulfadimethoxine	<LOQ	<LOQ	<LOQ	<LOQ	<LOQ	<LOQ		not detected	not detected
Sulfamethazine	7	<LOQ	<LOQ	<LOQ	<LOQ	<LOQ	64	not detected	64
Sulfamethoxazole	110	107	<LOQ	<LOQ	<LOQ	<LOQ	3	97	97
Sulfapyridine	57	164	<LOQ	<LOQ	<LOQ	<LOQ	-188	99	97
Terbutryn	51	28	<LOQ	<LOQ	<LOQ	<LOQ	45	89	95
Terbutylazine	20	16	7	8	7	6	20	56	60
Trimethoprim	69	76	<LOQ	<LOQ	<LOQ	<LOQ	-10	97	96

Sampling: 21.5.2008, 8:00 - 24.5.2008, 8:00
Ozone dose: 0.65 O_3/g DOC

Compounds	Primary effluent (ng/L)	Secondary effluent (ng/L)	Ozonation effluent (ng/L)	Sand filtration effluent (ng/L)	Furtbach upstream (ng(L)	Furtbach downstream (ng(L)	Elimination in secondary treatment (%)	Elimination by ozone (%)	Elimination of the whole treatment process (%)
N4-Acetylsulfamethoxazole	377	<LOQ	<LOQ	<LOQ	<LOQ	<LOQ	96	not detected	99
Atenolol	2771	1915	179	134	<LOQ	60	31	91	95
Atrazine	29	44	31	32	20	27	-52	30	-10
Atrazine-Desethyl	47	38	42	41	38	39	19	-11	13
Atrazine-Desisopropyl	<LOQ	<LOQ	<LOQ	<LOQ	<LOQ	<LOQ		not detected	not detected
Atrazine-Hydroxy	<LOQ	<LOQ	<LOQ	<LOQ	13	9		not detected	not detected
Benzotriazole	10287	6104	2105	1982	15	995	41	66	81
Bezafibrate	431	81	<LOQ	<LOQ	<LOQ	<LOQ	81	91	98
Carbamazepine	642	706	<LOQ	1	<LOQ	<LOQ	-10	100	100
Carbendazim	<LOQ	<LOQ	<LOQ	<LOQ	<LOQ	<LOQ		not detected	not detected
Clarithromycin	392	162	2	1	<LOQ	<LOQ	59	99	100
Clindamycin	58	31	<LOQ	<LOQ	<LOQ	<LOQ	47	95	97
Clofibric acid	28	24	12	9	<LOQ	4	14	50	68
Diatrizoate	<LOQ	nicht gemessen	<LOQ	<LOQ	<LOQ	<LOQ			not detected
Diazinion	694	197	67	61	<LOQ	23	72	66	91
Diclofenac	1318	1096	<LOQ	<LOQ	<LOQ	<LOQ	17	100	100
Diuron	<LOQ	<LOQ	<LOQ	<LOQ	<LOQ	<LOQ		not detected	not detected
N,N-Dimethylaminosulfanilid	<LOQ	<LOQ	<LOQ	<LOQ	<LOQ	<LOQ		not detected	not detected
Dimethyltolylsulfamid	<LOQ	<LOQ	<LOQ	<LOQ	<LOQ	<LOQ		not detected	not detected
Erythromycin z.T. mit Metabolit	57	32	<LOQ	<LOQ	<LOQ	<LOQ	44	69	82
Ibuprofen	4732	<LOQ	<LOQ	<LOQ	<LOQ	<LOQ	99	not detected	100
Iohexol	<LOQ	nicht gemessen	79		<LOQ	102			not detected
Iomeprol	<LOQ	nicht gemessen	<LOQ		<LOQ	<LOQ			not detected
Iopamidol	84	nicht gemessen	50		<LOQ	74			100
Iopromide	5910	nicht gemessen	1854		<LOQ	1435			100
Ioxitalamic acid	1400	nicht gemessen	41		<LOQ	<LOQ			100
Irgarol	22	18	<LOQ	<LOQ	<LOQ	<LOQ	18	92	93
Irgarol-Descyclopropyl	<LOQ	<LOQ	<LOQ	<LOQ	<LOQ	<LOQ		not detected	not detected
Isoproturon	24	45	<LOQ	<LOQ	18	10	-88	97	94
Mecoprop	153	433	129	127	68	95	-183	70	17
Mefenamic acid	2761	181	<LOQ	<LOQ	<LOQ	<LOQ	93	98	100
Methylbenzotriazole	2096	1481	224	223	<LOQ	105	29	85	89
Metoprolol	615	476	39	25	<LOQ	10	23	92	96
Naproxen	689	309	<LOQ	<LOQ	<LOQ	<LOQ	55	98	99
N-Nitrosodi-n-butylamine	3.4	<LOQ	<LOQ	<LOQ			56	not detected	56
N-Nitrosodiethylamine	16.4	0.7	1.1	1.7			96	-60	89
N-Nitrosodimethylamine	**180.3**	12.9	21.0	10.1			93	-64	94
N-Nitrosomorpholine	21.7	5.1	4.4	3.8			76	14	82
N-Nitrosopiperidine	1	<LOQ	<LOQ	<LOQ			21	not detected	21
N-Nitrosodiphenylamine	<LOQ	<LOQ	<LOQ	<LOQ	<LOQ	<LOQ	not detected	not detected	not detected
N-Nitrosodipropoylamine	<LOQ	<LOQ	<LOQ	<LOQ	<LOQ	<LOQ	not detected	not detected	not detected
N-Nitrisodipyrrolidine	<LOQ	<LOQ	<LOQ	<LOQ	<LOQ	<LOQ	not detected	not detected	not detected
N-Nitrosomethylethylamine	<LOQ	<LOQ	<LOQ	<LOQ	<LOQ	<LOQ	not detected	not detected	not detected
Paracetamol	36337	<LOQ	<LOQ	<LOQ	<LOQ	<LOQ	99	not detected	100
Phenazone	nicht auswertbar	75	<LOQ	<LOQ	<LOQ	<LOQ	#VALUE!	91	#VALUE!
Primidone	88	58	29	26	<LOQ	13	34	50	70
Propanolol	54	85	17	<LOQ	<LOQ	<LOQ	-57	80	95
Roxithromycin	12	<LOQ	<LOQ	<LOQ	<LOQ		88	not detected	88
Sotalol	566	520	<LOQ	<LOQ	<LOQ	<LOQ	8	98	99
Sulcotrione	<LOQ	<LOQ	<LOQ	<LOQ	<LOQ	<LOQ		not detected	not detected
Sulfadiazine	<LOQ	<LOQ	<LOQ	<LOQ	<LOQ	<LOQ		not detected	not detected
Sulfadimethoxine	<LOQ	<LOQ	<LOQ	<LOQ	<LOQ	<LOQ		not detected	not detected
Sulfamethazine	26	7	<LOQ	<LOQ	<LOQ	1	73	64	90
Sulfamethoxazole	139	99	<LOQ	<LOQ	<LOQ	<LOQ	29	96	98
Sulfapyridine	98	70	<LOQ	<LOQ	<LOQ	<LOQ	29	98	98
Terbutryn	41	30	<LOQ	<LOQ	<LOQ	<LOQ	27	90	94
Terbutylazine	<LOQ	<LOQ	4	5	41	16		not detected	not detected
Trimethoprim	139	98	<LOQ	<LOQ	<LOQ	<LOQ	29	97	98

Sampling: 24.5.2008, 8:00 - 26.5.2008, 8:00
Ozone dose: 0.60 O_3/g DOC

Compounds	Primary effluent (ng/L)	Secondary effluent (ng/L)	Ozonation effluent (ng/L)	Sand filtration effluent (ng/L)	Furtbach upstream (ng(L)	Furtbach downstream (ng(L)	Elimination in secondary treatment (%)	Elimination by ozone (%)	Elimination of the whole treatment process (%)
N4-Acetylsulfamethoxazole	552	<LOQ	<LOQ	<LOQ	<LOQ	<LOQ	97	not detected	99
Atenolol	2590	1692	146	108	<LOQ	60	35	91	96
Atrazine	20	28	17	16	20	17	-40	39	20
Atrazine-Desethyl	38	36	31	30	39	34	5	14	21
Atrazine-Desisopropyl	<LOQ	<LOQ	<LOQ	<LOQ	<LOQ	<LOQ		not detected	not detected
Atrazine-Hydroxy	<LOQ	<LOQ	<LOQ	<LOQ	14	8		not detected	not detected
Benzotriazole	9898	5207	1682	1660	24	818	47	68	83
Bezafibrate	389	67	<LOQ	<LOQ	<LOQ	5	83	90	98
Carbamazepine	442	578	<LOQ	<LOQ	<LOQ	<LOQ	-31	100	100
Carbendazim	<LOQ	<LOQ	<LOQ	<LOQ	<LOQ	<LOQ		not detected	not detected
Clarithromycin	398	283	<LOQ	2	<LOQ	1	29	99	99
Clindamycin	84	64	<LOQ	<LOQ	<LOQ	<LOQ	24	98	98
Clofibric acid	<LOQ	<LOQ	6	5	<LOQ	<LOQ		not detected	not detected
Diatrizoate	<LOQ	<LOQ	nicht gemessen	<LOQ	<LOQ	<LOQ		not detected	not detected
Diazinion	306	492	160	147	3	70	-61	67	52
Diclofenac	1326	1236	<LOQ	<LOQ	<LOQ	<LOQ	7	100	100
Diuron	127	70	18	<LOQ	<LOQ	<LOQ	45	74	92
N,N-Dimethylaminosulfanilid	<LOQ	<LOQ	<LOQ	<LOQ	<LOQ	<LOQ		not detected	not detected
Dimethyltolylsulfamid	<LOQ	<LOQ	<LOQ	<LOQ	<LOQ	<LOQ		not detected	not detected
Erythromycin z.T. mit Metabolit	72	49	<LOQ	<LOQ	<LOQ	<LOQ	32	80	86
Ibuprofen	4368	<LOQ	<LOQ	<LOQ	<LOQ	<LOQ	99	not detected	100
Iohexol	<LOQ	<LOQ	<LOQ	<LOQ	<LOQ	4		not detected	not detected
Iomeprol	<LOQ	<LOQ	nicht gemessen	<LOQ	<LOQ	4		not detected	not detected
Iopamidol	<LOQ	<LOQ	nicht gemessen	<LOQ	<LOQ	11	not detected	not detected	not detected
Iopromide	740	610	nicht gemessen	280	<LOQ	200	18	#VALUE!	62
Ioxitalamic acid	1220	1390	nicht gemessen	1185	<LOQ	613	-14	#VALUE!	3
Irgarol	<LOQ	<LOQ	<LOQ	<LOQ	<LOQ	<LOQ	not detected	not detected	not detected
Irgarol-Descyclopropyl	<LOQ	<LOQ	<LOQ	<LOQ	<LOQ	<LOQ		not detected	not detected
Isoproturon	29	38	<LOQ	<LOQ	14	<LOQ	-31	96	95
Mecoprop	110	163	40	28	25	28	-48	75	75
Mefenamic acid	2914	160	<LOQ	<LOQ	<LOQ	<LOQ	95	98	100
Methylbenzotriazole	2592	2386	308	312	<LOQ	131	8	87	88
Metoprolol	539	470	29	30	<LOQ	<LOQ	13	94	94
Naproxen	649	329	<LOQ	<LOQ	<LOQ	<LOQ	49	98	99
N-Nitrosodi-n-butylamine	4	2	2	<LOQ			63	-7	63
N-Nitrosodiethylamine	<LOQ	2.4	2.6	0.9				-8	not detected
N-Nitrosodimethylamine	77.4	4.4	18.7	12.6			94	-328	84
N-Nitrosomorpholine	6.4	5.6	4.8	5.8			13	14	9
N-Nitrosopiperidine	12.6	<LOQ	0.7	1.0			91	not detected	92
N-Nitrosodiphenylamine	<LOQ	<LOQ	<LOQ	<LOQ	<LOQ	<LOQ	not detected	not detected	not detected
N-Nitrosodipropoylamine	<LOQ	<LOQ	<LOQ	<LOQ	<LOQ	<LOQ	not detected	not detected	not detected
N-Nitrisodipyrrolidine	<LOQ	<LOQ	<LOQ	<LOQ	<LOQ	<LOQ	not detected	not detected	not detected
N-Nitrosomethylethylamine	<LOQ	<LOQ	<LOQ	<LOQ	<LOQ	<LOQ	not detected	not detected	not detected
Paracetamol	34246	<LOQ	<LOQ	<LOQ	<LOQ	<LOQ	99	not detected	100
Phenazone	nicht auswertbar	34	<LOQ	<LOQ	<LOQ	<LOQ		81	#VALUE!
Primidone	78	58	27	25	<LOQ	14	26	53	68
Propanolol	59	67	<LOQ	<LOQ	<LOQ	<LOQ	-14	96	96
Roxithromycin	15	5	<LOQ	<LOQ	1	1	67	70	90
Sotalol	700	492	<LOQ	<LOQ	<LOQ	<LOQ	30	98	99
Sulcotrione	<LOQ	<LOQ	<LOQ	<LOQ	<LOQ	<LOQ		not detected	not detected
Sulfadiazine	<LOQ	<LOQ	<LOQ	<LOQ	<LOQ	<LOQ		not detected	not detected
Sulfadimethoxine	<LOQ	<LOQ	<LOQ	<LOQ	<LOQ	<LOQ		not detected	not detected
Sulfamethazine	<LOQ	<LOQ	<LOQ	<LOQ	<LOQ	<LOQ		not detected	not detected
Sulfamethoxazole	242	155	<LOQ	<LOQ	<LOQ	<LOQ	36	98	99
Sulfapyridine	283	125	<LOQ	<LOQ	<LOQ		56	99	99
Terbutryn	45	26	<LOQ	<LOQ	<LOQ	<LOQ	42	88	94
Terbutylazine	15	6	6	5	584	391	60	0	67
Trimethoprim	156	111	<LOQ	<LOQ	<LOQ	<LOQ	29	98	98

Sampling: 17.6.2008, 8:00 - 19.6.2008, 8:00
Ozone dose: 1.16 O_3/gDOC

Compounds	Primary effluent (ng/L)	Secondary effluent (ng/L)	Ozonation effluent (ng/L)	Sand filtration effluent (ng/L)	Furtbach upstream (ng(L)	Furtbach downstream (ng(L)	Elimination in secondary treatment (%)	Elimination by ozone (%)	Elimination of the whole treatment process (%)
N4-Acetylsulfamethoxazole	247	<LOQ	<LOQ	<LOQ	<LOQ	<LOQ	94	not detected	99
Atenolol	2044	1504	<LOQ	<LOQ	<LOQ	<LOQ	26	100	100
Atrazine	31	37	14	13	37	25	-19	62	58
Atrazine-Desethyl	47	35	28	29	50	37	26	20	38
Atrazine-Desisopropyl	<LOQ	<LOQ	<LOQ	<LOQ			not detected	not detected	not detected
Atrazine-Hydroxy	<LOQ	<LOQ	<LOQ	<LOQ	16		not detected	not detected	not detected
Benzotriazole	6684	4968	100	135	12	60	26	98	98
Bezafibrate	322	63	<LOQ	<LOQ	<LOQ	<LOQ	80	89	98
Carbamazepine	485	714	<LOQ	<LOQ	<LOQ	<LOQ	-47	100	100
Carbendazim							#DIV/0!	#DIV/0!	#DIV/0!
Clarithromycin	352	197	<LOQ	<LOQ	<LOQ	<LOQ	44	99	100
Clindamycin	27	36	<LOQ	<LOQ	<LOQ	<LOQ	-31	96	95
Clofibric acid	16	11	<LOQ	<LOQ	<LOQ	<LOQ	36	86	91
Diatrizoate	<LOQ	<LOQ	<LOQ	<LOQ	<LOQ	<LOQ	not detected	not detected	not detected
Diazinion	44	39	1	3	1	1	11	97	93
Diclofenac	1477	957	<LOQ	<LOQ	<LOQ	<LOQ	35	99	100
Diuron		<LOQ	<LOQ	<LOQ	<LOQ	<LOQ	#DIV/0!	not detected	#DIV/0!
N,N-Dimethylaminosulfanilid		<LOQ	<LOQ	<LOQ	<LOQ	<LOQ	#DIV/0!	not detected	#DIV/0!
Dimethyltolylsulfamid		<LOQ	<LOQ	<LOQ	<LOQ	<LOQ	#DIV/0!	not detected	#DIV/0!
Erythromycin z.T. mit Metabolit	<LOQ	<LOQ	<LOQ	<LOQ	<LOQ	<LOQ	not detected	not detected	not detected
Ibuprofen	3330	<LOQ	<LOQ	<LOQ	<LOQ	<LOQ	99	not detected	100
Iohexol	<LOQ	<LOQ	<LOQ	<LOQ	<LOQ	<LOQ	not detected	not detected	not detected
Iomeprol	<LOQ	<LOQ	<LOQ	<LOQ	<LOQ	8	not detected	not detected	not detected
Iopamidol	163	<LOQ	45	44	<LOQ	24	92	not detected	73
Iopromide	14800	1880	953	794	<LOQ	348	87	49	95
Ioxitalamic acid	372	75	120	38	<LOQ	37	80	-60	90
Irgarol		<LOQ	<LOQ	<LOQ	<LOQ	<LOQ	#DIV/0!	not detected	#DIV/0!
Irgarol-Descyclopropyl		<LOQ	<LOQ	<LOQ	<LOQ	<LOQ	#DIV/0!	not detected	#DIV/0!
Isoproturon	14	17	<LOQ	<LOQ	10	<LOQ	-21	91	89
Mecoprop	178	251	<LOQ	<LOQ	55		-41	96	94
Mefenamic acid	2542	186	<LOQ	<LOQ	<LOQ	<LOQ	93	98	100
Methylbenzotriazole	1325	940	6	<LOQ	<LOQ	<LOQ	29	99	100
Metoprolol	487	326	<LOQ	<LOQ	<LOQ	<LOQ	33	97	98
Naproxen	462	196	<LOQ	<LOQ	<LOQ	<LOQ	57	97	99
N-Nitrosodi-n-butylamine	<LOQ	2	4	<LOQ			not detected	-95	not detected
N-Nitrosodiethylamine	2.7	4.3	6.0	<LOQ			-57	-40	87
N-Nitrosodimethylamine	24.3	19.4	20.2	4.6			20	-4	81
N-Nitrosomorpholine	14.1	9.9	6.0	2.7			30	40	81
N-Nitrosopiperidine	6	<LOQ	<LOQ	<LOQ			81	not detected	81
N-Nitrosodiphenylamine	<LOQ	<LOQ	<LOQ	<LOQ	<LOQ	<LOQ	not detected	not detected	not detected
N-Nitrosodipropoylamine	<LOQ	<LOQ	<LOQ	<LOQ	<LOQ	<LOQ	not detected	not detected	not detected
N-Nitrisodipyrrolidine	<LOQ	<LOQ	<LOQ	<LOQ	<LOQ	<LOQ	not detected	not detected	not detected
N-Nitrosomethylethylamine	<LOQ	<LOQ	<LOQ	<LOQ	<LOQ	<LOQ	not detected	not detected	not detected
Paracetamol	27923	<LOQ		<LOQ	<LOQ	<LOQ	99	not detected	100
Phenazone	44	26		<LOQ	<LOQ	<LOQ	41	100	86
Primidone	120	54	<LOQ	<LOQ	<LOQ	<LOQ	55	91	96
Propanolol	79	96	<LOQ	7	9	3	-21	97	91
Roxithromycin	<LOQ	<LOQ	<LOQ	<LOQ	<LOQ	<LOQ	not detected	not detected	not detected
Sotalol	434	392	<LOQ	<LOQ	<LOQ	<LOQ	10	98	99
Sulcotrione		<LOQ	<LOQ	<LOQ	<LOQ	<LOQ	#DIV/0!	not detected	#DIV/0!
Sulfadiazine	359	127	<LOQ	<LOQ	<LOQ	<LOQ	65	86	95
Sulfadimethoxine	<LOQ	<LOQ	<LOQ	<LOQ	<LOQ	<LOQ	not detected	not detected	not detected
Sulfamethazine	9	7		<LOQ	<LOQ	<LOQ	27	100	73
Sulfamethoxazole	165	96	<LOQ	<LOQ	<LOQ	<LOQ	42	96	98
Sulfapyridine	248	184	<LOQ	<LOQ	<LOQ	<LOQ	26	99	99
Terbutryn		<LOQ	<LOQ	<LOQ	30	14	#DIV/0!	not detected	#DIV/0!
Terbutylazine	22	19	9	9	57	33	14	53	59
Trimethoprim	105	85	<LOQ	<LOQ	<LOQ	<LOQ	18	97	98

Sampling: 26.8.2008, 8:00 - 28.8.2008, 8:00
Ozone dose: 0.77 g O_3 / g DOC

Compounds	Primary effluent (ng/L)	Secondary effluent (ng/L)	Ozonation effluent (ng/L)	Sand filtration effluent (ng/L)	Furtbach upstream (ng(L)	Furtbach downstream (ng(L)	Elimination in secondary treatment (%)	Elimination by ozone (%)	Elimination of the whole treatment process (%)
N4-Acetylsulfamethoxazole	844	<LOQ	<LOQ	<LOQ	<LOQ	<LOQ	98	not detected	100
Atenolol	2495	1428	16	11	<LOQ	<LOQ	43	99	100
Atrazine	18	16	8	9	21	15	11	50	50
Atrazine-Desethyl	60	37	29	28	52	38	38	22	53
Atrazine-Desisopropyl	<LOQ	<LOQ	<LOQ	<LOQ	<LOQ	<LOQ	not detected	not detected	not detected
Atrazine-Hydroxy	17	<LOQ	<LOQ	<LOQ	<LOQ	<LOQ	12	not detected	85
Benzotriazole	5817	3720	568	578	16	263	36	85	90
Bezafibrate	539	37	<LOQ	<LOQ	<LOQ	<LOQ	93	81	99
Carbamazepine	941	680	<LOQ	<LOQ	<LOQ	<LOQ	28	100	100
Carbendazim	31	31	<LOQ	<LOQ	100	41	0	65	65
Clarithromycin	239	122	<LOQ	<LOQ	<LOQ	<LOQ	49	99	99
Clindamycin	124	35	<LOQ	<LOQ	<LOQ	<LOQ	72	96	99
Clofibric acid	20	11	<LOQ	<LOQ	<LOQ	<LOQ	46	86	92
Diatrizoate	36	<LOQ	158	119	<LOQ	58	65	not detected	-231
Diazinion	17	16	2	3	6	1	6	88	82
Diclofenac	1907	1004	<LOQ	<LOQ	<LOQ	<LOQ	47	100	100
Diuron	<LOQ	<LOQ	<LOQ	<LOQ	76	33	not detected	not detected	not detected
N,N-Dimethylaminosulfanilid	<LOQ	<LOQ	<LOQ	<LOQ	<LOQ	<LOQ	not detected	not detected	not detected
Dimethyltolylsulfamid	<LOQ	<LOQ	<LOQ	<LOQ	<LOQ	<LOQ	not detected	not detected	not detected
Erythromycin z.T. mit Metabolit	85	73	<LOQ	<LOQ	<LOQ	<LOQ	14	86	88
Ibuprofen	4705	<LOQ	<LOQ	<LOQ	<LOQ	<LOQ	99	not detected	100
Iohexol	792	62	38	20	<LOQ	15	92	39	97
Iomeprol	<LOQ	<LOQ	<LOQ	<LOQ	<LOQ	<LOQ	not detected	not detected	not detected
Iopamidol	33	<LOQ	<LOQ	<LOQ	<LOQ	<LOQ	62	not detected	62
Iopromide	6630	990	648	510	<LOQ	242	85	35	92
Ioxitalamic acid	2930	1130	1083	993	<LOQ	473	61	4	66
Irgarol	<LOQ	<LOQ	<LOQ	<LOQ	<LOQ	<LOQ	not detected	not detected	not detected
Irgarol-Descyclopropyl	<LOQ	<LOQ	<LOQ	<LOQ	<LOQ	<LOQ	not detected	not detected	not detected
Isoproturon	70	69	<LOQ	<LOQ	6	3	1	98	98
Mecoprop	171	226	23	16	7	14	-32	90	91
Mefenamic acid	2812	93	<LOQ	<LOQ	<LOQ	<LOQ	97	97	100
Methylbenzotriazole	2326	1658	50	58	<LOQ	22	29	97	97
Metoprolol	651	468	10	<LOQ	<LOQ	<LOQ	28	98	99
Naproxen	636	181	<LOQ	<LOQ	<LOQ	<LOQ	72	97	99
N-Nitrosodi-n-butylamine	<LOQ	<LOQ	<LOQ	<LOQ			not detected	not detected	not detected
N-Nitrosodiethylamine	1.7	1.1	1.0	0.6			36	5	62
N-Nitrosodimethylamine	8	4	16	5			57	-344	45
N-Nitrosomorpholine	5.0	3.8	3.2	2.7			25	14	47
N-Nitrosopiperidine	5	<LOQ	<LOQ	<LOQ			78	not detected	78
N-Nitrosodiphenylamine	<LOQ	<LOQ	<LOQ	<LOQ	<LOQ	<LOQ	not detected	not detected	not detected
N-Nitrosodipropoylamine	<LOQ	<LOQ	<LOQ	<LOQ	<LOQ	<LOQ	not detected	not detected	not detected
N-Nitrisodipyrrolidine	<LOQ	<LOQ	<LOQ	<LOQ	<LOQ	<LOQ	not detected	not detected	not detected
N-Nitrosomethylethylamine	<LOQ	<LOQ	<LOQ	<LOQ	<LOQ	<LOQ	not detected	not detected	not detected
Paracetamol	31417	<LOQ	<LOQ	<LOQ	<LOQ	<LOQ	99	not detected	100
Phenazone	<LOQ	13	<LOQ	<LOQ	<LOQ	<LOQ	not detected	50	not detected
Primidone	78	75	23	17	<LOQ	<LOQ	4	69	78
Propanolol	94	112	<LOQ	10	<LOQ	14	-19	98	89
Roxithromycin	<LOQ	<LOQ	<LOQ	<LOQ	<LOQ	<LOQ	not detected	not detected	not detected
Sotalol	367	388	<LOQ	<LOQ	<LOQ	<LOQ	-6	98	98
Sulcotrione	<LOQ	<LOQ	<LOQ	<LOQ	<LOQ	<LOQ	not detected	not detected	not detected
Sulfadiazine	83	17	<LOQ	<LOQ	<LOQ	<LOQ	80	-5	79
Sulfadimethoxine	<LOQ	<LOQ	<LOQ	<LOQ	<LOQ	<LOQ	not detected	not detected	not detected
Sulfamethazine	<LOQ	<LOQ	<LOQ	<LOQ	<LOQ	<LOQ	not detected	not detected	not detected
Sulfamethoxazole	380	282	<LOQ	<LOQ	<LOQ	<LOQ	26	99	99
Sulfapyridine	197	129	<LOQ	<LOQ	<LOQ	<LOQ	35	99	99
Terbutryn	39	34	<LOQ	<LOQ	3	1	13	91	94
Terbutylazine	<LOQ	<LOQ	<LOQ	<LOQ	10	7	not detected	not detected	not detected
Trimethoprim	185	105	<LOQ	<LOQ	<LOQ	<LOQ	43	98	99

Sampling: 23.9.2008, 8:00 - 25.9.2008, 8:00
Ozone dose: 0.81 g O_3 / g DOC

Compounds	Primary effluent (ng/L)	Secondary effluent (ng/L)	Ozonation effluent (ng/L)	Sand filtration effluent (ng/L)	Elimination in secondary treatment (%)	Elimination by ozone (%)	Elimination of the whole treatment process (%)
N4-Acetylsulfamethoxazole	536	<LOQ	<LOQ	<LOQ	97	not detected	99
Atenolol	2245	1637	<LOQ	<LOQ	27	99	100
Atrazine	21	18	6	7	14	67	67
Atrazine-Desethyl	47	37	30	31	21	19	34
Atrazine-Desisopropyl	<LOQ	<LOQ	<LOQ	<LOQ	not detected	not detected	not detected
Atrazine-Hydroxy	<LOQ	<LOQ	<LOQ	<LOQ	not detected	not detected	not detected
Benzotriazole	7983	4055	556	609	49	86	92
Bezafibrate	478	67	<LOQ	<LOQ	86	51	99
Carbamazepine	340	384	<LOQ	<LOQ	-13	98	100
Carbendazim	46	51	<LOQ	<LOQ	-11	15	76
Clarithromycin	413	137	<LOQ	<LOQ	67	98	100
Clindamycin	32	18	<LOQ	<LOQ	44	86	95
Clofibric acid	32	18	<LOQ	<LOQ	44	86	95
Diatrizoate	<LOQ	16	84	108	not detected	-425	not detected
Diazinion	30	20	<LOQ	<LOQ	33	75	97
Diclofenac	1681	1288	<LOQ	<LOQ	23	98	100
Diuron	<LOQ	<LOQ	<LOQ	<LOQ	not detected	not detected	not detected
N,N-Dimethylaminosulfanilid	<LOQ	<LOQ	<LOQ	<LOQ	not detected	not detected	not detected
Dimethyltolylsulfamid	<LOQ	<LOQ	<LOQ	<LOQ	not detected	not detected	not detected
Erythromycin z.T. mit Metabolit	55	48	<LOQ	<LOQ	13	22	82
Ibuprofen	4184	<LOQ	<LOQ	<LOQ	99	not detected	100
Iohexol	<LOQ	<LOQ	<LOQ	<LOQ	not detected	not detected	not detected
Iomeprol	138	61	<LOQ	26	56	80	81
Iopamidol	106	190	78	82	-79	59	23
Iopromide	7560	1620	930	738	79	43	90
Ioxitalamic acid	2090	206	335	258	90	-63	88
Irgarol	<LOQ	<LOQ	<LOQ	<LOQ	not detected	not detected	not detected
Irgarol-Descyclopropyl	<LOQ	<LOQ	<LOQ	<LOQ	not detected	not detected	not detected
Isoproturon	19	85	<LOQ	<LOQ	-347	94	92
Mecoprop	<LOQ	53	<LOQ	<LOQ	not detected	6	not detected
Mefenamic acid	3359	161	<LOQ	<LOQ	95	95	100
Methylbenzotriazole	2374	1059	8	14	55	99	99
Metoprolol	552	439	<LOQ	<LOQ	20	90	98
Naproxen	670	291	<LOQ	<LOQ	57	70	99
N-Nitrosodi-n-butylamine	3	<LOQ	<LOQ	<LOQ	40	not detected	40
N-Nitrosodiethylamine	7.9	1.4	2.2	3.2	82	-55	60
N-Nitrosodimethylamine	21.8	2.4	13.7	7.2	89	-471	67
N-Nitrosomorpholine	8.9	4.6	4.9	3.5	48	-5	60
N-Nitrosopiperidine	19	<LOQ	<LOQ	<LOQ	94	not detected	94
N-Nitrosodiphenylamine	<LOQ	<LOQ	<LOQ	<LOQ	not detected	not detected	not detected
N-Nitrosodipropoylamine	<LOQ	<LOQ	<LOQ	<LOQ	not detected	not detected	not detected
N-Nitrisodipyrrolidine	<LOQ	<LOQ	<LOQ	<LOQ	not detected	not detected	not detected
N-Nitrosomethylethylamine	<LOQ	<LOQ	<LOQ	<LOQ	not detected	not detected	not detected
Paracetamol	43796	<LOQ	<LOQ	<LOQ	99	not detected	100
Phenazone	<LOQ	20	<LOQ	<LOQ	not detected	-38	not detected
Primidone	121	115	21	22	5	82	82
Propanolol	106	110	7	44	-4	94	58
Roxithromycin	<LOQ	<LOQ	<LOQ	<LOQ	not detected	not detected	not detected
Sotalol	422	488	<LOQ	<LOQ	-16	95	98
Sulcotrione	<LOQ	<LOQ	<LOQ	<LOQ	not detected	not detected	not detected
Sulfadiazine	<LOQ	<LOQ	<LOQ	<LOQ	not detected	not detected	not detected
Sulfadimethoxine	<LOQ	<LOQ	<LOQ	<LOQ	not detected	not detected	not detected
Sulfamethazine	10	9	<LOQ	<LOQ	10	72	75
Sulfamethoxazole	287	189	<LOQ	<LOQ	34	93	99
Sulfapyridine	271	147	<LOQ	<LOQ	46	95	99
Terbutryn	62	59	<LOQ	<LOQ	5	79	96
Terbutylazine	10	6	<LOQ	<LOQ	40	-133	70
Trimethoprim	149	125	<LOQ	<LOQ	16	88	98

References

(1) Elovitz, M. S.; von Gunten, U. Hydroxyl radicals/ozone ratios during ozonation processes. I. The Rct concept. *Ozone Sci. Eng.* **1999**, *21*, 239-260.

(2) von Gunten, U. Ozonation of drinking water: Part I. Oxidation kinetics and product formation. *Water Res.* **2003**, *37*, 1443-1467.

(3) Sein, M. M.; Zedda, M.; Tuerk, J.; Schmidt, T. C.; Golloch, A.; von Sonntag, C. Oxidation of diclofenac with ozone in aqueous solution. *Environ. Sci. Technol.* **2008**, *42*, 6656-6662.

(4) Gromadzka, K.; Nawrocki, J. Degradation of diclofenac and clofibric acid using ozone-loaded perfluorinated solvent. *Ozone Sci. Eng.* **2006**, *28*, 85-94.

(5) Ikehata, K.; Jodeiri Naghashkar, N.; Gamal El-Din, M. Degradation of aqueous pharmaceuticals by ozonation and advanced oxidation processes: A review. *Ozone Sci. Eng.* **2006**, *28*, 353-414.

(6) Göbel, A. M., C.S.; Suter, M.J.F.; Giger, W. Trace determination of macrolide and sulfonamide antimicrobials, a human sulfonamide metabolite, and trimethoprim in wastewater using liquid chromatography coupled to electrospray tandem mass spectrometry. *Anal. Chem.* **2004**, *76*, 4756-4764.

(7) Krauss, M.; Hollender, J. Analysis of nitrosamines in wastewater: Exploring the trace level quantification capabilities of a hybrid linear ion trap/orbitrap mass spectrometer. *Anal. Chem.* **2008**, *80*, 834-842.

(8) Singer, H.; Jaus, S.; Hanke, I.; Lück, A.; Hollender, J.; Alder, A. C. Determination of biocides and pesticides by on-line solid phase extraction coupled with mass spectrometry and their behaviour in wastewater and surface water. *Environmental Pollution* **2010,** *158 (10)*, 3054-3064.

(9) Weissbrodt, D. K., L; Pazhepurackel, V.; Ort, C.; Moser, R.; Hollender, J.; Siegrist H.;. McArdell C.S. Mass flows of X-ray contrast media and cytostatics in hospital wastewater. *Environ. Sci. Technol.* **2009**, *43,* 4810-4817.

(10) Kern, S.; Fenner, K.; Singer, H.P., Schwarzenbach, R.P.; Hollender, J. Identification of transformation products of organic contaminants in natural waters by computer-aided prediction and high-resolution mass spectrometry. *Environ. Sci. Technol.* **2009**, *43*, 7039-7046.

(11) Hoigné, J.; Bader, H. Rate constants of reactions of ozone with organic and inorganic compounds in water - I Non-dissociating organic compounds. *Water Res.* **1983** *17*, 173-183.

(12) Huber, M. M.; Canonica, S.; Park, G. Y.; von Gunten, U. Oxidation of pharmaceuticals during ozonation and advanced oxidation processes. *Environ. Sci. Technol.* **2003**, *37*, 1016-1024.

(13) Huber, M. M.; Göbel, A.; Joss, A.; Hermann, N.; Löffler, D.; McArdell, C. S.; Ried, A.; Siegrist, H.; Ternes, T. A.; von Gunten, U. Oxidation of pharmaceuticals during ozonation of municipal wastewater effluents: A pilot study. *Environ. Sci. Technol.* **2005**, *39*, 4290-4299.

(14) Benner, J.; Salhi, E.; Ternes, T.; von Gunten, U. Ozonation of reverse osmosis concentrate: Kinetics and efficiency of beta blocker oxidation. *Water Res.* **2008**, *42*, 3003-3012.

(15) Beltrán, F. J. G., M.; Rivas, J.; Marin, M. Oxidation of mecoprop in water with ozone and ozone combined with hydrogen peroxide. *Ind. Eng. Chem. Res.* **1994,** *33*, 125-136.

(16) Lutze, H. Ozonung von Benzotriazolen. *Bachelor Thesis, University Duisburg - Essen* **2005**.

(17) Naik, D. B. M., P. N. Studies on the Transient Species Formed in the Pulse-Radiolysis of Benzotriazole. . *Radiat. Phys. Chem.* **1995**, *46*, 353-357.

(18) Acero, J. L.; Stemmler, K.; von Gunten, U. Degradation kinetics of atrazine and its degradation products with ozone and OH radicals: A predictive tool for drinking water treatment. *Environ. Sci. Technol.* **2000**, *34*, 591-597.

Chapter 3

Kinetic assessment and modeling of an ozonation step for full-scale municipal wastewater treatment: Micropollutant oxidation, by-product formation and disinfection

Reprinted from *Water Research* 45 (2), Zimmermann, S.G.; Wittenwiler, M.; Hollender, J.; Krauss, M.; Ort, C.; Siegrist, H.; von Gunten, U., Kinetic assessment and modeling of an ozonation step for full-scale municipal wastewater treatment: Micropollutant oxidation, by-product formation and disinfection, 605-617.

http://www.sciencedirect.com/science/article/pii/S0043135410005634

Abstract

The kinetics of oxidation and disinfection processes during ozonation in a full-scale reactor treating secondary wastewater effluent were investigated for seven ozone doses ranging from 0.21 - 1.24 g O_3 g^{-1} dissolved organic carbon (DOC). Substances reacting fast with ozone, such as diclofenac or carbamazepine (k_{P,O_3} > 10^4 M^{-1} s^{-1}), were eliminated within the gas bubble column, except for the lowest ozone dose of 0.21 g O_3 g^{-1} DOC. For this low dose, this could be attributed to short-circuiting within the reactor. Substances with lower ozone reactivity (k_{P,O_3} < 10^4 M^{-1} s^{-1}) were only fully eliminated for higher ozone doses.

The predictions of micropollutant oxidation based on coupling reactor hydraulics with ozone chemistry and reaction kinetics were up to a factor of 2.5 higher than full-scale measurements. Monte Carlo simulations showed that the observed differences were higher than model uncertainties. The overestimation of micropollutant oxidation was attributed to a protection of micropollutants from ozone attack by the interaction with aquatic colloids. Laboratory-scale batch experiments using wastewater from the same full-scale treatment plant could predict the oxidation of slowly-reacting micropollutants on the full-scale level within a factor of 1.5. The R_{ct} value, the experimentally determined ratio of the concentrations of hydroxyl radicals and ozone, was identified as a major contribution to this difference.

An increase in the formation of bromate, a potential human carcinogen, was observed with increasing ozone doses. The final concentration for the highest ozone dose of 1.24 g O_3 g^{-1} DOC was 7.5 µg L^{-1}, which is below the drinking water standard of 10 µg L^{-1}. *N*-nitrosodimethylamine (NDMA) formation of up to 15 ng L^{-1} was observed in the first compartment of the reactor, followed by a slight elimination during sand filtration. Assimilable organic carbon (AOC) increased up to 740 µg AOC L^{-1}, with no clear trend when correlated to the ozone dose, and decreased by up to 50 % during post-sand filtration. The disinfection capacity of the ozone reactor was assessed to be 1 - 4.5 log units in terms of total cell counts (TCC) and 0.5 to 2.5 log units for *Escherichia coli (E. coli)*. Regrowth of up to 2.5 log units during sand filtration was observed for TCC while no regrowth occurred for *E. coli*. *E. coli* inactivation could not be accurately predicted by the model approach, most likely due to shielding of *E. coli* by flocs.

3.1 Introduction

In recent years, mitigation strategies to lower micropollutant loads from wastewater treatment plant (WWTP) effluents to receiving waters have been discussed intensively. Ozonation is a promising technique to upgrade WWTPs with a tertiary treatment step because it has been demonstrated to be efficient for the oxidation of pharmaceuticals and other micropollutants in drinking water *(1,2)* and wastewater *(3-8)*. Oxidation does not usually result in complete mineralization, but in the formation of transformation products, which in many cases have a much lower biological activity than the parent compounds *(9-11)*. In addition to the formation of transformation products, other undesired by-products can be formed such as bromate, a potential human carcinogen, formed during ozonation of bromide-containing waters by a complicated mechanism involving both ozone and hydroxyl radicals *(12)*. *N*-nitrosodimethylamine (NDMA) formation was reported during ozonation of drinking water *(13)* and wastewater *(8,14)*, while *N*-nitrosomorpholine (NMOR) formation occurred during ozonation of lake water *(15)*. Other organic by-products are formed from the oxidative breakdown of complex dissolved organic matter (DOM), which are usually readily biodegradable and can be measured as e.g. assimilable organic carbon (AOC) *(12,16)*. AOC is an important water quality parameter for the biological stability of drinking water and can influence river water quality after discharge of ozonated wastewater. For all of these known oxidation by-products, no information is available on the extent and kinetics of their formation during ozonation of secondary wastewater effluent. Concerning the toxicity of ozonated secondary wastewater effluent, a decrease in specific and unspecific toxicity after ozonation was demonstrated by an *in vitro* test battery using different toxicological endpoints *(17)*, while *in vivo* tests with rainbow trout suggested an increased toxicity that disappeared after sand filtration *(18)*. This can be explained by the formation of potentially toxic by-products from DOM oxidation, such as aldehydes, ketones and other oxygen-rich compounds *(12)*, which might not be enriched during solid phase extraction necessesary for the *in vitro* test battery. These oxygen-rich compounds are typically removed during sand filtration *(16)*.

Besides its role as an oxidant, ozone is mainly used in drinking water production because it is an effective disinfectant for viruses, bacteria and protozoa *(12)*. In the present study, the main focus is on micropollutant oxidation, however, disinfection is an additional benefit especially in reference to the amended bathing water directive of the European Union (2006/7/EC). Both objectives can be achieved by ozonation at a reasonable and manageable cost as demonstrated by Hollender et al. 2009 *(8)*.

Prediction of the oxidation and disinfection capacity of a full-scale ozonation step is of practical and scientific interest to ensure optimum performance. The design of the reactor as well as site-specific wastewater composition are important parameters influencing oxidation and disinfection performance of ozonation steps. von Gunten et al. *(19,20)* developed a concept to predict the behavior of oxidants and micropollutants in an ozone reactor treating lake water for drinking water purposes. This concept is based on the coupling of reactor hydraulics with ozone chemistry and reaction kinetics, and has been successfully applied for the simulation of ozone reactors treating spring *(21)* and river water *(22)*.

The objectives of the present study were to assess the oxidation and disinfection capacity of a full-scale ozonation step by quantitatively describing the kinetics of the following processes occurring during ozonation of secondary wastewater effluent: (i) micropollutant oxidation, (ii) oxidation by-product formation, (iii) AOC formation, and (iv) disinfection. (v) Finally, two different approaches to predict ozone reactor performance in terms of micropollutant oxidation were tested: (a) a model based on the concept of von Gunten et al *(19,20)* which could also be used for disinfection prediction, and (b) spiked laboratory-scale batch experiments using secondary effluent from the same full-scale WWTP.

3.2 Materials and Methods

3.2.1 Standards and Reagents

All chemicals and solvents were of analytical purity (≥ 95 %) and purchased from various suppliers. The micropollutants analyzed in the sampling campaigns are compiled in Table S3.1 of the Supporting Information.

3.2.2 Ozone reactor

A detailed description of WWTP Wüeri in Regensdorf, Switzerland, including rapid sand filtration as final biological treatment step after ozonation was given by *(8)*. A mixing chamber for final flocculation was retrofitted to a full-scale six compartment ozone reactor with a volume of 38 m^3 (Figure 3.1). A gaseous ozone/oxygen mixture was added in counter-current mode through a series of disc diffusers into the first compartment. Since DOM - measured as dissolved organic carbon (DOC) - is the main matrix component determining the ozone consumption in wastewater, a DOC load-proportional ozone dosing was chosen to account for varying DOC concentrations in the secondary effluent. Hence, the flow to the ozone reactor was determined online by an ultrasonic device (Prosonic, Endress + Hauser, Germany), and the DOC concentration was measured online by an S::can sensor (S::can, Austria) using UV absorption. The S::can sensor was calibrated using grab samples filtered to 0.45 µm and measured by a total organic carbon analyzer (Shimadzu, Switzerland). Seven sampling points (P1-P7) were distributed along the ozone reactor (Figure 3.1), each consisting of a stainless steel pipe with an inner diameter of 5.5 mm reaching 80 cm into the ozone reactor. This resulted in residence times between 5 and 22 s in the sampling tubes, depending on the length and the flow within the tubes.

3.2.3 Tracer tests

The hydraulic behavior of the ozone reactor was characterized using fluoresceine as a conservative tracer during Dirac pulse tracer tests and as a reactive tracer during a continuous tracer test. Further information can be found in Text S3.1.

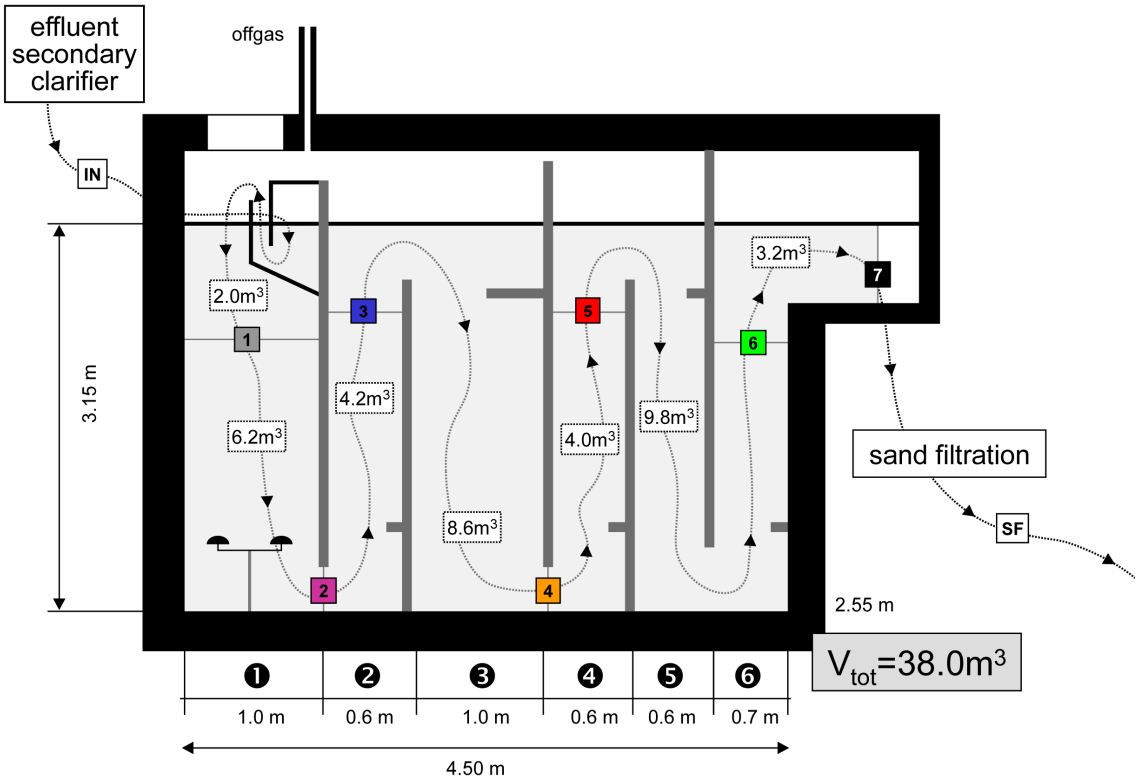

Figure 3.1. Scheme of the ozone reactor at WWTP Wüeri in Regensdorf, Switzerland

3.2.4 Sampling campaigns

Seven ozone doses were applied ranging from 0.21 – 1.24 g O_3 g^{-1} DOC by adding a fixed gas volume of either 15 or 20 m^3 h^{-1} and by automatically adjusting the ozone concentration in the process gas (Table 3.1, Table S3.2). Each ozone dose was injected for at least 20 h prior to sampling to guarantee equilibration of the sand filter (hydraulic retention time (HRT) 0.5 - 1 h). Grab samples were taken from the influent to the ozone reactor (IN), along the ozone reactor (P2, P3, P7 or P3, P5, P7), and after sand filtration (SF). Depending on the ozone dose, either sampling point P2 or P5 was sampled. Dissolved ozone was quenched with sulfite (nitrosamine analysis) or nitrite (all other analyses) in at least 10-fold excess during sampling. Samples along the ozone reactor were taken accounting for the different travel times between sampling points in order to sample from the same water package each time.

Table 3.1. Ozonation process and wastewater quality parameters of the influent grab samples collected during the sampling campaigns

		Transferred ozone dose[a] [g O_3 g^{-1} DOC]						
		0.21	**0.41**	**0.60**	**0.74**	**0.81**	**0.90**	**1.24**
Transferred ozone dose[a]	[mg O_3 L^{-1}]	0.8	1.2	2.6	3.0	3.8	4.3	5.2
Ozone exposure[b]	[M s]	n.d.	6.9 ± 0.7 x 10^{-4}	3.1 ± 0.6 x 10^{-3}	4.1 ± 0.4 x 10^{-3}	6.1 ± 0.4 x 10^{-3}	1.1 ± 0.1 x 10^{-2}	1.9 ± 0.1 x 10^{-2}
Ozone exposure[b]	[mg min L^{-1}]	n.d.	0.5 ± 0.1	2.5 ± 0.5	3.3 ± 0.4	4.9 ± 0.4	8.9 ± 0.4	14.9 ± 0.7
k_{O_3}	[s^{-1}]	n.d.	2.1 ± 0.3 x 10^{-2}	9.3 ± 1.2 x 10^{-3}	8.4 ± 0.7 x 10^{-3}	6.0 ± 0.5 x 10^{-3}	3.8 ± 0.0 x 10^{-3}	3.6 ± 0.2 x 10^{-3}
R_{ct}	[-]	n.d.	1.3 ± 0.3 x 10^{-7}	3.6 ± 0.2 x 10^{-8}	4.6 ± 0.4 x 10^{-8}	2.6 ± 0.1 x 10^{-8}	1.7 ± 0.0 x 10^{-8}	2.2 ± 0.3 x 10^{-8}
Temperature	[°C]	20	20	13	20	13	13	22
DOC	[mg L^{-1}]	3.4	2.4	4.4	3.4	4.7	4.8	4.1
pH[c]	[-]	7.0	7.0	7.0	7.0	7.0	7.0	7.2

n.d. - not determined

[a]Applied ozone dose minus the ozone lost in the off-gas (($c_{O_3\ process\ gas}$ x $Q_{process\ gas}$) - ($c_{O_3\ offgas}$ x Q_{offgas}) / $Q_{wastewater}$ / $c_{DOC\ wastewater}$)

[b]Measured average ozone exposure after complete ozone decay with standard deviation based on 2 or 3 laboratory batch experiments with the same wastewater

[c]No change in pH by ozonation was observed

3.2.5 Analyses of micropollutants and oxidation by-products

A total of 22 micropollutants (Table S3.1 without nitrosamines) were analyzed by online SPE-LC-MS/MS *(8)*, while NDMA and NMOR (Table S3.1) were extracted using offline SPE and analyzed by LC-MS/HRMS *(23)*. Bromide and bromate concentrations were determined using ion chromatography followed by a post-column reaction *(24)*. Quenching the wastewater samples with sulfite (nitrosamines) or nitrite (micropollutants and bromide/bromate) did not influence quantification. Relative residual concentrations [%] were calculated by dividing the measured concentration at each sampling point with the concentration in the ozone reactor influent.

3.2.6 Disinfection and AOC measurement

The concentration of *Escherichia coli (E. coli)* was determined according to the Swiss standard method *(25)*. Total cell counts (TCC) were analyzed by flow cytometry using a nucleic acid staining by SYBR® Green *(26)*. The AOC concentration was measured by inoculation of the wastewater samples with a natural microbial consortium for 4 d at 30 °C and determination of the cell numbers by flow cytometry. The value of 1 x 10^7 bacteria to 1 µg AOC L^{-1} allowed the conversion of the natural microbial consortium growth into AOC concentrations *(16,27)*.

3.2.7 Determination of pseudo first-order ozone decay constants, ozone and hydroxyl radical exposures and R_{ct} values

The pseudo first-order ozone decay constants k_{O_3} as well as the ozone and hydroxyl radical exposures were determined by means of a laboratory dispenser system *(28)* (Table 3.1). *p*-Chlorobenzoic acid (*p*CBA) was spiked as ozone-resistent probe compound to measure the transient hydroxyl radical concentrations and to calculate the R_{ct} values (Table 3.1). Further experimental details can be found in Text S3.2.

3.2.8 Modeling of micropollutant oxidation and *E. coli* inactivation

The oxidation of a micropollutant P typically follows a second-order rate law *(29)*. During an ozonation process, both ozone and hydroxyl radicals have to be considered as oxidants:

$$-\frac{d[P]}{dt} = k_{P,O_3}\,[O_3][P] + k_{P,OH\bullet}\,[OH\bullet][P] \qquad (3.1)$$

with k_{P,O_3} and $k_{P,OH\bullet}$ being second-order reaction rate constants for the reaction of the micropollutant with ozone and hydroxyl radicals, respectively, and $[O_3]$ and [OH•] as ozone and hydroxyl radical concentrations.

To model micropollutant oxidation as well as *E. coli* inactivation in the full-scale ozone reactor, a four-step approach based on the combination of reactor hydraulics, laboratory-scale characterization of the wastewater with regard to ozone chemistry, and reaction kinetics was used *(19,20)*:

i. Characterization of the hydraulics of the ozone reactor with a conservative tracer and fitting of the breakthrough curves by a series of ideal reactors (section 3.3.1).

ii. Laboratory-scale experiments to determine the pseudo first-order rate constant for ozone decomposition and the R_{ct} value (ratio between hydroxyl radical and ozone concentrations, eq 3.3, *(30)*) at the respective wastewater pH and temperature (section 3.2.7).

iii. Determination of the second-order rate constants for the oxidation of micropollutants by ozone (k_{P,O_3}) and hydroxyl radicals ($k_{P,OH\bullet}$) and for *E. coli* inactivation by ozone for the respective wastewater pH and temperature. The second-order rate constants were compiled from literature (Table S3.3) and corrected for pH by taking the acid-base speciation of the respective micropollutant into account and by using the species-specific reaction rate constants with ozone. Furthermore, the Arrhenius equation was used for temperature correction. An activation energy of 50 kJ mol^{-1} was assumed which is in the range of typical activation energies for reactions with ozone *(31)*.

iv. Coupling of reactor hydraulics with chemical kinetics by using software capable of solving coupled differential equations such as Berkeley Madonna *(32)*.

The hydraulic model as well as eqs 3.1, 3.2 and 3.3 were used to describe the chemical kinetics during ozonation and were solved simultaneously:

Ozone decay: $$-\frac{dO_3}{dt} = k_{O_3}\,[O_3] \quad (3.2)$$

Hydroxyl radical concentration: $$[OH\bullet] = R_{ct}\,[O_3] \quad (3.3)$$

The arithmetic mean and standard deviation of the model were calculated by running Monte Carlo simulations (batch runs with n = 1000) with k_{P,O_3}, $k_{P,OH\bullet}$, k_{O_3} and R_{ct} as random uniform distributions between the published or experimentally determined uncertainties of the respective parameter (Table 3.2).

Table 3.2. Ozone chemistry parameters used within the Monte Carlo simulations for ozone doses of 0.41 and 0.74 g O_3 g^{-1} DOC, including the respective range of their random uniform distributions

		Transferred ozone dose[a] [g O_3 g^{-1} DOC]		**Reference**
		0.41	**0.74**	
$k_{O_3,\ benzotriazole}$[b]	[M^{-1} s^{-1}]	1.86 - 2.70 x 10^2		*(33)*
$k_{OH\bullet,\ benzotriazole}$[c]	[M^{-1} s^{-1}]	7.10 - 8.10 x 10^9		*(34)*
$k_{O_3,\ atenolol}$	[M^{-1} s^{-1}]	1.30 - 2.10 x 10^3		*(35)*
$k_{OH\bullet,\ atenolol}$	[M^{-1} s^{-1}]	7.50 - 8.50 x 10^9		*(35)*
k_{O_3}	[s^{-1}]	1.97 - 2.42 x 10^{-2}	7.60 - 8.80 x 10^{-3}	present study
R_{ct}	[-]	1.14 - 4.71 x 10^{-7}	4.26 - 28.50 x 10^{-8}	present study

[a]Applied ozone dose minus the ozone lost in the off-gas (($c_{O_3\ process\ gas}$ x $Q_{process\ gas}$) - ($c_{O_3\ offgas}$ x Q_{offgas}) / $Q_{wastewater}$ / $c_{DOC\ wastewater}$)

[b]$k_{O_3,\ benzotriazole}$ determined at pH 2 and 5 (18 and 22 M^{-1} s^{-1}, respectively, *(36)*) support the $k_{O_3,\ benzotriazole}$ value determined by *(33)* at pH 7. Standard deviation of $k_{O_3,\ benzotriazole}$ at pH 7 was set as difference between the measured (2.28 x 10^2 M^{-1} s^{-1}) and modeled (1.86 x 10^2 M^{-1} s^{-1}) value determined in *(33)*, and the measured value was used as average value.

[c]Standard deviation of $k_{OH\bullet,\ benzotriazole}$ was estimated to be equal to the standard deviation of $k_{OH\bullet,\ atenolol}$.

3.2.9 Laboratory-scale batch experiments for micropollutant oxidation

In addition to the hydraulic model, a second approach based on laboratory-scale batch experiments was tested to predict micropollutant oxidation on the full-scale level. The concept included the use of wastewater from the same WWTP and the application of ozone under the same conditions (pH, T) as in the full-scale campaign, but with spiked micropollutants to allow for direct HPLC-UV/FL analysis. Accordingly, grab samples from the influent to the ozone reactor were taken, filtered (0.45 µm) and stored at 4 °C until use. Batch experiments were prepared and carried out as described in section 3.2.7, however, with spiked micropollutants (0.2 - 1.0 µM) and by applying ozone doses yielding the same ozone exposures as in the full-scale campaigns. Relative residual concentrations of micropollutants were subsequently determined by HPLC-UV/FL, while ozone and hydroxyl radical exposures and R_{ct} values were determined as described in section 3.2.7.

In addition, micropollutant transformation within the laboratory batch system was predicted according to eq 3.4, the integrated form of eq 3.1, which is only valid for a constant R_{ct} and for perfectly mixed and homogeneous solutions such as in a batch reactor:

$$\ln\frac{[P]}{[P_0]} = -k_{P,O_3}\int[O_3]\,dt - k_{P,OH\bullet}\int[OH\bullet]\,dt = -(k_{P,O_3} + k_{P,OH\bullet}\cdot R_{ct})\int[O_3]\,dt \qquad (3.4)$$

with $\int [O_3]\,dt$ and $\int [OH\bullet]\,dt$ being the ozone and hydroxyl radical exposures, respectively. Eq 3.4 shows that the relative elimination of a micropollutant reacting with second-order kinetics during an ozonation process is concentration-independent with regard to micropollutants concentration, as long as the micropollutant does not significantly affect the oxidant stability.

3.3 Results and Discussion

3.3.1 Hydraulics of the ozone reactor

The HRT of the ozone reactor varied between 3 to 15 min for storm (250 L s^{-1}) and dry weather conditions at night (35 L s^{-1}), respectively. For dry weather during daytime hours (80 – 100 L s^{-1}), the HRT was determined to be 7 – 8 min. The breakthrough curves derived from the Dirac pulse tracer tests could be modeled empirically for two flows as a series of five continuously stirred tank reactor (CSTR) cascades starting from P2 or P3 to P7 (Figure 3.2). Table S3.4 summarizes the number of CSTRs in each cascade for the two flows and shows that the difference is marginal. Inclusion of a recirculation/back-mixing did not significantly improve the model fit. The hydraulic model started at P2 or P3, depending on the selected first sampling point within the ozone reactor for micropollutants or *E. coli* analysis. The first compartment of the ozone reactor was not included because short-circuiting occurred from P1 to P2 which was stronger when wastewater flows were < 150 L s^{-1}. In case of ideal mixing within a CSTR, breakthrough curves at P2 should decrease in height and increase in width as compared to P1. However, the breakthrough curve at P1 was only as high as and slightly wider than the breakthrough curve at P2 under these flow conditions (Figure 3.2a). Results from a reactive continuous tracer test support the hypothesis of short-circuiting *(37)*. In addition, 0.1 ± 0.02 % of the tracer mass was detected prior to the main breakthrough curves at P7 (Figure S3.1), but not at P1 to P6. This hints on short-circuiting of a water fraction through the ozone reactor directly to P7, most likely on top of the reactor along the concrete walls. It remains unclear whether this small water fraction was exposed to ozone or not.

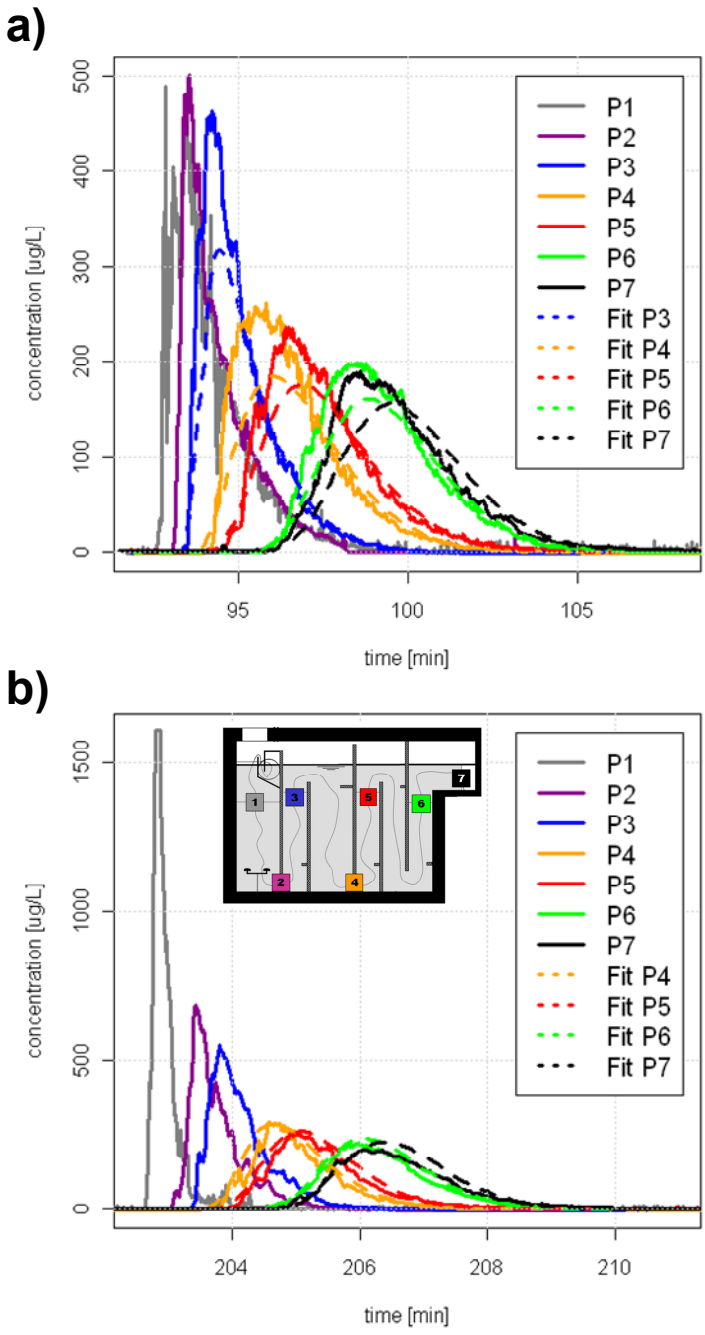

Figure 3.2. Breakthrough curves from the Dirac pulse tracer test of the conservative tracer fluoresceine at the ozone reactor for wastewater flows of a) 87 L s^{-1} and b) 170 L s^{-1}, both with 15 m^3 h^{-1} oxygen gas flow. Experimental data are shown as solid curves for P1 to P7 and hydraulic model calculations are depicted as dashed lines from a) P3 and b) P4 to P7.

3.3.2 Kinetics of full-scale micropollutant oxidation

Figure 3.3 shows the relative residual concentrations of three representative micropollutants with different second-order rate constants for their reaction with ozone. The fast-reacting substance diclofenac with a $k_{O_3} > 10^4$ M^{-1} s^{-1} (Table S3.3) was completely oxidized for ozone doses ≥ 0.41 g O_3 g^{-1} DOC within the first compartment of the ozone reactor (Figure 3.3a). Based on eq 3.4, this was expected from the ozone exposures (Table 3.1) and its k_{O_3}. Surprisingly, ~ 8 % of diclofenac resisted ozonation at a dose of 0.21 g O_3 g^{-1} DOC. According to eq 3.4, an ozone exposure of 6.7 x 10^{-6} M s is needed to achieve 99 % oxidation of diclofenac with k_{O_3} = 6.8 x 10^5 M^{-1} s^{-1}. Although the ozone exposure resulting from the 0.21 g O_3 g^{-1} DOC dose could not be determined by means of the laboratory dispenser system *(28)*, because ozone was consumed too fast, the ozone exposure needed for 99 % oxidation is less than 1 % of the final exposure of the 0.41 g O_3 g^{-1} DOC dose. Hence, a 99 % oxidation was expected even for an ozone dose of 0.21 g O_3 g^{-1} DOC. The incomplete oxidation of diclofenac and other fast-reacting substances such as carbamazepine, sulfamethoxazole and clarithromycin (Figure S3.2), can be attributed to short-circuiting from the first into the second compartment (section 3.1). 8 – 21 % of the mentioned micropollutants were not oxidized at a dose of 0.21 g O_3 g^{-1} DOC which is in agreement with the percentage of non-oxidized water (about 15 %) obtained during the reactive continuous fluoresceine tracer test carried out under identical conditions *(37)*. The short-circuiting is a hydraulic phenomenon and therefore independent of the ozone dose. However, for the 0.21 g O_3 g^{-1} DOC dose, dissolved ozone was completely consumed up to P2, leading to the observed residual fraction of fast-reacting micropollutants due to non-ozonated water packages. For all higher ozone doses, residual ozone was measured at P2. This may have led to a mixing of water packages containing dissolved ozone with others not containing ozone before reaching P2. As a consequence, the intrinsically fast oxidation of the fast-reacting micropollutants resulted in their complete oxidation.

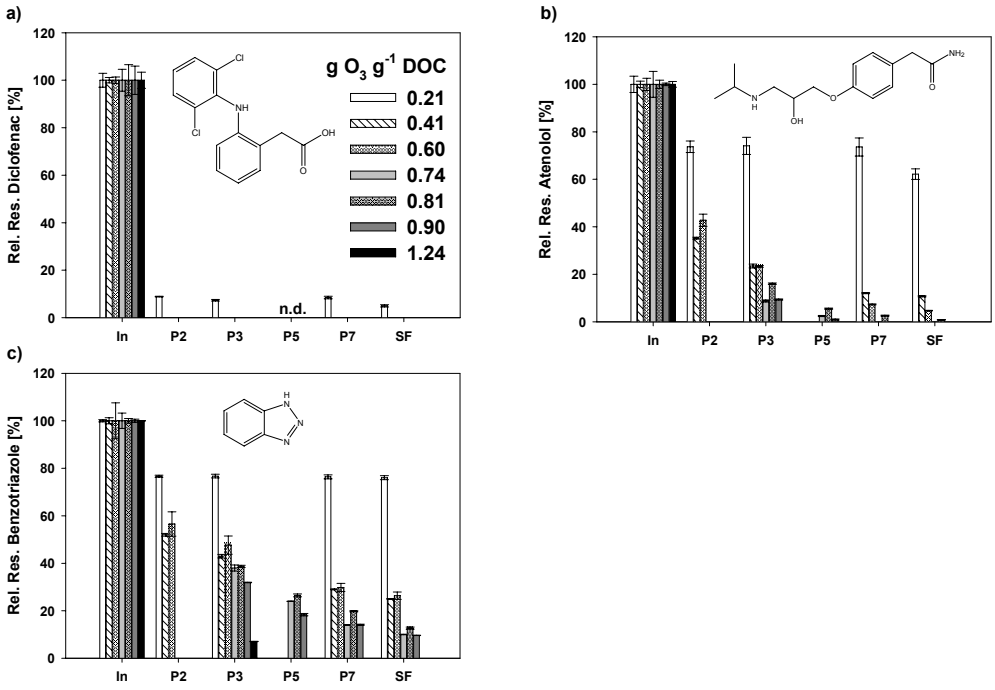

Figure 3.3. Relative residual concentrations of a) diclofenac, b) atenolol and c) benzotriazole for seven ozone doses ranging from 0.21 to 1.24 g O_3 g^{-1} DOC in the influent to the ozone reactor (IN), along the ozone reactor (P2, P3, P7 or P3, P5, P7) and after sand filtration (SF). Error bars were calculated by linear error propagation derived from duplicate measurements. n.d. = not determined.

The other fast-reacting substances clindamycin, erythromycin, mefenamic acid, naproxen, sulfapyridine and trimethoprim as well as sotalol ($k_{O_3} > 10^3$ M^{-1} s^{-1}), were oxidized below their limit of quantification (LOQ) (Table S3.1) at a dose of 0.21 g O_3 g^{-1} DOC at P2. This is not caused by a different oxidation behavior as compared to diclofenac, carbamazepine or sulfamethoxazole, but by their low influent concentrations which render them non-detectable even for ≤ 70 % relative residual concentration. Mefenamic acid with an unknown k_{O_3} was classified as fast-reacting compound from its structure. Its k_{O_3} was estimated to be higher than that of diclofenac because the two methyl groups increase the electron density of the aromatic system in contrast to the two electron-withdrawing chlorine atoms of diclofenac (Table S3.1).

Micropollutants reacting slower with ozone ($k_{P,O_3} < 10^4$ M^{-1} s^{-1}), such as atenolol and benzotriazole, were oxidized along the ozone reactor with increasing ozone and hydroxyl radical exposure (Figure 3.3b and c). The degree of transformation also increased with increasing k_{O_3} ($k_{O_3,atenolol}$ = 1.7 x 10^3 M^{-1} s^{-1} > $k_{O_3,benzotriazole}$ = 2.3 x 10^2 M^{-1} s^{-1} at pH 7). Ibuprofen, paracetamol and sulfamethazine were not detected in the influent of the ozone reactor, and sulfadiazine and phenanzone were only detected once and as expected fully oxidized at a dose of 0.81 and 1.24 g O_3 g^{-1} DOC, respectively. The slowly-reacting bezafibrate was detected in the influent on three sampling days, and was oxidized below the LOQ at the three highest ozone doses ≥ 0.60 g O_3 g^{-1} DOC (Figure S3.2).

3.3.3 Prediction of micropollutant oxidation based on a model coupling reactor hydraulics with ozone chemistry and reaction kinetics

The modeled ozone and hydroxyl radical concentration profiles for the two ozone doses 0.41 and 0.74 g O_3 g^{-1} DOC are illustrated in Figure 3.4. The relatively high number of reactors in the CSTR cascades (Table S3.4) indicates that the ozone reactor behaves similar to a plug flow reactor (PFR) after the first compartment. Hence, the ozone reactor was also modeled as a PFR by combining eqs 3.1, 3.2 and 3.3 to determine the influence of the hydraulic model on the prediction of ozone concentration profiles and micropollutant oxidation. The CSTR and PFR models predicted very similar ozone profiles, showing that the hydraulic model structure was of minor importance for this specific ozone reactor. Resulting ozone exposures were predicted to be 60 % (0.41 g O_3 g^{-1} DOC) and 26 % (0.74 g O_3 g^{-1} DOC) lower by the hydraulic models than for the full-scale measurements (Figure 3.4). Based on the lower ozone exposures and eq. 3.3, the modeled hydroxyl radical exposures were significantly smaller than the effective exposures in the full-scale system. The different ozone addition and mixing in the full-scale reactor (bubble column, non-homogeneously mixed) compared to the batch reactor (dosage of a stock solution, homogeneously mixed) may have affected the ozone behavior during the second phase of ozone decay, leading to different k_{O_3} values in both

set-ups. However, differences in the initial phase of ozone decay (first ~ 20 s, *(38)*) can be excluded as a factor for the observed deviations of the ozone profiles because the ozone decay in the full-scale ozone reactor already followed the second phase of ozone decay at the starting point of the hydraulic model (P2: HRT 18 s relative to P1), and can hence be described by k_{O_3} *(29)*.

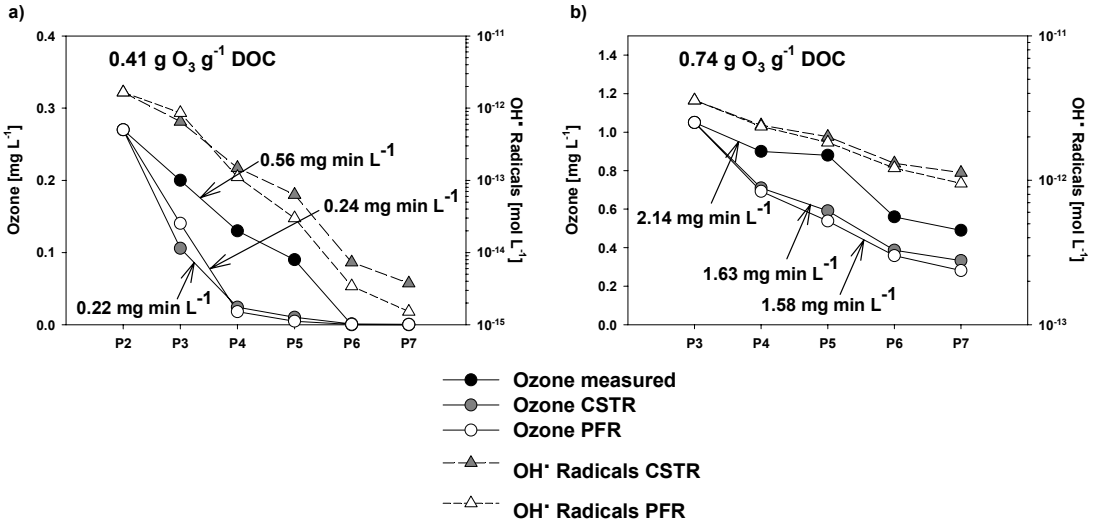

Figure 3.4. Measured ozone (black circles) and modeled ozone and hydroxyl radical profiles for the continuously stirred tank reactor (CSTR) model (grey circles and triangles) and the plug flow reactor (PFR) model (open circles and triangles) along the ozone reactor (P2/P3 - P7) for an ozone dose of a) 0.41 g O_3 g^{-1} DOC and b) 0.74 g O_3 g^{-1} DOC. Measured and modeled standard deviations are given but smaller than the respective symbols. The ozone exposures from P2/P3 to P7 are indicated in mg min L^{-1}. Storm weather conditions occurred during the 0.74 g O_3 g^{-1} DOC campaign, leading to a HRT of only 3-4 min (Table S3.2) and a DOC of 3.4 mg L^{-1} (Table 3.1).

Figure 3.5 shows the results of the CSTR and PFR models for benzotriazole and atenolol. As for the ozone profiles, predictions by the PFR model were very similar to the CSTR model. For an ozone dose of 0.41 g O_3 g^{-1} DOC, the measured and predicted values correlated well, while for an ozone dose of 0.74 g O_3 g^{-1} DOC, model predictions were about a factor of 2.5 higher than full-scale measurements. Monte Carlo simulations showed that deviations between measurements and model predictions were larger than

model uncertainties (standard deviations CSTR and PFR models, Figure 3.5). This is independent evidence that the model overestimated micropollutant oxidation for the ozone dose of 0.74 g O_3 g^{-1} DOC.

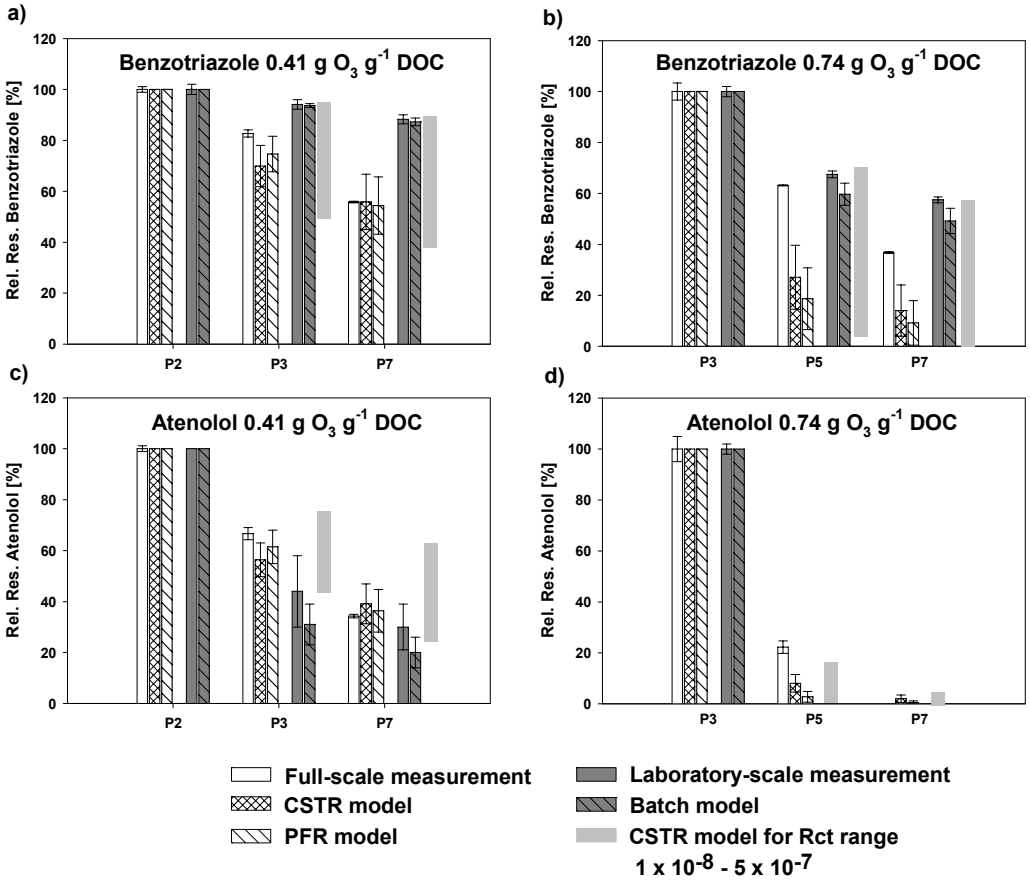

Figure 3.5. Relative residual micropollutant concentrations in various scenarios for benzotriazole with a) 0.41 and b) 0.74 g O_3 g^{-1} DOC and for atenolol with c) 0.41 and d) 0.74 g O_3 g^{-1} DOC starting from sampling point P2 or P3. Abbreviations: CSTR Model = Continuously Stirred Tank Reactor Model; PFR Model = Plug Flow Reactor Model. Laboratory-scale measurements were carried out in a batch experiment with secondary effluent from WWTP Wüeri under the same experimental conditions (ozone dose, pH, temperature) as in the full-scale measurement. The batch model is based on oxidant exposures determined during laboratory-scale measurements. Error bars from full- and laboratory-scale measurements were calculated by linear error propagation derived from duplicate measurements. Standard deviations of CSTR and PFR model predictions were calculated by Monte Carlo simulations.

The underestimation of oxidant exposures (Figure 3.4) should have led to underestimation of micropollutant oxidation in the model predictions. However, the contrary was observed. Therefore, counteracting processes must have lowered micropollutant oxidation in wastewater at the full-scale level, to compensate for the underestimation of oxidant exposures in the model predictions. Huber et al. *(5)* attributed the overestimation of micropollutant oxidation based on ozone and hydroxyl radical exposures to sorption of some compounds to sludge particles or the interaction with colloids which might offer some protection against ozone attack. We did not distinguish between micropollutants in the colloidal (particles between 1 nm and 1 µm) and dissolved phase in this study, but micropollutants in both phases were concentrated on and eluted from SPE cartridges *(39)*. The deviations between model predictions and measurements for benzotriazole and atenolol at a dose of 0.74 g O_3 g^{-1} DOC correspond to 45 % and 19 % at P5, respectively, and to 22 % for benzotriazole at P7. These deviations are in the range of the percentage of chemicals sorbed to aquatic colloids *(40,41)*. Since both benzotriazole and atenolol show sorption capabilities *(42,43)*, it might be possible that these micropollutants were protected from ozone attack by the interaction with aquatic colloids.

In contrast to these slower-reacting substances, fast-reacting substances with a k_{O_3} > 10^4 M^{-1} s^{-1} were already completely oxidized within the first compartment of the ozone reactor (section 3.3.2). This may be attributed to their intrinsic fast oxidation, leading to lower concentrations in the aqueous phase. This in turn causes a shift in the colloid/micropollutant equilibrium leading to quick desorption of micropollutants from colloids. Maskaoui et al. *(41)* determined 5 min to be sufficient to reach the colloid/pharmaceutical equilibrium. Although desorption kinetics have not been reported, quick desorption and subsequent fast oxidation by ozone are possible, leading to the observed oxidation of fast-reacting micropollutants below the LOQ in both the colloidal and dissolved phase. The same processes (sorption equilibrium, oxidation, desorption, further oxidation) apply to slower-reacting micropollutants as well. However, micropollutant desorption from the colloidal to the aqueous phase is much slower due to a slower oxidation of these compounds in aqueous solution.

In addition, model predictions were calculated based on minimum and maximum R_{ct} values (1×10^{-8} - 5×10^{-7}) determined in secondary effluent from WWTP Wüeri sampled under varying weather conditions over a period of 16 months (light grey bars, Figure 3.5). These calculations show that the R_{ct} value is highly important for the oxidation of slowly reacting micropollutants, since hydroxyl radicals contribute significantly to their oxidation. Predictions for the relative residual concentrations at P7 for the two modeled ozone doses varied from 39 to 93 % and 0 to 58 % for benzotriazole, respectively, and from 27 to 64 % and 0 to 6 % for atenolol, respectively. Hence, differences between the R_{ct} value in the full-scale reactor and laboratory batch experiments could directly contribute to the observed variations. Different R_{ct} values may be derived from different modes of ozone addition and mixing in the full-scale reactor (bubble column, non-homogeneously mixed) compared to the batch experiment (dosage of a stock solution, homogeneously mixed).

In conclusion, the two counteracting processes i) underestimation of modeled oxidant exposures (leading to an underestimation of micropollutants oxidation in the hydraulic model) and ii) protection of the sorbed micropollutants fraction from ozone attack (leading to an overestimation of micropollutants oxidation in the hydraulic model) may have compensated each other to varying extents. In combination with possibly different R_{ct} values in the full-scale vs. batch reactor, this resulted in a good prediction of micropollutants oxidation for the 0.41 g O_3 g^{-1} DOC dose, and in an overestimation within the factor of 2.5 for the 0.74 g O_3 g^{-1} DOC dose. The factor of 2.5 hence represents the range of possible deviations of the hydraulic model from the full-scale measurements at the ozone reactor at WWTP Wüeri in Regensdorf.

3.3.4 Prediction of full-scale micropollutant oxidation by laboratory-scale batch experiments

Figure 3.5 illustrates that micropollutant oxidation derived from laboratory-scale batch experiments and the respective laboratory-scale predictions based on eq 3.4 are in good agreement, but deviate up to a factor of 1.5 from full-scale measurements. Since different wastewater grab samples were used during laboratory- and full-scale experiments, and the comparison was based on the same ozone exposures, the R_{ct} value was identified as a major source for the observed deviations. It was 3 to 5 times lower in the batch experiments (data not shown) compared to batch experiments with wastewater from the full-scale sampling campaigns. Hence, it is highly important to determine the possible range of R_{ct} values, which strongly depends on the organic and inorganic matrix, of a specific wastewater under all conditions (rain, temperature, season, daytime). Due to the important contribution of hydroxyl radicals to the oxidation of slowly-reacting micropollutants, the R_{ct} is a critical parameter for these cases. This is underlined by a recent study investigating the uncertainty during micropollutant ozonation *(44)*. The R_{ct} value (and not k_{P,O_3} or $k_{P,OH\bullet}$) was found to be the most influential parameter for slowly-reacting substances, while the accuracy of the hydraulic model of a reactor was determined to be most important for fast-reacting substances.

Finally, the complete oxidation of the fast-reacting substances carbamazepine, diclofenac, sulfamethoxazole and 17α-ethinylestradiol ($k_{O_3,17\alpha\text{-ethinylestradiol}}$ = 1.6 x 10^6 M^{-1} s^{-1} at pH 7 *(45)*) in the laboratory-scale batch experiments was achieved for ozone exposures occurring at P2/P3 during full-scale sampling campaigns (data not shown), and is in accordance with full-scale measurements. Micropollutants interacting with colloids were of minor importance within the batch experiments since their respective concentrations in the aqueous phase were much higher (spiking of micropollutants), and accordingly, the fraction of micropollutants interacting with colloids was much lower. In addition, low residual concentrations could not be detected due to higher LOQs of the LC-UV/FL method as compared to the online-SPE-LC-MS/MS method.

3.3.5 Oxidation by-products

Bromate, a potential human carcinogen, forms during ozonation of bromide-containing waters through a combination of reactions involving ozone and secondary oxidants such as hydroxyl and carbonate radicals *(12)*. Bromide levels in the influent to the ozone reactor varied from 6 µg L^{-1} (due to dilution) to 32 µg L^{-1} (Table S3.2). These values are in accordance with low bromide levels (< 5 – 50 µg L^{-1}) found in a survey of 85 water resources for drinking water treatment in Switzerland *(46)*. Figure 3.6a shows that only ozone doses ≥ 0.74 g O_3 g^{-1} DOC yielded bromate concentrations above the LOQ of 2 µg L^{-1}. Bromate formation is a slow process *(12)*, reflected in a bromate increase from P3 to P7 for the highest ozone dose. As expected, aerobic sand filtration did not remove bromate. The final bromate concentrations (max. 7.5 µg L^{-1}) were below the drinking water standard of 10 µg L^{-1} for all ozone doses and hence also below a proposed ecotoxicological threshold value of 3 mg L^{-1} *(47)*.

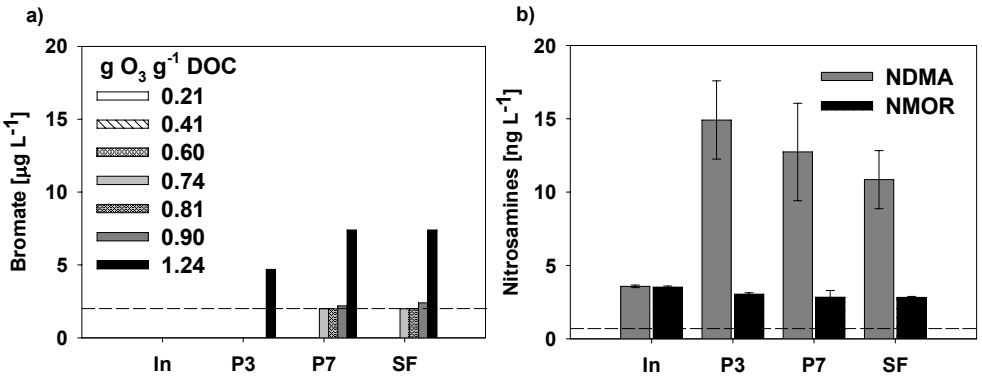

Figure 3.6. Oxidation by-products concentrations in the influent to the ozone reactor (IN), along the ozone reactor (P3, P7) and after sand filtration (SF): a) Bromate concentrations for seven ozone doses ranging from 0.21 to 1.24 g O_3 g^{-1} DOC. The limit of quantification (LOQ) was 2 µg L^{-1} and bromide concentrations varied between 6 - 32 µg L^{-1} (Table S3.2). b) *N*-nitrosodimethylamine (NDMA) and *N*-nitrosomorpholine (NMOR) concentrations for an ozone dose of 1.24 g O_3 g^{-1} DOC (LOQ = 1 ng L^{-1}). Error bars were calculated by linear error propagation derived from duplicate measurements. Note the different concentration units in Figures a) and b).

The concentrations of NDMA and NMOR in the reactor are illustrated in Figure 3.6b for the highest ozone dose (1.24 g O_3 g^{-1} DOC). A previous study showed that NDMA formation from secondary effluent did not correlate with the ozone dose *(8)* and might strongly depend on the concentrations and conversion rate of precursors as well as matrix composition. In the present study, NDMA formation was observed to be a fast process (strong increase up to P3), which was followed by a slight decrease within the ozone reactor to P7. The fast formation of NDMA points towards specific precursors rather than moieties of DOM as precursors *(48)*. As observed in a previous study *(8)*, sand filtration resulted in a decrease of NDMA concentration due to biodegradation, leading to concentrations slightly above the notification level of 10 ng L^{-1} for NDMA in drinking water in California *(49)*. An ecotoxicological threshold value does currently not exist for NDMA. In contrast to NDMA, neither ozonation nor sand filtration did have an influence on NMOR concentrations (Figure 3.6b).

3.3.6 AOC formation

Figure 3.7a shows that the AOC levels in the secondary effluent varied between 40 to 200 µg L^{-1}, which is in the range of concentrations found in lake water *(16)*. Hence, AOC was either not completely consumed during biological wastewater treatment or it might have been released from lysating cells due to a natural turnover of the microbial sewage sludge community. During ozonation, AOC levels increased up to a factor of 6, reaching a maximum concentration of 740 µg L^{-1}. AOC formation was a fast process since no substantial increase was observed after the initial increase at P1. Similar results were found during ozonation of lake water *(16)*. Still, no clear trend could be found when correlating AOC formation with the ozone dose, ozone exposure or influent AOC concentrations. The rapid sand filter finally decreased the AOC levels by 14 - 46 %, leading to AOC concentrations above the level before ozonation in some cases, as previously observed for ozonated drinking water followed by GAC/sand filtration *(50)*. Interestingly, the AOC levels after sand filtration depended on the wastewater temperature, and not on the AOC levels prior to sand filtration. AOC levels after sand filtration of 390 – 440 µg L^{-1} were found in April 2008 (wastewater temperature 13 °C), while 120 – 150 µg L^{-1} AOC were determined in August 2008 (wastewater temperature 20 - 22 °C).

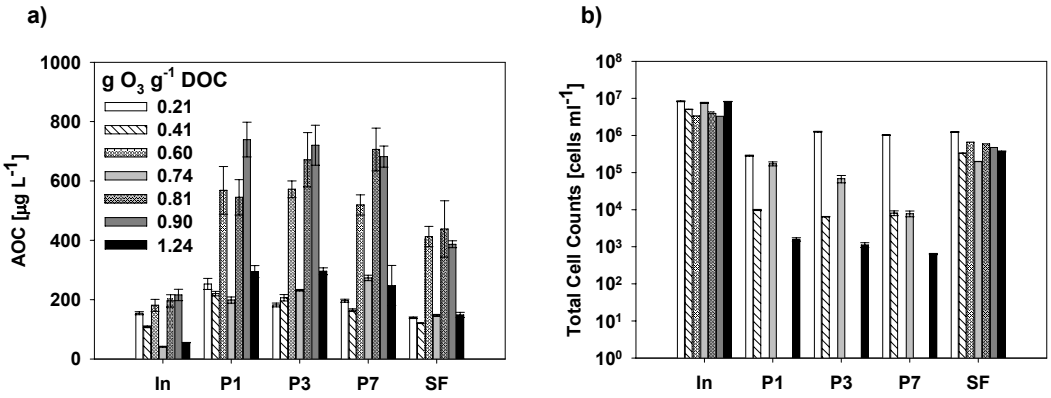

Figure 3.7. a) Assimilable organic carbon (AOC) concentrations and b) total cell counts (TCC) for seven ozone doses ranging from 0.21 to 1.24 g O_3 g^{-1} DOC in the influent to the ozone reactor (IN), along the ozone reactor (P1, P3, P7) and after sand filtration (SF). Error bars indicate standard deviations based on triplicate measurements.

3.3.7 Removal of total cell counts (TCC) and *E. coli*

Ozone is an excellent disinfectant and inactivates a broad range of microorganisms *(12)*. TCC in the influent to the ozone reactor were relatively stable and varied from 3.3 – 8.4 x 10^6 cells ml^{-1} (Figure 3.7b), as determined by flow cytometry. Ozonation decreased TCC by 1 - 4.5 log units, not consistently correlating with the ozone doses. A distinct regrowth of TCC was observed during sand filtration, since AOC formed during ozonation could act as a carbon source for microorganisms which were subsequently released from the sand filter. The release of TCC from the sand filter seemed to be independent of the TCC or AOC level after ozonation (Figure 3.7) and ΔTCC could not be correlated with ΔAOC concentrations (data not shown). Overall, TCC could be lowered by 0.5 to 1.5 log units by the combination of ozonation and sand filtration.

E. coli concentrations were lowered by 0.5 to 2.5 log units during ozonation (Figure 3.8, Table S3.2), and only partially correlated with the ozone exposure (Table 3.1). After a fast initial inactivation during the first compartment of the ozone reactor up to P3, *E. coli* was not further eliminated substantially from P3 to P7. This was unexpected for ozone doses ≥ 0.41 g O_3 g^{-1} DOC since dissolved ozone was still apparent from P3 to P7. *E. coli* inactivation by ozone is a fast process and well predicted in drinking water treatment based on the concept of reactor hydraulics coupled with ozone chemistry and

reaction kinetics *(12)*. However, in the present study, the same concept applied to wastewater treatment strongly overestimated *E. coli* inactivation (Figure S3.3). The water fraction of 0.1 % short-circuiting directly to P7 cannot be the main reason for the large discrepancy. In a worst case scenario with 0.1 % of the water not getting in contact with ozone at all, a maximum *E. coli* inactivation of 3 log units would be achieved. In case of the short-circuiting water packages getting in contact with ozone, the overall expected inactivation should be higher. However, a maximum inactivation of ~ 0.5 log units from P3 to P7 was observed (Figure S3.3). The large differences between measured and modeled *E. coli* inactivation can hence be explained by the shielding of *E. coli* in activated sludge flocs, which can experience lower ozone exposures than the aqueous solution *(5)*. Accordingly, *E. coli* present in activated sludge flocs might not be inactivated during ozonation, but could be released from the activated sludge flocs at a later stage and lead to a positive result in plating techniques. Finally, no regrowth of *E. coli* was observed upon sand filtration. Combining ozonation and sand filtration is hence an efficient barrier against *E. coli* and possibly other pathogens.

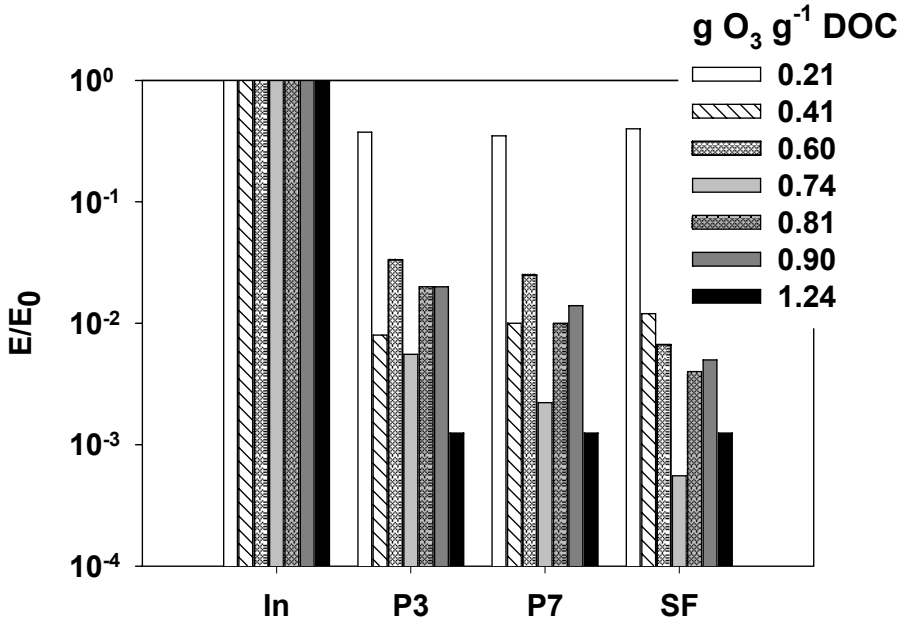

Figure 3.8. Relative residual concentrations of *Escherichia coli (E. coli)* for seven ozone doses ranging from 0.21 to 1.24 g O_3 g^{-1} DOC in the influent to the ozone reactor (IN), along the ozone reactor (P3 - P7) and after sand filtration (SF).

3.4 Conclusions

- The predicted oxidation of slowly-reacting micropollutants based on coupling reactor hydraulics with ozone chemistry and reaction kinetics was up to a factor of 2.5 higher than full-scale measurements. This overestimation was attributed to a protection of micropollutants from ozone attack by the interaction with aquatic colloids in the real system.
- Laboratory-scale batch experiments using wastewater from the same full-scale WWTP could predict the oxidation of slowly-reacting micropollutants ($k_{O_3} < 10^4$ M^{-1} s^{-1}) on the full-scale level within a factor of 1.5. The R_{ct} value (depending strongly on the organic and inorganic wastewater matrix) was identified as a major source to this deviation. Hence, it is important to determine the spectrum of R_{ct} values for various conditions in wastewater of a specific WWTP. Oxidation of fast-reacting substances could be well predicted since their oxidation does not significantly depend on the formation of hydroxyl radicals.
- An increase in bromate and NDMA concentrations to non-problematic levels was observed during ozonation, while no influence on NMOR concentrations could be shown. AOC was formed during ozonation of wastewater of up to 740 µg L^{-1} and subsequently degraded by up to 46 % during rapid sand filtration. Along with the slight decrease of NDMA during sand filtration, this finding highlights the importance of sand filtration after an ozonation step for removal of oxidation by-products (AOC, NDMA).
- Disinfection during ozonation in the full-scale reactor was demonstrated by the fast decrease of TCC and inactivation of *E. coli*. However, predictions of *E. coli* inactivation did strongly deviate from full-scale measurements, which can be attributed to the shielding of *E. coli* by activated sludge flocs.

Acknowledgements

This study was part of the project Strategy MicroPoll funded by the Swiss Federal Office for the Environment (FOEN). Support for S. G. Zimmermann was provided by the EU project Neptune (Contract No 036845, SUSTDEV-2005-3.II.3.2), which was financially supported by grants obtained from the EU Commission within the Energy, Global Change and Ecosystems Program of the Sixth Framework (FP6-2005-Global-4). The authors gratefully acknowledge S. Brocker and D. Rensch for installation and help with maintenance of the ozone reactor, the staff at WWTP Wüeri for general support, S. Koepke for SPE-LC-MS/MS measurements, E. Salhi for laboratory assistance and bromate measurements, F. Hammes and H. P. Füchslin for AOC and TCC determination, E. Gansner and M. Koch for *E. coli* measurements, J. Helbing and C. Abegglen for help with the tracer tests, M. Gresch for support during modeling, and J. L. Kormos for language corrections. The authors also thank CWQRC at Curtin University, Australia, and BfG, Germany, where the modeling and writing took place, Jaehong Kim for fruitful discussions as well as two anonymous reviewers for their helpful comments.

3.5 References

(1) Westerhoff, P.; Yoon, Y.; Snyder, S.; Wert, E. Fate of endocrine-disruptor, pharmaceutical, and personal care product chemicals during simulated drinking water treatment processes. *Environ. Sci. Technol.* **2005**, *39*, 6649-6663.

(2) Ternes, T. A.; Meisenheimer, M.; McDowell, D.; Sacher, F.; Brauch, H. J.; Gulde, B. H.; Preuss, G.; Wilme, U.; Seibert, N. Z. Removal of pharmaceuticals during drinking water treatment. *Environ. Sci. Technol.* **2002**, *36*, 3855-3863.

(3) Wert, E. C.; Rosario-Ortiz, F. L.; Snyder, S. A. Using Ultraviolet Absorbance and Color To Assess Pharmaceutical Oxidation during Ozonation of Wastewater. *Environ. Sci. Technol.* **2009**, *43*, 4858-4863.

(4) Wert, E. C.; Rosario-Ortiz, F. L.; Snyder, S. A. Effect of ozone exposure on the oxidation of trace organic contaminants in wastewater. *Water Res.* **2009**, *43*, 1005-1014.

(5) Huber, M. M.; Göbel, A.; Joss, A.; Hermann, N.; Löffler, D.; McArdell, C. S.; Ried, A.; Siegrist, H.; Ternes, T. A.; von Gunten, U. Oxidation of pharmaceuticals during ozonation of municipal wastewater effluents: A pilot study. *Environ. Sci. Technol.* **2005**, *39*, 4290-4299.

(6) Ternes, T. A.; Stuber, J.; Herrmann, N.; McDowell, D.; Ried, A.; Kampmann, M.; Teiser, B. Ozonation: a tool for removal of pharmaceuticals, contrast media and musk fragrances from wastewater? *Water Res.* **2003**, *37*, 1976-1982.

(7) Nakada, N.; Shinohara, H.; Murata, A.; Kiri, K.; Managaki, S.; Sato, N.; Takada, H. Removal of selected pharmaceuticals and personal care products (PPCPs) and endocrine-disrupting chemicals (EDCs) during sand filtration and ozonation at a municipal sewage treatment plant. *Water Res.* **2007**, *41*, 4373-4382.

(8) Hollender, J.; Zimmermann, S. G.; Koepke, S.; Krauss, M.; McArdell, C. S.; Ort, C.; Singer, H.; von Gunten, U.; Siegrist, H. Elimination of organic micropollutants in a municipal wastewater treatment plant upgraded with a full-scale post-ozonation followed by sand filtration. *Environ. Sci. Technol.* **2009**, *43*, 7862-7869.

(9) Dodd, M. C.; Kohler, H. P. E.; von Gunten, U. Oxidation of antibacterial compounds by ozone and hydroxyl radical: elimination of biological activity during aqueous ozonation processes. *Environ. Sci. Technol.* **2009**, *43*, 2498-2504.

(10) Huber, M. M.; Ternes, T. A.; von Gunten, U. Removal of estrogenic activity and formation of oxidation products during ozonation of 17 alpha-ethinylestradiol. *Environ. Sci. Technol.* **2004**, *38*, 5177-5186.

(11) Lee, Y.; Escher, B. I.; von Gunten, U. Efficient Removal of Estrogenic Activity during Oxidative Treatment of Waters Containing Steroid Estrogens. *Environ. Sci. Technol.* **2008**, *42*, 6333-6339.

(12) von Gunten, U. Ozonation of drinking water: Part II. Disinfection and by-product formation in presence of bromide, iodide or chlorine. *Water Res.* **2003**, *37*, 1469-1487.

(13) Schmidt, C. K.; Brauch, H.-J. *N,N*-Dimethylsulfamide as Precursor for *N*-Nitrosodimethylamine (NDMA) Formation upon Ozonation and its Fate During Drinking Water Treatment. *Environ. Sci. Technol.* **2008**, *42*, 6340-6346.

(14) Yang, L.; Chen, Z. L.; Shen, J. M.; Xu, Z. Z.; Liang, H.; Tian, J. Y.; Ben, Y.; Zhai, X.; Shi, W. X.; Li, G. B. Reinvestigation of the Nitrosamine-Formation Mechanism during Ozonation. *Environ. Sci. Technol.* **2009**, *43*, 5481-5487.

(15) Zhao, Y. Y.; Boyd, J. M.; Woodbeck, M.; Andrews, R. C.; Qin, F.; Hrudey, S. E.; Li, X. F. Formation of *N*-nitrosamines from eleven disinfection treatments of seven different surface waters. *Environ. Sci. Technol.* **2008**, *42*, 4857-4862.

(16) Hammes, F.; Salhi, E.; Koster, O.; Kaiser, H. P.; Egli, T.; von Gunten, U. Mechanistic and kinetic evaluation of organic disinfection by-product and assimilable organic carbon (AOC) formation during the ozonation of drinking water. *Water Res.* **2006**, *40*, 2275-2286.

(17) Escher, B. I.; Bramaz, N.; Ort, C. Monitoring the treatment efficiency of a full scale ozonation on a sewage treatment plant with a mode-of-action based test battery *J. Environ. Monit.* **2009**, *11*, 1836-1846.

(18) Stalter, D.; Magdeburg, A.; Weil, M.; Knacker, T.; Oehlmann, J. Toxication or detoxication? In vivo toxicity assessment of ozonation as advanced wastewater treatment with the rainbow trout. *Water Res.* **2009**, *44*, 439-448.

(19) von Gunten, U.; Elovitz, M.; Kaiser, H. P. Characterization of ozonation processes with conservative and reactive tracers: prediction of the degradation of micropollutants. *Analusis* **1997**, *25*, 29-31.

(20) von Gunten, U.; Elovitz, M.; Kaiser, H. P. Calibration of full-scale ozonation systems with conservative and reactive tracers. *J. Water Supply Res. Technol., AQUA* **1999**, *48*, 250-256.

(21) Boller, M.; von Gunten, U.; Pianta, R.; Solcà, L. In *9th Gothenburg Symposium: Chemical Water and Wastewater Treatment VI*; Springer, Berlin: Istanbul, Turkey, 2000; pp 125-136.

(22) Gallard, H.; von Gunten, U.; Kaiser, H. P. Prediction of the disinfection and oxidation efficiency of full-scale ozone reactors. *J. Water Supply Res. Technol., AQUA* **2003**, *52*, 277-290.

(23) Krauss, M.; Hollender, J. Analysis of nitrosamines in wastewater: Exploring the trace level quantification capabilities of a hybrid linear ion trap/orbitrap mass spectrometer. *Anal. Chem.* **2008**, *80*, 834-842.

(24) Salhi, E.; von Gunten, U. Simultaneous determination of bromide, bromate and nitrite in low mu g 1(-1) levels by ion chromatography without sample pretreatment. *Water Res.* **1999**, *33*, 3239-3244.

(25) Mikrobiologie. In *Schweizerisches Lebensmittelhandbuch*; Ettel, W., Ed.; Bundesamt für Gesundheit: Bern, 2000.

(26) Hammes, F.; Berney, M.; Wang, Y. Y.; Vital, M.; Koster, O.; Egli, T. Flow-cytometric total bacterial cell counts as a descriptive microbiological parameter for drinking water treatment processes. *Water Res.* **2008**, *42*, 269-277.

(27) Hammes, F. A.; Egli, T. New method for assimilable organic carbon determination using flow-cytometric enumeration and a natural microbial consortium as inoculum. *Environ. Sci. Technol.* **2005**, *39*, 3289-3294.

(28) Hoigné, J.; Bader, H. Characterization of Water-Quality Criteria for Ozonation Processes. 2. Lifetime of Added Ozone. *Ozone-Sci. Eng.* **1994**, *16*, 121-134.

(29) von Gunten, U. Ozonation of drinking water: Part I. Oxidation kinetics and product formation. *Water Res.* **2003**, *37*, 1443-1467.

(30) Elovitz, M. S.; von Gunten, U. Hydroxyl radical ozone ratios during ozonation processes. I-The R-ct concept. *Ozone-Sci. Eng.* **1999**, *21*, 239-260.

(31) Hoigné, J.; Bader, H. Rate Constants of Reactions of Ozone with Organic and Inorganic-Compounds in Water. 1. Non-Dissociating Organic-Compounds. *Water Res.* **1983**, *17*, 173-183.

(32) University of California. *Berkeley Madonna*; 2001.

(33) Lutze, H. Ozonung von Benzotriazolen. *Bachelor Thesis* **2005**, Universität Duisburg - Essen.

(34) Naik, D. B.; Moorthy, P. N. Studies on the Transient Species Formed in the Pulse-Radiolysis of Benzotriazole. *Radiat. Phys. Chem.* **1995**, *46*, 353-357.

(35) Benner, J.; Salhi, E.; Ternes, T.; von Gunten, U. Ozonation of reverse osmosis concentrate: Kinetics and efficiency of beta blocker oxidation. *Water Res.* **2008**, *42*, 3003-3012.

(36) Karpel Vel Leitner, N.; Roshani, B. Kinetic of benzotriazole oxidation by ozone and hydroxyl radical. *Water Res.* **2010**, *44*, 2058-2066.

(37) Helbing, J.; Gresch, M.; von Gunten, U. Fluorescein as an easy to use tracer for analysis of treatment trains, *in preparation*.

(38) Buffle, M. O.; Schumacher, J.; Salhi, E.; Jekel, M.; von Gunten, U. Measurement of the initial phase of ozone decomposition in water and wastewater by means of a continuous quench-flow system: Application to disinfection and pharmaceutical oxidation. *Water Res.* **2006**, *40*, 1884-1894.

(39) Zhang, Z. L.; Zhou, J. L. Simultaneous determination of various pharmaceutical compounds in water by solid-phase extraction-liquid chromatography-tandem mass spectrometry. *J. Chromatogr. A* **2007**, *1154*, 205-213.

(40) Zhou, J. L.; Liu, R.; Wilding, A.; Hibberd, A. Sorption of selected endocrine disrupting chemicals to different aquatic colloids. *Environ. Sci. Technol.* **2007**, *41*, 206-213.

(41) Maskaoui, K.; Hibberd, A.; Zhou, J. L. Assessment of the interaction between aquatic colloids and pharmaceuticals facilitated by cross-flow ultrafiltration. *Environ. Sci. Technol.* **2007**, *41*, 8038-8043.

(42) Yamamoto, H.; Nakamura, Y.; Moriguchi, S.; Nakamura, Y.; Honda, Y.; Tamura, I.; Hirata, Y.; Hayashi, A.; Sekizawa, J. Persistence and partitioning of eight selected pharmaceuticals in the aquatic environment: Laboratory photolysis, biodegradation, and sorption experiments. *Water Res.* **2009**, *43*, 351-362.

(43) Hinterbuchner, T. Das Verhalten von Benzotriazolen in Abwasser-reinigungsanlagen. *Diploma Thesis* **2006**, Fachhochschule Wels, Wels.

(44) Neumann, M. B.; Gujer, W.; von Gunten, U. Global sensitivity analysis for model-based prediction of oxidative micropollutant transformation during drinking water treatment. *Water Res.* **2009**, *43*, 997-1004.

(45) Deborde, M.; Rabouan, S.; Duguet, J.-P.; Legube, B. Kinetics of Aqueous Ozone-Induced Oxidation of Some Endocrine Disruptors. *Environ. Sci. Technol.* **2005**, *39*, 6086-6092.

(46) von Gunten, U.; Salhi, E. Bromate in drinking water a problem in Switzerland? *Ozone: Sci. Eng.* **2003**, *25*, 159-166.

(47) Hutchinson, T. H.; Hutchings, H. J.; Moore, K. W. A review of the effects of bromate on aquatic organisms and toxicity of bromate to oyster (Crassostrea gigas) embryos. *Ecotoxicol. Environ. Saf.* **1997**, *38*, 238-243.

(48) von Gunten, U.; Salhi, E.; Schmidt, C. K.; Arnold, W. A. Kinetics and Mechanisms of *N*-Nitrosodimethylamine Formation upon Ozonation of *N,N*-Dimethylsulfamide-Containing Waters: Bromide Catalysis. *Environ. Sci. Technol.* **2010**, *44*, 5762-5768.

(49) California Department of Public Health. NDMA and other nitrosamines - Drinking water issues. 2009, http://www.cdph.ca.gov/certlic/drinkingwater /Pages/NDMA.aspx. December, 15, 2009.

(50) van der Kooij, D.; Hijnen, W. A. M.; Kruithof, J. C. The effects of ozonation, biological filtration and distribution on the concentration of easily assimilable organic carbon (AOC) in drinking water. *Ozone-Sci. Eng.* **1989**, *11*, 297-311.

Supporting Information for Chapter 3

Kinetic assessment and modeling of an ozonation step for full-scale municipal wastewater treatment: Micropollutant oxidation, by-product formation and disinfection

4 tables, 3 figures and 2 texts

Reprinted from *Water Research* 45 (2), Zimmermann, S.G.; Wittenwiler, M.; Hollender, J.; Krauss, M.; Ort, C.; Siegrist, H.; von Gunten, U., Kinetic assessment and modeling of an ozonation step for full-scale municipal wastewater treatment: Micropollutant oxidation, by-product formation and disinfection, 605-617.

http://www.sciencedirect.com/science/article/pii/S0043135410005634

Table S3.1. Micropollutants analyzed with CAS number, structure and limit of quantification (LOQ) of the analytical method

Substance	CAS-Nr.	Structure	LOQ		
			Ozonation Influent [ng/L]	Ozonation Effluent [ng/L]	Sand filtration [ng/L]
Atenolol	29122-86-7	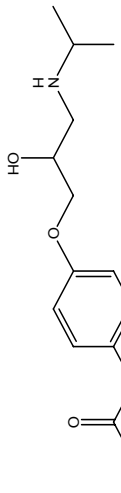	12	8	6
Benzotriazole	95-14-7	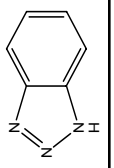	56	52	51
Bezafibrate	41859-67-0	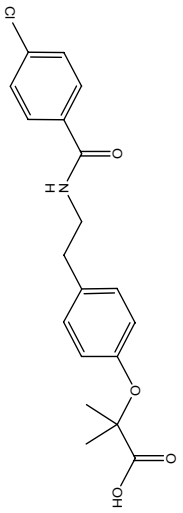	20	20	20
Carbamazepine	298-46-4	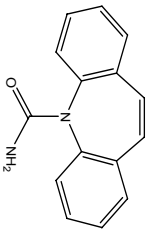	7	6	5
Clarithromycin	81103-11-9	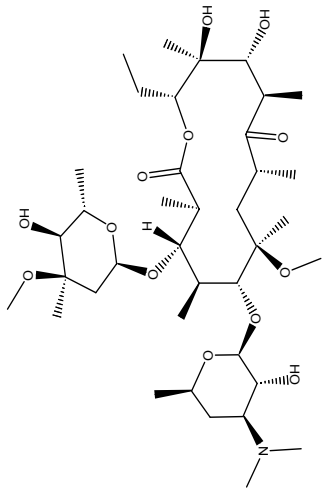	4	3	3

Substance	CAS-Nr.	Structure	LOQ Ozonation Influent [ng/L]	LOQ Ozonation Effluent [ng/L]	LOQ Sand filtration [ng/L]
Clindamycin	21462-39-5	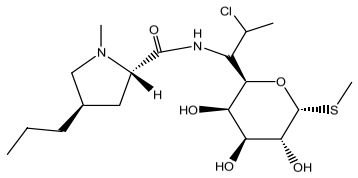	5	5	5
Clofibric Acid	882-09-7	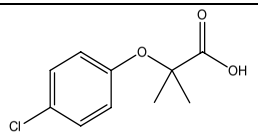	10	10	10
Diclofenac	15307-86-5	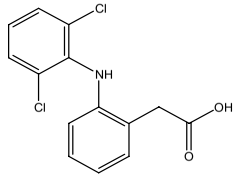	6	5	5
Erythromycin	114-07-8	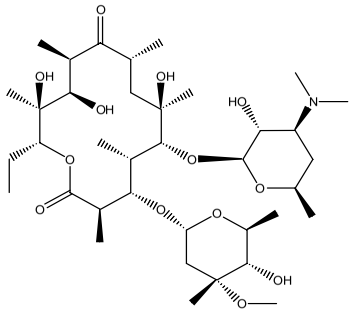	19	15	10
Ibuprofen	15687-27-1	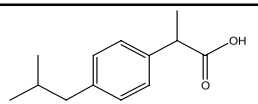	80	20	20
Mefenamic Acid	61-68-7	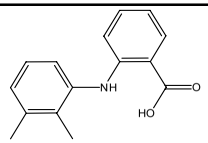	13	12	11

Substance	CAS-Nr.	Structure	LOQ		
			Ozonation Influent [ng/L]	Ozonation Effluent [ng/L]	Sand filtration [ng/L]
5-Methyl-Benzotriazole	136-85-6	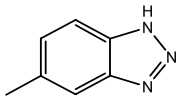	22	20	20
Metoprolol	56392-17-7	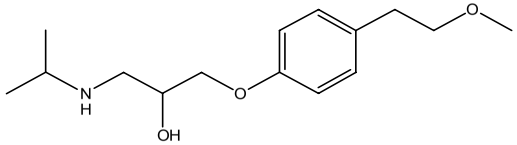	53	42	39
Naproxen	22204-53-1	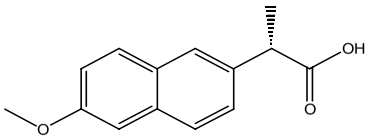	21	20	19
N-nitrosodimethylamine	62-75-9	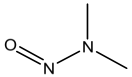	2	2	2
N-nitrosomorpholine	59-89-2	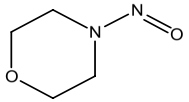	2	2	2
Paracetamol	103-90-2	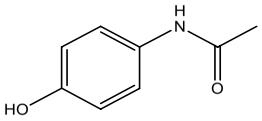	590	118	106
Phenanzone	60-80-0	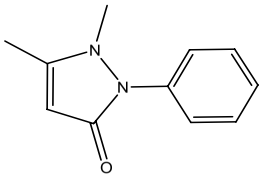	10	8	7

Substance	CAS-Nr.	Structure	LOQ		
			Ozonation Influent	Ozonation Effluent	Sand filtration
			[ng/L]	[ng/L]	[ng/L]
Sotalol	959-24-0	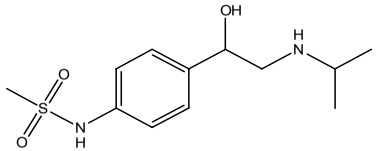	31	24	19
Sulfadiazine	68-35-9	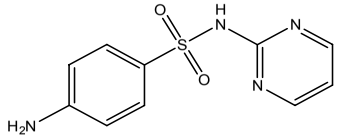	100	35	35
Sulfamethazine	57-68-1	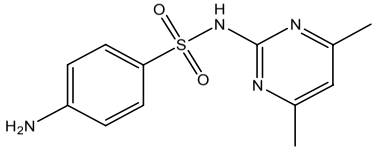	3	2	2
Sulfamethoxazole	723-46-6	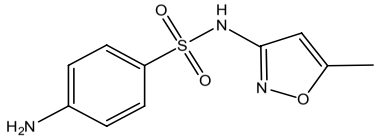	11	11	11
Sulfapyridine	144-83-2	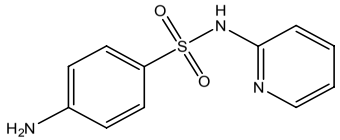	12	11	11
Trimethoprim	738-70-5	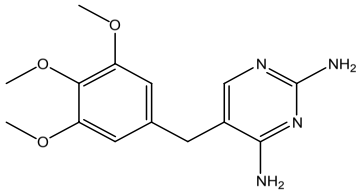	21	15	14

Text S3.1. Tracer tests

The breakthrough curves from both the Dirac pulse tracer tests and the continuous tracer test were monitored by a fiber-optical multi-port fluorometer at P1 to P7 *(1)*. The wastewater (35 to 250 L s^{-1}) and process gas flows (15 and 20 m^3 h^{-1}) were varied during the Dirac pulse tracer tests, and the process gas was injected as oxygen because ozone oxidizes fluoresceine. The hydraulic retention times (HRT) were calculated from the centers of mass using the software R *(2)* and the breakthrough curves were fitted by using the Berkeley Madonna code *(3)*. The procedure and results for the continuous tracer test can be found in *(1)*.

Table S3.2. Operational and wastewater quality parameters of the influent grab samples collected during the sampling campaigns

		Transferred ozone dose[a] [g O_3 g^{-1} DOC]						
		0.21	**0.41**	**0.60**	**0.74**	**0.81**	**0.90**	**1.24**
Transferred ozone dose[a]	[mg O_3 L^{-1}]	0.8	1.2	2.6	3.0	3.8	4.3	5.2
Sampling date		14 august 2008	13 august 2008	8 april 2008	12 august 2008	7 april 2008	9 april 2008	11 august 2008
$Q_{wastewater}$	[L s^{-1}]	80	90	80	170	110	80	70
$Q_{process\ gas}$	[Nm^3 h^{-1}]	15	15	15	15	15	20	20
Hydraulic retention time reactor[b]	[min:sec]	07:55	07:02	07:55	03:43	05:45	07:55	09:03
$Q_{cumulated}$[c]	[m^3]	10500	17000	7900	10500	11000	6300	4400
$Q_{wastewater}$ (tracer test)	[L s^{-1}]	-	87	-	170	-	-	80
$Q_{process\ gas}$ (tracer test)	[Nm^3 h^{-1}]	-	15	-	20	-	-	15
TOC	[mg L^{-1}]	4.1	2.7	n.d.	3.9	n.d.	5.2	4.2
Ammonium	[μg_N L^{-1}]	n.d.	n.d.	n.d.	n.d.	n.d.	31.8	n.d.
Alkalinity	[mmol L^{-1}]	3.5	2.0	n.d.	2.8	n.d.	3.5	3.8
Total water hardness	[mmol L^{-1}]	2.1	1.2	n.d.	1.8	n.d.	2.3	2.6
Nitrate	[mg_N L^{-1}]	6.8	3.4	n.d.	4.2	n.d.	6.0	10.3
Bromide	[μg L^{-1}]	20	6	32	19	31	31	28
E. coli	[cfu $100ml^{-1}$]	20000	5000	6000	9000	5000	5000	4000

n.d. - not determined

[a]Calculated from the ozone dose lost by out gassing subtracted from the applied ozone dose (calculated from $c_{O3\ Offgas}$ x Q_{Offgas} / $Q_{wastewater}$)

[b]Theoretical calculation based on a plug flow behavior and 38 m^3 total volume

[c]Flow cumulated over 24h from 8am the day before – 8am at the sampling date

Text S3.2. Determination of pseudo first-order ozone decay constants, ozone and hydroxyl radical exposures and R_{ct} values

The stability of ozone in wastewater depends strongly on the composition of the matrix. The influence of water quality parameters such as pH, DOC, alkalinity and temperature on ozone decay kinetics may be avoided by direct measurement of the ozone decay under the actual treatment conditions. Therefore, grab samples from the influent to the ozone reactor were taken during each sampling day, filtered (0.45 µm) and stored at 4 °C until use. The filtration step should not significantly influence the ozone decay because it is mainly controlled by DOM *(4)*. The pseudo first-order ozone decay constants as well as the ozone and hydroxyl radical exposures were subsequently determined by means of a laboratory dispenser system *(5)*. Samples were buffered to the pH of the respective sampling campaign (Table 3.1), and *p*CBA was spiked as ozone-resistant probe compound to measure the transient hydroxyl radical concentrations *(6)*. Experiments were carried out at the same temperature and with the same ozone dose as in the respective full-scale experiment (Table 3.1). After ozone addition, samples were withdrawn at regular time intervals starting from 10 s until complete ozone consumption. Ozone was quenched with indigo for residual ozone measurements *(7)*, and the residual *p*CBA concentration was determined by reverse-phase HPLC (55/45 methanol/10 mM H_3PO_4 buffer eluent, flow 1 ml min^{-1} and UV detection at 234 nm). Ozone exposures were calculated by integrating the respective decay curves over time. Hydroxyl radical exposures were directly derived from the relative decrease of *p*CBA, while the R_{ct} values were calculated from the slopes of the $\ln([pCBA]/[pCBA_0])$ vs. ozone exposure plot *(8)* (Table 3.1).

Table S3.3. pK_a values, species-specific and apparent second-order rate constants including standard deviations at pH 7 of the investigated micropollutants and *E. coli* for the reaction with ozone and hydroxyl radicals at 20 °C

Substance	pK_a	k_{O_3} [M^{-1} s^{-1}]			k_{O_3} at pH 7	$k_{OH\cdot}$	Reference
		deprotonated	monoprotonated	diprotonated	[M^{-1} s^{-1}]	[M^{-1} s^{-1}]	
Atenolol	9.6	6.3 x 10^5*	1.1 x 10^2	-	1.7 ± 0.4 x 10^3	8.0 ± 0.5 x 10^9	*(9)*
Benzotriazole[a]	1.6 8.2	2.4x x10^3	3.7 x 10^1*	-	2.3 ± 0.4 x 10^2	7.6 ± 0.5 x 10^9	*(10-12)*
Bezafibrate	3.6	5.9 x 10^2	-	-	5.9 x 10^2 - 4.2 x 10^3	7.4 x 10^9	*(4,13,14)*
Carbamazepine	-	-	3.0 x 10^5*	-	3.0 x 10^5	8.8 x 10^9	*(4,14)*
Clarithromycin	-	-	-	-	7.0 x 10^4	-	*(15)*
Clindamycin	-	-	-	-	1.0 x 10^5	-	*(14)*
Clofibric acid	4.5	-	-	-	2.0 x 10^1	4.7 x 10^9	*(4)*
Diclofenac	4.2	6.8 x 10^5	-	-	6.8 x 10^5	7.5 x 10^9	*(4,16)*
Erythromycin	-	-	-	-	1.0 x 10^5	-	*(14)*
Ibuprofen	4.9	9.6 x 10^0	-	-	9.1 x 10^0	7.4 x 10^9	*(4,14)*
Mefenamic acid	-	-	-	-	-	-	
5-Methyl-Benzotriazole	-	1.0 x 10^4	1.8 x 10^2*	-	4.0 x 10^2	1.0 x 10^9 - 1.0 x 10^{10}	*(8,10)*
Metoprolol	9.7	8.6 x 10^5*	3.3 x 10^2	-	2.0 x 10^3	7.3 x 10^9	*(9)*
Naproxen	4.2	-	-	-	2.0 x 10^5	9.6 x 10^9	*(4,14)*
NDMA	-	-	-	-	5.2 x 10^{-2}	4.5 x 10^8	*(17)*
NMOR	-	-	-	-	-	-	
Paracetamol	9.4	9.9 x 10^8	1.4 x 10^3*	-	4.1 x 10^6	2.2 x 10^9	*(18)*

Substance	pK_a	k_{O_3} [M^{-1} s^{-1}]			k_{O_3} at pH 7	$k_{OH\bullet}$	Reference
		depro-tonated	monopro-tonated	dipro-tonated	[M^{-1} s^{-1}]	[M^{-1} s^{-1}]	
Phenanzone	-	-	-	-	-	-	
Sotalol	-	-	-	-	1.0 x 10^3-10^4	-	*(14)*
Sulfadiazine	-	-	-	-	1.0 x 10^5	3.7 x 10^9	*(14,19)*
Sulfamethazine	-	-	-	-	1.0 x 10^5	5.0 x 10^9	*(14,19)*
Sulfamethoxazole	1.7 5.6	5.7 x 10^5	*4.7 x 10^4**	-	5.5 x 10^5	5.5 x 10^9	*(20)*
Sulfapyridine	-	-	-	-	1.0 x 10^5	-	*(14)*
Trimethoprim	3.2 7.1	5.2 x 10^5*	7.4 x 10^4	3.3 x 10^4	2.7 x 10^5	6.9 x 10^9	*(20)*
E. coli	-	-	-	-	1.0 x 10^5		*(21)*

*neutral species, s*ulfonamides are zwitterions and written in italic.*

[a]$k_{O_3,benzotriazole}$ determined at pH 2 and 5 (18 and 22 M^{-1} s^{-1}, respectively, *(22)*) support the $k_{O_3,benzotriazole}$ value determined by Lutze (2005) *(10)* at pH 7. Standard deviation of $k_{O_3,benzotriazole}$ at pH 7 was set as difference between the measured (2.28 x 10^2 M^{-1} s^{-1}) and modeled (1.86 x 10^2 M^{-1} s^{-1}) value determined in Lutze (2005) *(10)*, and the measured value was used as average value. Standard deviation of $k_{OH\bullet,benzotriazole}$ was estimated to be equal to the standard deviation of $k_{OH\bullet,atenolol}$.

Table S3.4. Number (n) of continuously stirred tank reactors (CSTRs) in each cascade of CSTRs of the hydraulic model for different combinations of wastewater and process gas flows

n in each cascade of CSTRs	$Q_{wastewater}$ = 87 L s^{-1} $Q_{process\ gas}$ = 15 m^3 h^{-1}	$Q_{wastewater}$ = 170 L s^{-1} $Q_{process\ gas}$ = 20 m^3 h^{-1}
P2 – P3	4	-
P3 – P4	2	3
P4 – P5	3	2
P5 – P6	9	9
P6 – P7	2	2

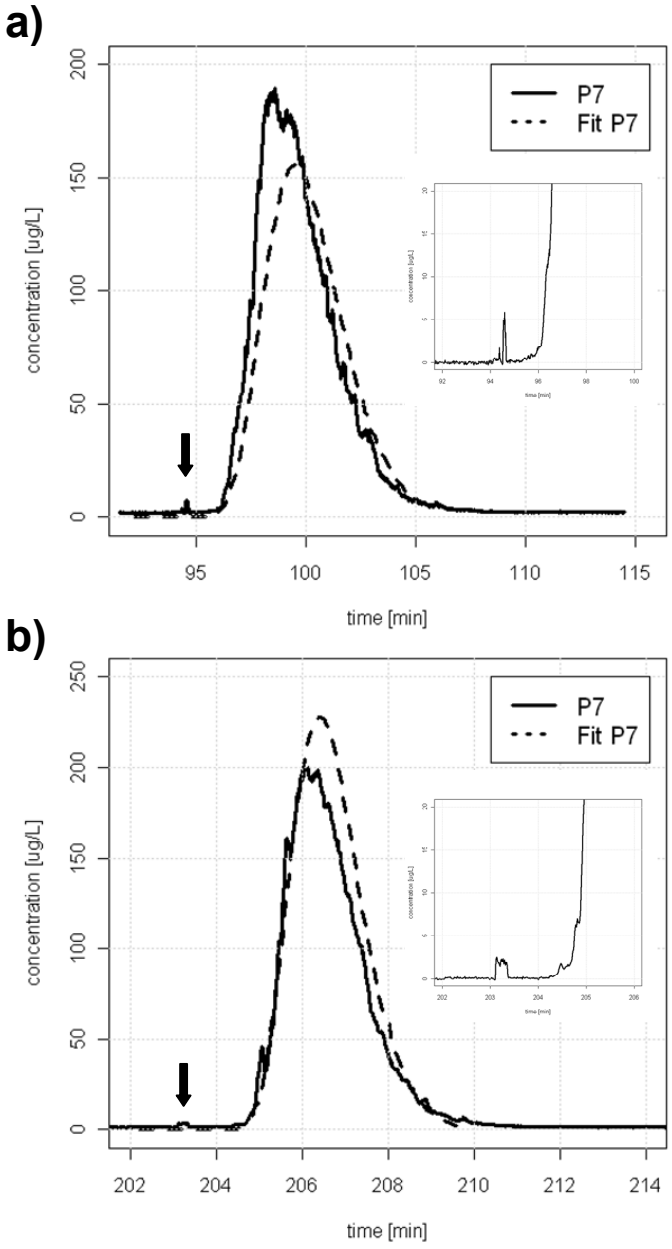

Figure S3.1. Breakthrough curves from the Dirac pulse tracer test of the conservative tracer fluoresceine at P7 of the ozone reactor for wastewater flows of a) 87 L s^{-1} and b) 170 L s^{-1}, both with 15 m^3 h^{-1} oxygen gas flow. Experimental data are shown as solid curves, and hydraulic model calculations are depicted as dashed lines. Black arrows point at a fraction eluting prior to the main breakthrough curves at P7. Integrating the breakthrough curves yielded 0.1 ± 0.02 % of the total area for the fraction eluting prior, and 99.9 ± 0.02 % of the total area for the main breakthrough curves, respectively.

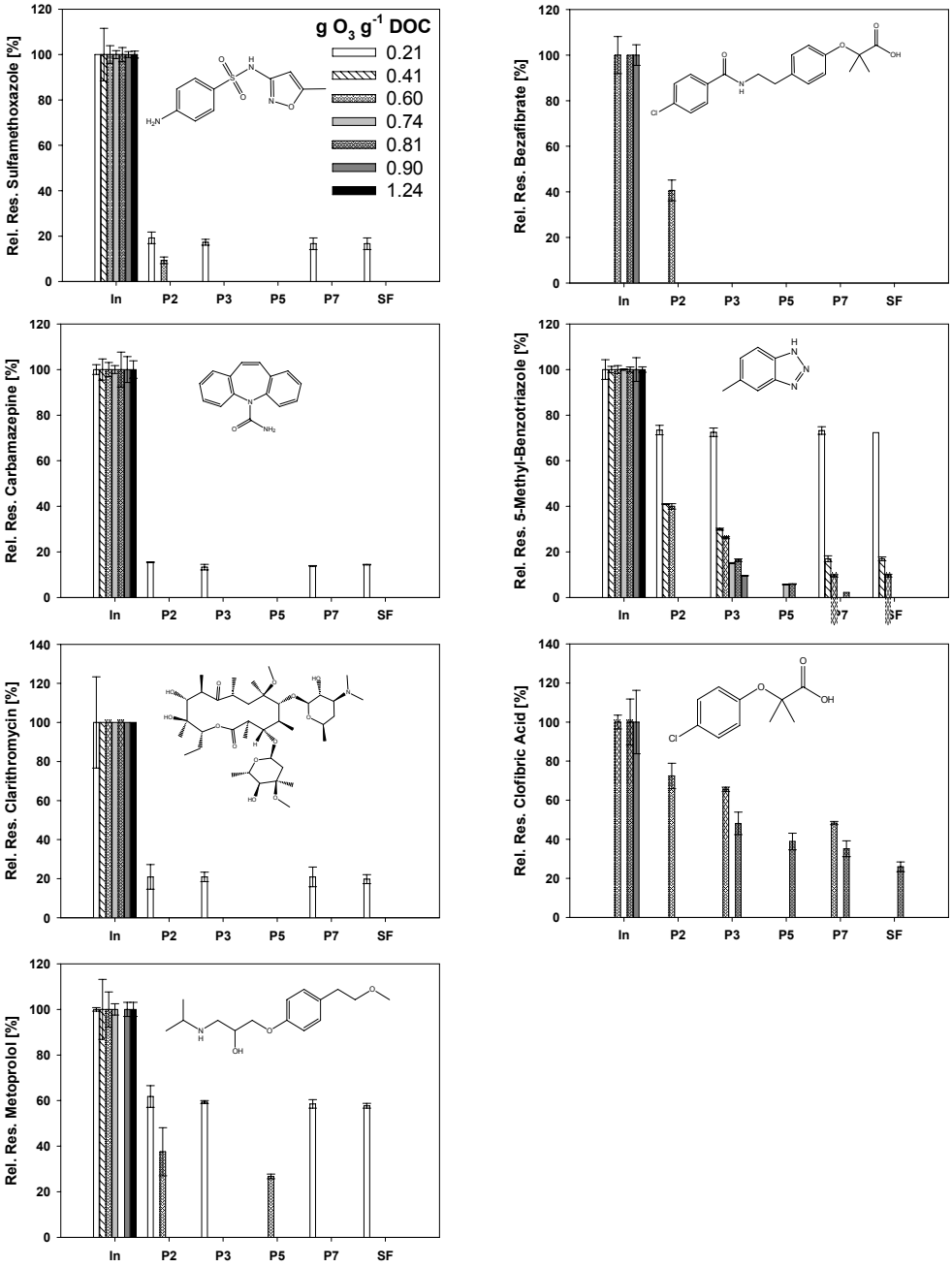

Figure S3.2. Relative residual concentrations of various micropollutants for seven ozone doses ranging from 0.21 to 1.24 g O_3 g^{-1} DOC in the influent to the ozone reactor (IN), along the ozone reactor (P2, P3, P7 or P3, P5, P7) and after sand filtration (SF). Error bars were derived from duplicate measurements and calculated by linear error propagation. Micropollutants are arranged according to their decreasing second-order rate constants for their reaction with ozone from sulfamethoxazole to clofibric acid (Table S3.3). n.d. = not determined.

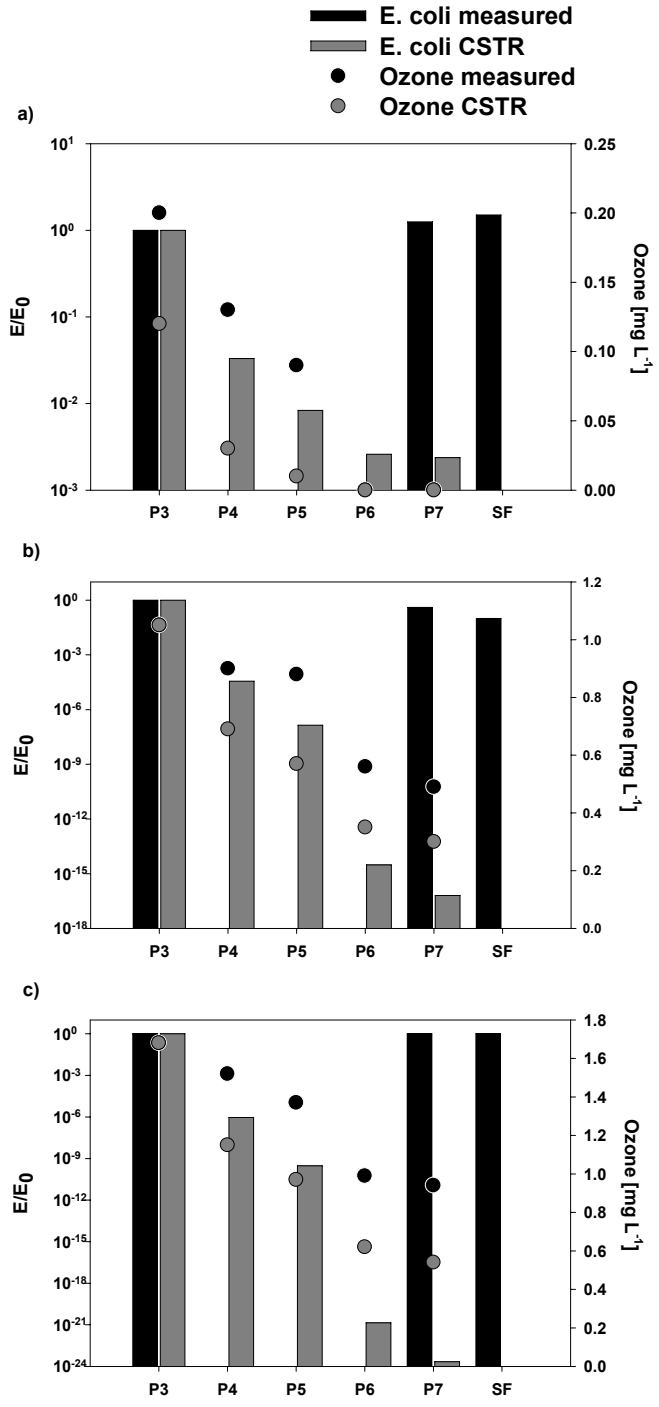

Figure S3.3. Measured and modeled (based on the CSTR model) relative residual concentrations of *Escherichia coli (E. coli)* based on the concentrations at P3 as well as absolute ozone concentrations for an ozone dose of a) 0.41 g O_3 g^{-1} DOC, b) 0.74 g O_3 g^{-1} DOC and c) 1.24 g O_3 g^{-1} DOC along the ozone reactor (P3 – P7) and after sand filtration (SF). *E. coli* concentrations were not measured at P4 to P6.

References

(1) Helbing, J.; Gresch, M.; von Gunten, U. Fluorescein as an easy to use tracer for analysis of treatment trains, *in preparation.*

(2) R Foundation for statistical Computing. *R: A language and environment for statistical computing*; 2006.

(3) University of California. *Berkeley Madonna*; 2001.

(4) Huber, M. M.; Göbel, A.; Joss, A.; Hermann, N.; Löffler, D.; McArdell, C. S.; Ried, A.; Siegrist, H.; Ternes, T. A.; von Gunten, U. Oxidation of pharmaceuticals during ozonation of municipal wastewater effluents: A pilot study. *Environ. Sci. Technol.* **2005**, *39*, 4290-4299.

(5) Hoigné, J.; Bader, H. Characterization of Water-Quality Criteria for Ozonation Processes. 2. Lifetime of Added Ozone. *Ozone-Sci. Eng.* **1994**, *16*, 121-134.

(6) Hoigné, J. Inter-calibration of OH radical sources and water quality parameters. *Water Sci. Technol.* **1997**, *35*, 1-8.

(7) Bader, H.; Hoigné, J. Determination of ozone in water by the indigo method. *J Water Research* **1981**, *15*, 449-456.

(8) von Gunten, U. Ozonation of drinking water: Part I. Oxidation kinetics and product formation. *Water Res.* **2003**, *37*, 1443-1467.

(9) Benner, J.; Salhi, E.; Ternes, T.; von Gunten, U. Ozonation of reverse osmosis concentrate: Kinetics and efficiency of beta blocker oxidation. *Water Res.* **2008**, *42*, 3003-3012.

(10) Lutze, H. Ozonung von Benzotriazolen. *Bachelor Thesis* **2005**, Universität Duisburg - Essen.

(11) Naik, D. B.; Moorthy, P. N. Studies on the Transient Species Formed in the Pulse-Radiolysis of Benzotriazole. *Radiat. Phys. Chem.* **1995**, *46*, 353-357.

(12) Fagel, J. E.; Ewing, G. W. The Ultraviolet Absorption of Benzotriazole. *J. Am. Chem. Soc.* **1951**, *73*, 4360-4362.

(13) Dantas, R. F.; Canterino, M.; Marotta, R.; Sansa, C.; Esplugas, S.; Andreozzi, R. Bezafibrate removal by means of ozonation: Primary intermediates, kinetics, and toxicity assessment. *Water Res.* **2007**, *41*, 2525-2532.

(14) Huber, M. M.; Canonica, S.; Park, G. Y.; von Gunten, U. Oxidation of pharmaceuticals during ozonation and advanced oxidation processes. *Environ. Sci. Technol.* **2003**, *37*, 1016-1024.

(15) Lange, F.; Cornelissen, S.; Kubac, D.; Sein, M. M.; von Sonntag, J.; Hannich, C. B.; Golloch, A.; Heipieper, H. J.; Möder, M.; von Sonntag, C. Degradation of macrolide antibiotics by ozone: A mechanistic case study with clarithromycin. *Chemosphere* **2006**, *65*, 17-23.

(16) Sein, M. M.; Zedda, M.; Tuerk, J.; Schmidt, T. C.; Golloch, A.; von Sonntag, C. Oxidation of Diclofenac with Ozone in Aqueous Solution. *Environ. Sci. Technol.* **2008**, *42*, 6656-6662.

(17) Lee, C.; Yoon, J.; Von Gunten, U. Oxidative degradation of *N*-nitrosodimethylamine by conventional ozonation and the advanced oxidation process ozone/hydrogen peroxide. *Water Res.* **2007**, *41*, 581-590.

(18) Andreozzi, R.; Caprio, V.; Marotta, R.; Vogna, D. Paracetamol oxidation from aqueous solutions by means of ozonation and H2O2/UV system. *Water Res.* **2003**, *37*, 993-1004.

(19) Boreen, A. L.; Arnold, W. A.; McNeill, K. Triplet-sensitized photodegradation of sulfa drugs containing six-membered heterocyclic groups: Identification of an SO2 extrusion photoproduct. *Environ. Sci. Technol.* **2005**, *39*, 3630-3638.

(20) Dodd, M. C.; Buffle, M. O.; von Gunten, U. Oxidation of antibacterial molecules by aqueous ozone: Moiety-specific reaction kinetics and application to ozone-based wastewater treatment. *Environ. Sci. Technol.* **2006**, *40*, 1969-1977.

(21) Hunt, N. K.; Marinas, B. J. Kinetics of Escherichia coli inactivation with ozone. *Water Res.* **1997**, *31*, 1355-1362.

(22) Karpel Vel Leitner, N.; Roshani, B. Kinetic of benzotriazole oxidation by ozone and hydroxyl radical. *Water Res.* **2010**, *44*, 2058-2066.

Chapter 4

Ferrate (Fe(VI)) application for municipal wastewater treatment: A novel process for simultaneous micropollutant oxidation and phosphate removal

Reproduced with permission from Lee, Y.*; Zimmermann, S. G.*; Kieu, A. T.; von Gunten, U. *Environmental Science and Technology* **2009**, *43*, 3831-3838.

http://pubs.acs.org/doi/abs/10.1021/es803588k

*Co-primary authors contributed equally to this work

Abstract

A novel technology for enhanced municipal wasterwater treatment was assessed based on the dual functions of Fe(VI) to oxidize micropollutants and remove phosphate by formation of ferric hydroxides. Second-order rate constants (k) for the reactions of selected pharmaceuticals, endocrine disruptors, and organic model compounds with Fe(VI) were in the range of 1 (trimethylamine) to 9000 M^{-1} s^{-1} (aniline) in the pH range 7 – 8. The selected compounds contained electron-rich moieties (ERM) such as phenols, anilines, amines, and olefins. Oxidation experiments in wastewater spiked with micropollutants at concentrations in the low μM range at pH 7 and 8 showed that Fe(VI) doses higher than 5 mg Fe L^{-1} are capable of eliminating various ERM-containing micropollutants by more than 85 %. In comparison to ozone, Fe(VI) was as effective or slightly less effective in terms of micropollutants oxidation, with Fe(VI) having the benefit of phosphate removal. To lower phosphate from 3.5 to 0.8 mg PO_4-P L^{-1} (regulatory limit for wastewater discharge in Switzerland), a Fe(VI) dose of 7.5 mg Fe L^{-1} was needed. Overall, this study demonstrates Fe(VI) as a promising tool for an enhanced wastewater treatment to remove micropollutants as well as to control phosphate in a single treatment step.

4.1 Introduction

Phosphate removal from municipal wastewater has been practiced for a long time to prevent eutrophication of the receiving waters. In Switzerland, the regulatory limit for phosphate in wastewater effluents is 0.8 mg PO_4-P L^{-1} (*1*). Addition of ferric salts and subsequent ferric-phosphate precipitation is one of the common practices in municipal wastewater treatment plants (WWTPs) to meet the phosphate standards (*2*). Recently, effluents of municipal WWTPs have also been identified as a major source of emerging micropollutants, such as hormones, pharmaceuticals and personal care products for the aquatic environments (*3*). Strategies for the removal of these compounds from municipal wastewaters are currently discussed. Oxidation processes with ozone (O_3) in laboratory- and pilot-scale studies have been shown to be an option for the removal of micropollutants (*4,5*).

As an alternative, ferrate (Fe(VI)) is a potential water treatment chemical due to its dual functions as an oxidant and a subsequent coagulant/precipitant as ferric hydroxide (*6,7*). Hence, an application of Fe(VI) to wastewater could achieve both oxidative elimination of various micropollutants and removal of phosphate by a subsequent ferric-phosphate precipitation. However, up to now, Fe(VI) has neither been suggested nor investigated in detail for this novel application.

Fe(VI) has been known to react with electron-rich organic moieties (ERM), such as phenols (*8,9*), anilines (*10–12*), amines (*10,13,14*), and olefines (*15*). Therefore, ERM-containing compounds can be potentially transformed during Fe(VI) oxidation. This has been demonstrated in a few previous kinetic studies for the Fe(VI) reaction with emerging micropollutants such as steroid estrogens (*9*), sulfonamide antimicrobials (*12*), and carbamazepine (*15*). Nevertheless, kinetic information is still limited for the reactions of Fe(VI) with various organic compounds in the pH range relevant to water treatment (pH 6 – 9).

The aim of this study was to assess the potential of Fe(VI) to oxidize selected micropollutants and remove phosphate during enhanced treatment of municipal wastewater in a single treatment step. Second-order rate constants (k) for the reaction of Fe(VI) with selected micropollutants and organic model compounds were determined as

a function of pH. The oxidative elimination of a wide range of micropollutants was then investigated in wastewater for varying experimental conditions for pH (7 and 8) and Fe(VI) dose (0.1 – 15 mg Fe L^{-1}). In addition, the performance of Fe(VI) to oxidize micropollutants in a wastewater matrix was compared to O_3. Furthermore, jar tests with Fe(VI) were performed in wastewater to evaluate the oxidative elimination of selected micropollutants in combination with the subsequent removal of phosphate. Finally, Fe(VI) was compared to Fe(III) and Fe(II) with regard to the phosphate removal efficiency.

4.2 Materials and Methods

4.2.1 Standards and reagents

All chemicals and solvents (purity ≥ 95 %) were purchased from various commerical suppliers. Description on preparation and quantification of oxidants (Fe(VI) and O_3), coagulants (Fe(II) and Fe(III)), stock solutions of micropollutants and organic model compounds are provided in the Supporting Information, Text S4.1.

4.2.2 Kinetics of Fe(VI) reactions with micropollutants and organic model compounds

All kinetic experiments were performed at room temperature (23±2 °C). Second-order rate constants were mostly determined by measuring the Fe(VI) decrease in presence of excess compound (pseudo first-order kinetic method) in the pH range 5–11. For diclofenac, second-order rate constants were determined by measuring the diclofenac decrease in presence of excess Fe(VI). For details, see Text S4.2.

4.2.3 Oxidation of micropollutants by Fe(VI) in a wastewater matrix

Bench-scale experiments were performed to investigate the elimination of micropollutants spiked in a secondary effluent from a pilot WWTP in Dübendorf, Switzerland (DDWW) at various Fe(VI) doses at 23±2 °C and pH 7 and 8. Secondary effluent was chosen to investigate the potential of Fe(VI) as a polishing step for enhanced removal of micropollutants as well as phosphate. The micropollutants were selected as representative substances with different reactive moieties that belong to different usage classes and have an environmental relevance (*3*). Each micropollutant was spiked separately at concentrations of 0.2 – 1 μM into 20 mL of the wastewater buffered at pH 7 (10 mM carbonate buffer) or 8 (20 mM borate buffer). After Fe(VI) was completely consumed (3–5 hours after Fe(VI) addition), residual micropollutant concentrations were analyzed with a HPLC/UV-fluorescence system (Text S4.3). Fe(VI) decrease was measured spectrophotometrically as a function of the reaction time with the ABTS method (*16*). Further experimental details, the characteristics of the wastewater and the analytical procedures are described in Text S4.4.

4.2.4 Oxidation of micropollutants by Fe(VI) and O_3 in the same wastewater matrix

DDWW was spiked with each of the selected micropollutants at pH 8 (20 mM borate buffer) and treated with a range of Fe(VI) or O_3 doses. After 3–5 hours (total Fe(VI) or O_3 consumption), residual micropollutant concentrations were analyzed by a HPLC/UV-fluorescence system (Text S4.3).

4.2.5 Jar tests for phosphate removal

Phosphate removal experiments were carried out with a standard jar test apparatus with a reactor volume of 0.5 L. DDWW was spiked with phosphate (3.5 mg PO_4-P L^{-1}, a realistic scenario for a high phosphate concentration) and selected micropollutants at pH 7 (typical pH conditions of municipal wastewaters). Carbamazepine, diclofenac, and sulfamethoxazole were chosen based on their moderate reactivity toward Fe(VI) and relevance in municipal wastewaters. Thereafter, a range of Fe(VI) doses (1–15 mg Fe L^{-1}) were added. For comparison of the phosphate removal efficiency, Fe(II) ($FeCl_2$) and Fe(III) ($FeCl_3$) were also used. Concentrated stock solutions of Fe(II) and Fe(III) were freshly prepared and quickly applied to the wastewater (see Text S4.1 for details). The jar test procedure for the removal of phosphate was composed of three steps: i) rapid mixing at 200 rpm for 0.5 min, ii) slow mixing at 50 rpm for 15 min, and iii) settling for >15 min. After settling, the supernatant samples were collected and filtered through 0.45 μm Nylon or RC filters (BGB Analytik AG, Switzerland) prior to analysis of the residual phosphate and micropollutant concentrations. Phosphate concentrations were analyzed according to a standard method (ascorbic acid-molybdate blue method, (*17*)). All experiments were performed in triplicate.

4.3 Results and Discussion

4.3.1 Kinetics for the reactions of Fe(VI) with micropollutants and organic model compounds

To assess the reactivity of Fe(VI) towards a broad range of micropollutants, second-order rate constants (k) were determined for the reaction of Fe(VI) with selected micropollutants and organic model compounds as a function of pH. The investigated micropollutants were selected based on their environmental relevance and their reactivity to other water treatment oxidants, such as O_3 (*4,18*), due to electron-rich moieties (ERM). For example, 17α-ethinylestradiol contains a phenolic-, carbamazepine an olefine-, ciprofloxacin and enrofloxacin an amine-, and sulfamethoxazole and diclofenac an aniline-moiety.

Fe(VI) shows an appreciable reactivity with the selected micropollutants. In the pH range 7 – 8, the second order rate constant k varied between 20 and 2090 M^{-1} s^{-1} (Figure 4.1a). In general, k for the selected micropollutants (Figure 4.1a) and organic model compounds (Figure 4.1b) increases with decreasing pH. These pH-dependent variations in k could be explained by considering species-specific reactions between Fe(VI) species ($HFeO_4^- \Leftrightarrow FeO_4^{2-} + H^+$, $pK_{HFeO_4} = 7.2$) and acid-base species of an ionizable substrate ($XH \Leftrightarrow X^- + H^+$, $pK_{a,XH}$) (*9,13*). The speciation of Fe(VI) as a function of pH can be found in Figure S4.5. According to that, eq 4.1 applies for the loss of Fe(VI):

$$-\frac{d[Fe(VI)_{tot}]}{dt} = k[Fe(VI)_{tot}][XH_{tot}]$$

$$= k_1[HFeO_4^-][XH] + k_2[HFeO_4^-][X^-] + k_3[FeO_4^{2-}][XH] + k_4[FeO_4^{2-}][X^-] \qquad (4.1)$$

and therefore, k can be expressed by eq 4.2:

$$k = k_1\alpha_1\beta_1 + k_2\alpha_1\beta_2 + k_3\alpha_2\beta_1 + k_4\alpha_2\beta_2 \qquad (4.2)$$

where $[Fe(VI)_{tot}] = [HFeO_4^-] + [FeO_4^{2-}]$ and $[XH_{tot}] = [XH] + [X^-]$, k_1, k_2, k_3 and k_4 represent species-specific rate constants, α_1 and α_2 represent the fraction of $HFeO_4^-$ and FeO_4^{2-}, respectively, and β_1 and β_2 represent the fraction of XH and X^-, respectively. Similarily, for the reaction of Fe(VI) with non-ionizable substrate, k can be expressed by eq 4.3:

$$k = k_5\alpha_1 + k_6\alpha_2 \quad (4.3)$$

The species-specific second-order rate constants, k_1 – k_6 were calculated from least-square non-linear regressions of the experimental k data by using the software GraphPad Prism (www.graphpad.com). In all cases, the model could explain the experimental k well ($R^2 \geq 0.94$). For reactions of Fe(VI) with ionizable substrates, the reactions of FeO_4^{2-} ($k_3\alpha_2\beta_1$ and $k_4\alpha_2\beta_2$) did not appear to contribute significantly to the overall kinetics and thus were neglected. Table 4.1 summarizes the determined species-specific rate constants.

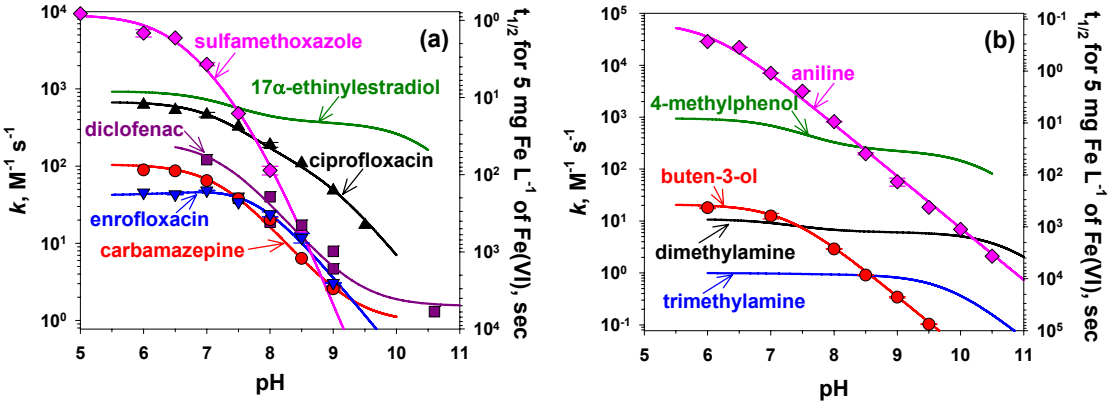

Figure 4.1. Second-order rate constants and half-lives ($t_{1/2}$) for the reactions of Fe(VI) with (a) selected micropollutants and (b) organic model compounds as a function of pH (5–11) and at T = 23±2 °C. The symbols represent the measured data and the lines represent the model fits from the present study. The half-lives are calculated for a Fe(VI) concentration of 5 mg Fe L^{-1} (90 µM). Kinetic data for 17α-ethinylestradiol and 4-methylphenol are taken from *ref.* (*9*) and for dimethylamine and trimethylamine from *ref.* (*13*) and only the model fits are provided here.

Table 4.1. Second-order rate constants k (M^{-1} s^{-1}) for the reaction of Fe(VI) and O_3 with selected pharmaceuticals, endocrine disruptors and organic model compounds (standard deviation (±σ) is given for the rate constants determined in this study)

Compound	Structure	pK_a	Fe(VI)				O_3		
			Reacting species	k_1/k_2 (k_5/k_6) [a]	k (pH 7)	k (pH 8)	k_1/k_2 [b]	k (pH 7)	k (pH 8)
17α-ethinyl-estradiol		10.4 [c]	$HFeO_4^- + XH$/ $HFeO_4^- + X^-$	9.4×10^2 / 5.4×10^5 [d]	7.3×10^2	4.5×10^2	1.8×10^5 / 3.7×10^9 [c]	1.6×10^6	1.5×10^7
17β-estradiol		10.4 [c]	$HFeO_4^- + XH$/ $HFeO_4^- + X^-$	1.0×10^3 / 5.4×10^5 [d]	7.6×10^2	4.6×10^2	2.2×10^5 / 3.7×10^9 [c]	1.7×10^6	1.5×10^7
bisphenol-A		9.6 10.2 [c]	$HFeO_4^- + XH_2$/ $HFeO_4^- + XH^-$/ $HFeO_4^- + X^{2-}$	8.2×10^2 / 8.0×10^4 / 2.6×10^5 [d]	6.4×10^2	4.1×10^2	1.7×10^4 / 1.1×10^9 / 1.1×10^9 [c]	2.7×10^6	2.6×10^7
triclosan		8.1 [e]	$HFeO_4^- + XH$/ $HFeO_4^- + X^-$	– / $2.5(\pm0.2)\times10^4$ [f]	1.1×10^3	1.6×10^3	1.3×10^3 / 5.1×10^8 [e]	3.8×10^7	2.3×10^8
4-methylphenol		10.3 [g]	$HFeO_4^- + XH$/ $HFeO_4^- + X^-$	9.6×10^2 / 2.4×10^5 [d]	6.9×10^2	3.3×10^2	3.0×10^4 [g]/ 2.0×10^9 [h]	1.1×10^6	1.1×10^7
carbamazepine		–	$HFeO_4^- + X$/ $FeO_4^{2-} + X$	$1.1(\pm0.1)\times10^2$ / $0.9(\pm0.3)$	67	16	3×10^5 [i]	3×10^5	3×10^5
buten-3-ol		–	$HFeO_4^- + X$/ $FeO_4^{2-} + X$	$19(\pm0.6)$ / $0.01(\pm0.003)$	12	3	7.9×10^4 [j]	7.9×10^4	7.9×10^4
ciprofloxacin		6.2(I) 8.8(II) [k]	$HFeO_4^- + XH$/ $HFeO_4^- + X^-$	$6.9(\pm0.4)\times10^2$/ $4.4(\pm0.3)\times10^3$ [l]	4.7×10^2	1.7×10^2	7.5×10^3 / 9.0×10^5 [k, l]	1.9×10^4	1.3×10^5
dimethylamine		10.7 [g]	$HFeO_4^- + XH$/ $HFeO_4^- + X^-$	11 / 1.8×10^4 [m]	9	7	– / 1.9×10^7 [g]	3.8×10^3	3.8×10^4

Compound	Structure	pK_a	Fe(VI) Reacting species	Fe(VI) k_1/k_2 (k_5/k_6) [a]	Fe(VI) k (pH 7)	Fe(VI) k (pH 8)	O_3 k_1/k_2 [b]	O_3 k (pH 7)	O_3 k (pH 8)
enrofloxacin	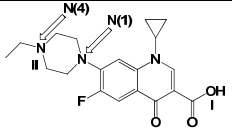	6.1(I) 7.7(II)[k]	$HFeO_4^- + XH$/ $HFeO_4^- + X^-$	43(±4) / $2.2(\pm0.2)\times10^2$ [l]	46	24	4.6×10^4 / 7.8×10^5 [k, l]	1.5×10^5	5.3×10^5
trimethylamine		9.8 [g]	$HFeO_4^- + XH$/ $HFeO_4^- + X^-$	1 / 3.5×10^2 [m]	1	1	– / 4.1×10^6 [g]	6.5×10^3	6.4×10^4
sulfamethox-azole	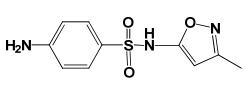	6.4 (±0.2), 7.8 (±0.3) [n]	– [o]	$9.2(\pm1.7)\times10^3$	1.8×10^3	77	2.5×10^6 [i]	2.5×10^6	2.5×10^6
aniline	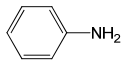	6.0 (±0.2) [p]	– [q]	$6.8(\pm2.8)\times10^4$	6.6×10^3	7.2×10^2	1.4×10^7 [r]	1.4×10^7	1.4×10^7
diclofenac	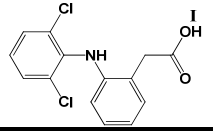	4.2 (I) [i]	$HFeO_4^- + X^-$/ $FeO_4^{2-} + X^-$	$2.1(\pm0.4)\times10^2$ / 1.5(±0.6)	1.3×10^2	32	1×10^6 [i]	1×10^6	1×10^6

[a] k_1 and k_2 represent the reaction rate constants of $HFeO_4^-$ with protonated and deprotonated species of substrates, respectively. Exceptions are: bisphenol-A for which the reaction rate constants of $HFeO_4^-$ with protonated, mono-, and di-deprotonated species are given; carbamazepine, buten-3-ol, and diclofenac of which the reaction rate constants with $HFeO_4^-$ (k_5) and FeO_4^{2-} (k_6) are given; k_3 and k_4 are not of importance as discussed in the text, [b] k_1 and k_2 represent the reaction rate constants of O_3 with protonated and deprotonated species of substrates, respectively. [c]from *ref.* (*20*), [d]from *ref.* (*9*), [e]from *ref.* (*21*), [f]estimated from the competition kinetics in DDWW at pH 7 (see Figure S4.8), [g]from *ref.* (*22*), [h]estimated from Brown-Okamoto correlations in *ref.* (*21*), [i]from *ref.* (*4*), [j]from *ref.* (*23*), [k]from *ref.* (*18*), [l] k_1 for ciprofloxacin and enrofloxacin represent an 'effective' rate constant for the combination of zwitterionic and neutral species, [m] k from *ref.* (*13*), [n] pK_a values of hypothesized Fe(VI)-sulfamethoxazole intermediate, [o]the reaction of the fully protonated species of the intermediate (Fe(VI)–SMX–H_2^+) with sulfamethoxazole, [p] pK_a value of hypothesized Fe(VI)-aniline intermediate, [q]the reaction of the protonated species of the intermediate (Fe(VI)–AN–H) with aniline, [r] k from *ref.* (*24*).

4.3.1.1 17α-ethinylestradiol and 4-methylphenol

The pH-dependence of *k* for 17α-ethinylestradiol is well explained by considering the reactions of $HFeO_4^-$ with the protonated (k_1 = 9.4×10^2 M^{-1} s^{-1}) and the deprotonated species of 17α-ethinylestradiol (k_2 = 5.4×10^5 M^{-1} s^{-1}) at the 17α-ethinylestradiol's phenolic-moiety (pK_a = 10.4, Table 4.1) (*9*). The magnitude and pH-dependence of *k* for 17α-ethinylestradiol are consistent with those for 4-methylphenol (Figure 4.1).

4.3.1.2 Carbamazepine and buten-3-ol

Both compounds are not ionizable in the tested pH range 5–11. As a consequence, *k* for these two compounds mainly depends on the fraction of the $HFeO_4^-$ species as a function of pH. Hence, the magnitude of *k* exhibits a one-log decrease for each unit increase in pH. k_5 for carbamazepine is 1.1(±0.1)×10^2 M^{-1} s^{-1}, which is about a factor of five higher than that for buten-3-ol (Table 4.1). It is assumed that Fe(VI) only attacks at the double bond and that the presence of electron-donating benzene-groups increases the reactivity to Fe(VI). k_5 for carbamazepine from this study is comparable to the value reported recently by Hu et al (k_5 = 1.4×10^2 M^{-1} s^{-1}) (*15*).

4.3.1.3 Ciprofloxacin and dimethylamine

The pH-dependence of *k* for ciprofloxacin is well explained by considering the reactions of $HFeO_4^-$ with the protonated (k_1 = 6.9(±0.4)×10^2 M^{-1} s^{-1}) and the deprotonated species of ciprofloxacin (k_2 = 4.4(±0.3)×10^3 M^{-1} s^{-1}) at the ciprofloxacin's secondary amine moiety (N(4), p$K_{a,\,II}$ = 8.8, Table 4.1). This is consistent with the case of O_3 where only the N(4) amine, not the N(1) amine nor the quinolone moiety, of the ciprofloxacin is the main site for oxidation (*18*). The pH-dependent *k* for ciprofloxacin is much higher than that of dimethylamine, because of the higher pK_a value of dimethylamine (10.7, Table 4.1).

4.3.1.4 Enrofloxacin and trimethylamine

Similar to the case of ciprofloxacin, the pH-dependence of *k* for enrofloxacin is governed by deprotonation at the enrofloxacin's tertiary amine moiety (N(4), $pK_{a,\,II}$ = 7.7, Table 4.1) which was shown for ozone as well (*18*). *k* of enrofloxacin is much higher than that of trimethylamine, because of the higher pK_a value of trimethylamine (9.8, Table 4.1). In addition, enrofloxacin reacts with Fe(VI) at lower rates than ciprofloxacin which is consistent with the lower reactivity of tertiary amines.

4.3.1.5 Sulfamethoxazole and aniline

These two compounds show a strong pH-dependence with *k* increasing more than four orders of magnitude with a decrease of the pH from 11 to 5. The pH- dependence of *k* for sulfamethoxazole and aniline could not be explained by eq 4.1 or eq 4.2. *k* steadily increases even at pH < 7.2 where the $HFeO_4^-$ concentration is at its maximum. Furthermore, *k* for sulfamethoxazole exhibits more than a one-log unit increase for each unit decrease of pH from 9 to 7. Including the reactions of H_2FeO_4 ($H_2FeO_4 \Leftrightarrow HFeO_4^- + H^+$, $pK_{H_2FeO_4}$ = 3.5 (*19*)) into the model calculations did not improve the predictions. However, this unusual pH-dependence could be explained by employing the following tentative reaction mechanism: Fe(VI) reacts with R–NH_2 by forming an intermediate complex, such as 'Fe(VI)–NH_2–R' which also has an acid-base equilibrium. For aniline, the pK_a of the corresponding intermediate was estimated to be 6.0(±0.2) (i.e. Fe(VI)–AN–H $\Leftrightarrow$ Fe(VI)–AN^- + H^+, pK_a = 6.0 where AN represents the aniline side). For sulfamethoxazole, the existence of two pK_a at 6.4(±0.2) and 7.8(±0.3) was necessary to explain the observed pH-dependence of *k* (i.e. Fe(VI) –SMX–H_2^+ $\Leftrightarrow$ Fe(VI)–SMX–H + H^+, $pK_{a,1}$ = 6.4 and Fe(VI)–SMX–H $\Leftrightarrow$ Fe(VI)–SMX^- + H^+, $pK_{a,2}$ = 7.8 where SMX represents the sulfamethoxazole side). The (de)-protonation may occur either at the Fe(VI)- or aniline-side of the intermediate. The rate determining step will be the reaction of these intermediates with an additional aniline (or sulfamethoxazole) because the reaction was found to be first-order with respect to both Fe(VI) and aniline (or sulfamethoxazole) (Figure S4.3). A similar reaction mechanism has been proposed in a previous study for the aniline oxidation by Fe(VI) (*10*). The non-linear regression of the

k with the above proposed model revealed that only the reaction of the protonated species of the intermediate (Fe(VI)–AN–H) with aniline (k = 6.8(±2.8)×10^4 M^{-1} s^{-1}, Table 4.1) is contributing to the pH-dependence for the reaction between Fe(VI) and aniline. Similary, for the reaction between Fe(VI) and sulfamethoxazole, the reaction of the fully protonated species of the intermediate (Fe(VI)–SMX–H_2^+) with sulfamethoxazole (k = 9.2(±1.7)×10^3 M^{-1} s^{-1}, Table 4.1) is controlling the pH-dependence. Further details of the reaction scheme for aniline and sulfamethoxazole are described in Text S4.5.

The *k* for aniline and sulfamethoxazole has been reported in previous studies (*10–12*). The *k* values for aniline and sulfamethoxazole determined in the present study are comparable to those of Huang et al. 2001 (*11*) and Sharma et al. 2006 (*12*), respectively, but different within a factor of 5 from those of Hornstein 1999 (*10*). In addition, the intepretation of the pH- dependence of *k* in the studies of Huang et al. (*11*) and Sharma et al. (*12*) is different from that of the present study. A comparison of the *k* for aniline and sulfamethoxazole with literature data is provided in Text S4.6.

4.3.1.6 Diclofenac

The pH-dependence of *k* for diclofenac in the pH-range 7 – 11 is well explained by considering the reactions of diclofenac with $HFeO_4^-$ (k_5 = 2.1(±0.4)×10^2 M^{-1} s^{-1}) and FeO_4^{2-} (k_6 = 1.5(±0.6) M^{-1} s^{-1}). It is assumed that the protonation on diclofenac's carboxylic acid moiety (pK_a = 4.2, Table 4.1) does not have any influence on the kinetics within the tested pH range.

4.3.2 Oxidation of individually spiked micropollutants by Fe(VI) in a wastewater matrix

The significant reactivity of Fe(VI) toward the ERMs shown in the previous section indicates that many micropollutants containing these ERMs can be considerably eliminated during oxidation by Fe(VI). To confirm this, experiments for the elimination of selected micropollutants were performed in real wastewaters.

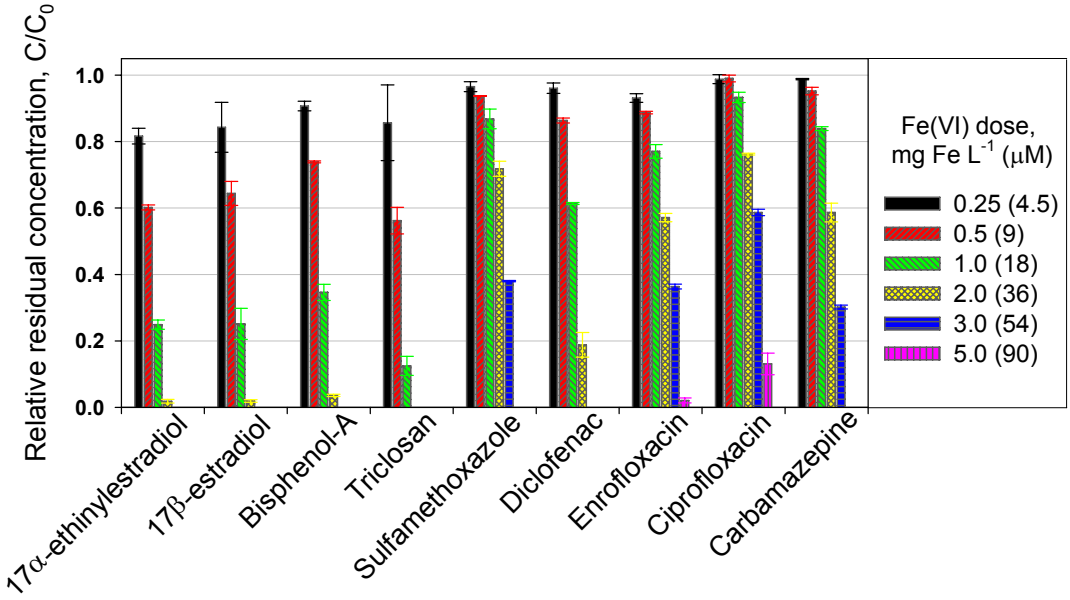

Figure 4.2. Relative residual concentration of selected micropollutants during treatment of a wastewater (DDWW) as a function of the Fe(VI) dose (0.25 –5.0 mg Fe L^{-1}) after complete Fe(VI) consumption (3–5 hours). Experimental conditions: $[micropollutants]_0$ = 0.2 – 1 μM (0.05 – 0.32 mg L^{-1}), $[phosphate]_0$ = 3.5 mg PO_4-P L^{-1}, [DOC] = 5.1 mg C L^{-1}, pH = 7 (10 mM bicarbonate buffer), and T = 23±2 °C. For the four phenolic micropollutants, Fe(VI) doses were applied up to 2.0 mg Fe L^{-1}. If no bar is shown, the residual concentration was below 4 % of the initial concentration.

Figure 4.2 shows the oxidative elimination of individually spiked ERM-containing micropollutants in a wastewater (DDWW) at a concentration of 0.2 – 1.0 μM (0.05 – 0.32 mg L^{-1}) and at pH 7 for Fe(VI) doses ranging from 0.25 to 5.0 mg Fe L^{-1}. For the micropollutants containing a phenolic-moiety, such as 17α-ethinylestradiol,

17β-estradiol, bisphenol-A, and triclosan, a Fe(VI) dose of 2 mg Fe L^{-1} achieved an elimination of > 95 %. The rate constant k for the reaction of triclosan with Fe(VI) at pH 7 could be estimated from the elimination of triclosan relative to the other phenolic micropollutants in DDWW. Figure S4.8 shows a competition kinetic plot for triclosan versus 17α-ethinylestradiol, 17β-estradiol, and bisphenol-A, respectively. A second-order rate constant of $1.1(\pm 0.1)\times 10^3$ M^{-1} s^{-1} was obtained for triclosan at pH 7. Based on this rate constant, the second-order rate constant (k_2) between $HFeO_4^-$ and deprotonated triclosan species was estimated to be $2.5(\pm 0.2)\times 10^4$ M^{-1} s^{-1}. Even though k_2 for triclosan is > 10-fold lower than the corresponding rate constants for the other phenolic micropollutants, the reactivity of triclosan at pH 7 or 8 is higher due to a lower pK_a value of triclosan (pK_a = 8.1, Table 4.1).

An electrophilic attack on phenolic moieties is expected for both Fe(VI) and O_3. Therefore, a correlation between the corresponding Fe(VI) and O_3 rate constants can be developed. Figure S4.9 shows a good linear correlation between $\log(k_{HFeO_4^-})$ and $\log(k_{O_3})$ for selected phenolic compounds. $k_{HFeO_4^-}$ and k_{O_3} represent the second-order rate constant of $HFeO_4^-$ and O_3, respectively, with deprotonated phenolic compounds. The obtained correlation was $\log(k_{HFeO_4^-}) = 1.91\cdot(\pm 0.19)\ \log(k_{O_3}) - 12.50\ (\pm 1.74)$, $R^2 = 0.94$, n = 8. For a given phenolic compound, the rate constant for O_3 is about 4–5 orders of magnitude higher than for $HFeO_4^-$.

For the other micropollutants such as sulfamethoxazole, diclofenac, enrofloxacin, ciprofloxacin, and carbamazepine, a Fe(VI) dose of 5 mg Fe L^{-1} was necessary to obtain an elimination of > 85 %. The compounds with an amine or olefine moiety have a lower reactivtiy with Fe(VI) (Table 4.1) and were therefore eliminated less efficiently than the phenolic compounds.

Compounds without the ERMs were also treated by Fe(VI) in the same wastewater. Figure S4.10 shows that bezafibrate, iopromide, and ibuprofen were eliminated by less than 40 % even at a Fe(VI) dose of 15 mg Fe L^{-1}. Therefore, significant eliminations are not expected for other micropollutants without the ERMs.

The oxidative elimination of a micropollutant (P) by Fe(VI) can be predicted by using the determined second-order rate constants ($k_{Fe(VI)}$, Table 4.1) according to eq 4.4:

$$\frac{[P]_\tau}{[P]_0} = \exp\left[-k_{Fe(VI)} \int_0^\tau [Fe(VI)]dt\right] \quad (4.4)$$

where $\int_0^\tau [Fe(VI)]dt$ represents the Fe(VI) exposure (Fe(VI) concentration integrated over time). Eq 4.4 is derived from the second-order reaction kinetics for the reaction between P and Fe(VI) under the condition of [P] << [Fe(VI)].

Figure S4.11 shows the time-dependent Fe(VI) concentrations in DDWW at pH 7 for various Fe(VI) doses. Most of Fe(VI) added to the wastewater was consumed within 30 min. In general, the Fe(VI) decrease is caused by its reaction with the ERMs in the dissolved organic matter and by the Fe(VI) self-decay (*9,19*). Hence, as an example, when a Fe(VI) dose of 2.5 mg Fe L^{-1} was applied to the wastewater, a Fe(VI) exposure of 7.7 mg Fe L^{-1} min (= 8.3 mM sec) was obtained (Figure S4.11). Based on the Fe(VI) exposures in Figure S4.11, the measured and predicted relative residual concentrations of selected micropollutants are compared in Figure S4.12 during treatment of DDWW with Fe(VI) at pH 7. For 17α-ethinylestradiol, carbamazepine and enrofloxacin, the eliminations were reasonably well predicted. However, the predictions overestimated the eliminations of ciprofloxacin and sulfamethoxazole and underestimated the elimination of diclofenac (Figure S4.12).

The oxidative elimination experiments of selected compounds by Fe(VI) were also performed at pH 8 in DDWW to investigate the effect of pH. Figure 4.3 shows that similar degrees of elimination were observed for the selected micropollutants at pH 8 compared to the data at pH 7 presented in Figure 4.2. 17α-ethinylestradiol as a phenolic micropollutant was oxidized by > 95 % at a Fe(VI) dose of 1 mg Fe L^{-1}. The other investigated micropollutants, such as sulfamethoxazole, diclofenac, ciprofloxacin, enrofloxacin and carbamazepine, were eliminated by > 95 % at a Fe(VI) dose of 5 mg Fe L^{-1}. The similar degrees of the elimination at pH 7 and 8 (Figure 4.2 vs. Figure 4.3), even though the apparent *k* for the selected micropollutants is higher at pH 7 than pH 8 (Table 4.1), can be understood by considering the longer lifetime of Fe(VI) and hence the higher Fe(VI) exposure at pH 8 (Figure S4.13) compared to pH 7 (Figure S4.11). For example, when a Fe(VI) dose of 5 mg Fe L^{-1} was applied, a Fe(VI) exposure of 58 mg Fe L^{-1} min was obtained at pH 8 (Figure S4.13), whereas at pH 7 it

was only 20 mg Fe L^{-1} min (Figure S4.11). Based on the Fe(VI) exposures derived from Figure S4.13, a comparison of the predicted relative residual concentration of selected micropollutants at pH 8 in DDWW with the measured data is shown in Figure 4.4. Comparable to pH 7 (Figure S4.12), 17α-ethinylestradiol and enrofloxacin eliminations were well predicted while ciprofloxacin elimination was again overestimated (Figure 4.4). Carbamazepine and diclofenac eliminations were well predicted at a Fe(VI) dose of 1 mg Fe L^{-1}, however, increasingly underestimated by increasing the Fe(VI) doses to 3 and 4 mg Fe L^{-1}. Sulfamethoxazole elimination was well predicted at Fe(VI) doses of 1 and 3 mg Fe L^{-1}, however, underestimated at a Fe(VI) dose of 4 mg Fe L^{-1} (Figure 4.4).

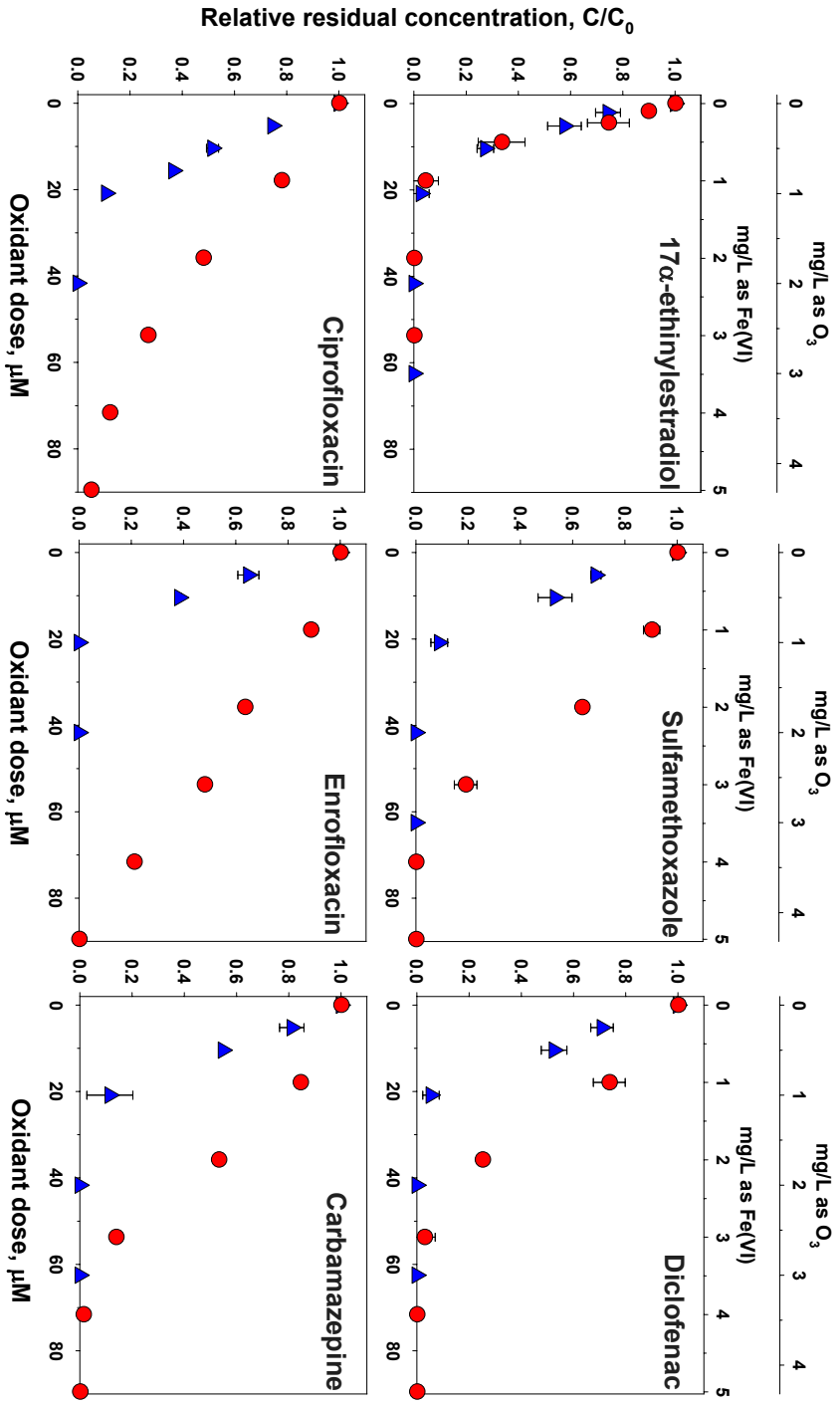

Figure 4.3. Comparison of the relative residual concentration after oxidation of selected micropollutants by Fe(VI) (red circles) and O_3 (blue triangles) as a function of the oxidant dose in a wastewater (DDWW). Experimental conditions: $[micropollutants]_0$ = 0.2 – 1 µM (0.05 – 0.32 mg L–1), [DOC] = 5.0 mg C L–1, pH = 8 (20 mM borate buffer), T = 23±2 °C.

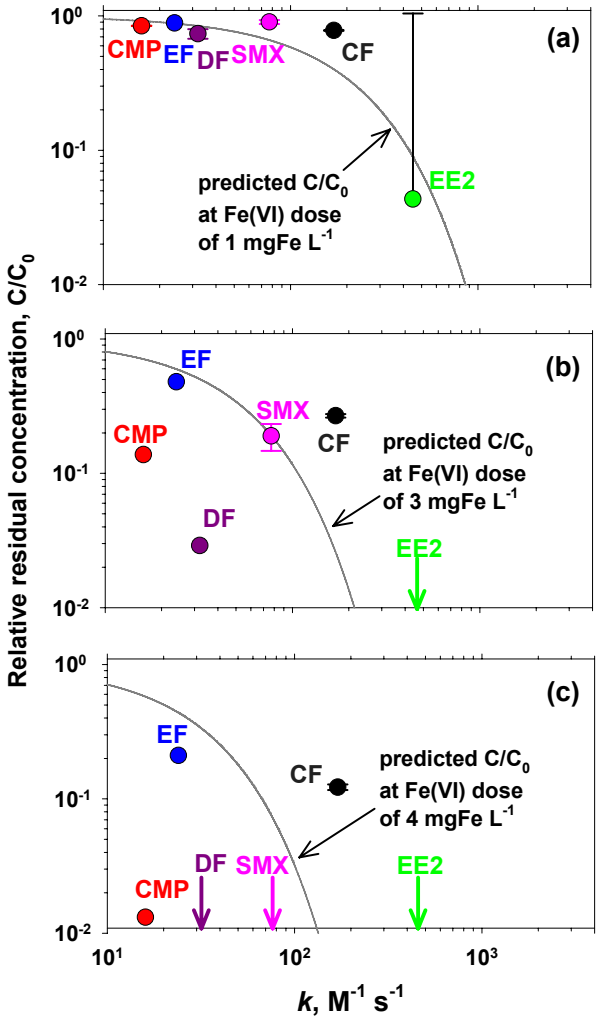

Figure 4.4. Measured and predicted relative residual concentration (C/C_0) of selected micropollutants during treatment of a wastewater (DDWW) wastewater at pH 8 with Fe(VI). Predicted relative residual concentration (lines) at Fe(VI) doses of (a) 1.0 mg Fe L^{-1}, (b) 3.0 mg Fe L^{-1} and (c) 4.0 mg Fe L^{-1}, was calculated by using eq 4.4 and the resulting Fe(VI) exposures of (a) 5.0 mg Fe L^{-1} min, (b) 34 mg Fe L^{-1} min and (c) 46 mg Fe L^{-1} min (Figure S4.13). Abbreviations: EE2 = 17α-ethinylestradiol, EF = enrofloxacin, CF = ciprofloxacin, CMP = carbamazepine, SMX = sulfamethoxazole, DF = diclofenac. Circles represent measured relative residual concentrations at the respective Fe(VI) doses shown in Figure 4.3. The arrows indicate that the relative residual concentration of the respective micropollutant is below its quantification limit (4 % of the initial concentration) at the corresponding Fe(VI) dose.

There are several possible reasons for the discrepany between measured and predicted eliminations. One of the possibilities is the difference of *k* which is measured by Fe(VI) decay and micropollutant decay. The method monitoring the Fe(VI) decay (which is mainly employed in the current study) can yield a *k* which differs from that obtained by the method monitoring the micropollutant decay, by the stoichiometric factor η, which defines the number of Fe(VI) molecules consumed per molecule of target micropollutant under the experimental conditions. Deviations from η = 1 can be caused by fast side reactions of Fe(VI) with products of the primary (or secondary) reactions. Little is known about the η values of Fe(VI) reactions with organic compounds in literatures. Only Sharma et al 2006 (*12*) reported the η value of ~4 for the Fe(VI) reaction with sulfamethoxazole. If we assume that the η values for Fe(VI) reactions range from 1 to 4 (based on the case of sulfamethoxazole), the *k*, which is measured by monitoring Fe(VI) decay can overestimate the transformation of a micropollutant up to a factor of 4. The difference in the *k* from the two kinetic methods can partially explain the observed lower elimination of sulfamethoxazole and ciprofloxacin at pH 7 (Figure S4.12) and ciprofloxacin at pH 8 in DDWW (Figures 4.4) than model predictions.

The other possibility is the contribution of Fe(V) or Fe(IV) species to the enhanced oxidation of the compounds. Fe(VI) has been known to react via one-electron or two-electron transfer depending on its reaction counterparts, generating Fe(V) or Fe(IV) species, respectively (*8,10,19,25*). Since Fe(V) is known to be several orders of magnitude more reactive than Fe(VI) (*8,19,25*), oxidative elimination rates of micropollutants by Fe(VI) may be enhanced when reactions are conducted in presence of reducing substrates such as dissolved organic matter in wastewater. This might be the case for the higher elimination of diclofenac at pH 7 (Figure S4.12) and sulfamethoxazole, diclofenac, and carbamazepine at pH 8 in DDWW (Figure 4.4). The mechanisms of Fe(VI) reactions with organic compounds are currently poorly understood and therefore a comprehensive discussion of the underlying processes is beyond the scope of this study.

4.3.3 Comparison between Fe(VI) and O_3

Recent studies have demonstrated that ozonation might be a powerful tool for the elimination of various micropollutants during enhanced wastewater treatment (*5,18*). Therefore, it is of interest to compare the ability of Fe(VI) to oxidize various micropollutants in wastewater with O_3. Figure 4.3 shows a comparison between Fe(VI) and O_3 for the eliminations of ERM-containing micropollutants as a function of the oxidant dose in a wastewater (DDWW) at pH 8. For 17α-ethinylestradiol, Fe(VI) and O_3 showed almost the same elimination efficiency. An oxidant dose of 20 μM (~1 mg L^{-1} for Fe(VI) and O_3) achieved a > 95 % elimination of 17α-ethinylestradiol. For the other micropollutants, O_3 was more efficient than Fe(VI) within a factor of 3 in terms of oxidant dose required to achieve > 95 % elimination. The *k* values for Fe(VI) reactions with the investigated micropollutants in Figure 4.3 are several orders of magnitude lower than those for O_3 (Table 4.1). Nevertheless, the observed comparable elimination efficiency of Fe(VI) relative to O_3 can be understood because of the much higher stability of Fe(VI) in a wastewater matrix. As an example, Figure S4.14 shows the decrease of Fe(VI) and O_3 in a secondary effluent from WWTP in Regensdorf, Switzerland at pH 8 for an oxidant dose of 40–45 μM. Fe(VI) was consumed within > 30 min, whereas O_3 was completely consumed in less than 5 min.

4.3.4 Phosphate removal from a wastewater matrix

Figure 4.5a demonstrates the ability of Fe(VI) to eliminate micropollutants and subsequently remove phosphate during treatment of DDWW. A Fe(VI) dose of 7.5 mg Fe L^{-1} lowered the phosphate concentration from initially 3.5 to below 0.8 mg PO_4-P L^{-1} (~ 80 % removal), the regulatory limit for wastewater discharge in Switzerland. Selected micropollutants, sulfamethoxazole, diclofenac, and carbamazepine were eliminated > 97 % at a Fe(VI) dose of 5 mg Fe L^{-1}. It can be predicted that at Fe(VI) doses at which > 80 % removal of phosphate is achieved (≥ 8 mg Fe L^{-1}), many ERM-containing micropollutants can be significantly eliminated. Figure 4.5b compares the phosphate removal efficiency during treatment of DDWW with different forms of iron (Fe(VI), Fe(II) and Fe(III)). Fe(VI) shows a similar efficiency as Fe(II) and a

slightly better efficiency than Fe(III) (within a factor of 1.5). This can be understood by considering a relative homogeneous formation of Fe(III) by Fe(VI) and Fe(II) leading to higher specific surface areas compared to Fe(III) where larger aggregates are formed (*2*).

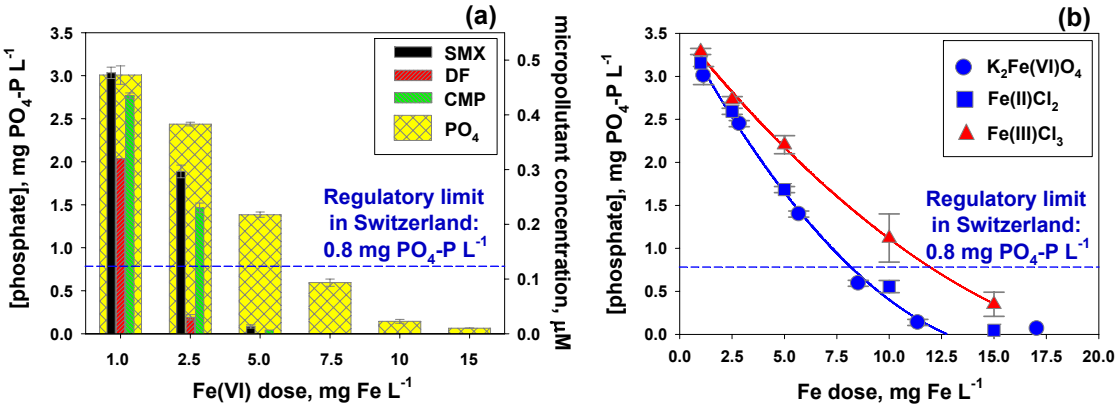

Figure 4.5. (a) Oxidative elimination of selected micropollutants and subsequent removal of phosphate during treatment of a wastewater (DDWW) as a function of the Fe(VI) dose (1.0 – 15 mg Fe L^{-1}) and (b) comparison of phosphate removal efficiency for various forms of iron. A standard jar test protocol was applied for ferric-phosphate precipitation (see materials and methods section for details). Experimental conditions: $[micropollutants]_0$ = 0.5 – 1 µM, $[phosphate]_0$ = 3.5 mg PO_4-P L^{-1}, [DOC] = 5.1 mg C L^{-1}, pH = 7 (10 mM bicarbonate buffer), and T = 23±2 °C. The blue dashed lines represent the regulatory limit for phosphate (0.8 mg PO_4-P L^{-1}) in effluents of wastewater treatment plants in Switzerland (*1*). Abbreviations: SMX = sulfamethoxazole, DF = diclofenac, and CMP = carbamazepine.

4.3.5 Implications for enhanced wastewater treatment

This study has demonstrated that Fe(VI) is a powerful tool to eliminate various micropollutants containing electron-rich moieties as well as to remove phosphate during enhanced treatment of secondary wastewater effluents. Fe(VI) doses required to achieve significant eliminations of micropollutants in the tested wastewater (e.g. > 5 mg Fe L^{-1} per 5 mg C L^{-1} of DOC) were lower than those for a significant phosphate removal (≥ 8 mg Fe L^{-1} for 3.5 to 0.8 mg PO_4-P L^{-1}, the regulatory limit for wastewater

discharge in Switzerland). Therefore, a combined use of Fe(VI) and Fe(III) as an additional coagulant could be a practical method, since Fe(VI) is significantly more expensive than Fe(III). This study mainly focused on the application of Fe(VI) to secondary effluents to eliminate micropollutants and lower the phosphate level in the final effluent significantly (e.g. < 0.8 mg PO_4-P L^{-1}). The application of Fe(VI) can also be considered during primary or secondary treatment of wastewater. In this case, a higher consumption of Fe(VI) by higher concentrations of suspended (e.g. sludge) or dissolved organic matter is expected, which decreases the oxidation efficiency for micropollutants. Finally, for the wastewater treatment plants already practicing a chemical phosphorus removal, it can be straightforward to switch to a Fe(VI) treatment because the existing facilities for pumping and mixing can be used. However, technologies for on-site production of aqueous Fe(VI) and its rapid application is required because of the unstable nature of Fe(VI) in contact with water. Furthermore, additional research is needed to assess the feasibility of the Fe(VI) treatment process in pilot- or full-scale wastewater treatment plants.

Acknowledgements

This study was part of the EU Neptune project (Contract No 036845, SUSTDEV-2005-3.II.3.2), which was financially supported by grants obtained from the EU Commission within the Energy, Global Change and Ecosystems Program of the Sixth Framework (FP6-2005-Global-4). Support for Y. Lee was partially provided by Korean Research Foundation Grant (MOEHRD) (KRF-2005-214-D00258). The authors would like to thank E. Salhi and H. Laubscher for laboratory assistance; and J. Ma for providing a Fe(VI) sample. Four anonymous reviewers are acknowledged for their constructive comments. Y. Lee and S. G. Zimmermann contributed equally to this study.

4.4 References

(1) Swiss Water Protection Ordinance (Gewässerschutzverordnung, SR no. 814.201), 1998. Available at http://www.admin.ch/ch/d/sr/c814_201.html (April, 2009).

(2) Valsami-Jones, E. *Phosphorus in Environmental Technology: Principles and Applications*; IWA Publishing: London, 2004.

(3) Ternes, T. A.; Joss, A. *Human Pharmaceuticals, Hormones and Fragrances. The Challenge of Micropollutants in Urban Water Management*, IWA Publishing: London, 2006.

(4) Huber, M. M.; Canonica, S.; Park, G. Y.; von Gunten, U. Oxidation of pharmaceuticals during ozonation and advanced oxidation processes. *Environ. Sci. Technol.* **2003**, *37*, 1016–1024.

(5) Huber, M. M.; Göbel, A.; Joss, A.; Hermann, N.; Löffler, D.; McArdell, C. S.; Ried, A.; Siegrist, H.; Ternes, T. A.; von Gunten, U. Oxidation of pharmaceuticals during ozonation of municipal wastewater effluents: A pilot study. *Environ. Sci. Technol.* **2005**, *39*, 4290–4299.

(6) Yuan, B. L.; Qu, J. H.; Fu, M. L. Removal of cyanobacterial microcystin-LR by ferrate oxidation-coagulation. *Toxicon* **2002**, *40*, 1129–1134.

(7) Lee, Y.; Um, I. H.; Yoon, J. Arsenic(III) oxidation by iron(VI) (ferrate) and subsequent removal of arsenic(V) by iron(III) coagulation. *Environ. Sci. Technol.* **2003**, *37*, 5750–5756.

(8) Rush, J. D.; Cyr, J. E.; Zhao, Z.; Bielski, B. H. J. The oxidation of phenol by ferrate(VI) and ferrate(V). A pulse radiolysis and stopped-flow study. *Free Rad. Res.* **1996**, *22*, 349–360.

(9) Lee, Y.; Yoon, J.; Von Gunten, U. Kinetics of the oxidation of phenols and phenolic endocrine disruptors during water treatment with ferrate (Fe(VI)). *Environ. Sci. Technol.* **2005**, *39*, 8978–8984.

(10) Hornstein, B. J. Reaction mechanisms of hypervalent iron: The oxidation of amines and hydroxylamines by potassium ferrate, K_2FeO_4. Ph.D. Thesis. New Mexico State University, Las Cruces, NM, 1999.

(11) Huang, H.; Sommerfeld, D.; Dunn, B. C.; Lloyd, C. R.; Eyring, E. M. Ferrate(VI) oxidation of aniline. *J. Chem. Soc., Dalton Trans.* **2001**, 1301–1305.

(12) Sharma, V. K.; Mishra, S. K.; Nesnas, N. Oxidation of sulfonamide antimicrobials by ferrate(VI) [$Fe^{VI}O_4^{2-}$]. *Environ. Sci. Technol.* **2006**, *40*, 7222–7227.

(13) Lee, C.; Lee, Y.; Schmidt, C.; Yoon, J.; Von Gunten, U. Oxidation of suspected N-nitrosodimethylamine (NDMA) precursors by ferrate (VI): Kinetics and effect on the NDMA formation potential of natural waters. *Water Res.* **2008**, *42*, 433–441.

(14) Noorhasan, N. N.; Sharma, V. K. Kinetics of the reaction of aqueous iron(VI) ($Fe^{VI}O_4^{2-}$) with ethylenediaminetetraacetic acid. *Dalton Transactions* **2008**, 1883–1887.

(15) Hu, L.; Martin, H. M.; Arce-Bulted, O.; Sugihara, M. N.; Keating, K. A.; Strathmann, T. J. Oxidation of carbamazepine by Mn(VII) and Fe(VI): reaction kinetics and mechanism. *Environ. Sci. Technol.* **2009,** *43*, 509–515.

(16) Lee, Y.; Yoon, J.; von Gunten, U. Spectrophotometric determination of ferrate (Fe(Vl)) in water by ABTS. *Water Res.* **2005**, *39*, 1946–1953.

(17) *Standard Methods for the Examination of Water and Wastewater*; 20th ed.; APHA, AWWA, WPCF: Washington DC, 1998.

(18) Dodd, M. C.; Buffle, M. O.; von Gunten, U. Oxidation of antibacterial molecules by aqueous ozone: Moiety-specific reaction kinetics and application to ozone-based wastewater treatment. *Environ. Sci. Technol.* **2006**, *40*, 1969–1977.

(19) Rush, J. D.; Zhao, Z. W.; Bielski, B. H. J. Reaction of ferrate(VI)/ferrate(V) with hydrogen peroxide and superoxide anion - A stopped-flow and premix pulse radiolysis study. *Free Rad. Res.* **1996**, *24*, 187–198.

(20) Deborde, M.; Rabouan, S.; Duguet, J. P.; Legube, B. Kinetics of aqueous ozone-induced oxidation of some endocrine disruptors. *Environ. Sci. Technol.* **2005**, *39*, 6086–6092.

(21) Suarez, S.; Dodd, M. C.; Omil, F.; von Gunten, U. Kinetics of triclosan oxidation by aqueous ozone and consequent loss of antibacterial activity: Relevance to municipal wastewater ozonation. *Water Res.* **2007**, *41*, 2481–2490.

(22) Hoigné, J.; Bader, H. Rate constants of reactions of ozone with organic and inorganic compounds in water–II. Dissociating organic compounds. *Water Res.* **1983**, *17*, 185–194.

(23) Dowideit, P.; von Sonntag, C. Reaction of ozone with ethene and its methyl- and chlorine-substituted derivatives in aqueous solution. *Environ. Sci. Technol.* **1998**, *32*, 1112–1119.

(24) Pierpoint, A. C.; Hapeman, C. J.; Torrents, A. Linear free energy study of ring-substituted aniline ozonation for developing treatment of aniline-based pesticide wastes. *J. Agric. Food Chem.* **2001**, *49*, 3827–3832.

(25) Sharma, V. K.; O'Connor, D. B.; Cabelli, D. E. Sequential one-electron reduction of Fe(V) to Fe(III) by cyanide in alkaline medium. *J. Phys. Chem. B* **2001**, *105*, 11529–11532.

Supporting Information for Chapter 4

Ferrate (Fe(VI)) application for municipal wastewater treatment: A novel process for simultaneous micropollutant oxidation and phosphate removal

14 figures and 9 texts

http://pubs.acs.org/doi/abs/10.1021/es803588k

*Co-primary authors contributed equally to this work

Text S4.1. Standard and reagents

Oxidants and coagulants

Potassium ferrate ($K_2Fe(VI)O_4$) was prepared by the method of Thompson et al. (*1*). The prepared potassium ferrate had a purity of 88 % as Fe(VI) (w/w). This was determined by dissolving known amounts of solid samples in phosphate buffer solutions (5 mM Na_2HPO_4/ 1 mM borate, pH ≈ 9.2), subsequent filtration through 0.45 μm nylon syringe filters (BGB Analytik AG, Switzerland), and measuring the Fe(VI) concentration by both the direct 510 nm method (ε = 1150 $M^{-1}\,cm^{-1}$) and the ABTS method (*2*). The remaining 12 % of Fe of the prepared potassium ferrate were ferric oxide, which was determined by the modified ferrozine method (*3,4*). Stock solutions of Fe(VI) (0.2–3 mM) were freshly prepared by dissolving solid samples of potassium ferrate in pure water (pH ≈ 9.2). The fresh stock solution was also quickly filtered through a 0.45 μm nylon syringe filter (BGB Analytik AG, Switzerland) and then standardized spectrophotometrically at 510 nm. Ozone (O_3) was produced with a Fischer 502 ozone generator by using pure oxygen as feed gas. Ozone stock solutions (~1.5 mM) were produced by sparging ozone-containing oxygen through Milli-Q water that was cooled in an ice bath and were standardized spectrophotometrically at 260 nm (ε = 3000 $M^{-1}\,cm^{-1}$) (*5*). For ferric coagulant, 0.1 M of $FeCl_3$ stock solution was freshly prepared in pure water. The 0.1 M ferric coagulant solution can be classified as type A based on the analysis of Hong-Xiao and Stumm (*6*). Type A ferric solution is in the initial stage of hydrolysis (pH ~ 1.7) and contains monomers (Fe^{3+}, $FeOH^{2+}$, $Fe(OH)_2^{+}$, and complexes with chlorides) and some portions of polynuclear species. Type A was chosen because ferric coagulant solutions with concentrations higher than 0.1 M have been known to be more effective than those of lower concentration (*6*). For ferrous coagulant, a 0.05 M $FeCl_2$ stock solution was freshly prepared in 0.01 M $HClO_4$ to prevent ferrous oxidation by oxygen. In all coagulation experiments, these iron stock solutions were added directly to the water.

Stock solutions of micropollutants and organic model compounds

Several methods were used to prepare stock solutions. Aqueous stock solutions were used for kinetic experiments of Fe(VI) and for the oxidative elimination experiments of micropollutants in the μM-range in a wastewater matrix. For the compounds with a high

aqueous solubility (>> 200 μM at room temperature), the stock solutions were prepared by dissolving known amounts of a compound directly in pure water. For compounds with a low aqueous solubility (< 200 μM), such as carbamazepine, diclofenac and 17α-ethinylestradiol, saturated solutions were first prepared by dissolving excess amounts of a compound in pure water. After mixing a few days in the dark, the saturated solutions were filtered through 0.45 μm PTFE syringe filters (BGB Analytik AG, Switzerland) to get a final aqueous stock solution. The concentrations of these aqueous stock solutions were determined by comparing them with those of the corresponding stock solution prepared in methanol at known concentrations. For the comparison, peak areas in the HPLC/UV chromatogram were compared between the aqueous and the methanol stock solution.

The stock solutions of carbamazepine, enrofloxacin and ciprofloxacin were also prepared in an acetonitrile-water mixture (50/50 %). These stock solutions were used for the determination of second-order rate constants of Fe(VI). The concentrations of micropollutants during kinetic experiments were higher than their aqueous solubility (up to 1 mM) assisted by 2 % acetonitrile. In addition, Fe(VI) decreases were not affected by the presence of 2 % acetonitrile.

Text S4.2. Kinetics of Fe(VI) reactions with compounds: micropollutants and organic model compounds

Second-order rate constants for the reactions of Fe(VI) with compounds were determined in the pH range 5.5–10.5. 10 mM acetic acid/10 mM phosphate was used as a buffer for the pH range 5.0–5.5, 10 mM phosphate for the pH range 6.0–8.5, and 10 mM borate/10 mM phosphate for the pH range 9.0–11.0. Phosphate, borate, and acetic acid have been widely used as a choice of buffer in previous Fe(VI) kinetics studies (*7–9*, as representative examples) as well as in kinetics studies of other water treatment oxidants such as ozone, chlorine, and chlorine dioxide etc (*10–12*, as representative examples) (for ozone, the use of acetic acid as a buffer should be avoided). This is because these compounds have a very low reactivity to oxidants. For example, the second-order rate constant (k) of ozone (O_3) with phosphate, borate, and acetic acid are: $k(O_3 + H_2PO_4^-) = < 2\times10^{-4}$ M^{-1} s^{-1} (*10*), $k(O_3 + H_2BO_3^-) = < 6\times10^{-2}$ M^{-1} s^{-1} (*10*),

and $k(O_3 + CH_3CO_2^-) = \leq 3\times10^{-5}$ M^{-1} s^{-1} (*13*). Given that Fe(VI) is generally far less reactive than O_3 (e.g. see Table 4.1 in the main text), the k of Fe(VI) with these buffers are expected to be very low (k << 0.1 M^{-1} s^{-1} at pH 5 – 11), thus small effects on the Fe(VI) reactions of interest can be expected. In addition, the presence of phosphate is required in all pH conditions because it prevents the precipitation of Fe(III) by forming soluble ferric-phosphate complex. Without phosphate or other proper complexing agents, a ferric oxyhydroxide-precipitate is formed and can interfere with the Fe(VI) reactions of interest.

For all investigated compounds except diclofenac, kinetic experiments were conducted under pseudo-first-order conditions with the target compound in excess to Fe(VI) ($[compound]_0$ >> $10\times[Fe(VI)]_0$, and $[Fe(VI)]_0$ = 0.5–5 μM) and the decrease of the concentration of Fe(VI) was measured as a function of the reaction time. Fe(VI) is unstable at pH < 9 and decompose to Fe(III), oxygen (O_2), and hydrogen peroxide (H_2O_2) as final products (*7*,*8*,*14*). This Fe(VI) self-decomposition follows a second-order reaction kinetic with respect to Fe(VI) concentration, indicating that the reaction between two Fe(VI) is the rate-limiting step for the Fe(VI) self-decomposition. To minimize the Fe(VI) self-decomposition during our kinetic experiments, low initial Fe(VI) concentrations (0.5–5 μM) or high compound concentrations (>> 5 μM) were employed. To choose a proper inital Fe(VI) concentration at a given pH condition, the second-order rate constant (k_{self}) for the Fe(VI) self-decomposition was considered to predict the Fe(VI) self-decomposition as a function of time. For example, the k_{self} at different pH conditions are: 450 M^{-1} s^{-1} at pH 5, 130 M^{-1} s^{-1} at pH 6, 52 M^{-1} s^{-1} at pH 7, and 6.2 M^{-1} s^{-1} at pH 8 (*14*). Since the self-decomposition of Fe(VI) follows the second-order kinetics with respect to Fe(VI), the Fe(VI) concentration as a function of time (τ) can be predicted based on eq S4.1:

$$[Fe(VI)]_\tau = \frac{[Fe(VI)]_0}{1 + 2k_{self}[Fe(VI)]_0\,\tau} \qquad \text{(S4.1)}$$

where $[Fe(VI)]_0$ and τ represent the initial Fe(VI) concentration and the reaction time, respectively.

Figure S4.1 shows the predicted Fe(VI) self-decomposition as a function of time at different pH and initial Fe(VI) concentrations at pH 5 – 8. The different time window at

each condition shows the maximum reaction time allowed in the experiments to determine second-order rate constants of Fe(VI) reactions with compounds (e.g. Figure S4.2). For all pH conditions, the Fe(VI) self-decomposition was less than 5 % of the initial Fe(VI) concentration for a given reaction time. Therefore, the Fe(VI) self-decomposition was not considered in evaluating the rate constants of Fe(VI) reactions with the selected compounds.

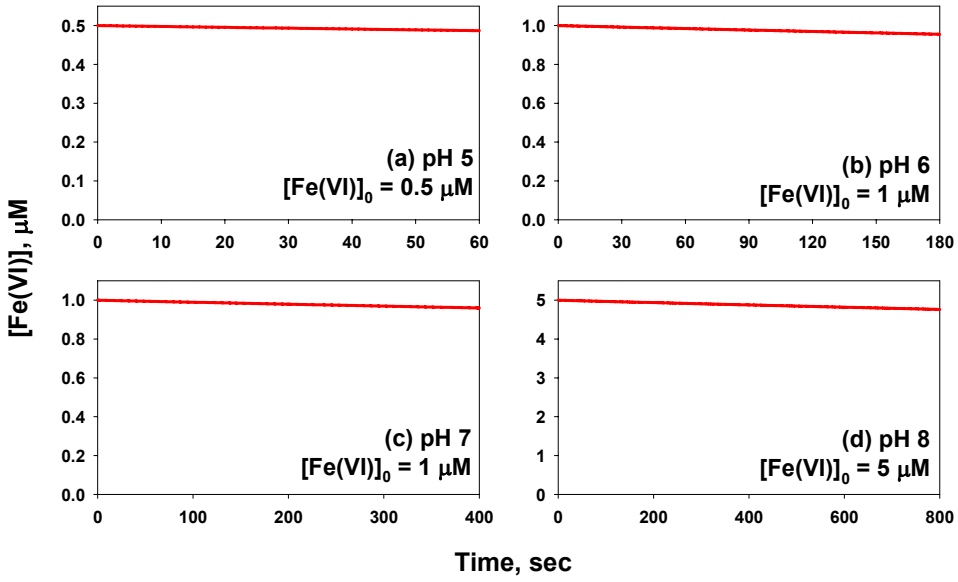

Figure S4.1. Predicted Fe(VI) self-decomposition as a function of time at different pH and initial Fe(VI) concentrations. (a) pH 5 and $[Fe(VI)]_0$ = 0.5 μM, (b) pH 6 and $[Fe(VI)]_0$ = 1 μM, (c) pH 7 and $[Fe(VI)]_0$ = 1 μM, and (d) pH 8 and $[Fe(VI)]_0$ = 5 μM. The predictions were made by using the eq S4.1 $(Fe(VI)]_\tau = \frac{[Fe(VI)]_0}{1 + 2k_{self}[Fe(VI)]_0 \tau}$) and the known second-order rate constants for Fe(VI) self-decomposition (k_{self} = 450 M^{-1} s^{-1} at pH 5, 130 M^{-1} s^{-1} at pH 6, 52 M^{-1} s^{-1} at pH 7, and 6.2 M^{-1} s^{-1} at pH 8 (*14*)). The different time window at different pH and initial Fe(VI) concentrations shows the maximum reaction time allowed in the experiments to determine second-order rate constants of Fe(VI) reactions with compounds (e.g. Figure S4.2).

Kinetic runs were started by injecting an aliquot of a Fe(VI) stock solution (0.2–3 mM) under rapid mixing. At proper time intervals, 1–20 mL of the reaction solution was sampled and quenched with the ABTS solution to measure residual Fe(VI) concentrations (*2*). The pseudo-first order rate constants (k_{app}') were calculated from the slope of the linear curve resulting from a plot of log-decrease of Fe(VI) concentration vs. the reaction time (see Figure S4.2 as an example). For all investigated compounds, Fe(VI) followed a pseudo-first order decrease, confirming that the reaction is first-order with respect to Fe(VI) (Figure S4.2).

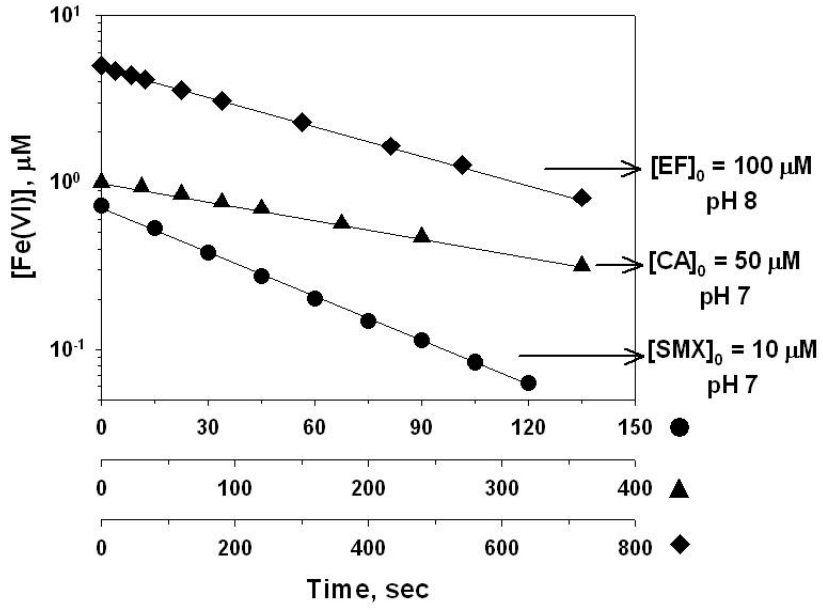

Figure S4.2. Examples of the pseudo-first-order kinetic plot for the decrease of Fe(VI) concentration vs. reaction time in presence of excess compound in aqueous solution at 23±2 °C. SMX = sulfamethoxazole, CA = carbamazepine, and EF = enrofloxacin.

The k_{app}' values were also determined at various concentrations of compounds. For all investigated compounds, k_{app}' increases linearly with increasing concentration of compounds, confirming the reaction to be also first-order with respect to the target compounds. Figure S4.3 shows an example of the linearity of k_{app}' vs. the concentration of aniline at pH 9. The second-order rate constants k were then obtained by dividing the pseudo first-order rate constants by the concentration of the compound.

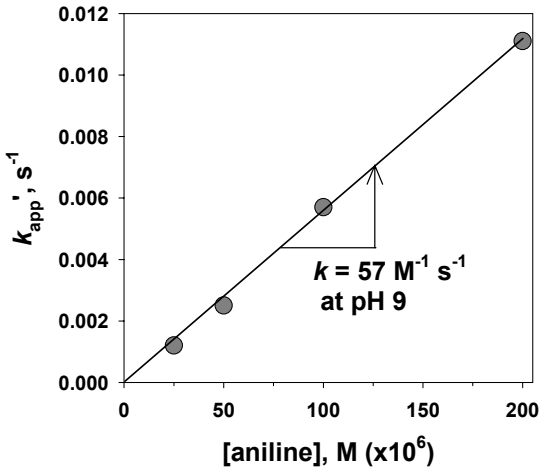

Figure S4.3. Plot of the pseudo first-order rate constant for the decrease of Fe(VI) (k_{app}') vs. the initial aniline concentration at pH 9 and 23±2 °C

For diclofenac, kinetic experiments were conducted under pseudo-first-order conditions with Fe(VI) in excess to diclofenac ($[Fe(VI)]_0 >> 10\times[diclofenac]_0$, and $[diclofenac]_0$ = 0.6 – 1 μM) and the decrease of the diclofenac and Fe(VI) concentrations were measured as a function of the reaction time. The kinetic runs were started by adding an aliquot of a Fe(VI) stock solution (1 – 2 mM) under rapid mixing. At proper time intervals, 1–5 mL of the reaction solution were sampled and quenched with a thiosulfate solution (5 mM) to measure residual diclofenac concentrations as well as with an ABTS solution to measure residual Fe(VI) concentrations (*2*). It was necessary to measure the rate of Fe(VI) decrease because Fe(VI) decomposed more than 10 % by its self-decomposition at initial Fe(VI) concentrations of > 10 μM and at pH < 9. The data was evaluated by plotting the natural logarithm of the diclofenac concentration vs. the Fe(VI) exposure, i.e., Fe(VI) concentration integrated over time, as shown in eq S4.2:

$$\ln([diclofenac]/[diclofenac]_0) = -k \int_0^t [Fe(VI)]\,dt \qquad (S4.2)$$

where the term $\int_0^t [\mathrm{Fe(VI)}]\,dt$ represents the Fe(VI) exposure, the time integrated concentration of Fe(VI) and k (the slope of the resulting straight line) represents the second-order rate constant.

Figure S4.4a shows the concentration time profiles of diclofenac and Fe(VI) during the oxidation of diclofenac (1 μM) by excess Fe(VI) (18 μM) at pH 8 as representative data. Even though Fe(VI) was unstable, the Fe(VI) concentration was always in excess to the concentration of diclofenac within the studied reaction time. Figure S4.4b clearly shows that eq S4.2 successfully represents the kinetics of diclofenac elimination by Fe(VI) oxidation ($R^2 > 0.99$). From the slope of the line in Figure S4.4b, the k was determined as $k = 18.7\ M^{-1}\ s^{-1}$ at pH 8.

Text S4.3. Determinations of micropollutants

Micropollutant concentrations at sub to low μM range were determined with an Agilent 1100 series HPLC system equipped with a Nucleosil 100-5 C18 column (125 mm × 4 mm or 250 mm × 4 mm) and a UV (diode array) and fluorescence detector. Separation was achieved by different gradient programs with the aqueous phase consisting either of 10 mM phosphoric acid or 10 mM citric acid (pH 5) and the solvent phase either of acetonitrile or methanol. The injection volume was 100 μL and the flow rate was set to 1 ml min^{-1}. The repeatability was determined to be 4 % while limit of quantifications (LOQ) were inferred from the lowest standard concentrations used. The limits of quantification were in all cases sufficient to determine an elimination of micropollutants of more than 96 %.

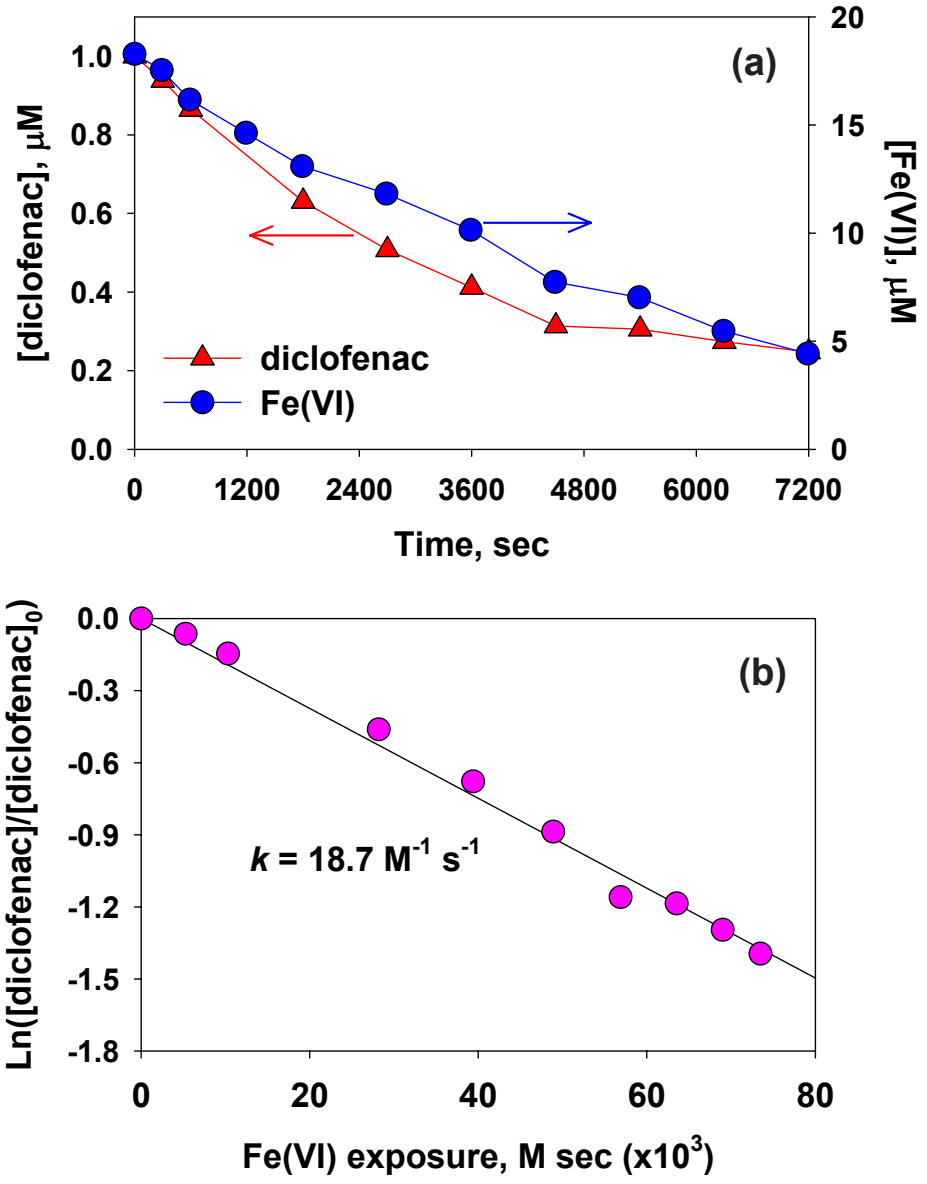

Figure S4.4. (a) Concentration time profiles of diclofenac and Fe(VI). $[diclofenac]_0$ = 1 μM, $[Fe(VI)]_0$ = 18 μM, pH 8, and (b) fit of diclofenac oxidation by Fe(VI) with second-order reaction kinetics (eq S4.2).

Text S4.4. Oxidation of micropollutants by Fe(VI) in a wastewater matrix

A 15 L grab sample of secondary wastewater effluent was obtained from the Dübendorf pilot WWTP (DDWW) which is located near Zürich, Switzerland. The samples were transported to the laboratory in a polypropylene carboy within several hours of sampling and vacuum-filtered with a 0.45 μm cellulose-nitrate membrane. The filtered samples were stored at 4 °C until used. DDWW was sampled twice, for experiments at pH 7 and pH 8, respectively. Characteristics of the two DDWW samples were very similar: the pH, alkalinity, DOC, and phosphate concentration of the original DDWW were 8.0–8.2, 6.6–7.3 mM as HCO_3^-, 7.2–7.6 mg C L^{-1}, and ~0.5 mg PO_4-P L^{-1}, respectively. Typical concentrations of micropollutants present in municipal wastewater secondary effluents are sub to a few μg L^{-1} (*15*). These levels are negligible relative to the concentrations spiked to DDWW, which were 0.2 – 1 μM for each micropollutant (e.g. 0.2 μM of bisphenol-A is equivalent to 46 μg L^{-1}).

DDWW was buffered by adding 10 mM bicarbonate buffer or 20 mM borate buffer and then spiked with a single micropollutant (0.1–1 μM). During this step, DDWW was diluted to have a DOC value of 5.0 – 5.1 mg C L^{-1}. The pH of the wastewater was then adjusted to pH 7 (bicarbonate) and 8 (borate) which is the pH range of municipal wastewater and subsequently transferred into several 25 mL serum vials. In a next step, Fe(VI) doses of 0.1–15 mg Fe L^{-1} were injected into the vials while the water was vigorously stirred for a few seconds. After Fe(VI) was completely consumed (usually after 3 – 5 hours), residual micropollutant concentrations were measured with the HPLC/UV-fluorescence system (Text S4.3). At Fe(VI) doses higher than 2 mg Fe L^{-1}, the treated samples were filtered through a 0.45 μm PTFE filter (BGB Analytik AG, Switzerland) to remove iron-precipitates and then subjected to the HPLC/UV-fluorescence analysis. Losses of micropollutants during the filtration were negligible. Each experiment for a single micropollutant was conducted in duplicate or triplicate.

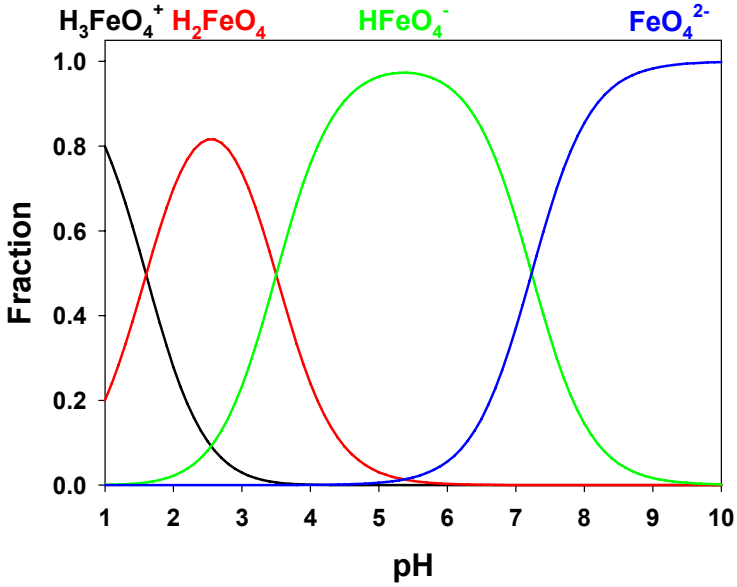

Figure S4.5. Speciation of ferrate as a function of pH based on an equilibrium calculation of dissolved species concentration. The values of $pK_{H_3FeO_4^+}$ = 1.5 for $H_3FeO_4^+ \Leftrightarrow H_2FeO_4 + H^+$ and $pK_{H_2FeO_4}$ = 3.5 for $H_2FeO_4 \Leftrightarrow HFeO_4^- + H^+$ were taken from *(8)*. The value of $pK_{HFeO_4^-}$ = 7.2 for $HFeO_4^- \Leftrightarrow FeO_4^{2-} + H^+$ was taken from *(16)*.

Text S4.5. Reaction scheme for the oxidation of aniline and sulfamethoxazole by Fe(VI)

Aniline

The following reaction scheme is proposed for the aniline oxidation by Fe(VI). In eq S4.3, Fe(VI) reacts with aniline (AN–H) by forming an intermediate complex, such as 'Fe(VI)–AN–H'. The intermediate complex has an acid-base equilibrium as shown in eq S4.4. The forward and backward reactions of eq S4.3 and S4.4 are fast with the corresponding equilibrium constants as K_3 and K_4, respectively. Even though the (de)-protonation may occur either at the Fe(VI)- or aniline-side of the intermediate complex, the (de)-protonation is given only in the aniline-side of the complex in eq S4.4 for the sake of simplicity. The rate limiting step is the reaction of these intermediates with an additional aniline as shown in eq S4.5 and S4.6, which leads to a consumption of Fe(VI) and oxidation of aniline.

$$\text{Fe(VI)} + \text{AN–H} \Leftrightarrow \text{Fe(VI)–AN–H} \qquad k_3/k_{-3} = K_3 \qquad \text{(S4.3)}$$

$$\text{Fe(VI)–AN–H} \Leftrightarrow \text{Fe(VI)–AN}^- + \text{H}^+ \qquad k_4/k_{-4} = K_4 \qquad \text{(S4.4)}$$

$$\text{Fe(VI)–AN–H} + \text{AN–H} \rightarrow \rightarrow \text{products} \qquad k_5 \text{ (rate limiting step)} \qquad \text{(S4.5)}$$

$$\text{Fe(VI)–AN}^- + \text{AN–H} \rightarrow \rightarrow \text{products} \qquad k_6 \text{ (rate limiting step)} \qquad \text{(S4.6)}$$

In the present study, we used the ABTS method to determine the decrease of Fe(VI) concentration as a function of time during the reaction of Fe(VI) with excess of aniline. We assume that the intermediate complex species (Fe(VI)–AN–H/Fe(VI)–AN$^-$) can oxidize ABTS and produce the same amount of ABTS$\bullet^+$ as Fe(VI) does in the ABTS method. Therefore, the total Fe(VI) concentration is given as shown in eq S4.7:

$$[\text{Fe(VI)}]_{\text{tot}} = [\text{Fe(VI)}] + [\text{Fe(VI)–AN–H}] + [\text{Fe(VI)–AN}^-] \qquad \text{(S4.7)}$$

Based on the assumption that eq S4.5 and S4.6 are the rate limiting step, the loss of Fe(VI) can be written as eq S4.8:

$$-\frac{\text{d}[\text{Fe(VI)}]_{\text{tot}}}{\text{dt}} = k[\text{Fe(VI)}]_{\text{tot}}[\text{AN–H}]$$

$$= k_5[\text{Fe(VI)–AN–H}][\text{AN–H}] + k_6[\text{Fe(VI)–AN}^-][\text{AN–H}] \qquad \text{(S4.8)}$$

and therefore, k can be expressed by eq S4.9:

$$k = k_5\alpha_1 + k_6\alpha_2 \qquad \text{(S4.9)}$$

where α_1 and α_2 represent the fraction of Fe(VI)–AN–H and Fe(VI)–AN$^-$, respectively.

By using eq S4.3, S4.4, and S4.7, α_1 and α_2 can be expressed as eq S4.10 and S4.11, respectively:

$$\alpha_1 = \frac{[\text{Fe(VI)} - \text{AN} - \text{H}]}{[\text{Fe(VI)}]_{\text{tot}}} = \frac{1}{\left(\frac{1}{K_3[\text{AN} - \text{H}]} + 1 + \frac{K_4}{[\text{H}^+]}\right)} \qquad \text{(S4.10)}$$

$$\alpha_2 = \frac{[\text{Fe(VI)} - \text{AN}^-]}{[\text{Fe(VI)}]_{\text{tot}}} = \frac{\frac{K_4}{[\text{H}^+]}}{\left(\frac{1}{K_3[\text{AN} - \text{H}]} + 1 + \frac{K_4}{[\text{H}^+]}\right)} \quad \text{(S4.11)}$$

Under conditions of K_3[AN–H] > 10, eq S4.10 and S4.11 can be changed to eq S4.12 and S4.13, respectively. This means that if K_3 or [AN–H] is large enough, most of the Fe(VI) exists as the form of Fe(VI)–AN–H and Fe(VI)–AN$^-$. In this case, the pH-dependence of k in eq S4.9 is determined only by the k_5, k_6 and K_4. The species specific rate constants, k_5 and k_6, and the equilibrium constant, K_4, were fitted by least-square non-linear regressions of the experimental k data with eq S4.9 by using the software GraphPad Prism (www.graphpad.com).

$$\alpha_1 = \frac{[\text{Fe(VI)} - \text{AN} - \text{H}]}{[\text{Fe(VI)}]_{\text{tot}}} = \frac{[\text{H}^+]}{[\text{H}^+] + K_4} \quad \text{(S4.12)}$$

$$\alpha_2 = \frac{[\text{Fe(VI)} - \text{AN}^-]}{[\text{Fe(VI)}]_{\text{tot}}} = \frac{K_4}{[\text{H}^+] + K_4} \quad \text{(S4.13)}$$

The above proposed model could explain the experimental k well (R^2 = 0.94), which supports the above proposed reaction scheme. The fitted values by non-linear regression analysis were k_5 = 6.8(±2.8)×10^4 M^{-1} s^{-1}, $k_6 \approx 0$, and pK_4 = 6.0(±0.2), respectively. Therefore, only the reaction of the protonated species of the intermediate with aniline (eq S4.5) is contributing to the pH-dependence for the reaction between Fe(VI) and aniline.

Sulfamethoxazole

Sulfamethoxazole contains an aniline moiety, and therefore it is assumed that it reacts with Fe(VI) through the same reaction scheme proposed for aniline. The initiation step is the reaction of Fe(VI) with sulfamethoxazole to form an intermediate complex, such as 'Fe(VI)–SMX–H' as shown in eq S4.14.

$$\text{Fe(VI)} + \text{SMX–H} \Leftrightarrow \text{Fe(VI)–SMX–H} \qquad k_{14}/k_{-14} = K_{14} \quad \text{(S4.14)}$$

However, eq S4.9 could not explain the pH-dependence of *k* for sulfamethoxazole. The *k* for sulfamethoxazole exhibits more than one-log unit increase for each unit decrease of pH from 9 to 7 (see Figure 4.1 in the main text). To explain this high pH-dependence of *k*, the existence of two acid-base equilibria for Fe(VI)–SMX–H is proposed as shown in eq S4.15 and S4.16.

$$\text{Fe(VI)–SMX–H}_2^+ \Leftrightarrow \text{Fe(VI)–SMX–H} + \text{H}^+ \qquad k_{15}/k_{-15} = K_{15} \qquad \text{(S4.15)}$$

$$\text{Fe(VI)–SMX–H} \Leftrightarrow \text{Fe(VI)–SMX}^- + \text{H}^+ \qquad k_{16}/k_{-16} = K_{16} \qquad \text{(S4.16)}$$

The rate limiting step for sulfamethoxazole oxidation by Fe(VI) is the reaction of the intermediates with an additional sulfamethoxazole as shown in eq S4.17, S4.18, and S4.19.

$$\text{Fe(VI)–SMX–H}_2^+ + \text{SMX–H} \rightarrow \rightarrow \text{products} \qquad k_{17} \text{ (rate limiting step)} \qquad \text{(S4.17)}$$

$$\text{Fe(VI)–SMX–H} + \text{SMX–H} \rightarrow \rightarrow \text{products} \qquad k_{18} \text{ (rate limiting step)} \qquad \text{(S4.18)}$$

$$\text{Fe(VI)–SMX}^- + \text{SMX–H} \rightarrow \rightarrow \text{products} \qquad k_{19} \text{ (rate limiting step)} \qquad \text{(S4.19)}$$

Therefore, the *k* for sulfamethoxazole can be expressed by eq S4.20:

$$k = k_{17}\beta_1 + k_{18}\beta_2 + k_{19}\beta_3 \qquad \text{(S4.20)}$$

where β_1, β_2, and β_3 represent the fraction of Fe(VI)–SMX–H_2^+, Fe(VI)–SMX–H, and Fe(VI)–SMX^-, respectively. In the condition of K_{14}[SMX–H] > 10 which was also assumed for the case of aniline, β_1, β_2, and β_3 can be expressed as eq S4.21, S4.22, and S4.23, respectively.

$$\beta_1 = \frac{[\text{Fe(VI)} - \text{SMX} - \text{H}^+]}{[\text{Fe(VI)}]_{\text{tot}}} = \frac{[\text{H}^+]^2}{[\text{H}^+]^2 + [\text{H}^+]K_{15} + K_{15}K_{16}} \qquad \text{(S4.21)}$$

$$\beta_2 = \frac{[\text{Fe(VI)} - \text{SMX} - \text{H}]}{[\text{Fe(VI)}]_{\text{tot}}} = \frac{[\text{H}^+]K_{15}}{[\text{H}^+]^2 + [\text{H}^+]K_{15} + K_{15}K_{16}} \quad \text{(S4.22)}$$

$$\beta_3 = \frac{[\text{Fe(VI)} - \text{SMX}^-]}{[\text{Fe(VI)}]_{\text{tot}}} = \frac{K_{15}K_{16}}{[\text{H}^+]^2 + [\text{H}^+]K_{15} + K_{15}K_{16}} \quad \text{(S4.23)}$$

Non-linear regression analysis showed that the above proposed model could (eq S4.20) explain the experimental k well ($R^2 = 0.96$), which supports the above proposed reaction scheme. In addition, only the reaction of the di-protonated species of the intermediate with sulfamethoxazole (eq S4.17) is mainly contributing to the pH-dependence for the reaction between Fe(VI) and sulfamethoxazole ($k_{18} \approx 0$ and $k_{19} \approx 0$). The fitted values by non-linear regression analysis were $k_{17} = 9.2(\pm 1.7)\times 10^3$ M^{-1} s^{-1}, pK_{15} = 6.4 (±0.2), and pK_{16} = 7.8 (±0.3), respectively.

Text S4.6. Comparison of the second-order rate constants for aniline and sulfamethoxazole with literature data

The second-order rate constants (k) for the reaction of Fe(VI) with aniline and sulfamethoxazole have previously been measured by Hornstein 1999, Huang et al. 2001 (*17*,*18*) and Sharma et al. 2006 (*19*). In the following section, we compare these rate constants with our data.

Aniline

Figure S4.6 shows the pH dependent second-order rate constants (k) for the reaction of Fe(VI) with aniline from this study (pink diamonds and lines) with literature values. Hornstein (*17*) observed the formation of a Fe(VI)-aniline intermediate from the Fe(VI)/aniline reaction and the intermediate has a λ_{max} at 475 nm with a molar absorption coefficient of 1,200 M^{-1} cm^{-1}. The formation of the Fe(VI)-aniline intermediate was found to be first order with respect to Fe(VI) and aniline concentration. The k for the intermediate formation is shown as red circles in Figure S4.6. This initial step probably corresponds to the forward step of eq S4.3 in Text S4.5, and therefore the measured k corresponds to the k_3 in our reaction scheme. Hornstein also determined the k for the decay of the Fe(VI)-aniline intermediate. The k for the decay of the Fe(VI)-

aniline intermediate is shown as blue squares in Figure S4.6. This second step probably corresponds to the eq S4.5 in Text S4.5, and therefore the measured k corresponds to the $k_5\alpha_1$ in our reaction scheme. The k values from this study, which represent the reaction rate between Fe(VI)-aniline intermediate and aniline ($k_5\alpha_1$), are higher than those of Hornstein by a factor of up to 5. The k for the formation of the Fe(VI)-aniline intermediate (k_3) are higher than the k for the decay of the intermediate ($k_5\alpha_1$), which is consistent with the reaction scheme proposed in this study (Text S4.5).

Huang et al. 2001 (*18*) also determined the k for the Fe(VI)/aniline reaction. They monitored the progress of the reaction by measuring the absorbance change in a stopped-flow spectrophotometer. However, they did not specify which wavelength they used to monitor the reaction. Contrary to the case of Hornstein 1999, Huang et al. 2001 did not indicate the formation and decay of the intermediate. Therefore, it is not clear whether the k determined by Huang et al. corresponds to the k_3 or $k_5\alpha_1$ of this study. The k values of Huang et al. are shown as black triangles in Figure S4.6 and similar to the values determined in this study ($k_5\alpha_1$). It is noteworthy that 1) the Fe(VI)-aniline intermediate observed by Hornstein 1999 has a similar spectrum (ε = 1,200 M^{-1} cm^{-1} at λ_{max} of 475 nm) compared to Fe(VI) (ε = 1,150 M^{-1} cm^{-1} at λ_{max} of 510 nm) and 2) the formation rate of the intermediate is > 5-fold faster than its decay rate (*17*). Therefore, there is a possibility that Huang et al. 2001 measured the decay of the intermediate ($k_5\alpha_1$).

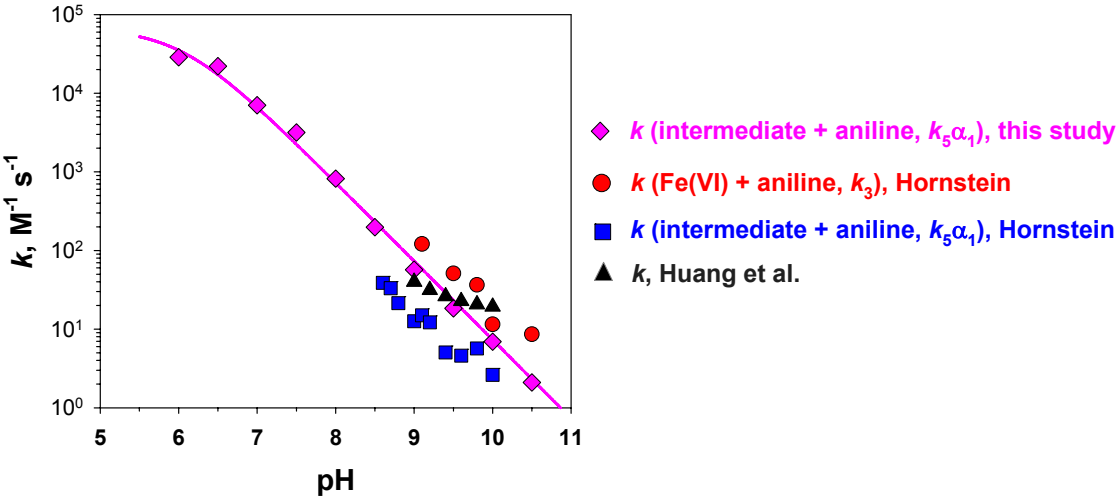

Figure S4.6. Comparison of the pH-dependent second-order rate constants (k) for the reaction of Fe(VI) with aniline. Pink diamonds (measured) and pink lines (model calculations) are from this study. Red circles represent the k for the formation of a Fe(VI)-aniline intermediate (*17*). Blue squares represent the k for the decay of the Fe(VI)-aniline intermediate (*17*). Black triangles represent the k from (*18)*, which is re-produced based on the rate equation in the corresponding reference.

Sulfamethoxazole

Figure S4.7 shows the pH-dependent k for the reaction of Fe(VI) with sulfamethoxazole from this study (pink diamonds and lines) and Sharma et al. 2006 (black triangles, (*19*)). Sharma et al. 2006 monitored the progress of the reaction by measuring the absorbance at 510 nm in a stopped-flow spectrophotometer. They did not indicate the formation and decay of a Fe(VI)-sulfamethoxazole intermediate. Therefore, it is not clear whether the k determined by Sharma et al. corresponds to the k_{15} or $k_{17}\beta_1$ of this study (Text S4.5). The k values of Sharma et al. 2006 are similar to the values determined in this study ($k_{17}\beta_1$). If the Fe(VI)-sulfamethoxazole intermediate has a similar spectrum compared to Fe(VI), which was the case for the aniline oxidation by Fe(VI) (*17*), there could be a possibility that Sharma et al. 2006 measured the decay of the intermediate ($k_{17}\beta_1$). Further studies are necessary to confirm this hypothesis.

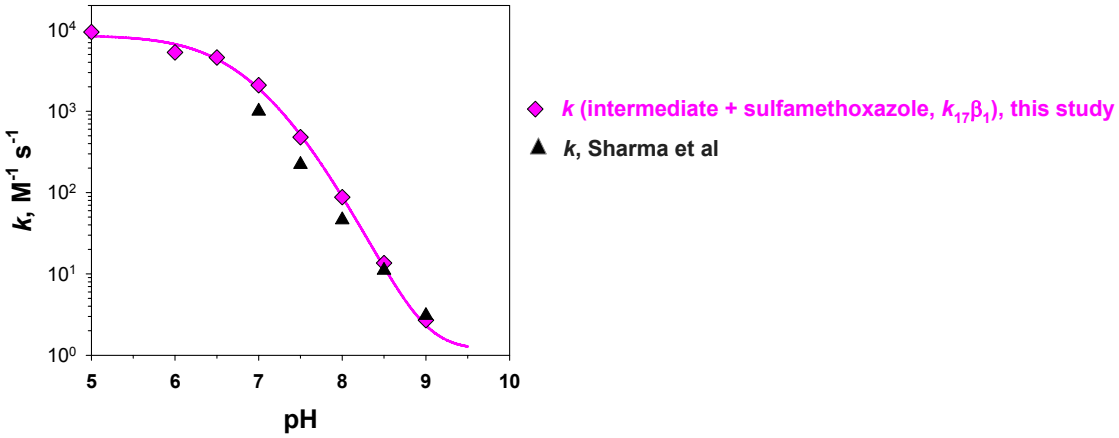

Figure S4.7. Comparison of the pH-dependent second-order rate constants (k) for the reaction of Fe(VI) with sulfamethoxazole. Pink diamonds (measured) and pink lines (model calculations) are from this study. Black triangles represent the k from (*19*), which is reproduced based on the rate equation in the corresponding reference.

Text S4.7. Determination of the rate constant for triclosan: competition kinetics

The second-order rate constant for the reaction of Fe(VI) with triclosan has not been known in literature and its determination in pure water (e.g synthetic buffer solutions) was not within the scope of the current study. However, the rate constant *k* for the reaction of triclosan with Fe(VI) at pH 7 could be estimated based on the elimination of triclosan relative to the other phenolic micropollutants in DDWW by Fe(VI) oxidation (Figure 4.2 in the main text). This so called 'competition kinetic method' is based on the following kinetic concept (*20*).

In competition kinetics, two substrates (here P and R) react with the oxidant (here Fe(VI)) in a batch reactor. P is the compound with unknown rate constant (triclosan) and R is the reference compound whose rate constant is well estabilished with the reagent (17α-ethinylestradiol, 17β-estradiol, and bisphenol-A). If the reaction rate is first order with respect to Fe(VI) and P/R, the loss of P and R per time is given by the following eq S4.24 and S4.25, respectively:

$$-\frac{\mathrm{d[P]}}{\mathrm{dt}} = k_{\mathrm{P}}[\mathrm{P}][\mathrm{Fe(VI)}] \tag{S4.24}$$

$$-\frac{\mathrm{d[R]}}{\mathrm{dt}} = k_{\mathrm{R}}[\mathrm{R}][\mathrm{Fe(VI)}] \tag{S4.25}$$

If neither P nor R is in excess, the integration of eq S4.24 and S4.25 with time (up to τ) generates eq S4.26 and S4.27, respectively.

$$\frac{1}{k_{\mathrm{P}}}\ln\frac{[\mathrm{P}]_\tau}{[\mathrm{P}]_0} = -\int_0^\tau [\mathrm{Fe(VI)}]\mathrm{dt} \tag{S4.26}$$

$$\frac{1}{k_{\mathrm{R}}}\ln\frac{[\mathrm{R}]_\tau}{[\mathrm{R}]_0} = -\int_0^\tau [\mathrm{Fe(VI)}]\mathrm{dt} \tag{S4.27}$$

with $\int_0^\tau [\mathrm{Fe(VI)}]\mathrm{dt}$ as the ferrate exposure. The combination of eq S4.26 and S4.27 generates eq S4.28.

$$\ln\left(\frac{[P]_\tau}{[P]_0}\right) = \ln\left(\frac{[R]_\tau}{[R]_0}\right)\frac{k_P}{k_R} \qquad \text{(S4.28)}$$

According to eq S4.28, k for triclosan ($k_{triclosan}$) could be determined from the slope of the straight line ($k_{triclosan}/k_R$) in a plot of $\ln([triclosan]_\tau/[triclosan]_0)$ vs. $\ln([R]_\tau/[R]_0)$. Figure S4.8 shows the resulting competition kinetic plot using 17α-ethinylestradiol (EE2, red circles), 17β-estradiol (E2, green triangles), and bisphenol-A (BPA, blue squares) as the reference compounds, respectively. In all cases, the relative eliminations of triclosan vs. the other phenolic micropollutants (EE2, E2, and BPA) were well described by eq S4.28 ($R^2 > 0.98$), which supports the validity of the competition kinetic concept even in the wastewater matrix. Finally, the second-order rate constant of $1.1(\pm0.1)\times10^3\ M^{-1}\ s^{-1}$ was obtained for triclosan at pH 7. Based on this rate constant, the species specific second-order rate constant (k_2) between $HFeO_4^-$ and deprotonated triclosan was estimated to be $2.5(\pm0.2)\times10^4\ M^{-1}\ s^{-1}$ by using the following eq S4.29.

$$k_2 = k(\text{pH 7})\ \frac{([H^+] + K_{HFeO4})([H^+] + K_{triclosan})}{[H^+]\,K_{triclosan}} \qquad \text{(S4.29)}$$

where k(pH 7) is the second-order rate constant of Fe(VI) with triclosan at pH 7 ($= 1.1\times10^3\ M^{-1}\ s^{-1}$); $K_{HFeO_4^-}$ ($= 10^{-7.2}$) and $K_{triclosan}$ ($= 10^{-8.1}$) represent the acid-base equilibrium constant of $HFeO_4^-$ and triclosan, respectively.

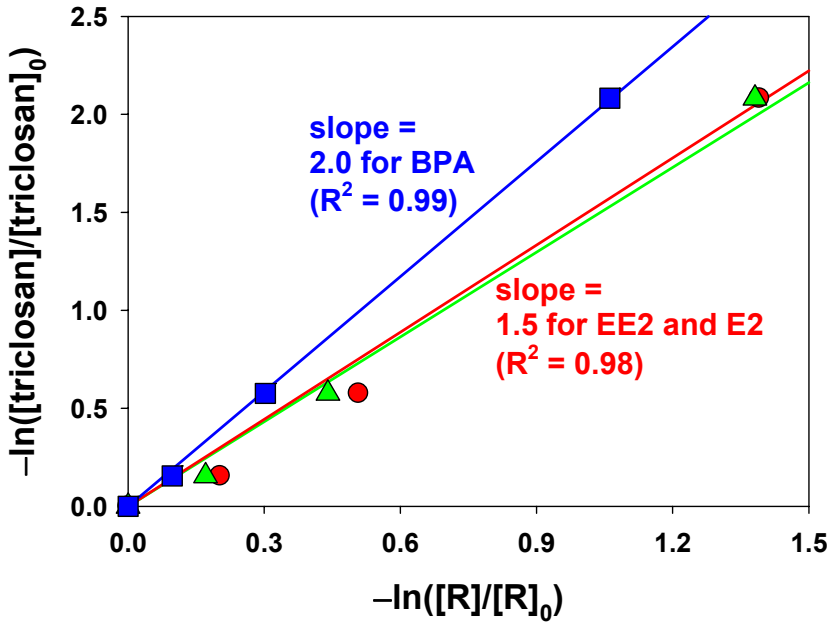

Figure S4.8. Evaluation of the second-order rate constant for the reaction of triclosan with Fe(VI) ($k_{triclosan}$) at pH 7 based on its eliminations in DDWW relative to a reference compound, R (17α-ethinylestradiol = EE2 = red circles, 17β-estradiol = E2 = green triangles, and bisphenol-A = BPA = blue squares). See Figure 4.2 in the main text for the original elimination data.

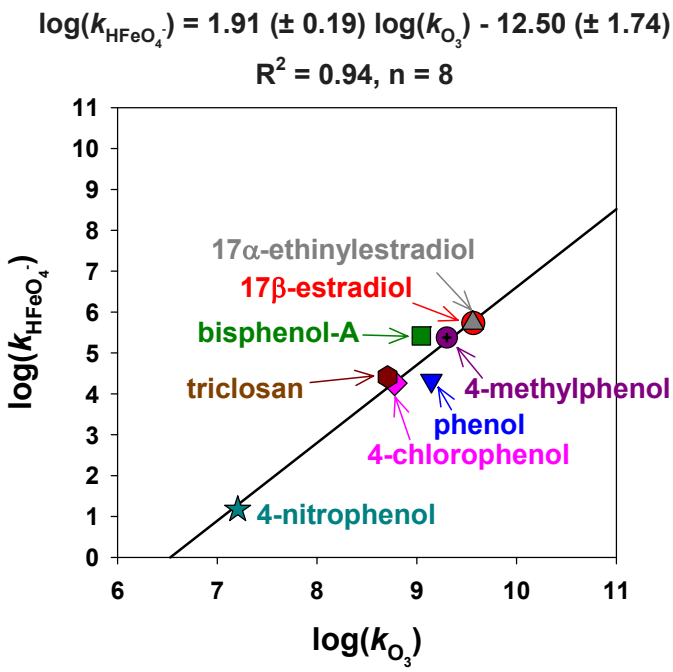

Figure S4.9. Linear correlation between the $\log(k_{HFeO_4^-})$ and $\log(k_{O_3})$ for selected phenolic compounds. $k_{HFeO_4^-}$ and k_{O_3} represent the second-order rate constant of $HFeO_4^-$ and O_3, respectively, with the deprotonated species of the phenolic compounds. All $k_{HFeO_4^-}$ were taken from *(21)* except triclosan. The $k_{HFeO_4^-}$ for triclosan was estimated in this study (Figure S4.8). The k_{O_3} for 17α-ethinylestradiol, 17β-estradiol, and bisphenol-A were taken from *(22)*. The k_{O_3} for phenol, 4-chlorophenol, and 4-nitrophenol were from *(13)*. The k_{O_3} for 4-methylphenol and triclosan were taken from *(23)*.

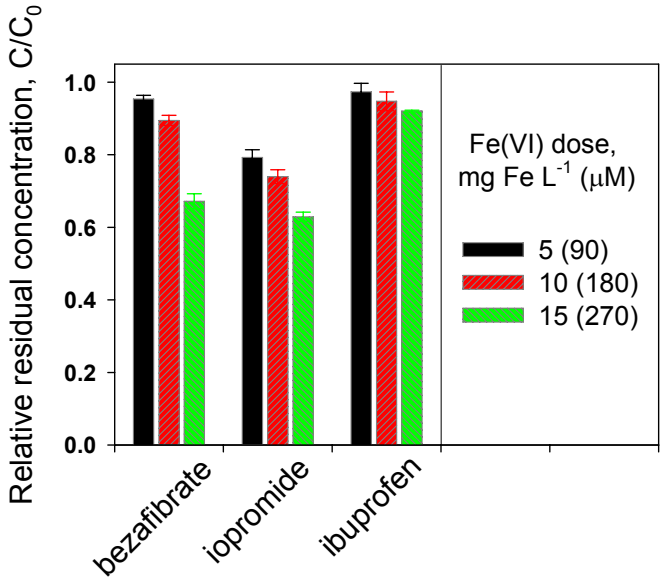

Figure S4.10. Relative residual concentration of selected micropollutants during treatment of wastewater (secondary effluent from Dübendorf WWTP (DDWW), Switzerland) as a function of the Fe(VI) dose (5–15 mg Fe L^{-1}). Experimental conditions: $[micropollutants]_0$ = 1 μM, $[phosphate]_0$ = 3.5 mg PO_4-P L^{-1}, [DOC] = 5.1 mg C L^{-1}, pH = 7 (10 mM bicarbonate buffer), and T = 23±2 °C.

Text S4.8. Determination of Fe(VI) exposures and prediction of micropollutants elimination in DDWW at pH 7

To predict the oxidative elimination of a micropollutant by Fe(VI), Fe(VI) exposures should be known (eq 4.4 in the main text, $\frac{[P]_\tau}{[P]_0} = e^{-k_{Fe(VI)}\int_0^\tau [Fe(VI)]dt}$). Fe(VI) exposures ($=\int_0^\tau [Fe(VI)]dt$) can be calculated from the area below the Fe(VI) decay curve as a function of time. Figure S4.11 shows the time-dependent Fe(VI) concentrations measured in DDWW at pH 7 for various Fe(VI) doses. To facilitate the kinetic modeling of micropollutant elimination, the consumption of Fe(VI) (blue circles, Figure S4.11) was fitted by using the chemical kinetics program Kintecus, version 3.953, www.kintecus.com (blue lines, Figure S4.11). The exploratory model for accounting the Fe(VI) consumption is based on the concept of Buffle et al. *(24)* that has described the reactivity of ozone towards the wastewater matrix or DOM by a continuous description of rate constants and concentrations. Similarly, the Fe(VI) consumption by DOM of the DDWW matrix was fitted iteratively by assuming the existence of three different reactive moieties towards Fe(VI) with the following concentrations and second-order rate constants: $[\text{moiety 1}]_0$ = 21 μM and $k_{\text{Fe(VI) + moiety 1}}$ = 1000 M^{-1} s^{-1}, $[\text{moiety 2}]_0$ = 23 μM and $k_{\text{Fe(VI) + moiety 2}}$ = 100 M^{-1} s^{-1}, and $[\text{moiety 3}]_0$ = 30 μM and $k_{\text{Fe(VI) + moiety 3}}$ = 10 M^{-1} s^{-1}. The determined parameters are purely empirical. In addition to the consumption of Fe(VI) by these three reactive moieties, the self-decay of Fe(VI) (Fe(VI) + Fe(VI) $\rightarrow$ products, $2k$ = 90 M^{-1} s^{-1} at pH 7) was also considered (*14*). With this empirical model, the consumption kinetics of Fe(VI) in DDWW at pH 7 were successfully fitted as shown in Figure S4.11.

Based upon the Fe(VI) exposures in Figure S4.11, the measured and predicted relative residual concentrations of selected micropollutants are compared in Figure S4.12 during treatment of DDWW with Fe(VI) at pH 7. Predicted relative residual concentration of micropollutants at a Fe(VI) dose of 2.5 mg Fe L^{-1} (line in Figure S4.12) were calculated by using eq 4.4 in the main text and a Fe(VI) exposure of 7.7 mg Fe L^{-1} min (Figure S4.11). As results, for 17α-ethinylestradiol, carbamazepine and enrofloxacin, the eliminations were reasonably well predicted. However, the predictions overestimated the

eliminations of ciprofloxacin and sulfamethoxazole and underestimated the elimination of diclofenac (Figure S4.12).

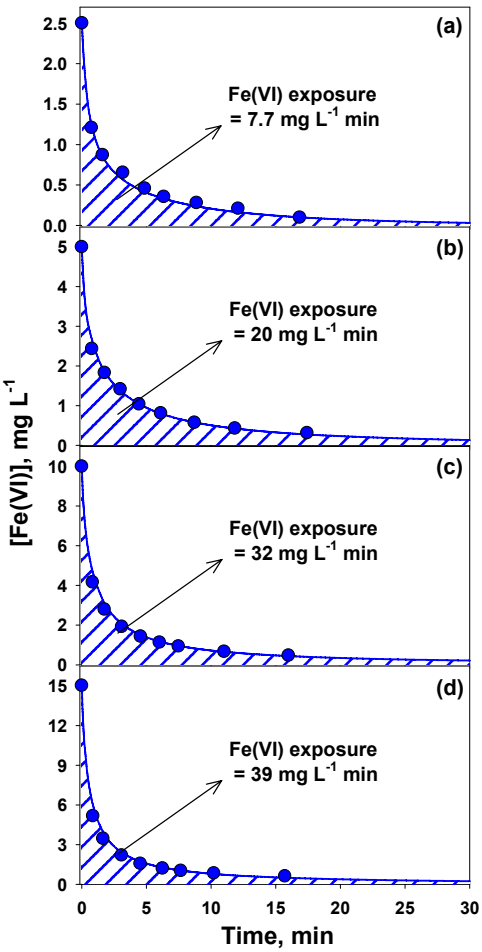

Figure S4.11. Decrease of Fe(VI) in Dübendorf wastewater (DDWW) at pH 7 (10 mM bicarbonate buffer). Experimental conditions: Fe(VI) dose = (a) 2.5, (b) 5, (c) 10, (d) 15 mg Fe L^{-1}. The initial Fe(VI) concentration is an assumed value while all other values are measured. Symbols represent experimental data and lines represent model predictions for Fe(VI) consumption (see Text S4.8).

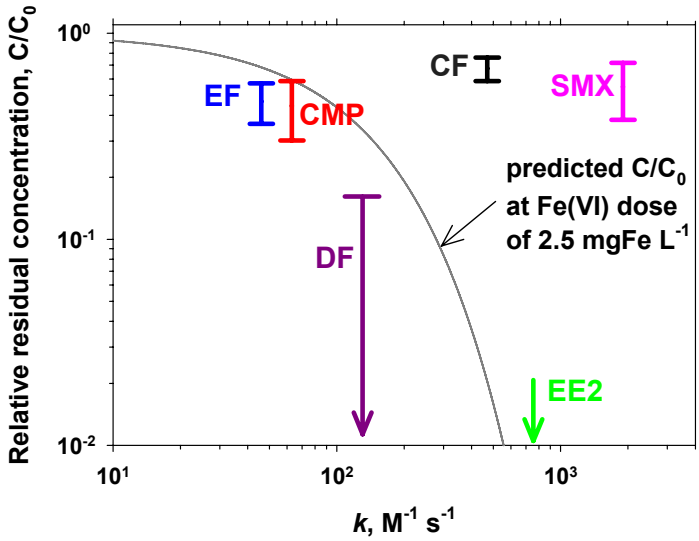

Figure S4.12. Measured and predicted relative residual concentration (C/C_0) of selected micropollutants during treatment of a wastewater (DDWW) at pH 7 with Fe(VI). Predicted relative residual concentration of micropollutants at a Fe(VI) dose of 2.5 mg Fe L^{-1} (line) were calculated by using eq 4.4 in the main text and a Fe(VI) exposure of 7.7 mg Fe L^{-1} min (Figure S4.11). Upper and lower bars represent measured relative residual concentration of micropollutants at Fe(VI) dose of 2 and 3 mg Fe L^{-1}, respectively (Figure 4.2 in the main text). The arrow for EE2 indicates that the relative residual concentration of EE2 is below its quantification limit (2 %) at a Fe(VI) dose of 2 mg Fe L^{-1}. The arrow for DF indicates that the relative residual concentration of DF is below its quantification limit (4 %) at a Fe(VI) dose of 3 mg Fe L^{-1}. Abbreviations represent: EE2 = 17α-ethinylestradiol, EF = enrofloxacin, CF = ciprofloxacin, CMP = carbamazepine, SMX = sulfamethoxazole, DF = diclofenac.

Text S4.9. Determination of Fe(VI) exposures and prediction of micropollutants elimination in DDWW at pH 8

To facilitate the kinetic modeling of micropollutant elimination in DDWW, consumption of Fe(VI) at pH 8 (blue circles, Figure S4.13) was fitted by the same procedure explained in the previous section, Text S4.8. The chemical kinetics program Kintecus, version 3.953, www.kintecus.com, was used for the fitting. The Fe(VI) consumption by DOM of the DDWW matrix was fitted itteratively by assuming the existence of three different reactive moieties towards Fe(VI) with the following concentrations and second-order rate constants: $[\text{moiety 1}]_0 = 15\ \mu M$ and $k_{\text{Fe(VI) + moiety 1}} = 350\ M^{-1}\ s^{-1}$, $[\text{moiety 2}]_0 = 20\ \mu M$ and $k_{\text{Fe(VI) + moiety 2}} = 20\ M^{-1}\ s^{-1}$, and $[\text{moiety 3}]_0 = 100\ \mu M$ and $k_{\text{Fe(VI) + moiety 3}} = 5\ M^{-1}\ s^{-1}$. The determined parameters are purely empirical. In addition to the consumption of Fe(VI) by these three reactive moieties, the self-decay of Fe(VI) (Fe(VI) + Fe(VI) $\rightarrow$ products, $2k = 15.2\ M^{-1}\ s^{-1}$ at pH 8) was considered *(14)*. Fe(VI) exposures were calculated from the area below the Fe(VI) decay curve. With this empirical model, the consumption kinetics of Fe(VI) in DDWW at pH 8 were successfully fitted as shown in Figure S4.13.

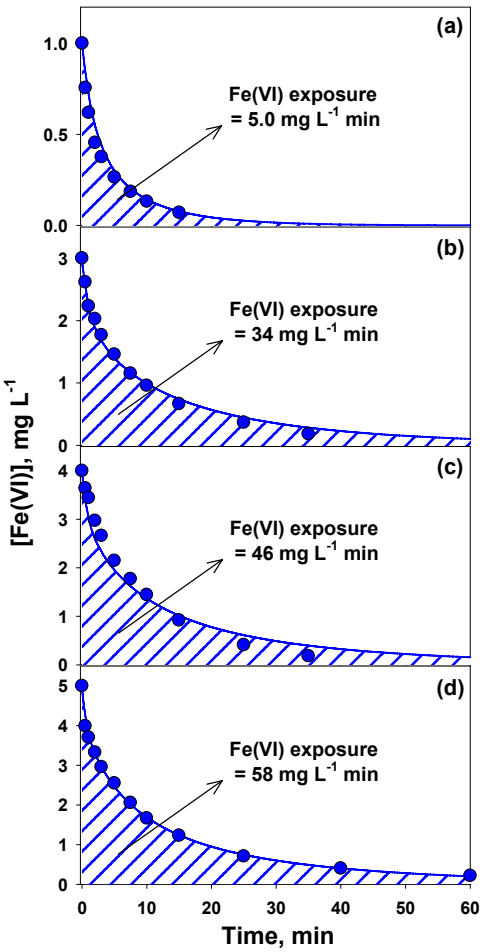

Figure S4.13. Decrease of Fe(VI) in Dübendorf wastewater (DDWW) at pH 8 (20 mM borate buffer). Experimental conditions: Fe(VI) dose = (a) 1.0, (b) 3.0, (c) 4.0, (d) 5.0 mg Fe L^{-1}. The initial Fe(VI) concentration is an assumed value while all other values are measured. Symbols represent experimental data and lines represent model predictions for Fe(VI) consumption (see Text S4.9).

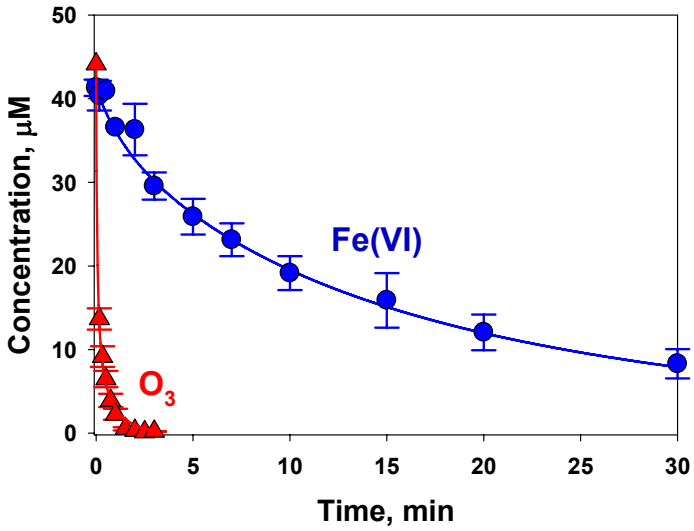

Figure S4.14. Decrease of Fe(VI) and O_3 in a wastewater matrix (secondary effluent from WWTP in Regensdorf, Switzerland, RDWW) at pH 8 (20 mM borate buffer). Symbols and lines represent measured and predicted data, respectively. O_3 was determined by the indigo method (*2*).

References

(1) Thompson, G. W.; Ockerman, L. T.; Schreyer, J. M. Preparation and purification of potassium ferrate.VI. *J. Am. Chem. Soc.* **1951**, *73*, 1379–1381.

(2) Lee, Y.; Yoon, J.; von Gunten, U. Spectrophotometric determination of ferrate (Fe(Vl)) in water by ABTS. *Water Res.* **2005**, *39*, 1946–1953.

(3) Stookey, L. L. Ferrozine–a new spectrophotometric reagent for iron. *Anal. Chem.* **1970**, *42*, 779–781.

(4) Voelker-Bartschat, B. M. Iron redox cycling in surface waters: effects of humic substances and light. Ph.D. Thesis. ETH Zürich, Zürich, 1994.

(5) Liu, Q.; Schurter, L. M.; Muller, C. E.; Aloisio, S.; Francisco, J. S.; Margerum, D. W. Kinetics and mechanisms of aqueous ozone reactions with bromide, sulfite, hydrogen sulfite, iodide, and nitrite ions. *Inorg. Chem.* **2001**, *40*, 4436–4442.

(6) Hong-Xiao, T.; Stumm, W. The coagulating behaviors of Fe(III) polymeric species–II. Preformed polymers in various concentrations. *Water Res.* **1987**, *21*, 123–128.

(7) Carr, J. D.; Kelter, P. B.; Tabatabai, A.; Splichal, D.; Erickson, J.; McLaughlin, C. W. Properties of ferrate(VI) in aqueous solution: an alternative oxidant in wastewater treatment. *Proc. Conf. Water Chlorination Chem. Environ. Impact. Health Effects* **1985**, *5*, 1285–1298.

(8) Rush, J. D.; Zhao, Z. W.; Bielski, B. H. J. Reaction of ferrate(VI)/ferrate(V) with hydrogen peroxide and superoxide anion - A stopped-flow and premix pulse radiolysis study. *Free Rad. Res.* **1996**, *24*, 187–198.

(9) Johnson, M. D.; Hornstein, B. J. The kinetics and mechanism of the ferrate(VI) oxidation of hydroxylamines. *Inorg. Chem.* **2003**, *42*, 6923–6928.

(10) Hoigné, J.; Bader, H.; Haag, W. R.; Staehelin, J. Rate constants of reactions of ozone with organic and inorganic compounds in water–III. Inorganic compounds and radicals. *Water Res.* **1985**, *19*, 993–1004.

(11) Kumar, K.; Margerum, D. W. Kinetics and mechanism of general-acid-assisted oxidation of bromide by hypochlorite and hypochlorous acid. *Inorg. Chem.* **1987**, *26*, 2706–2711.

(12) Huber, M. M.; Korhonen, S.; Ternes, T. A.; von Gunten, U. Oxidation of pharmaceuticals during water treatment with chlorine dioxide. *Water Res.* **2005**, *39*, 3607–3617.

(13) Hoigné, J.; Bader, H. Rate constants of reactions of ozone with organic and inorganic compounds in water–II. Dissociating organic compounds. *Water Res.* **1983**, *17*, 185–194.

(14) Lee, Y.; Kieu, A. T.; Kissner, R.; von Gunten, U. Self-decomposition of ferrate (Fe(VI)) in water: kinetics, mechanism, and formation of hydrogen peroxide, i*n preparation.*

(15) Ternes, T. A.; Joss, A. *Human Pharmaceuticals, Hormones and Fragrances. The Challenge of Micropollutants in Urban Water Management*, IWA Publishing: London, 2006.

(16) Sharma, V. K.; Burnett, C. R.; Millero, F. J. Dissociation constants of the monoprotic ferrate(VI) ion in NaCl media. *Phys. Chem. Chem. Phys.* **2001**, *3*, 2059–2062.

(17) Hornstein, B. J. Reaction mechanisms of hypervalent iron: The oxidation of amines and hydroxylamines by potassium ferrate, K_2FeO_4. Ph.D. Thesis. New Mexico State University, Las Cruces, NM, 1999.

(18) Huang, H.; Sommerfeld, D.; Dunn, B. C.; Lloyd, C. R.; Eyring, E. M. Ferrate(VI) oxidation of aniline. *J. Chem. Soc., Dalton Trans.* **2001**, 1301-1305.

(19) Sharma, V. K.; Mishra, S. K.; Nesnas, N. Oxidation of sulfonamide antimicrobials by ferrate(VI) [$Fe^{VI}O_4^{2-}$]. *Environ. Sci. Technol.* **2006**, *40*, 7222–7227.

(20) Huber, M. M.; Canonica, S.; Park, G. Y.; von Gunten, U. Oxidation of pharmaceuticals during ozonation and advanced oxidation processes. *Environ. Sci. Technol.* **2003**, *37*, 1016–1024.

(21) Lee, Y.; Yoon, J.; von Gunten, U. Kinetics of the oxidation of phenols and phenolic endocrine disruptors during water treatment with ferrate (Fe(VI)). *Environ. Sci. Technol.* **2005**, *39*, 8978–8984.

(22) Deborde, M.; Rabouan, S.; Duguet, J. P.; Legube, B. Kinetics of aqueous ozone-induced oxidation of some endocrine disruptors. *Environ. Sci. Technol.* **2005**, *39*, 6086–6092.

(23) Suarez, S.; Dodd, M. C.; Omil, F.; von Gunten, U. Kinetics of triclosan oxidation by aqueous ozone and consequent loss of antibacterial activity: Relevance to municipal wastewater ozonation. *Water Res.* **2007**, *41*, 2481–2490.

(24) Buffle, M.-O.; Schumacher, J.; Meylan, S.; Jekel, M.; von Gunten, U. Ozonation and advanced oxidation of wastewater: effect of O_3 dose, pH, DOM and $HO^{\cdot}$-scavengers on ozone decomposition and $HO^{\cdot}$ generation. *Ozone Sci. Eng.* **2006**, *28*, 247–259.

Chapter 5

Kinetic and mechanistic investigations of the oxidation of tramadol by ferrate and ozone

Reproduced with permission from *Environmental Science and Technology*, submitted for publication.

Abstract

The kinetics and oxidation products (OPs) of tramadol (TRA), an opioid, were investigated for its oxidation with ferrate (Fe(VI)) and ozone. The kinetics could be explained by the speciation of the tertiary amine moiety of TRA, with apparent second-order rate constants of 7.4 M^{-1} s^{-1} (Fe(VI)) and 4.2 x 10^4 M^{-1} s^{-1} (ozone) at pH 8, respectively. In total, six OPs of TRA were identified for both oxidants using Qq-LIT-MS, LTQ-FT-MS, GC-MS, and moiety-specific chemical reactions. In excess of oxidants, these OPs can be further transformed to unidentified OPs. Kinetics and OP identification confirmed that the lone electron pair of the amine-N is the predominant site of oxidant attack. An oxygen transfer mechanism can explain the formation of *N*-oxide-TRA, while a one-electron transfer may result in the formation of N-centered radical cation intermediates. These in turn could lead to the observed N-dealkylation, and to the identified formamide and aldehyde derivatives via several intermediate steps. The proposed radical intermediate mechanism is favored for Fe(VI) leading predominantly to *N*-desmethyl-TRA (≤ 40 %), whereas the proposed oxygen transfer prevails for O_3 attack resulting in *N*-oxide-TRA as the main OP (≤ 95 %).

5.1 Introduction

Tramadol (TRA) is a synthetic, centrally-acting analgesic agent used for the relief of moderate to severe acute and chronic pain, and shows a potency ranging between weak opioids and morphine *(1)*.

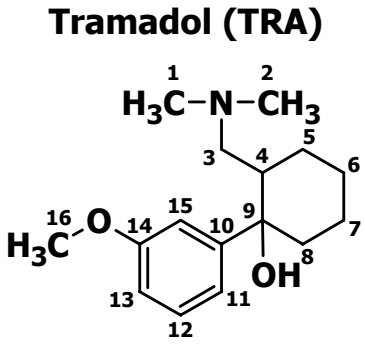

Figure 5.1. Chemical structure of tramadol (TRA)

Approximately 10 – 30 % of TRA is excreted unchanged via urine. In most species, the principle metabolites produced in the liver are *O*-desmethyltramadol (O-DES) and *N*-desmethyltramadol (N-DES). These primary metabolites may be further metabolized to *N*,*N*-bidesmethyltramadol (BIDES), *N*,*N*,*O*-tridesmethyltramadol, and *N*,*O*-desmethyltramadol. All metabolites can undergo conjugation reactions with glucuronic acid and sulfate prior to excretion via urine *(2)*.

TRA is used in both human and veterinary medicine *(3)*. In 2004, a total of 25.3 tons were prescribed in Germany *(4)*. Accordingly, concentrations of up to 97 µg L^{-1} and 6 µg L^{-1} were reported in secondary effluent and surface water, respectively, underlining the environmental relevance of TRA *(5)*.

Currently, ozonation of secondary effluents is discussed as one of the most promising options for the mitigation of micropollutants entering the aqueous environment via wastewater streams, and can be successfully operated at the full-scale level in municipal wastewater treatment plants (WWTPs) during tertiary treatment *(6,7)*. Fe(VI) is a promising new oxidant in wastewater treatment achieving both oxidation of a broad range of micropollutants as well as precipitation of phosphate from wastewater *(8)*. The use of Fe(VI) as an oxidant in the treatment of bromide-containing waters has the

additional advantage of not producing bromate *(9)*, a potentially carcinogenic by-product, which is formed during ozonation *(10)*. Research to implement Fe(VI) application in wastewater treatment is currently carried out, and mainly focuses on the development of on-site Fe(VI) production techniques by electrochemical methods *(11)*.

Oxidative treatment does not usually result in full mineralization but in the transformation of the target compounds. For a comprehensive environmental assessment of an oxidative technology especially with regard to ecotoxicological concerns, it is crucial to elucidate the transformation pathways of the micropollutants present. Mechanistic information on ozonation products formed from micropollutants containing reactive functional groups such as olefines *(12)*, phenols *(13)* or amines *(14-16)* is available, but much less is known about oxidation products (OPs) and mechanisms for Fe(VI) reactions. Studies for olefinic carbamazepine *(17)* as well as phenolic triclosan *(18)* and bisphenol A *(19)* are available, however, limited information is available for amine-containing micropollutants.

In general, Fe(VI) reacts with inorganic and organic compounds via one-electron transfer, hydrogen abstraction or oxygen transfer *(9,20)*. An example of a hydrogen abstraction mechanism is the oxidation of phenol by Fe(VI). This mechanism produces a phenoxy radical and Fe(V), resulting in the formation of quinone *(20)*. Oxygen transfer has been reported for the oxidation of AsO_3^{3-} to AsO_4^{3-}*(21)*.

Some studies investigating the oxidation of the N-containing compounds glycine and nitrilotriacetic acid by Fe(VI) showed cleavage of the N-C bond *(22,23)*. Nitrobenzene derived from oxygen transfer as well as coupling products were identified as Fe(VI) OPs from aniline *(24)*, and in analogy, nitroso- and nitro-sulfamethoxazole from sulfamethoxazole attack *(25)*.

In the present paper, the kinetics and OP formation of TRA, containing an aliphatic tertiary amine moiety, are investigated during Fe(VI) and O_3 oxidation. Reaction mechanisms are postulated based on kinetic data, identified OPs, respective mass balances in buffered solutions, and available information from literature.

5.2 Materials and Methods

5.2.1 Chemicals and Reagents

All chemicals and solvents were of analytical grade (≥ 95 %). Information on authentic reference standards and oxidant preparation is given in Table S5.1 and Text S5.1 of the Supporting Information.

5.2.2 Reaction Kinetics

All kinetic experiments were carried out at 22 ± 2 °C in duplicate or triplicate. Apparent second-order rate constants *k* for the reaction of TRA and N-DES with Fe(VI) were measured in excess Fe(VI) in the pH range 6.5 - 10.5. For BIDES, *N*-oxide-tramadol (N-OXID) and anisole, *k* values for the reaction with Fe(VI) were measured with excess compound at pH 8.0. For O_3, *k* values for the reaction with TRA were determined with excess O_3 in the pH range 3.0 - 7.5 by direct measurements in batch experiments, and with excess compound in the pH range 7.5 - 8.5 using competition kinetics. 20 mM tert-butanol was spiked as a radical scavenger. Competition experiments were also used for determining *k* values for the reaction of TRA with hydroxyl radicals at pH 8.0. Further details are given in Text S5.2.

5.2.3 Identification of Oxidation Products

5.2.3.1 Sample preparation

TRA OPs from Fe(VI) and O_3 treatment were produced in bench-scale experiments. A Fe(VI) stock solution was added to a 1670 µM TRA solution buffered to pH 8.5 (125 mM phosphate) to yield 200 µM Fe(VI). After complete Fe(VI) consumption, the procedure was repeated 14 times to compensate for loss of Fe(VI) due to self-decay. The pH was controlled after each step and if necessary, readjusted to pH 7.5 by the addition of H_3PO_4. The solution was kept at 4 °C until complete Fe(III) (hydr)oxide precipitation. The unfiltered supernatant was used for product identification. An O_3 stock solution was added to the reaction solution containing TRA (100 µM) and phosphate buffer (50 mM) at pH 8.0, resulting in O_3:TRA ratios of 1:5, 1:1, 5:1, and 10:1. To exclude the influence

of hydroxyl radicals during OPs formation, 100 mM tert-butanol was spiked as a radical scavenger. Pre-concentration of OPs formed by ozone was subsequently achieved by freeze-drying 1 L of the 10:1 reaction solution, and redissolving it in deionized water.

5.2.3.2 Separation by HPLC-UV/FLD-fraction collector

An Agilent 1100 system (Agilent Technologies, Santa Clara, CA) was used to separate the mixtures of OPs. HPLC conditions are described in Text S5.3 and Table S5.2. Fractions of the eluate were subsequently collected by a fraction collector (Advantec SF-2120 Super Fraction Collector, Techlab GmbH, Erkerode, Germany). Fe(VI) OPs fractions were concentrated in brown glass bottles heated to 40 °C in a water bath under a gentle N_2 stream.

5.2.3.3 Determination of molecular weights and fragmentation by mass spectrometry

Molecular weights of TRA OPs produced from Fe(VI) or O_3 were obtained from Q1 scans (50 - 1000 m/z) of a hybrid triple quadrupole-linear ion trap mass spectrometer (Qq-LIT-MS, Applied Biosystems Sciex 4000 Q Trap (Applied Biosystems, Langen, Germany)). Structural elucidation of TRA OPs was based on their MS^2 and MS^3 fragmentation pathways obtained from product ion (PI), precursor or MS^3 scans using Qq-LIT-MS. The exact masses and hence sum formula of the OPs were further determined by a linear triple quadrupole ion trap Fourier transformation mass spectrometer (LTQ-FT-MS, LTQ Orbitrap Velos, Thermo Scientific, Bremen, Germany). Both MS systems were equipped with an electrospray ionization source (ESI). The optimized MS conditions for each OP were written into one multiple reaction mode (MRM) transition method, and can be found in Table S5.3.

5.2.3.4 Derivatization and subsequent GC-MS detection

The fractions of OP 249 and OP 264a were derivatized with different agents and subsequently measured by GC-MS (Text S5.4).

5.2.3.5 Purpald® test

Each OP fraction was tested for aldehydes by the Purpald® test *(26,27)*. An aliquot (500 µl) of each fraction was added to 2 mL reactant solution, consisting of 150 mg 4-amino-3-hydrazino-5-mercapto-1,2,4-triazole (Purpald®) dissolved in 2 mL 1 N NaOH. Glutaraldehyde was used as positive control, and Milli-Q water and the final HPLC eluent mixture were used as negative controls.

5.2.3.6 pH dependence of LC retention time

The presence or absence of basic or acid moieties in isolated OP fractions was checked by determining the retention times (R_t) at pH 3.5, 7.0 and 10.0 (with ammoniumacetate and methanol as eluents) in RP-LC-Qq-LIT-MS, using a 4.6 x 100 mm non-modified, endcapped Chromolith C_{18} column (Merck, Darmstadt, Germany).

5.2.4 Mass balance

A mass balance experiment for TRA OPs with Fe(VI) was carried out at pH 8.0 in 100 mM phosphate buffer with $[TRA]_0$ = 50 µM, and $[Fe(VI)]_0$ = 500 µM. Fe(VI) was added nine times in order to keep [Fe(VI)] in excess to [TRA] until complete TRA oxidation was achieved (Figure S5.1). The pH was controlled after each Fe(VI) addition and if necessary, readjusted to pH 8.0 with 1 % H_3PO_4. At proper time intervals, [Fe(VI)] was determined by the ABTS method *(28)*, and 2 mL of the solution were quenched with 1 mL 10 mM thiosulfate. OP formation and residual [TRA] were measured by the optimized LC-Qq-LIT-MS method (Table S5.2 and S5.3) with an analytical Hydro-RP column (flow 0.3 mL min^{-1}). The two most intensive MRM transitions were used for quantification. To quantify TRA, N-OXID, N-DES and BIDES with authentic reference standards, each sample was divided into four aliquots, and a standard addition with no, single, double and triple analyte concentration of the four authentic standards was carried out. In addition, d_6-TRA was spiked as surrogate internal standard. The mass balance experiment for TRA OPs with ozone was conducted with a 50 µM TRA solution buffered to pH 8.0 (100 mM phosphate) by spiking different aliquots of the O_3 stock solution to yield O_3:TRA ratios of 1:5, 1:2.5, 1:1, 2.5:1, 5:1 and 10:1. tert-butanol (5 mM) was spiked as a radical scavenger.

5.3 Results and Discussion

5.3.1 Reaction Kinetics

At pH 8, Fe(VI) shows a moderate reactivity with TRA and N-DES, with rate constants of 7.4 and 7.6 M^{-1} s^{-1}, respectively. The reactivity decreases with increasing pH, and can be well explained by second-order kinetics and by considering the speciation of both Fe(VI) and the target compounds (Text S5.2 and Figure S5.2a). Table 5.1 summarizes the fitted species-specific rate constants. The rate constants k_2 for the reaction of the deprotonated amine moieties P of both TRA (tertiary amine) and N-DES (secondary amine) with $HFeO_4^-$ were two orders of magnitude higher than the rate constants for the respective protonated amine moieties PH^+ (k_1). This can be explained by the availability of the amine's lone electron pair in the unprotonated species. The increasing reactivity of the compound with increasing pH is compensated by a decreasing reactivity of Fe(VI), leading to the observed overall decrease of reactivity with increasing pH. k_1 values for the protonated amine moieties do not differ between TRA and N-DES, while k_2 for the deprotonated secondary amine (N-DES) is eight times higher than k_2 for the deprotonated tertiary amine (TRA). This is consistent with findings for the oxidation of dimethylamine/trimethylamine and ciprofloxacin/enrofloxacin by Fe(VI) *(8)*.

TRA also exhibits a strong pH dependence for the reaction with O_3 (Text S5.2 and Figure S5.2b). The apparent second-order rate constants k determined by competition kinetics ($pH \geq 7.5$) agree well with the rate constants determined directly without a competitor ($pH \leq 7.5$). In contrast to Fe(VI), the overall reactivity of TRA with O_3 increases with increasing pH. This can be exlained by the fact that O_3 does not undergo acid-base speciation. Similar to $HFeO_4^-$, the deprotonated amine moiety shows a much higher species-specific second-order rate constant k_6 with O_3 than the protonated amine moiety (k_5, Table 5.1).

When comparing both oxidants, O_3 is three orders of magnitude more reactive with the deprotonated amine moiety of TRA than $HFeO_4^-$, which is consistent with other studies *(8)*. No pH dependence was observed for the second-order rate constants for the reaction of TRA with hydroxyl radicals (6.3 (± 0.2) x 10^9 M^{-1} s^{-1}, Table 5.1). The apparent second-order rate constants k of BIDES and N-OXID with Fe(VI) were only determined

at pH 8 to support later kinetic modeling (Table 5.1). In addition, the rate constant *k* for the reaction of anisole with Fe(VI) showed that the anisole moiety of TRA is nearly non-reactive with Fe(VI) (Table 5.1).

Table 5.1. Second-order rate constants k [M^{-1} s^{-1}] for the reaction of Fe(VI), O_3 and hydroxyl radicals with tramadol as well as for the reaction of Fe(VI) with the tramadol oxidation products *N*-desmethyl-tramadol, *N,N*-bidesmethyl-tramadol and *N*-oxide-tramadol, and the model compound anisole at 22 ± 2 °C.

Substance	**pK_a**	**Reacting species**	**k_1 / k_2 (Fe(VI)) k_5 / k_6 (O_3)**	**k (pH 7)**	**k (pH 8)**
Tramadol (TRA)	9.4 [a]	$HFeO_4^-$ + PH^+/ $HFeO_4^-$ + P	1.7 (± 0.2) x 10^1/ 1.2 (± 0.1) x 10^3	1.4 x 10^1	7.4 x 10^0
		O_3 + PH^+/ O_3 + P	7.7 (± 0.2) x 10^1/ 1.0 (± 0.1) x 10^6	2.2 x 10^3	4.2 x 10^4
		$OH^\cdot$ + PH^+/P		6.3 (± 0.2) x 10^9 [b]	
N-desmethyl-tramadol (N-DES)	10.6 [c]	$HFeO_4^-$ + PH^+/ $HFeO_4^-$ + P	2.4 (± 0.6) x 10^1/ 7.9 (± 1.6) x 10^3	2.8 x 10^1	7.6 x 10^0
N,N-bidesmethyl-tramadol (BIDES)	n.a.	$HFeO_4^-$/FeO_4^{2-}/ + PH^+/P	-	-	3.5 x 10^1
N-oxide-tramadol (N-OXID)	n.a.	$HFeO_4^-$/FeO_4^{2-}/ + PH^+/P	-	-	1.3 x 10^0
Anisole	-	$HFeO_4^-$/FeO_4^{2-}/ + P	-	-	< 2.0 x 10^{-2}

[a] Ref. *(29,30)*

[b] Average second-order rate constant for the reaction of TRA with hydroxyl radicals for triplicate measurements at pH 3 and 8

[c] estimated from SPARC online V4.5 http://sparc.chem.uga.edu/sparc/

n.a. not available

5.3.2 Identification of Oxidation Products

Kinetic experiments showed that both Fe(VI) and O_3 are moderate to very reactive with TRA, leading to several OPs detectable by LC-MS/MS. For Fe(VI), a total of six OPs could be identified (Table S5.4) while the structure of three additional OPs could tentatively be proposed (Table S5.5). After ozonation, two main OPs were identified (Table S5.4).

5.3.2.1 Information derived from reference standards

To elucidate the chemical structures of TRA OPs by Qq-LIT-MS and LTQ-FT-MS, the MS, MS^2 and MS^3 spectra of TRA and the structurally related N-DES, BIDES and N-OXID (Schemes S5.1 - S5.4) provided the basis for interpretation. For instance, certain fragments indicated the presence of the intact aromatic ring (Scheme S5.1, 77 m/z (**9**)) including the methoxy group (Scheme S5.4, 107 m/z (**11**)), and with a varying number of carbon atoms originating from the hexyl ring that rearrange to ring structures (Scheme S5.1, 91 m/z (**8**), 115 m/z (**7**), 121 m/z (**6**), 159 m/z (**5**), 173 m/z (**4**)). The occurrence of the two fragments 189 m/z (Scheme S5.2, (**3**)) and 201 m/z (Scheme S5.1, (**3**)) indicated a fully intact hexyl ring. In reference to the amine function, fragment 58 m/z was assigned to the tertiary amine moiety for both TRA (Scheme S5.1, (**10**)) and N-OXID (Scheme S5.4, (**14**)), fragment 44 m/z to the secondary amine moiety for N-DES (Scheme S5.2, (**8**)), and fragment 30 m/z to the primary amine moiety for BIDES (Scheme S5.3, (**7**)).

5.3.2.2 Fe(VI) OPs

The formation of N-DES (OP 250a), BIDES (OP 236) and N-OXID (OP 280) during Fe(VI) treatment could be confirmed by comparing R_t, nominal masses as well as MS^2 and MS^3 spectra with the authentic reference standards (Schemes S5.2 - S5.4). All Fe(VI) OPs exhibited an intact anisole moiety and an intact hexyl ring. This is supported by Fe(VI) being practically unreactive towards anisole (Table 5.1). Furthermore, none of the previously mentioned amine fragments (58, 44, 30 m/z) could be detected for the other Fe(VI) OPs (Schemes S5.5 - S5.10), indicating further structural changes at the tertiary amine besides N-dealkylation or oxygen insertion.

Formamide derivative

For OP 278, an additional evaluation of the MS^3 fragmentation pattern 278 m/z → 260 m/z → 201 m/z (Scheme S5.5) by LTQ-FT-MS revealed the sum formulas $C_{16}H_{22}NO_2$ (260.16428 m/z) and $C_{14}H_{17}O$ (201.12726 m/z), respectively. The difference is 59.03702 m/z which corresponds to the sum formula C_2H_5NO and not to $CHNO_2$ as the leaving group. This indicates that one oxygen atom was inserted to the TRA tertiary amine moiety with the following information from the MS^3 spectra: no water loss from the fragment C_2H_5NO (= no hydroxyl group next to an extractable proton), no formation of a fragment 58 m/z as for N-OXID (= no loss of water from the amine function), and a parent mass 2 Da lower than N-OXID. Accordingly, one oxygen atom must have been added to one of the two methyl groups neighboring the nitrogen atom (C_1 or C_2 and not C_3 in Figure 5.1), while two hydrogen atoms are no longer present in the tertiary amine moiety. The only reasonable explanation is the formation of an aldehyde moiety at C_1 or C_2, which was confirmed by a positive Purpald® test *(26,27)*. Hence, a formamide derivative was identified containing the aldehyde moiety.

Dealkylation yielding aldehyde and carboxylic acid functional groups

Two OPs (OP 235 and OP 249) without a nitrogen atom but intact anisole and hexyl moieties were found (Schemes S5.6 and S5.7). The loss of nitrogen was evident from their uneven nominal masses (235 and 249 m/z in positive and negative ESI mode, respectively) in comparison to the even nominal mass of TRA (N-rule). The MS^3 fragmentation pathway 235 m/z → 217 m/z → 189 m/z (Scheme S5.6) revealed the presence of one hydroxyl group (-18 Da) and, in combination with the exact sum formula $C_{14}H_{19}O_3$ determined by LTQ-FT-MS (Table S5.4), hinted at the formation of an aldehyde moiety (loss of 28 Da as C=O) at C_3. A positive Purpald® test confirmed the presence of an aldehyde moiety, and hence the chemical structure. In contrast to all other OPs, OP 249 was detected in negative ESI mode (scheme S5.7). The sum formula revealed an additional oxygen atom compared to OP 235, and the MS^2 spectrum (Scheme S5.7) showed one hydroxyl group (-18 Da) and suggested the formation of a carboxylic group (fragment 45 m/z). When observing the pH-dependant R_t in RP-chromatography, OP 249 was the only OP showing a shift towards an earlier R_t with increasing pH (pH 3.5 → 10). This implies the presence of a carboxylic moiety in the

structure. Further evidence for one strongly acid proton was taken from 1-fold methylation of OP 249 by TMSH (Figure S5.4). When considering all the information, OP 249 was identified as the corresponding carboxylic acid to OP 235.

Intra-molecular ring formation

The chemical structure of three OPs formed could be proposed based on intra-molecular ring formation (Table S5.5). OP 264a was derived from ring closure of either C_1 or C_2 of the two methyl groups with C_5 of the hexyl ring, and OP 264b and OP 250b originated from a ring closure of the nitrogen atom with C_{15} of the aromatic ring (Figure 5.1). Corresponding MS fragmentation pathways are proposed in Schemes S5.8 - S5.10. Although no direct experimental proof for the intra-molecular ring formation was possible (quantity was not sufficient for NMR), several strong indications exist for the proposed chemical structures: (i) an intact anisole moiety and an intact hexyl ring (scheme S5.8, (**4**); scheme S5.9, (**6**); scheme S5.10, (**3**) and (**4**)), (ii) the respective exact parent mass determined by LTQ-FT-MS (Table S5.5), (iii) the nitrogen atom still present, (iv) the absence of fragments indicating a non-heterocyclic tertiary, secondary or primary amine, and (v) the occurrence of fragments including the nitrogen in connection to several carbon atoms (scheme S5.8, (**5**) and (**14**); scheme S5.9, (**10**) and (**13**); scheme S5.10, (**5**)). In addition, the loss of 32 Da from OP 264b implies the presence of a free methyl group (-14 Da) within the molecule, co-fragmenting with a hydroxyl group (-18 Da), which was not observed for OP 264a. These observations can only be explained if an intra-molecular ring formation occurred. In addition, the double loss of water indicates the presence of two hydroxyl groups next to an extractable proton for all three OPs, of which one hydroxyl group originates from TRA. For OP 264a, the position of the additional hydroxyl group was verified at the N atom by observing a two-fold silylation of the molecule (Figure S5.5). The additional hydroxyl groups in OP 264b and OP 250b are also tentatively assigned to the respective N atom, based on the structure of N-OXID and OP 264a.

5.3.2.3 O_3 OPs

As for Fe(VI), the formation of both N-DES (OP 250a) and N-OXID (OP 280) during O_3 treatment could be confirmed by comparing R_t, nominal masses as well as MS^2 and MS^3 spectra with the authentic reference standards (Schemes S5.2 and S5.4).

5.3.3 Mass balance experiment and proposed mechanisms of tramadol oxidation by Fe(VI)

5.3.3.1 Quantification of OPs

Mass balance experiments were conducted to elucidate the sequence of OP formation from TRA during Fe(VI) treatment at pH 8. TRA, N-DES, BIDES and N-OXID could be quantified by authentic reference standards. For OPs without available authentic reference standards, a semi-quantitative determination was used by normalizing the two most intensive MRM transitions to the respective highest peak area ratio. From a normalized plot, OPs can also be classified as primary or secondary OPs. Primary OPs evolve first and reach their maximum before the respective secondary OP. The proposed reaction mechanisms discussed in the following section are illustrated in Scheme 5.1.

5.3.3.2 Oxygen transfer

In the present study, the formation of N-OXID shows that Fe(VI) is able to oxidize tertiary amines by oxygen transfer to the corresponding *N*-oxide (**1**). This reaction has also been reported for other oxidants such as O_3 *(14,16)*, MnO_4^{2-} *(31)*, and MnO_2 *(32)*.
In analogy to the formation of phenoxy radicals from phenol by Fe(VI), further oxidation of N-OXID to a nitroxyl radical (**2**) is hypothesized, similar to the oxidation of *N*-oxides by MnO_2 *(33)*, or of hydroxylamine by Fe(VI) *(34)*. This would explain a certain reactivity of N-OXID towards Fe(VI) (Table 1), although the lone electron pair of the N atom is missing.

Scheme 5.1. Proposed reaction mechanisms for the oxidation of TRA by Fe(VI)

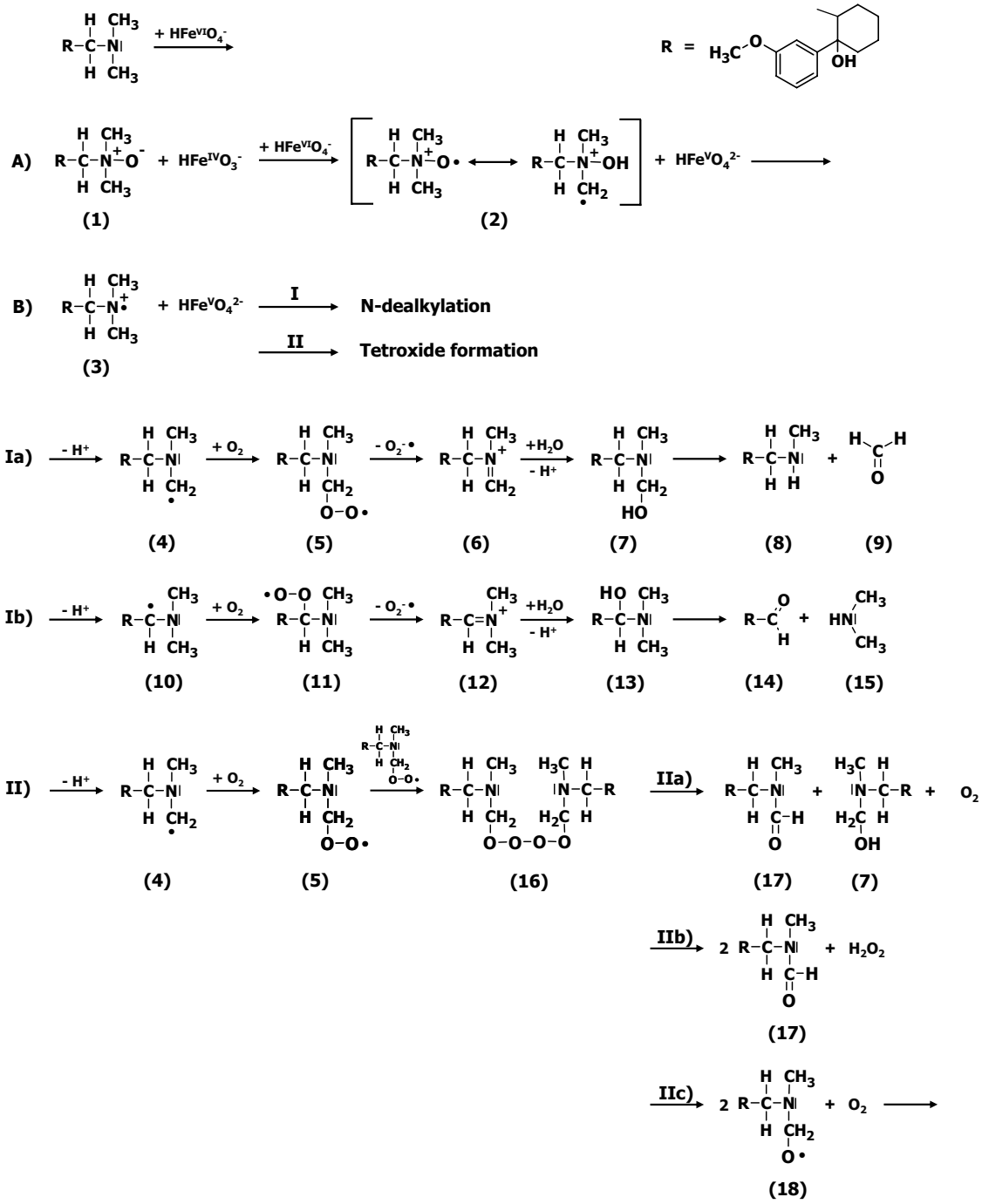

5.3.3.3 Aminium radical cation formation

The identification of OPs strongly indicates the formation of an aminium radical cation (**3**) via electron abstraction from the N atom of TRA. The proposed aminium radical cation was shown as intermediate in the oxidation of amines by ClO_2 *(35,36)*. The experimental evidence for an analogous anilino radical by Fe(VI) oxidation was given by electron paramagnetic resonance spectroscopy *(37)*. The proposed TRA radical cation can subsequently undergo several reaction pathways (reactions B I - II) to yield a range of products:

Reaction I

In alkaline solution, the proposed TRA radical cation (**3)** would rapidly deprotonate into one of the three neighboring C-centered radicals ((**4**) and (**10**)). In the presence of oxygen, these are then converted with nearly diffusion-controlled reactions *(38)* into the corresponding peroxyl radicals ((**5**) and (**11**)). In both reactions Ia and Ib, the subsequent formation of superoxide ($O_2^{\bullet-}$) yields iminium cations ((**6**) and (**12**)). Depending on the position of the double bond, the iminium cation hydrolyzes via formation of unstable hemiaminals ((**7**) and (**13**)) to either N-DES (**8**) and formaldehyde (**9**) (B Ia), or to OP 235 (**14**) and dimethylamine (**15**) (B IIb). Further N-dealkylation of N-DES would yield BIDES and formaldehyde (B Ia), or again OP 235 and methylamine (B Ib). C-N bond cleavage has been shown to occur for nitrilotriacetic acid during Fe(VI) treatment *(22)*, and for other tertiary amines during oxidation by O_3 *(14)* and MnO_4^{2-} *(31)*. A similar reaction, the oxidation of trimethylamine by hydroxyl radicals, has been studied in detail starting from the C-centered radicals *(39,40)*.

Reaction II

The proposed peroxyl radicals of TRA (e.g. (**5**)) can also recombine to form a short-lived tetroxide structure (**16**) that may decompose via a number of pathways *(40)*. The Russell mechanism (B IIa) forms OP 278 (**17**) as a carbonyl compound, O_2 and an unstable hemiaminal (**7**) which in turn decomposes to N-DES (**8**) and formaldehyde (**9**) as in reaction Ia *(40)*. Decomposition pathway B IIb produces two OP 278 molecules (**17**)

and H_2O_2 from one tetroxide (**16**), whereas a third pathway is a non-terminating process resulting in the formation of two oxyl radicals (**18**) and oxygen (B IIc) *(40)*.

5.3.3.4 Intra-molecular ring formation

The mechanism for an intra-molecular ring formation leading to the proposed ring structures of OP 264a, OP 264b and OP 250b (Table S5.5) could not be elucidated from the literature. A speculative reaction mechanism could be hydrogen radical abstraction from C_5 or C_{15} after ring formation via N or C centered (C_1 or C_2) radicals to C_5 or C_{15} (Figure 5.1).

5.3.3.5 Kinetic modeling

Based on the above mechanistic information, a reaction sequence (eqs 5.1 - 5.7) is proposed with N-dealkylation of TRA via N-DES to BIDES, and direct N-OXID formation from TRA:

$$\text{TRA} \xrightarrow{\text{Fe(VI)}} \text{N} - \text{DES} \qquad k_{\text{TRA} \rightarrow \text{N-DES}} = \text{a x } 7.4\ \text{M}^{-1}\ \text{s}^{-1} \qquad (5.1)$$

$$\text{TRA} \xrightarrow{\text{Fe(VI)}} \text{N} - \text{OXID} \qquad k_{\text{TRA} \rightarrow \text{N-OXID}} = \text{b x } 7.4\ \text{M}^{-1}\ \text{s}^{-1} \qquad (5.2)$$

$$\text{TRA} \xrightarrow{\text{Fe(VI)}} \text{other products 1} \qquad k_{\text{TRA} \rightarrow \text{OTH PR 1}} = (1 - \text{a} - \text{b}) \text{ x } 7.4\ \text{M}^{-1}\ \text{s}^{-1} \qquad (5.3)$$

$$\text{N} - \text{DES} \xrightarrow{\text{Fe(VI)}} \text{BIDES} \qquad k_{\text{N-DES} \rightarrow \text{BIDES}} = \text{c x } 7.6\ \text{M}^{-1}\ \text{s}^{-1} \qquad (5.4)$$

$$\text{N} - \text{DES} \xrightarrow{\text{Fe(VI)}} \text{other products 2} \qquad k_{\text{N-DES} \rightarrow \text{OTH PR 3}} = (1 - \text{c}) \text{ x } 7.6\ \text{M}^{-1}\ \text{s}^{-1} \qquad (5.5)$$

$$\text{N} - \text{OXID} \xrightarrow{\text{Fe(VI)}} \text{other products 3} \qquad k_{\text{N-OXID} \rightarrow \text{OTH PR 2}} = 1.3\ \text{M}^{-1}\ \text{s}^{-1} \qquad (5.6)$$

$$\text{BIDES} \xrightarrow{\text{Fe(VI)}} \text{other products 4} \qquad k_{\text{BIDES} \rightarrow \text{OTH PR 4}} = 35\ \text{M}^{-1}\ \text{s}^{-1} \qquad (5.7)$$

Experimentally determined second-order rate constants for the reaction of TRA, N-OXID, N-DES and BIDES with Fe(VI) at pH 8.0 are compiled in Table 5.1. Parameters a, b and c correspond to the fraction of the products formed during the respective reaction and were fitted by minimizing the sum of squares between the resulting N-OXID, N-DES and BIDES model concentrations and the respective

experimental data. Figure 5.2 illustrates that kinetic simulations best explained the experimental data for an initial N-DES formation of 40 % from TRA (fraction a), and subsequent further oxidation of 14.5 % N-DES to BIDES (fraction c). In contrast, only 1 % of TRA is directly transformed into N-OXID (fraction b). All proposed oxidation pathways and yields for each reaction are shown in Figure 5.3.

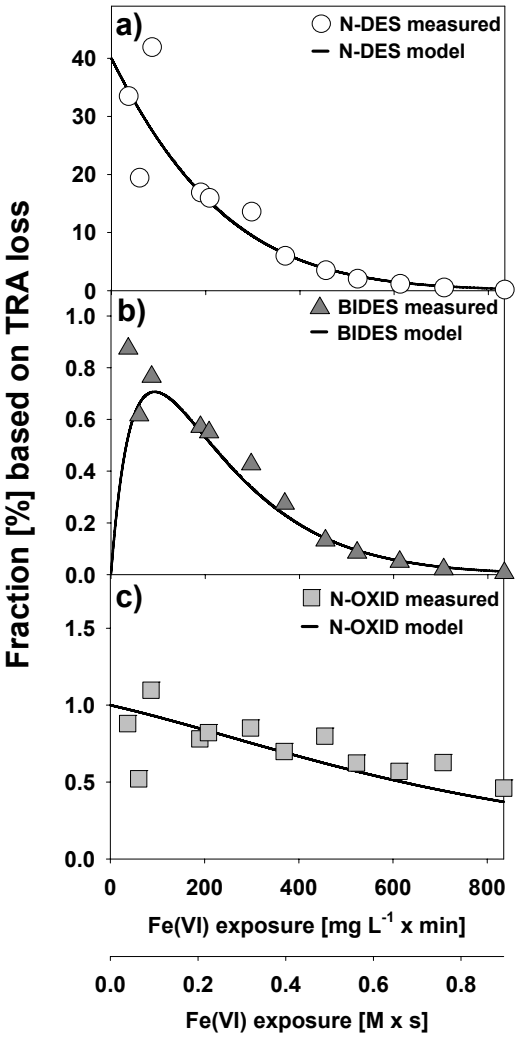

Figure 5.2. Experimental data and model calculations for the formation and further oxidation of a) *N*-desmethyl-tramadol (N-DES), b) *N,N*-bidesmethyl-tramadol (BIDES) and c) *N*-oxide-tramadol (N-OXID) during oxidative treatment of tramadol (TRA) by Fe(VI) at pH 8.0, based on TRA loss. $[TRA]_0$ = 50 µM.

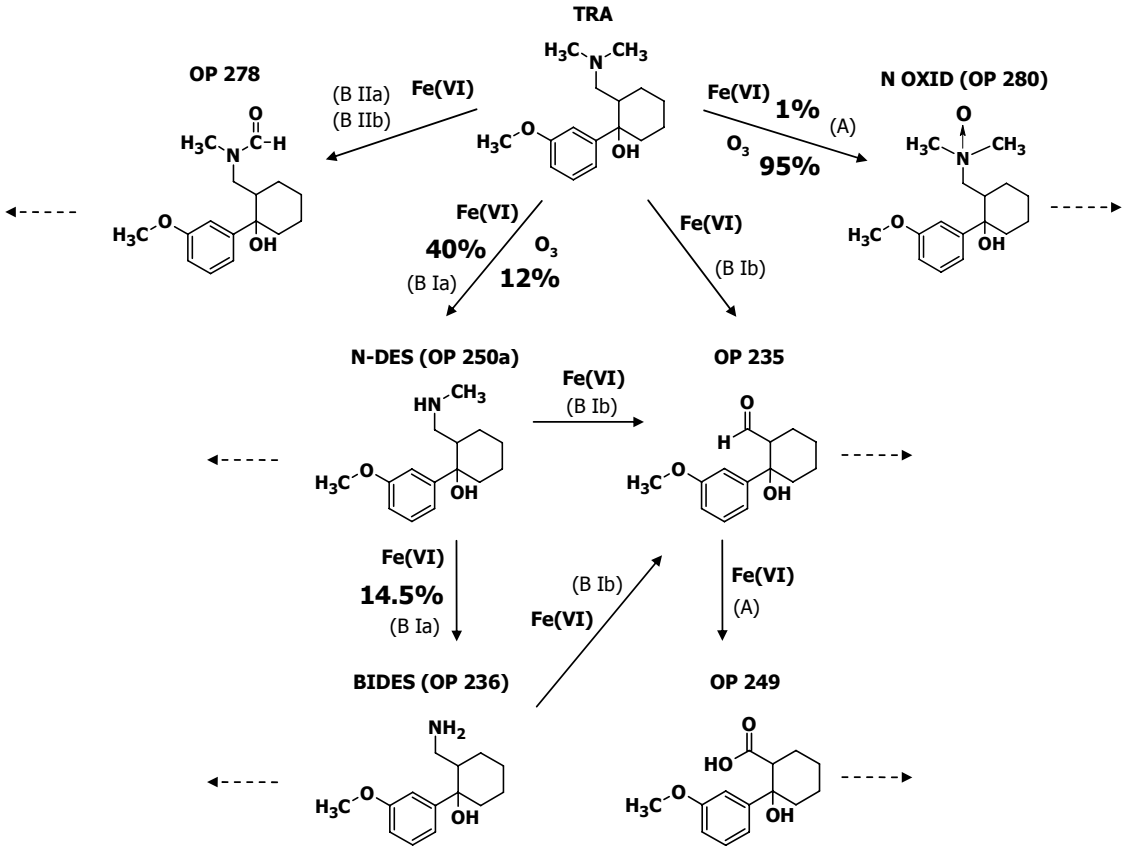

Figure 5.3. Proposed pathways of TRA oxidation by Fe(VI) and O_3. Yields for the formation of oxidation products (OP) are indicated for Fe(VI) and O_3. Reaction mechanisms A, B Ia, B Ib, B IIa and B IIb as proposed in Scheme 5.1 for Fe(VI) are given in brackets. Dashed lines indicate further oxidation of OPs.

5.3.3.6 Primary and secondary OPs

Since 41 % of TRA are initially oxidized to N-DES and N-OXID, the kinetic simulations imply that 59 % of TRA is transformed into OPs other than N-DES or N-OXID (BIDES is a secondary OP). Based on their identified structure, the discussed mechanisms and the sharp relative increase during the mass balance experiment, both OP 278 (Figure S5.6a) and OP 235 (Figure S5.6b) are identified as further primary Fe(VI) OPs of TRA, and may account for up to 59 % of initially oxidized TRA. However, OP 235 may also form from N-DES or BIDES, classifying it as a primary, secondary and tertiary OP of TRA. In contrast, OP 249 containing a carboxylic moiety is clearly a secondary OP due to its delayed relative formation (Figure S5.6b) that may derive from the oxidation of OP 235 by oxygen transfer similar to reaction A in Scheme 5.1. OP 264a shows a formation pattern with a sharp relative increase similar to primary OPs. Still, reaction mechanisms necessary to explain the proposed chemical structure (N-dealkylation, oxygen transfer, intra-molecular ring formation) would render it a secondary or tertiary OP. N-DES, which may act as a precursor from a mechanistic point of view, exhibits the same sharp relative increase and in addition, reaches its relative maximum prior to OP 264a (Figure S5.6). In additional experiments, OP 264a was found to be an OP of N-DES oxidation by Fe(VI) at pH 8. Hence, OP 264a is a secondary or even tertiary OP in the TRA-Fe(VI) system, despite its sharp relative increase typical for primary OPs. OP 264b and OP 250b exhibit a delayed relative formation pattern and may form from N-DES (OP 264b) and N-DES or BIDES (OP 250b), respectively. From mechanistic considerations, OP 250b might also derive from N-dealkylation of OP 264b (B Ia), however, their simultaneous formation suggests N-dealkylation of OP 264b being a minor pathway for the formation of OP 250b. It is important to note that all Fe(VI) OPs could be further oxidized at higher Fe(VI) exposures as indicated by the dashed arrows in Figure 5.3. However, realistic Fe(VI) exposures for wastewater treatment are in the range of 50 - 100 mg L^{-1} min *(8)*, indicating that the identified OPs will be prevailing under realistic conditions.

5.3.3.7 OPs of N-containing compounds reported in literature

In the present study, screening for C-Nitroso-TRA revealed a third peak with 250 m/z beside N-DES (250a) and OP 250b. However, a final identification was not possible. In addition, the theoretical m/z value for nitro-TRA (266 m/z) was not found. This indicated that the formation of nitro- and nitroso compounds which was reported for aniline containing compounds *(25,41)* is of minor relevance during oxidation of aliphatic tertiary amines by Fe(VI). Coupling products of TRA were also not identified.

5.3.4 Mass balance experiment and proposed mechanisms of TRA oxidation by O_3

The mass balance experiment for the oxidation of TRA by O_3 showed that the main OP is N-OXID with a yield of ~ 95 % of initially oxidized TRA. The second most abundant OP is N-DES with a yield of up to ~ 12 % (Fig. S5.7). For the lower ozone:TRA ratios of 1:5, 1:2.5 and 1:1, this leads to a mass balance of 100 - 107 % and clearly shows that these two OPs dominate the initial process. BIDES formation of only 0.1 % was determined, and can be neglected. The proposed oxidation pathways and yields for each reaction with O_3 are also shown in Figure 5.3. For ozone in excess to TRA (ozone:TRA ratios of 2.5:1, 5:1 and 10:1), no N-DES or BIDES could be quantified and the fraction of N-OXID decreased to 35 %. This shows that all three OPs can be further oxidized by O_3 reactions (dashed arrows in Figure 5.3) since hydroxyl radicals were excluded by the radical scavenger tert-butanol. The results are supported by OP formation and the respective yields reported for the ozonation of trimethylamine *(42)* and clarithromycin *(16)*. In analogy to these studies, the main reaction mechanism is oxygen transfer to the N atom, and a minor pathway leads to the formation of N-dealkylated TRA. In contrast to Fe(VI), the initial step of O_3 addition to the lone electron pair of the nitrogen atom is well-established *(42)* and leads to the formation of an ozonide ammonium zwitterion R_3N^+-O-O-O^-. This can subsequently decay via two pathways: it either looses a singlet oxygen ($^1O_2$) and yields an *N*-oxide, or it forms an ozonide radical anion ($O_3^{\bullet-}$) and an aminium radical cation. Once the aminium radical cation is formed, it is subjected to the same reactions in the presence of oxygen as described for Fe(VI) in Scheme 5.1,

reactions I - II. In addition, ozonated samples were screened for Fe(VI) OPs without authentic reference standards, and most of them (OP 278, 264a, 235 and 249) could be detected (Figure S5.8, Table S5.4 and S5.5), however, with extremely small peak areas compared to the formation during Fe(VI) treatment. Deaminated clarithromycin, which corresponds to OP 235, was < 1 % during the ozonation of clarithromycin, underlining the aminium radical cation pathway to be of minor importance during ozonation of tertiary amines *(16)*. For realistic conditions with O_3 in excess to TRA, OP 278, 264a, 235 and 249 will be further oxidized (Figure S5.8). Under such conditions, most fast-reacting amine moieties have been transformed (k_{TRA,O_3} = 4.2 x 10^4 M^{-1} s^{-1} at pH 8, Table 5.1), and the anisole moiety ($k_{anisole,O_3}$ = 290 M^{-1} s^{-1}, *(43)*) may also be attacked by O_3 according to the Criegee mechanism *(44)*. However, no such O_3 OP were identified in the present study.

5.3.5 Comparison of Fe(VI) and O_3 OPs

For both oxidants, the lone electron pair of the amine is the first site of attack. The formation of an aminium radical cation and oxygen transfer can explain some identified OPs which are observed for both oxidants. Still, the proposed aminium radical cation is favored during oxidation by Fe(VI) leading predominantly to N-DES formation, whereas the proposed oxygen transfer prevails for O_3 attack resulting in N-OXID as the main OP.

Acknowledgements

The authors gratefully acknowledge S. Canonica for support during determination of the hydroxyl radical rate constant with tramadol, M. Schlüsener and A. Wick for technical assistance, Y. Lee and R. Beel for fruitful discussions, and J.L. Kormos for language corrections. The study was financially supported by the Swiss Federal Office for the Environment (FOEN) within the Swiss National project MicroPoll, and the EU NEPTUNE project (Contract No 036845, SUSTDEV-2005-3.II.3.2), which was financially supported by grants obtained from the EU Commission within the Energy, Global Change and Ecosystems Program of the Sixth Framework (FP6-2005-Global-4).

5.4 References

(1) Flick, K.; Frankus, E.; Friderichs, E. Studies on Chemical-Structure and Analgetic Activity of Phenyl Substituted Aminomethylcyclohexanoles. *Arzneimittel-Forschung/Drug Research* **1978**, *28-1*, 107-113.

(2) Lintz, W.; Erlacin, S.; Frankus, E.; Uragg, H. Biotransformation of Tramadol in Man and Animal. *Arzneimittel-Forschung/Drug Research* **1981**, *31-2*, 1932-1943.

(3) De Leo, M.; Giorgi, M.; Saccomanni, G.; Manera, C.; Braca, A. Evaluation of tramadol and its main metabolites in horse plasma by high-performance liquid chromatography/fluorescence and liquid chromatography/electrospray ionization tandem mass spectrometry techniques. *Rapid Commun. Mass Spectrom.* **2009**, *23*, 228-236.

(4) Schwabe, U.; Paffrath, D. *Arzneiverordnungs-Report 2005*. Springer-Verlag: Berlin, Heidelberg, 2006.

(5) Kasprzyk-Hordern, B.; Dinsdale, R. M.; Guwy, A. J. The removal of pharmaceuticals, personal care products, endocrine disruptors and illicit drugs during wastewater treatment and its impact on the quality of receiving waters. *Water Res.* **2009**, *43*, 363-380.

(6) Hollender, J.; Zimmermann, S. G.; Koepke, S.; Krauss, M.; McArdell, C. S.; Ort, C.; Singer, H.; von Gunten, U.; Siegrist, H. Elimination of organic micropollutants in a municipal wastewater treatment plant upgraded with a full-scale post-ozonation followed by sand filtration. *Environ. Sci. Technol.* **2009**, *43*, 7862-7869.

(7) Zimmermann, S. G.; Wittenwiler, M.; Hollender, J.; Krauss, M.; Ort, C.; Siegrist, H.; von Gunten, U. Kinetic assessment and modeling of an ozonation step for full-scale municipal wastewater treatment: Micropollutant oxidation, by-product formation and disinfection. *Water Res.* **2011**, *45*, 605-617.

(8) Lee, Y.; Zimmermann, S. G.; Kieu, A. T.; von Gunten, U. Ferrate (Fe(VI)) Application for Municipal Wastewater Treatment: A Novel Process for Simultaneous Micropollutant Oxidation and Phosphate Removal. *Environ. Sci. Technol.* **2009**, *43*, 3831-3838.

(9) Sharma, V. K. Oxidation of Inorganic Compounds by Ferrate(VI) and Ferrate(V): One-Electron and Two-Electron Transfer Steps. *Environ. Sci. Technol.* **2010**, *44*, 5148-5152.

(10) von Gunten, U.; Hoigné, J. Bromate Formation During Ozonation of Bromide-Containing Waters - Interaction of Ozone and Hydroxyl Radical Reactions. *Environ. Sci. Technol.* **1994**, *28*, 1234-1242.

(11) Alsheyab, M.; Jiang, J.-Q.; Stanford, C. Engineering Aspects of Electrochemical Generation of Ferrate: A Step Towards Its Full Scale Application for Water and Wastewater Treatment. *Water Air and Soil Pollution* **2010**, *210*, 203-210.

(12) McDowell, D. C.; Huber, M. M.; Wagner, M.; von Gunten, U.; Ternes, T. A. Ozonation of carbamazepine in drinking water: Identification and kinetic study of major oxidation products. *Environ. Sci. Technol.* **2005**, *39*, 8014-8022.

(13) Huber, M. M.; Ternes, T. A.; von Gunten, U. Removal of estrogenic activity and formation of oxidation products during ozonation of 17 alpha-ethinylestradiol. *Environ. Sci. Technol.* **2004**, *38*, 5177-5186.

(14) De Witte, B.; Van Langenhove, H.; Hemelsoet, K.; Demeestere, K.; De Wispelaere, P.; Van Speybroeck, V.; Dewulf, J. Levofloxacin ozonation in water: Rate determining process parameters and reaction pathway elucidation. *Chemosphere* **2009**, *76*, 683-689.

(15) Benner, J.; Ternes, T. A. Ozonation of Propranolol: Formation of Oxidation Products. *Environ. Sci. Technol.* **2009**, *43*, 5086-5093.

(16) Lange, F.; Cornelissen, S.; Kubac, D.; Sein, M. M.; von Sonntag, J.; Hannich, C. B.; Golloch, A.; Heipieper, H. J.; Möder, M.; von Sonntag, C. Degradation of macrolide antibiotics by ozone: A mechanistic case study with clarithromycin. *Chemosphere* **2006**, *65*, 17-23.

(17) Hu, L.; Martin, H. M.; Arcs-Bulted, O.; Sugihara, M. N.; Keatlng, K. A.; Strathmann, T. J. Oxidation of Carbamazepine by Mn(VII) and Fe(VI): Reaction Kinetics and Mechanism. *Environ. Sci. Technol.* **2009**, *43*, 509-515.

(18) Yang, B.; Ying, G.; Zhao, J.-L.; Zhang, L.-J.; Fang, Y.-X.; Nghiem, L. D. Oxidation of triclosan by ferrate: Reaction kinetics, products identification and toxicity evaluation. *J. Hazard. Mater.* **2011**, *186*, 227-235.

(19) Li, C.; Li, X. Z.; Graham, N.; Gao, N. Y. The aqueous degradation of bisphenol A and steroid estrogens by ferrate. *Water Res.* **2008**, *42*, 109-120.

(20) Huang, H.; Sommerfeld, D.; Dunn, B. C.; Eyring, E. M.; Lloyd, C. R. Ferrate(VI) oxidation of aqueous phenol: Kinetics and mechanism. *J. Phys. Chem. A* **2001**, *105*, 3536-3541.

(21) Lee, Y.; Um, I. H.; Yoon, J. Arsenic(III) oxidation by iron(VI) (ferrate) and subsequent removal of arsenic(V) by iron(III) coagulation. *Environ. Sci. Technol.* **2003**, *37*, 5750-5756.

(22) Carr, J. D.; Kelter, P. B.; Ericson, A. T. Ferrate(VI) Oxidation of Nitrilotriacetic Acid. *Environ. Sci. Technol.* **1981**, *15*, 184-187.

(23) Noorhasan, N.; Patel, B.; Sharma, V. K. Ferrate(VI) oxidation of glycine and glycylglycine: Kinetics and products. *Water Res.* **2010**, *44*, 927-935.

(24) Johnson, M. D.; Hornstein, B. J.; Wischnewsky, J.: Ferrate(VI) Oxidation of Nitrogenous Compounds. In *Ferrates: Synthesis, Properties, and Applications in Water and Wastewater Treatment*; Sharma, V. K., Ed.; ACS Symposium Series: Washington D.C., 2008; pp 177-188.

(25) Sharma, V. K.; Mishra, S. K.; Nesnas, N. Oxidation of sulfonamide antimicrobials by ferrate(VI) [Fe(VI)O42-]. *Environ. Sci. Technol.* **2006**, *40*, 7222-7227.

(26) Dickinson, R. G.; Jacobsen, N. W. A New Sensitive and Specific Test for the Detection of Aldehydes: Formation of 6- Mercapto-3-substituted-s-triazolo[4,3-b]-s-tetrazines. *Journal of the Chemical Society D: Chemical Communications* **1970**, *24*, 1719-1720.

(27) Hopps, H. B. Purpald (R): A reagent that turns aldehydes purple! *Aldrichimica Acta* **2000**, *33*, 28-30.

(28) Lee, Y.; Yoon, J.; von Gunten, U. Spectrophotometric determination of ferrate (Fe(Vl)) in water by ABTS. *Water Res.* **2005**, *39*, 1946-1953.

(29) Pospisilova, M.; Polasek, M.; Jokl, V. Determination of tramadol in various dosage forms by capillary isotachophoresis. *J. Pharm. Biomed. Anal.* **1998**, *18*, 777-783.

(30) Wiczling, P.; Kawczak, P.; Nasal, A.; Kaliszan, R. Simultaneous determination of pK(a) and lipophilicity by gradient RP HPLC. *Anal. Chem.* **2006**, *78*, 239-249.

(31) Thabaj, K. A.; Kulkarni, S. D.; Chimatadar, S. A.; Nandibewoor, S. T. Oxidative transformation of ciprofloxacin by alkaline permanganate - A kinetic and mechanistic study. *Polyhedron* **2007**, *26*, 4877-4885.

(32) Zhang, H. C.; Huang, C. H. Oxidative transformation of fluoroquinolone antibacterial agents and structurally related amines by manganese oxide. *Environ. Sci. Technol.* **2005**, *39*, 4474-4483.

(33) Zhang, H. C.; Huang, C. H. Reactivity and transformation of antibacterial *N*-oxides in the presence of manganese oxide. *Environ. Sci. Technol.* **2005**, *39*, 593-601.

(34) Johnson, M. D.; Hornstein, B. J. The kinetics and mechanism of the ferrate(VI) oxidation of hydroxylamines. *Inorg. Chem.* **2003**, *42*, 6923-6928.

(35) Dennis, W. H.; Hull, L. A.; Rosenblatt. Oxidations of Amines. 4. Oxidative Fragmentation. *J. Org. Chem.* **1967**, *32*, 3783-3787.

(36) Hull, L. A.; Davis, G. T.; Rosenblatt; Williams, H. K.; Weglein, R. C. Oxidations of Amines. 3. Duality of Mechanism in Reaction of Amines with Chlorine Dioxide. *J. Am. Chem. Soc.* **1967**, *89*, 1163-1170.

(37) Huang, H.; Sommerfeld, D.; Dunn, B. C.; Lloyd, C. R.; Eyring, E. M. Ferrate(VI) oxidation of aniline. *J. Chem. Soc.-Dalton Trans.* **2001**, 1301-1305.

(38) Neta, P.; Huie, R. E.; Ross, A. B. Rate Constants for Reactions of Peroxyl Radicals in Fluid Solutions. *J. Phys. Chem. Ref. Data* **1990**, *19*, 413-513.

(39) Das, S.; Schuchmann, M. N.; Schuchmann, H. P.; von Sonntag, C. The Production of the Superoxide Radical-Anion by the Oh Radical-Induced Oxidation of Trimethylamine in Oxygenated Aqueous-Solution - the Kinetics of the Hydrolysis of (Hydroxymethyl)Dimethylamine. *Chemische Berichte-Recueil* **1987**, *120*, 319-323.

(40) von Sonntag, C.; Dowideit, P.; Fang, X. W.; Mertens, R.; Pan, X. M.; Schuchmann, M. N.; Schuchmann, H. P. The fate of peroxyl radicals in aqueous solution. *Water Sci. Technol.* **1997**, *35*, 9-15.

(41) Johnson, M. D.; Hornstein, B. J. Unexpected selectivity in the oxidation of arylamines with ferrate-preliminary mechanistic considerations. *Chemical Communications* **1996**, 965-966.

(42) Munoz, F.; von Sonntag, C. The reactions of ozone with tertiary amines including the complexing agents nitrilotriacetic acid (NTA) and ethylenediaminetetraacetic acid (EDTA) in aqueous solution. *Journal of the Chemical Society-Perkin Transactions 2* **2000**, 2029-2033.

(43) Hoigné, J.; Bader, H. Rate Constants of Reactions of Ozone with Organic and Inorganic-Compounds in Water .1. Non-Dissociating Organic-Compounds. *Water Res.* **1983**, *17*, 173-183.

(44) Dowideit, P.; von Sonntag, C. Reaction of ozone with ethene and its methyl- and chlorine-substituted derivatives in aqueous solution. *Environ. Sci. Technol.* **1998**, *32*, 1112-1119.

Supporting Information for Chapter 5

Kinetic and mechanistic investigations of the oxidation of tramadol by ferrate and ozone

5 tables, 8 figures, 4 texts and 10 schemes

Table S5.1. Substances analyzed with CAS number, supplier, structure and internal standard. n.a. = not available.

Substance ***internal standard***	**CAS number**	**Supplier**	**Structure**
Tramadol (TRA) *d6-Tramadol*	36282-47-0	Sigma-Aldrich *Toronto Research Chemicals*	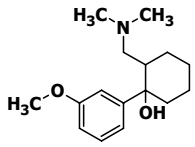
N-desmethyl-tramadol (N-DES)	1018989-94-0	LGC Standards	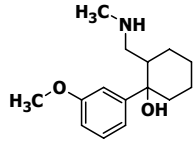
N,N-bidesmethyl-tramadol (BIDES)	n.a.	Toronto Research Chemicals	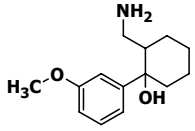
N-oxide-tramadol (N-OXID)	147441-56-3	LGC Standards	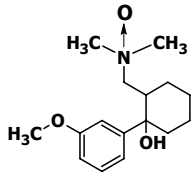
Anisole	100-66-3	Sigma-Aldrich	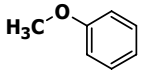

Text S5.1. Preparation of oxidants

Potassium ferrate ($K_2Fe(VI)O_4$) was prepared by the method of Thompson et al. *(1)* and its purity determined to be 88 %, as described in *(2)*. Stock solutions of Fe(VI) (0.2 - 3 mM) were freshly prepared by dissolving solid K_2FeO_4 in 5 mM phosphate / 1 mM borate buffer (pH 9.1) to stabilize Fe(VI) in aqueous solution *(3,4)*, quickly filtered through 0.45 µm PTFE syringe filters (BGB Analytik AG, Switzerland) and then quantified spectrophotometrically at 510 nm with $\varepsilon = 1150\ M^{-1}\ cm^{-1}$. Ozone ($O_3$) stock solutions (0.7 - 1.5 mM) were produced by sparging O_3 - containing oxygen through Milli-Q water cooled in an ice bath *(5)*, and standardized spectrophotometrically at 258 nm with $\varepsilon = 3000\ M^{-1}\ cm^{-1}$.

Text S5.2. Reaction kinetics of selected micropollutants and model compounds with Fe(VI), ozone and hydroxyl radicals

The apparent second-order rate constants *k* of tramadol (TRA) and *N*-desmethyl-tramadol (N-DES) with Fe(VI) were determined in the pH range 6.5 - 10.5 in batch experiments at 22 ± 2 °C using 0.25 L glass beakers. 100 mM phosphate solution was used as buffer for the pH range 6.5 - 8.5, and a 12.5 mM phosphate / 12.5 mM borate buffer solution for the pH range 9.0 - 10.5 *(2)*. For TRA and N-DES, kinetic experiments were conducted under pseudo-first-order conditions with Fe(VI) in excess to the compound ($[Fe(VI)]_0 : [compound]_0 \geq 10$, and $[compound]_0 = 1\ \mu M$). Kinetic runs were started by adding an appropriate amount of a Fe(VI) stock solution under rapid mixing, and if necessary, Fe(VI) stock solution was added several times during the kinetic run to keep [Fe(VI)] in excess to [compound]. The dilution factor was taken into account during data evaluation. At proper time intervals, 5 mL of the experimental solution were quenched with 10 mM thiosulfate solution to measure the residual compound concentration by HPLC-UV/FLD, while 1 mL of the experimental solution was quenched with ABTS solution to measure the residual Fe(VI) concentration *(3)*. The Fe(VI) exposure (Fe(VI) concentration integrated over time) corresponding to each residual compound measurement was calculated and plotted against the natural logarithm of the compound concentration (P) (eq S5.1):

$$\ln\left(\frac{[P]}{[P]_0}\right) = -k_{P,Fe(VI)} \times \int_0^t [Fe(VI)]dt \quad \text{(S5.1)}$$

The slope of the resulting straight line corresponded to the second-order rate constant $k_{P,Fe(VI)}$.

The apparent rate constants k for the reaction of Fe(VI) with TRA and N-DES were subsequently explained by second-order kinetics and by considering the reactions between Fe(VI) species ($HFeO_4^- \leftrightarrow FeO_4^{2-} + H^+$, p$K_a$ = 7.2 *(6)*) and compound species ($PH^+ \leftrightarrow P + H^+$, p$K_a$ see Table 5.1):

$$-\frac{d[P]_{tot}}{dt} = k\,[Fe(VI)]_{tot}\,[P]_{tot} = k_1[HFeO_4^-][PH^+] + k_2[HFeO_4^-][P] + k_3[FeO_4^{2-}][PH^+] + k_4[FeO_4^{2-}][P] \quad \text{(S5.2)}$$

The apparent second-order rate constant k can therefore be described by eq S5.3:

$$k = k_1\alpha_1\beta_1 + k_2\alpha_1\beta_2 + k_3\alpha_2\beta_1 + k_4\alpha_2\beta_2 \quad \text{(S5.3)}$$

with k_1, k_2, k_3 and k_4 being species-specific second-order rate constants, α_1 and α_2 representing the fraction of $HFeO_4^-$ and FeO_4^{2-}, respectively, and β_1 and β_2 representing the fraction of PH^+ and P, respectively. Based on eqs S5.1 and S5.2, the species-specific second-order rate constants k_1 - k_4 were fitted from the apparent second-order rate constants k by least-squares nonlinear regression using the software Sigma Plot V11.0. Similar to other studies, reactions of the deprotonated Fe(VI) species (FeO_4^{2-}) did not contribute significantly to the overall reactivity *(2,7)*, and were thus neglected. Table 5.1 of the main text summarizes therefore only the values for k_1 and k_2.

Second-order rate constants of *N,N*-bidesmethyl-tramadol (BIDES), *N*-oxide-tramadol (N-OXID) and anisole with Fe(VI) were determined with the compound in excess ($[compound)]_0$: $[Fe(VI)]_0 \geq 10$, and $[Fe(VI)]_0$ = 3 μM), and only at pH 8.0. 25 mM phosphate solution was used as a buffer, and experiments were carried out in 0.25 L glass beakers at 22 ± 2 °C. Kinetic runs were started by adding an appropriate amount of a Fe(VI) stock solution under rapid mixing, and at proper time intervals, 1 mL of the experimental solution was quenched with ABTS solution to measure the residual Fe(VI) concentration *(3)*. The plot of the natural logarithm of the Fe(VI) concentration vs. the

reaction time yielded a linear curve, corresponding to the pseudo-first order rate constant k_{app}'. The second-order rate constant $k_{P,Fe(VI)}$ was subsequently derived by dividing the pseudo-first order rate constant k_{app}' by the compound concentration.

For ozone, the second-order rate constant with TRA was determined in the pH range 3.0 to 7.5 under pseudo-first order conditions with excess ozone ($[ozone]_0 : [tramadol]_0 \geq 10$, and $[tramadol]_0$ = 1 µM). Experiments were carried out in 0.25 L glass bottles with a dispenser system *(8)* at 22 ± 2 °C. 50 mM phosphate solution was used as a buffer and 20 mM tert-butanol was used as a radical scavenger. An aliquot of ozone stock solution was injected with a syringe to start the kinetic run. 2 mL samples were withdrawn every 5-15 s and the residual ozone was quenched immediately by dispensing the sample into a tube containing indigo blue solution. This allowed for both the residual ozone *(5)* as well as TRA concentration to be measured by HPLC-UV/FLD. As for Fe(VI), the data was evaluated by plotting the natural logarithm of the remaining TRA concentration vs. the ozone exposure (equivalent to eq S5.1). The slope of the resulting straight line corresponded to the second-order rate constant. For higher second-order rate constants at the pH values 7.5, 8.0 and 8.5, competition kinetics were applied with excess TRA, using cephalexin ($k_{monoprotonated,O_3}$ = 8.2 (± 2.9) x 10^4 M^{-1} s^{-1}, and $k_{deprotonated,O_3}$ = 9.3 (± 2.2) x 10^4 M^{-1} s^{-1} *(9)*, pK_a = 7.1 *(10)*) as reference compound. Experiments were carried out in 0.25 L glass bottles with a dispenser system *(8)* and in solutions containing equal concentrations of TRA and cephalexin (5 µM) at 22 ± 2 °C. 50 mM phosphate solution was used as a buffer and 20 mM tert-butanol as a radical scavenger. After application of different ozone doses and subsequent complete ozone consumption, the remaining TRA and cephalexin concentrations were determined by HPLC-UV/FLD. According to eq S5.4, the second-order rate constant k_{P,O_3} could be derived from the slope of the plot of the natural logarithm of the remaining TRA concentration (P) vs. the natural logarithm of the remaining reference compound concentration (R), and the known second-order rate constant of the reference compound with ozone (k_{R,O_3}):

$$\ln\left(\frac{[P]}{[P]_0}\right) = \frac{k_{P,O_3}}{k_{R,O_3}} \times \ln\left(\frac{[R]}{[R]_0}\right) \qquad \text{(S5.4)}$$

The apparent rate constants k for the reaction of O_3 with TRA were subsequently explained by second-order kinetics similar to eq S5.1, however, without speciation of O_3. Thus eq S5.2 is adapted to eq S5.5:

$$-\frac{d[P]_{tot}}{dt} = k[O_3][P]_{tot} = k_5[O_3][PH^+] + k_6[O_3][P] \quad \text{(S5.5)}$$

The species-specific rate constant k_5 for the reaction of protonated TRA with O_3 was taken from the apparent k at pH 3.0 for which TRA speciation is dominated by its protonated form (pK_a 9.4). Equivalent to eq S5.3 for the reaction of TRA with Fe(VI), the apparent second-order rate constant k for the reaction of TRA with O_3 can be expressed as:

$$k = k_5(1-\beta) + k_6\beta \quad \text{(S5.6)}$$

with k_5 and k_6 as species-specific second-order rate constants and β representing the fraction of deprotonated TRA (P). The species-specific rate constant k_6 for the reaction of deprotonated TRA with O_3 was determined from the slope of the linear fit of the k vs. β plot as shown in Figure S5.3. Both values for k_5 and k_6 are given in Table 5.1.

The second-order rate constant for the reaction of TRA with hydroxyl radicals was also determined by competition kinetics, at pH 3 and 8 and at 22 ± 2 °C, using para-chlorobenzoic acid (*p*CBA) as reference compound ($k_{pCBA, OH\cdot}$ = 5.0 x 10^9 M^{-1} s^{-1} *(11)*. Hydroxyl radicals were generated by in situ UV photolysis (low-pressure mercury lamp) of 2 mM H_2O_2 solution *(12)*, while the pH was buffered with 50 mM phosphate buffer. The decrease of both TRA (1 µM) and *p*CBA (1 µM) was determined for different irradiation times and evaluated according to eq S5.4.

Text S5.3. HPLC-UV/FLD conditions for the separation of Fe(VI) and ozone OPs of tramadol

For Fe(VI) OPs, separation was achieved on a semipreparative 10 x 250 mm Synergi Hydro-RP column, and for the ozone OPs, a semipreparative 10 x 250 mm Synergi Polar-RP 80 A 4 µm column (both Phenomenex, Aschaffenburg, Germany) was used. Table S5.2 summarizes the optimized gradient conditions. TRA and its OPs were detected by a FLD at Ex/Em 275/300 nm (Fe(VI)) and 202/296 nm (ozone), respectively, and by a UVD at 254, 270 and 280 nm.

Table S5.2. HPLC gradient and further conditions for separation of tramadol OPs

Fe(VI)			**Ozone**		
time [min]	**A [%]**	**B [%]**	**time [min]**	**A [%]**	**B [%]**
0	60	40	0	90	10
26	60	40	15	70	30
27	40	60	25	35	65
100	40	60	27	90	10
101	60	40	29	90	10
120	60	40			
column temperature [°C]	25			room temperature	
injection volume [µL]	900			100	
flow rate [mL min^{-1}]	1.0			0.5	
eluent A	0.1% HCOOH			0.1 M NH_4COOH (pH 4)	
eluent B	methanol			acetonitrile	

Table S5.3. Optimized mass spectrometer parameters of the multiple reaction mode (MRM) method using the Qq-LIT-MS. positive mode: $M+H^+$; negative mode: $M-H^+$.

Q1 → Q3 [m/z]	Declustering Potential [V]	Collision Energy [V]	Collision Cell Exit Potential [V]	mode
264.1 → 246.1	46	17	12	positive
264.1 → 115.1	46	101	10	positive
264.1 → 91.1	46	63	14	positive
264.1 → 77	46	103	12	positive
270.1 → 252.1	31	17	14	positive
270.1 → 77.1	31	91	4	positive
280.1 → 262.1	56	21	22	positive
280.1 → 135.1	56	31	10	positive
280.1 → 121.1	56	47	10	positive
280.1 → 77.0	56	67	4	positive
250.1 → 232.1	41	13	12	positive
250.1 → 91.0	41	63	6	positive
250.1 → 77.0	41	95	12	positive
236.1 → 218.1	26	11	4	positive
236.1 → 121.1	26	35	8	positive
236.1 → 91.0	26	57	14	positive
236.1 → 77.0	26	63	4	positive
264.1 → 228.1	41	20	2	positive
264.1 → 200.1	41	31	8	positive
264.1 → 135.1	41	50	2	positive
264.1 → 121.1	41	50	2	positive
264.1 → 232.2	40	10	2	positive
264.1 → 214.1	40	15	2	positive
250.1 → 199.1	56	17	16	positive
250.1 → 171.1	56	40	2	positive
250.1 → 135.1	56	23	10	positive
250.1 → 121.1	56	50	2	positive

Q1 → Q3 [m/z]	Declustering Potential [V]	Collision Energy [V]	Collision Cell Exit Potential [V]	mode
278.1 → 260.1	21	11	10	positive
278.1 → 201.1	21	19	6	positive
278.1 → 121.1	21	40	2	positive
278.1 → 91.1	21	50	2	positive
278.1 → 77.0	21	67	4	positive
235.1 → 217.1	36	20	2	positive
235.1 → 189.1	36	20	2	positive
235.1 → 121.1	36	25	14	positive
235.1 → 91.1	36	50	2	positive
235.1 → 77.0	36	51	2	positive
249.1 → 217.1	-40	-40	-2	negative
249.1 → 199.1	-40	-40	-2	negative
249.1 →171.1	-40	-40	-2	negative
249.1 → 161.1	-40	-40	-2	negative
249.1 → 147.1	-40	-40	-2	negative
249.1 → 92.0	-40	-40	-2	negative

General parameters	
collision activated dissociation (CAD) gas	medium
curtain gas (CUR) [psi]	30
GS 1 [psi]	30
GS 2 [psi]	30
source temperature [°C]	400
capillary voltage pos./neg. mode (IS) [V]	4500 / -4500
entrance potential pos./neg. mode (EP) [V]	10 / -10

Text S5.4. Derivatization of OP 249 and OP 264a and subsequent GC-MS detection

The fraction of OP 249 was evaporated to dryness in a brown glass bottle heated to 40 °C in a water bath under a gentle N_2 stream. 100 µl of 0.2 M trimethylsulphonium hydroxide (TMSH) in methanol (Macherey-Nagel, Düren, Germany) were added and shaken for 30 s. Derivatization was achieved by injecting the mixture into the GC injector where the reaction took place at 275 °C. The fraction of OP 264a was dried analogously, and 500 µl N-methyl-N-trimethylsilyl-trifluoroacetamide (MSTFA) containing 1 % trimethylchlorosilane (TMCS) (Sigma-Aldrich, Germany) were added and heated to 60 °C in a water bath for 15 min. Both reaction solutions and both pure derivatization reagents were subjected to GC-MS analysis using a Thermo Finnigan Polaris-Q Trace GC (Thermo Scientific, Bremen, Germany), screening from 50 - 750 m/z.

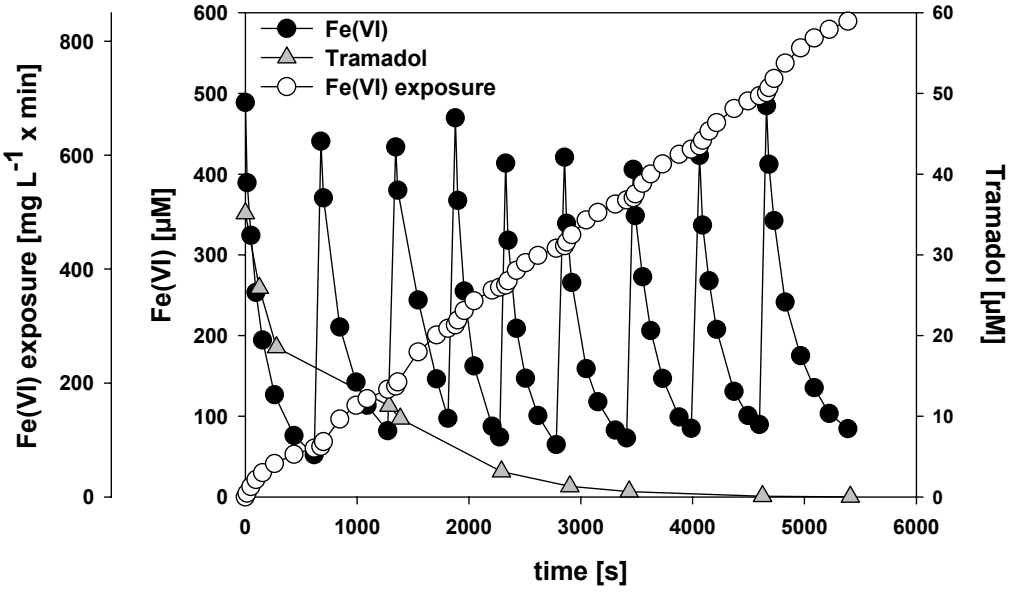

Figure S5.1. Fe(VI) and TRA concentrations as well as the resulting Fe(VI) exposure as a function of time during the mass balance experiment at pH 8.0

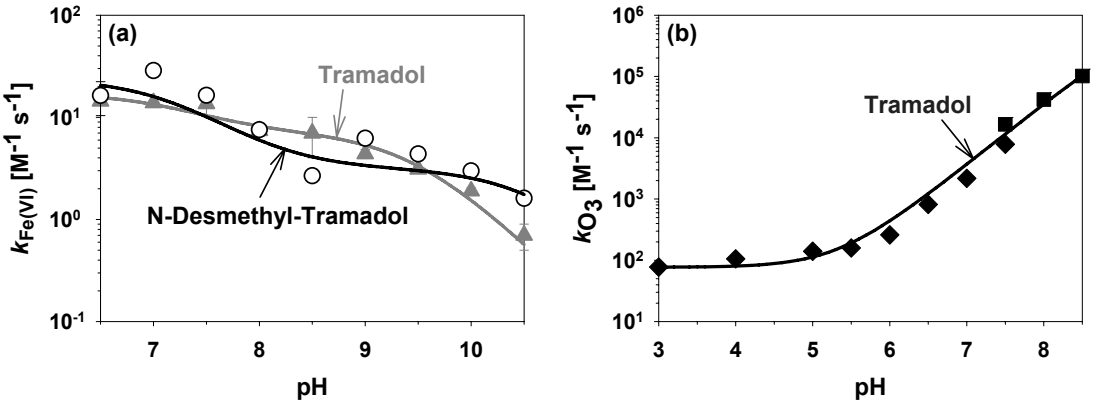

Figure S5.2. Apparent second-order rate constants *k* for the reaction of (a) Fe(VI) with tramadol (blue triangles) and *N*-desmethyl-tramadol (red circles) and (b) O_3 with tramadol determined directly (black diamonds) and determined with the help of a competitor (black squares) as a function of pH at 22 ± 2 °C. Lines represent model fits from the present study.

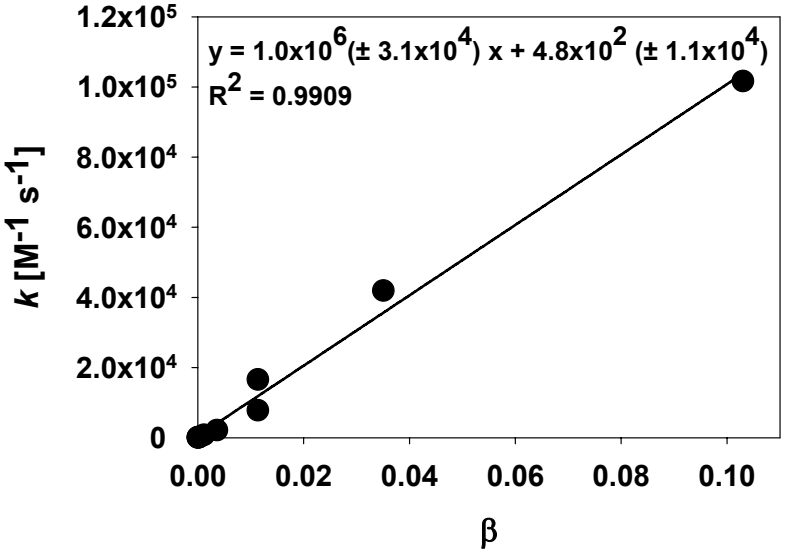

Figure S5.3. Plot of *k* for the reaction of ozone with tramadol within the pH range 3.0 to 8.5 (see Figure S5.2) versus the degree of dissociation of tramadol (β), which can be expressed as $\beta = 1/(1 + [H^+]/K)$ with *K* as dissociation constant of tramadol (Table 5.1, main text). According to eq S5.6, the slope of the linear fit gives the species-specific second-order reaction rate constant for the reaction of ozone with deprotonated tramadol (k_6).

Table S5.4. Structures, mass to charge ratios and sum formulas of tramadol and identified tramadol oxidation products from Fe(VI) and O_3 treatment

Compound ID	ESI (+) / (-)	Mass/charge ratio [m/z][a]	Sum formula[a]	Structure	Product of Fe(VI)	Product of O_3[c]
Tramadol (TRA)	+	264.19570[b]	$C_{16}H_{26}NO_2$	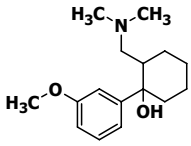		
OP 280 (N-OXID)	+	280.19037[b]	$C_{16}H_{26}NO_3$	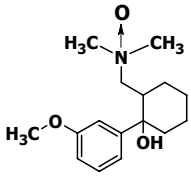	✓	✓
OP 278	+	278.17510[b]	$C_{16}H_{24}NO_3$	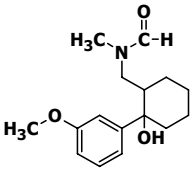	✓	(✓)
OP 250a (N-DES)	+	250.18016[b]	$C_{15}H_{24}NO_2$	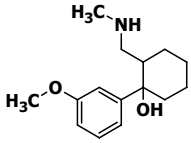	✓	✓
OP 249	-	249.11333[b]	$C_{14}H_{17}O_4$	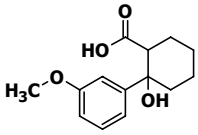	✓	(✓)
OP 236 (BIDES)	+	236	$C_{14}H_{22}NO_2$	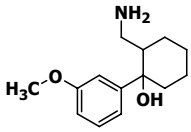	✓	(✓)
OP 235	+	235.13272[b]	$C_{14}H_{19}O_3$	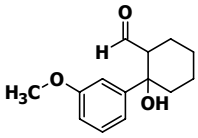	✓	(✓)

[a]Masses and sum formulas are given as $M+H^+$ or $M-H^+$ depending on the ESI mode.

[b]Exact mass/charge ratios determined by LTQ-FT-MS.

[c]Checkmarks in brackets indicate that OPs were identified as Fe(VI) OPs. Their formation during ozonation could be confirmed by the MRM method (Table S5.3).

Table S5.5. Structures, mass to charge ratios and sum formulas of tentatively proposed tramadol oxidation products from Fe(VI) and O_3 treatment

Compound ID	ESI (+) / (-)	Mass/charge ratio [m/z][a]	Sum formula[a]	Structure	Product of Fe(VI)	Product of O_3[c]
OP 264a	+	264.15944[b]	$C_{15}H_{22}NO_3$	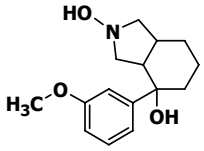	✓	(✓)
OP 264b	+	264.15912[b]	$C_{15}H_{22}NO_3$	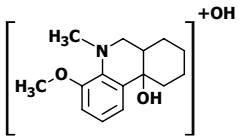	✓	-
OP 250b	+	250.14363[b]	$C_{14}H_{20}NO_3$	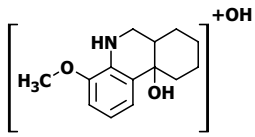	✓	-

[a]Masses and sum formulas are given as $M+H^+$ or $M-H^+$ depending on the ESI mode.

[b]Exact mass/charge ratios determined by LTQ-FT-MS.

[c]Checkmarks in brackets indicate that OPs were identified as Fe(VI) OPs. Their formation during ozonation could be confirmed by the MRM method (Table S5.3).

Scheme S5.1. Proposed fragmentation pathway and MS^2 and MS^3 spectra of tramadol (TRA)

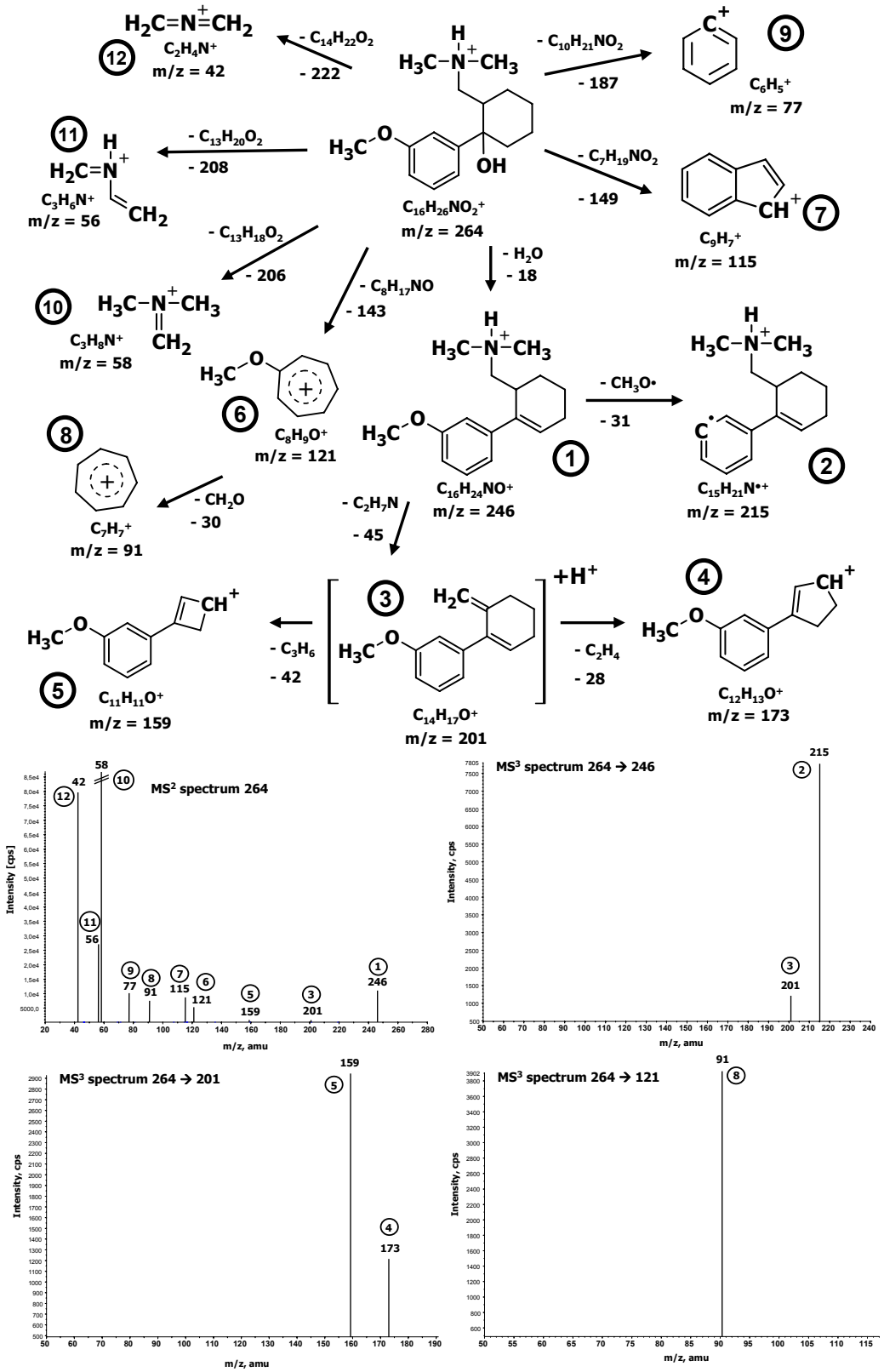

Scheme S5.2. Proposed fragmentation pathway and MS^2 and MS^3 spectra of *N*-desmethyl-tramadol (N-DES)

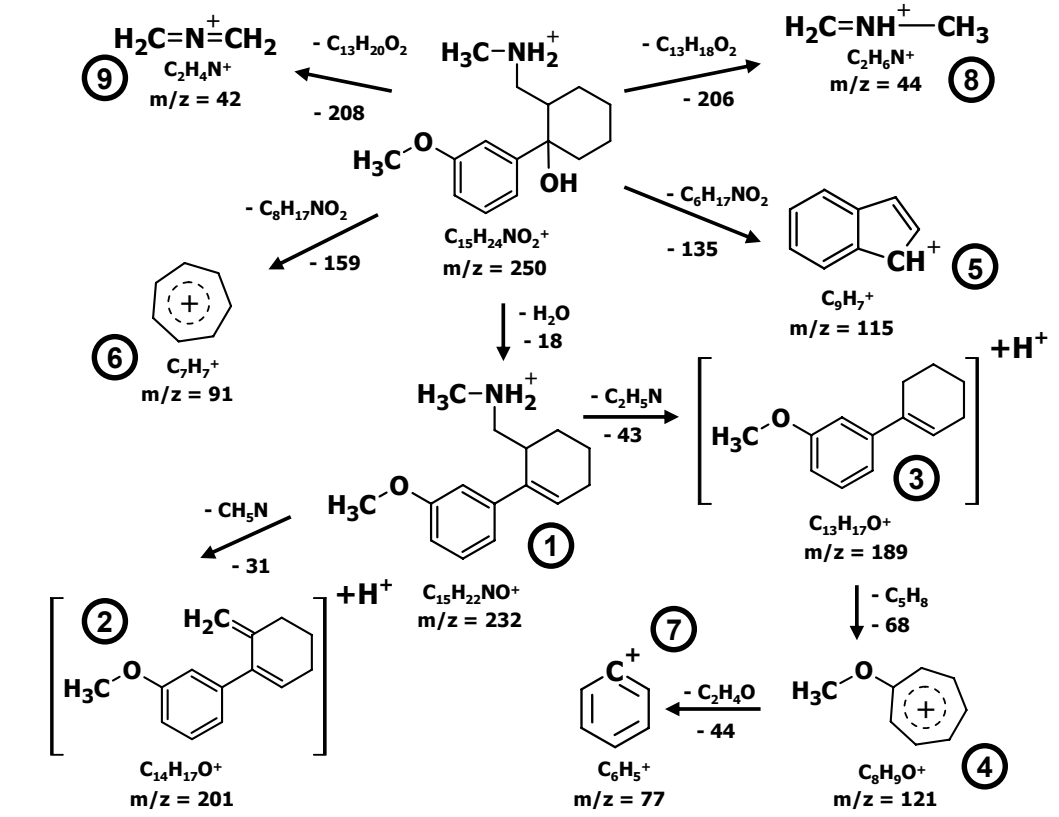

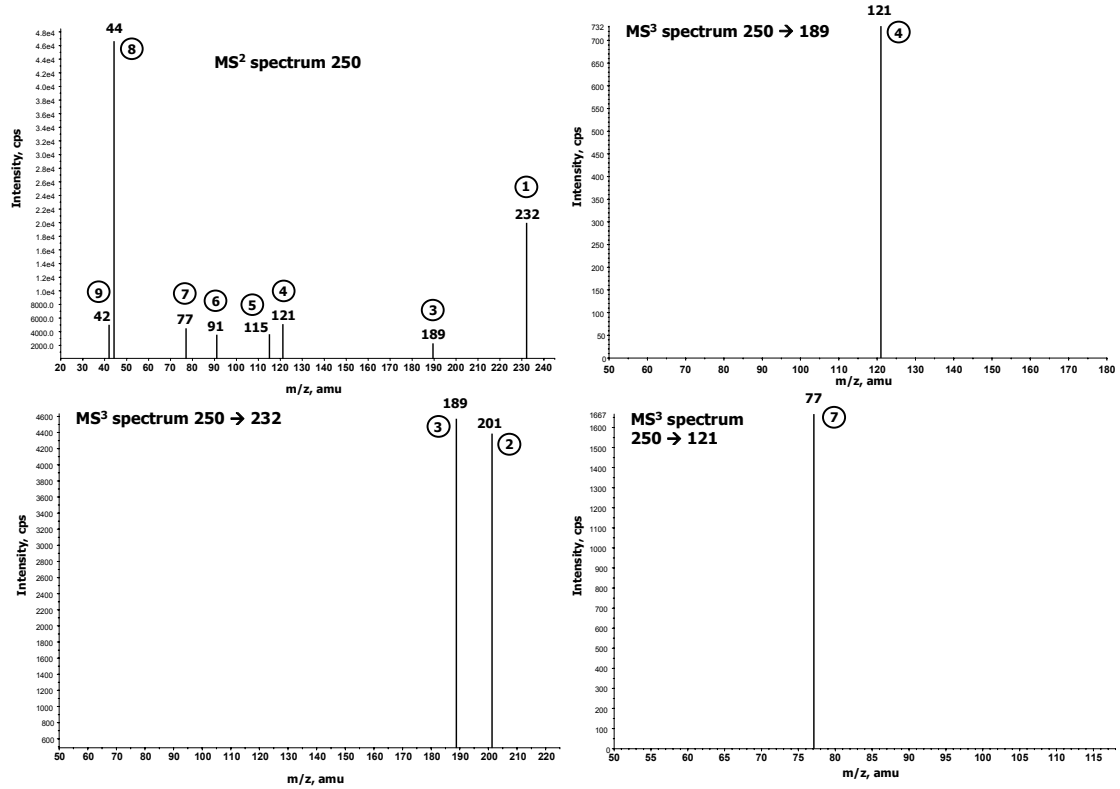

Scheme S5.3. Proposed fragmentation pathway and MS^2 of *N,N*-bidesmethyl-tramadol (BIDES)

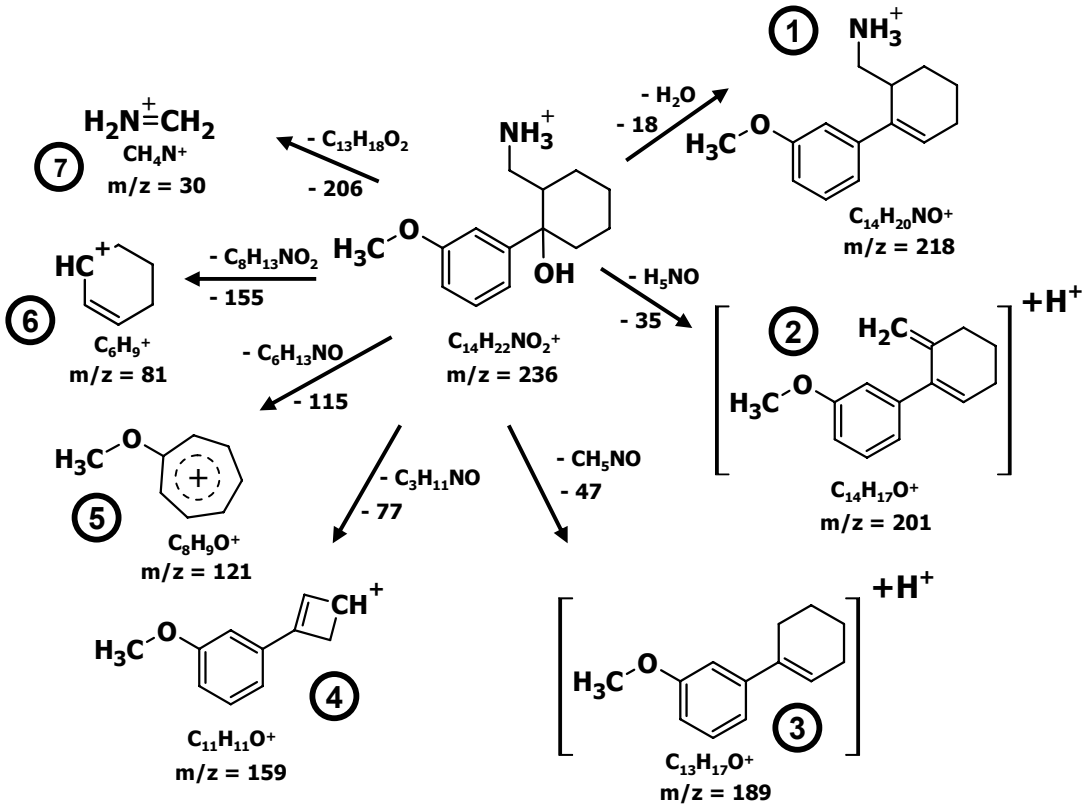

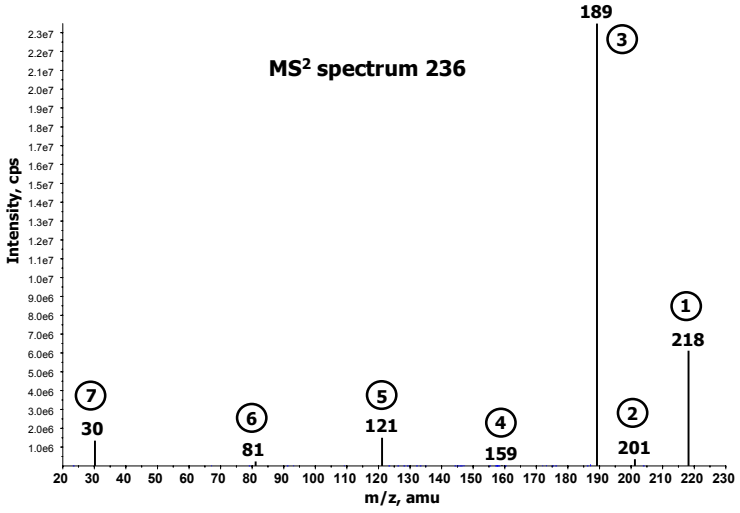

Scheme S5.4. Proposed fragmentation pathway and MS^2 and MS^3 spectra of *N*-oxide-tramadol (N-OXID)

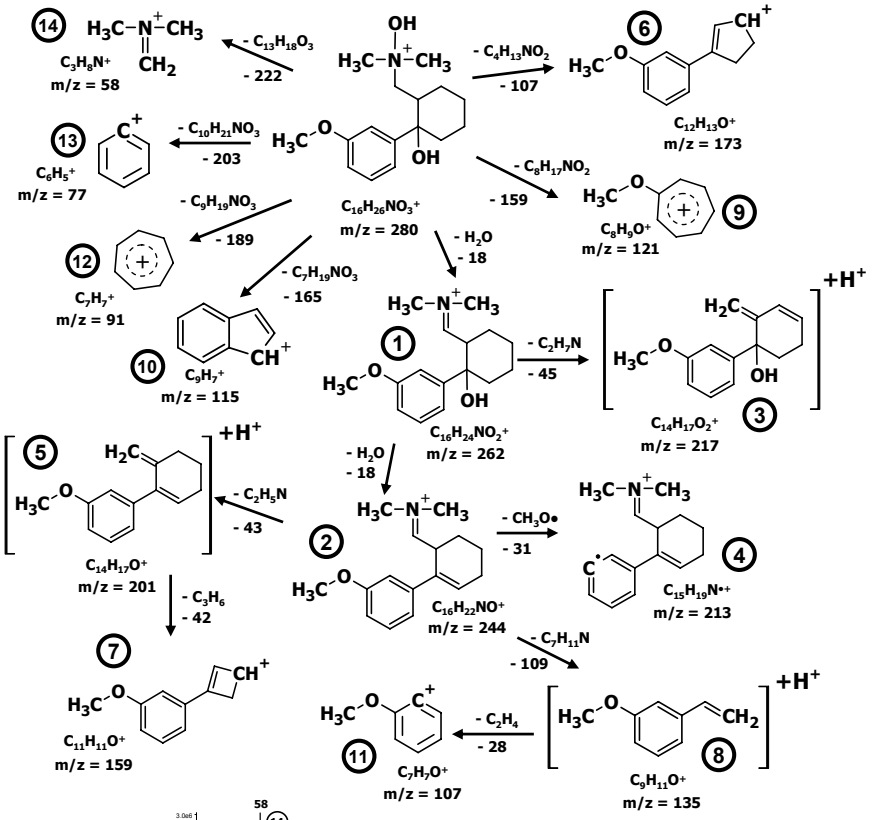

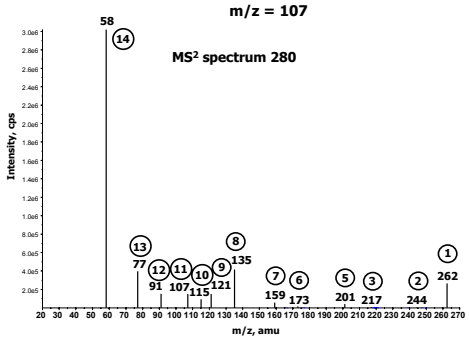

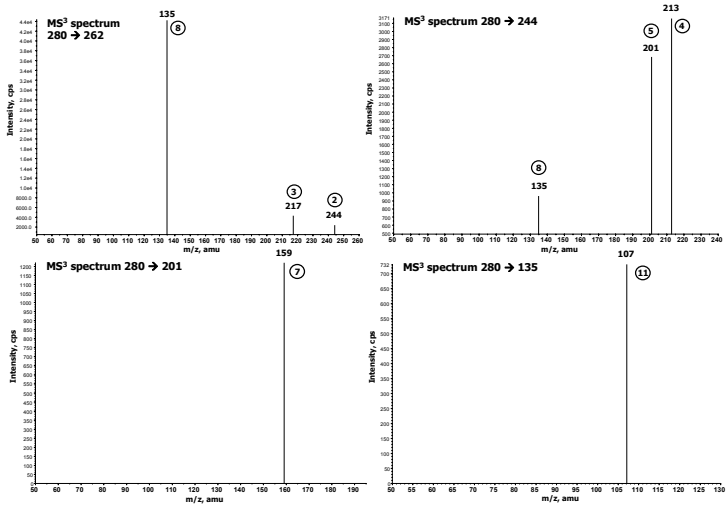

Scheme S5.5. Proposed fragmentation pathway and MS^2 and MS^3 spectra of OP 278

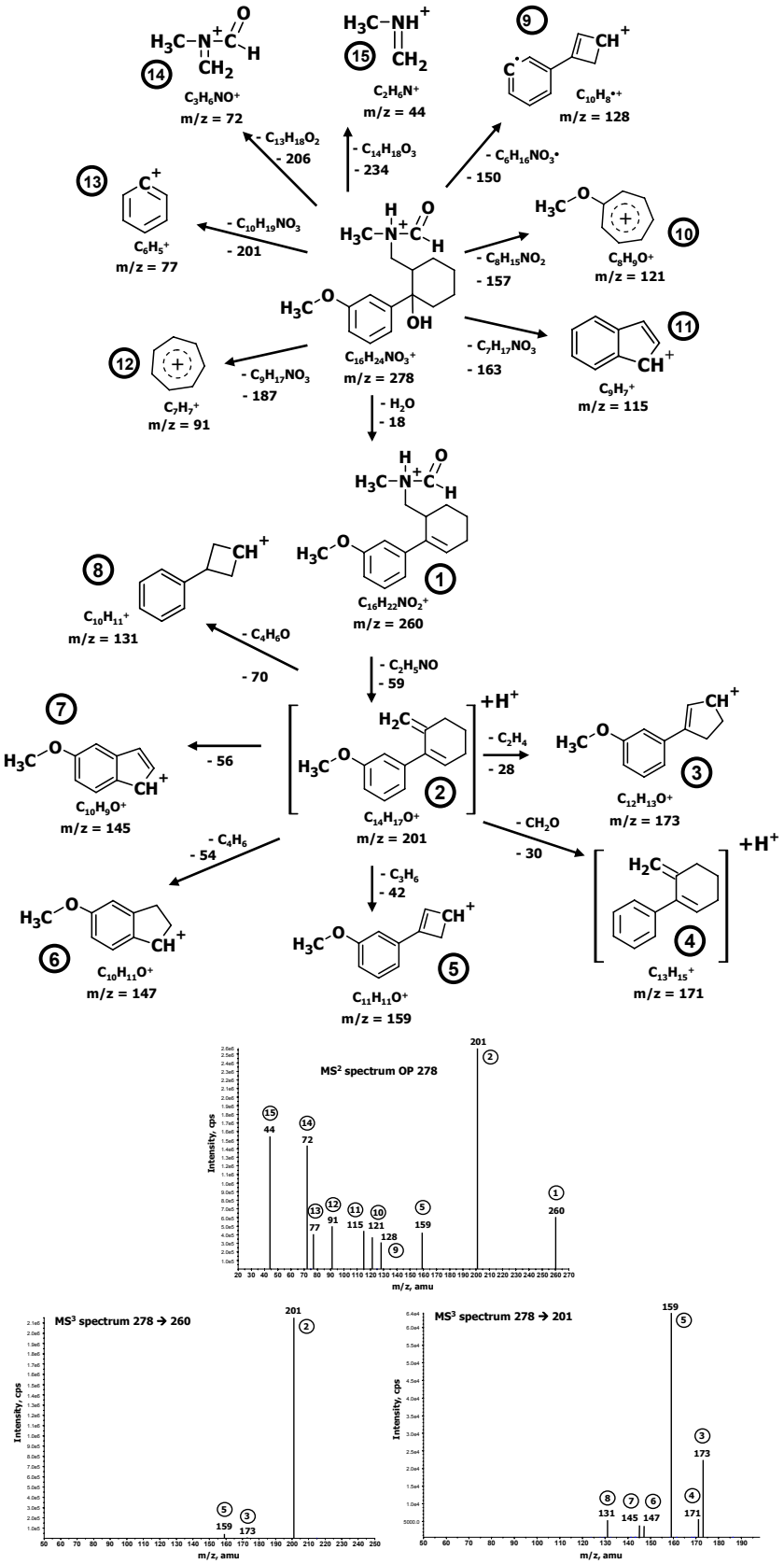

Scheme S5.6. Proposed fragmentation pathway and MS^2 and MS^3 spectra of OP 235

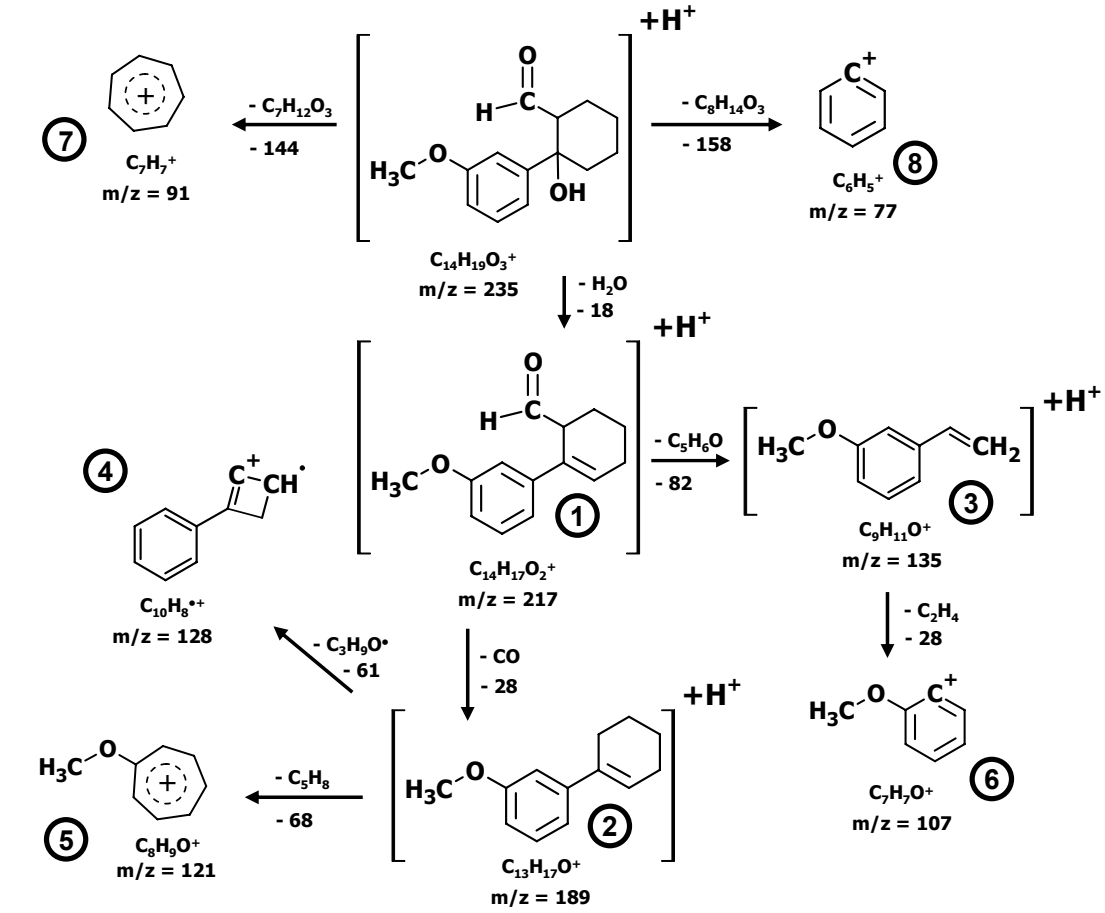

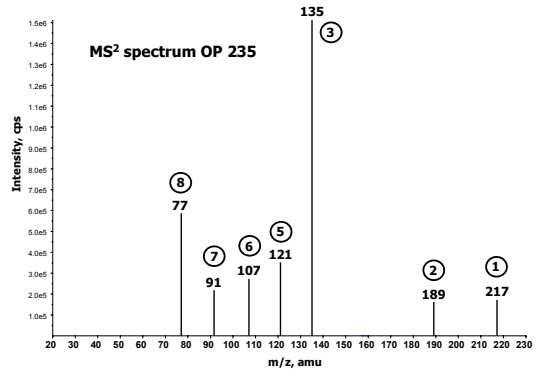

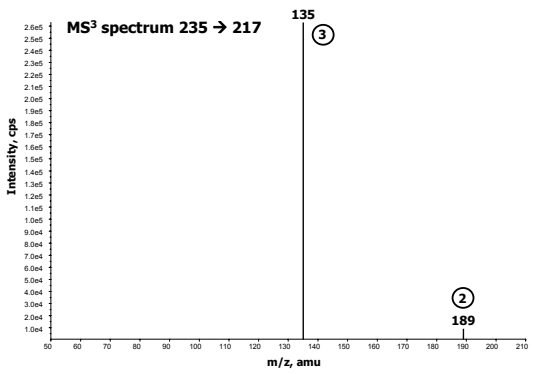

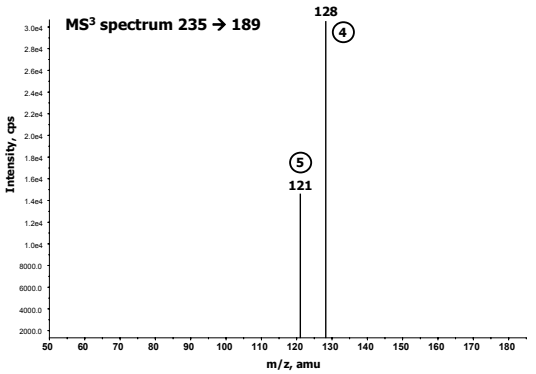

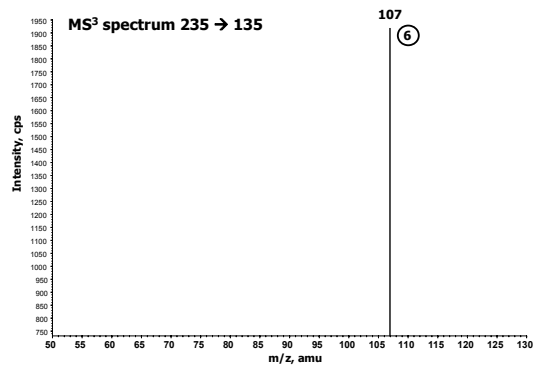

Scheme S5.7. Proposed fragmentation pathway and MS^2 and MS^3 spectra of OP 249

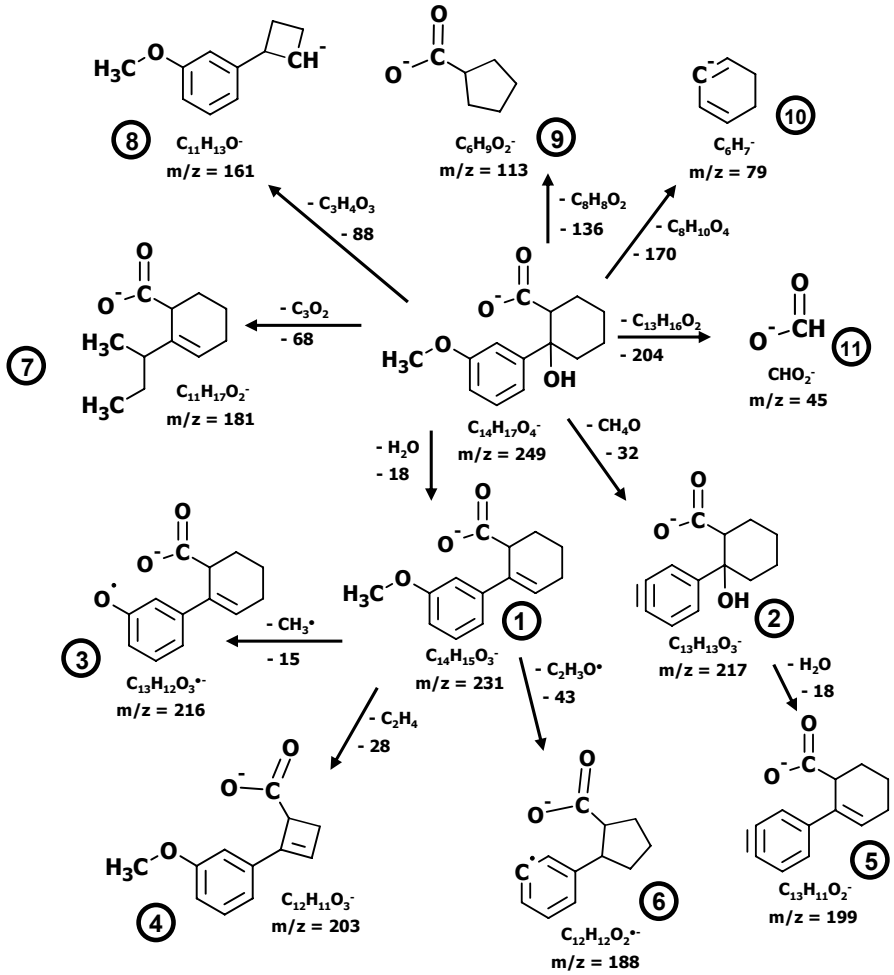

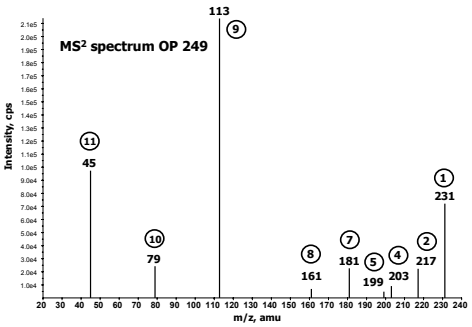

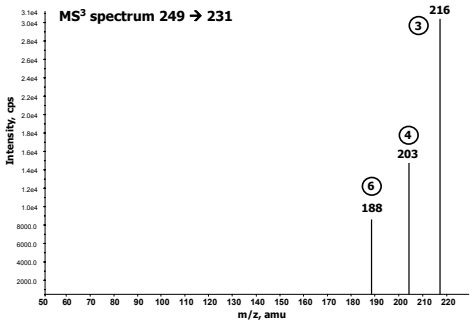

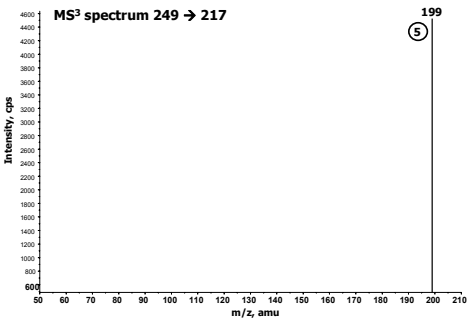

Scheme S5.8. Proposed fragmentation pathway and MS^2 and MS^3 spectra of OP 264a

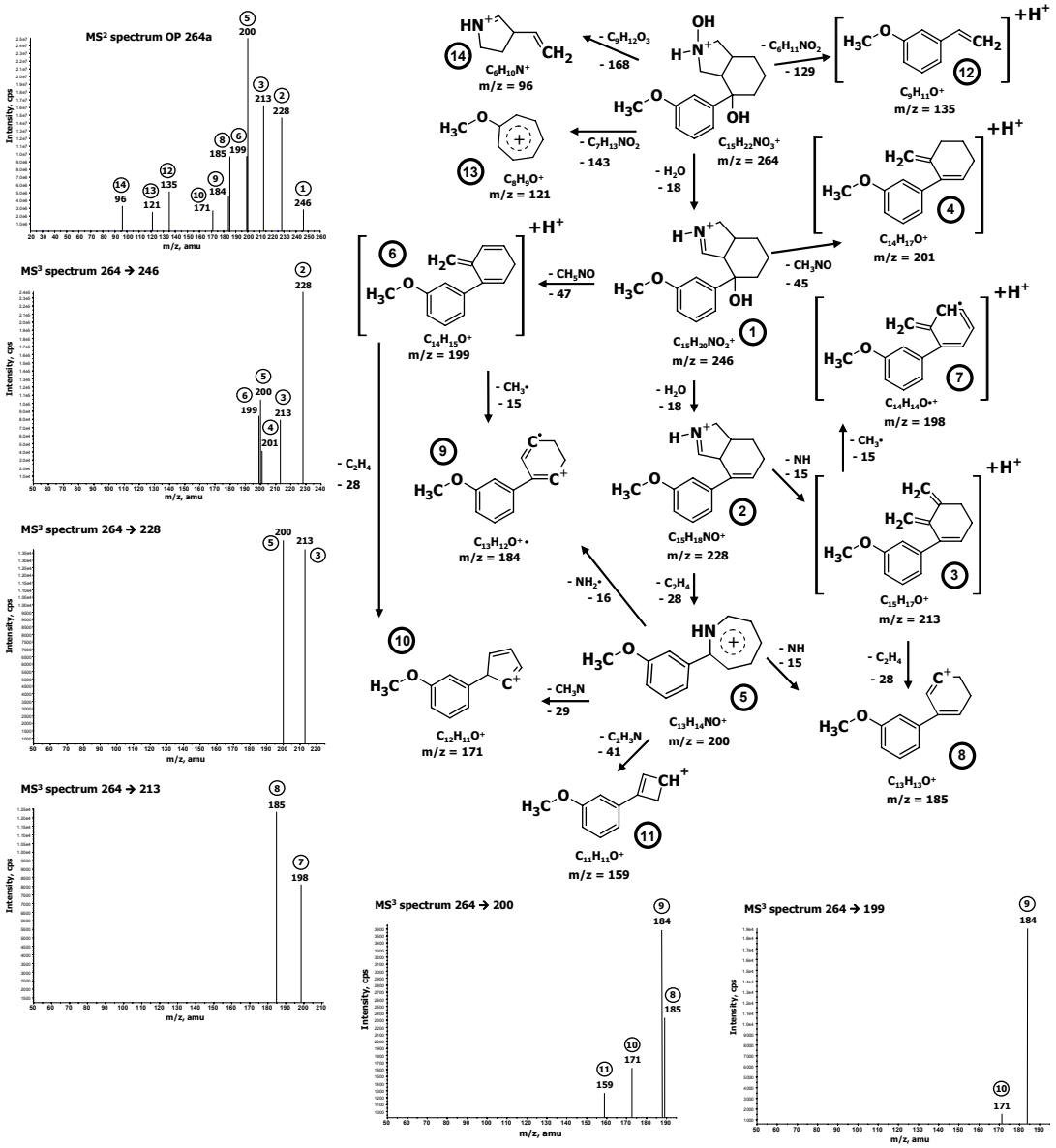

Scheme S5.9. Proposed fragmentation pathway and MS^2 and MS^3 spectra of OP 264b

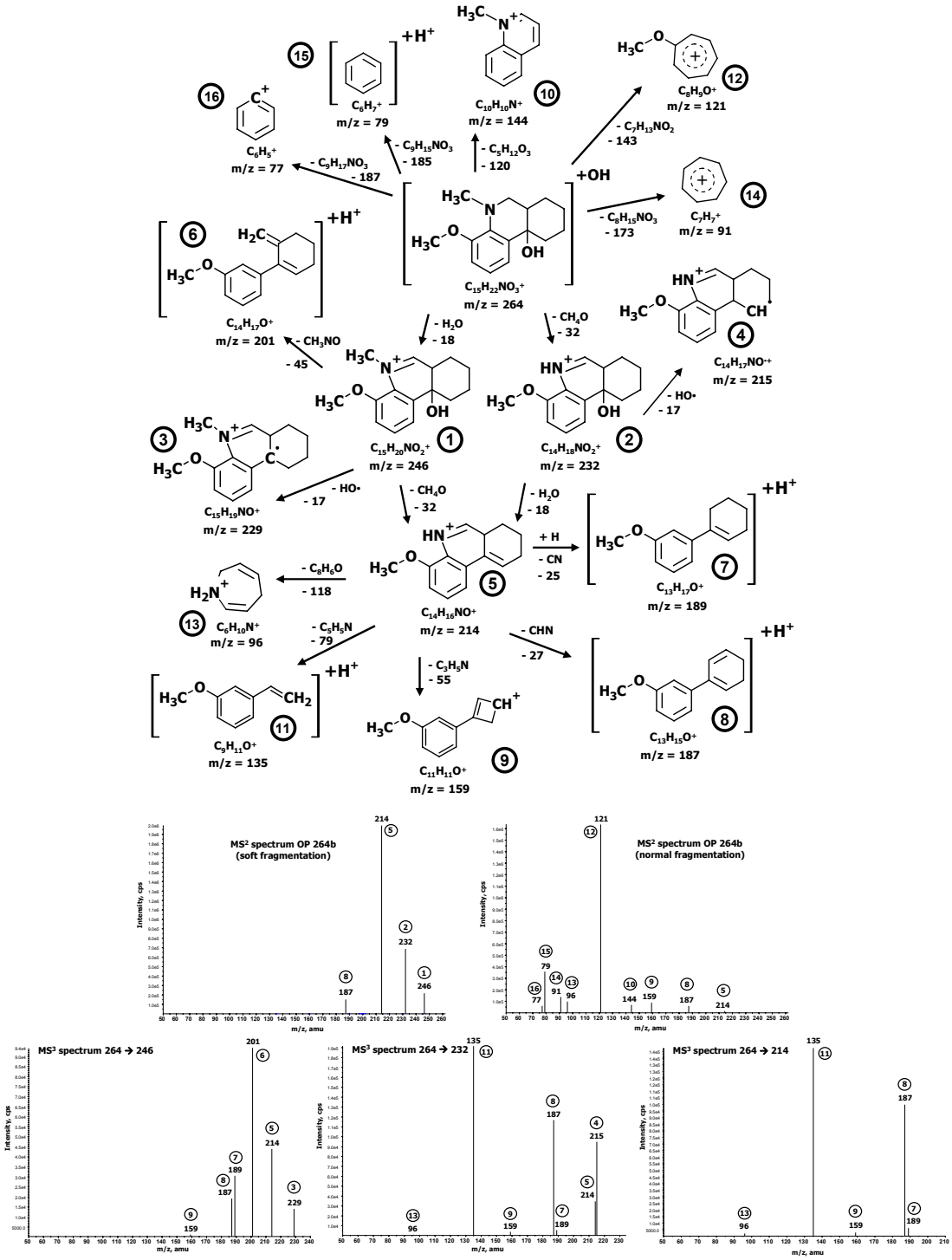

Scheme S5.10. Proposed fragmentation pathway and MS^2 and MS^3 spectra of OP 250b

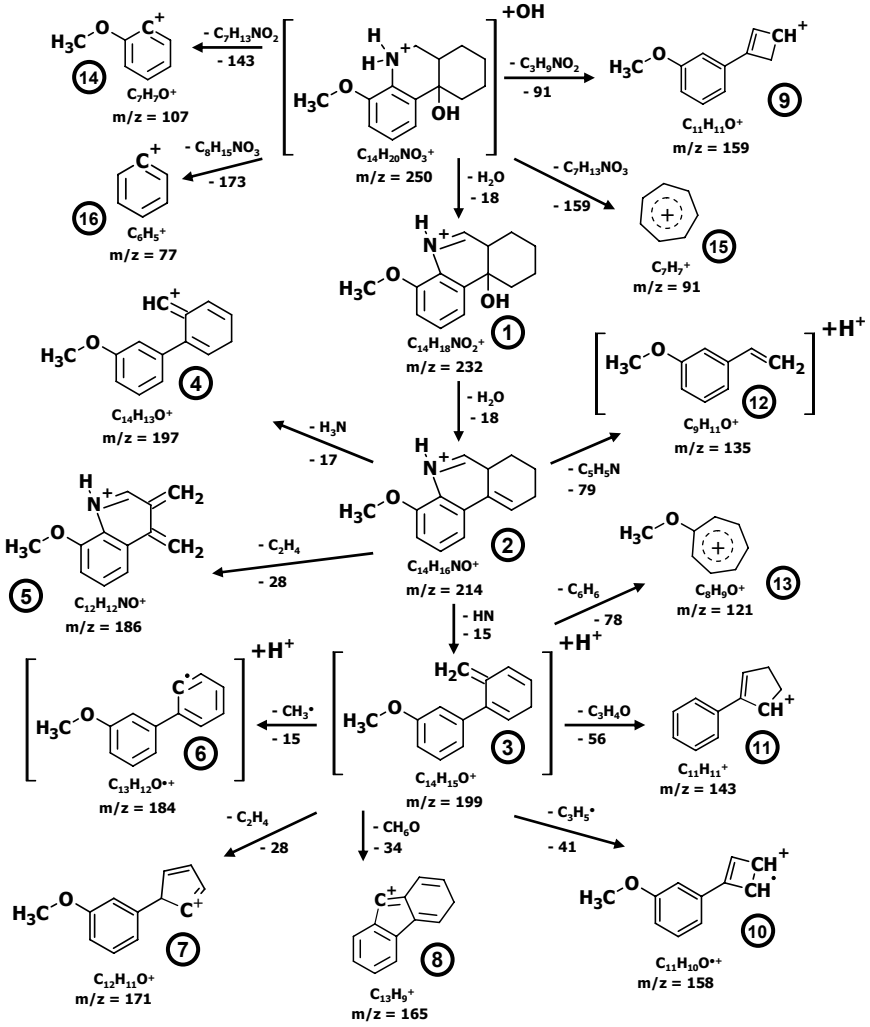

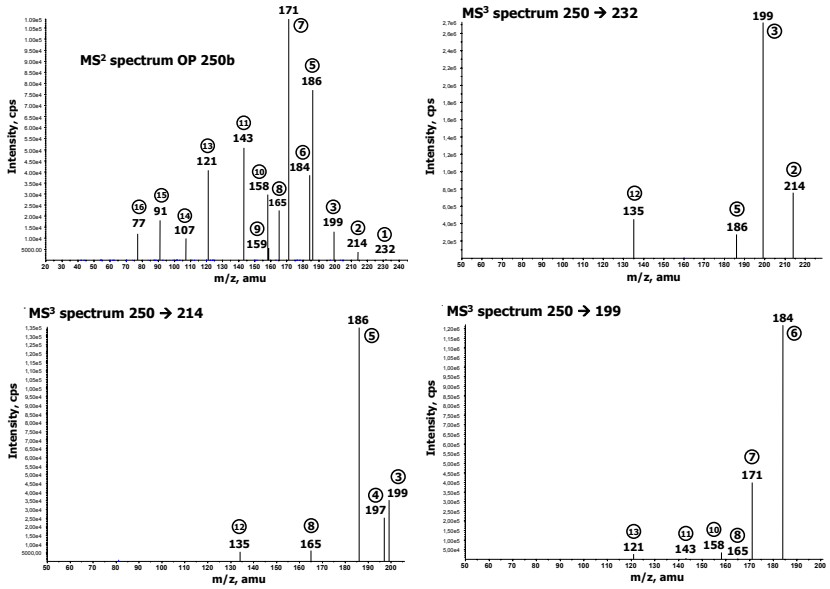

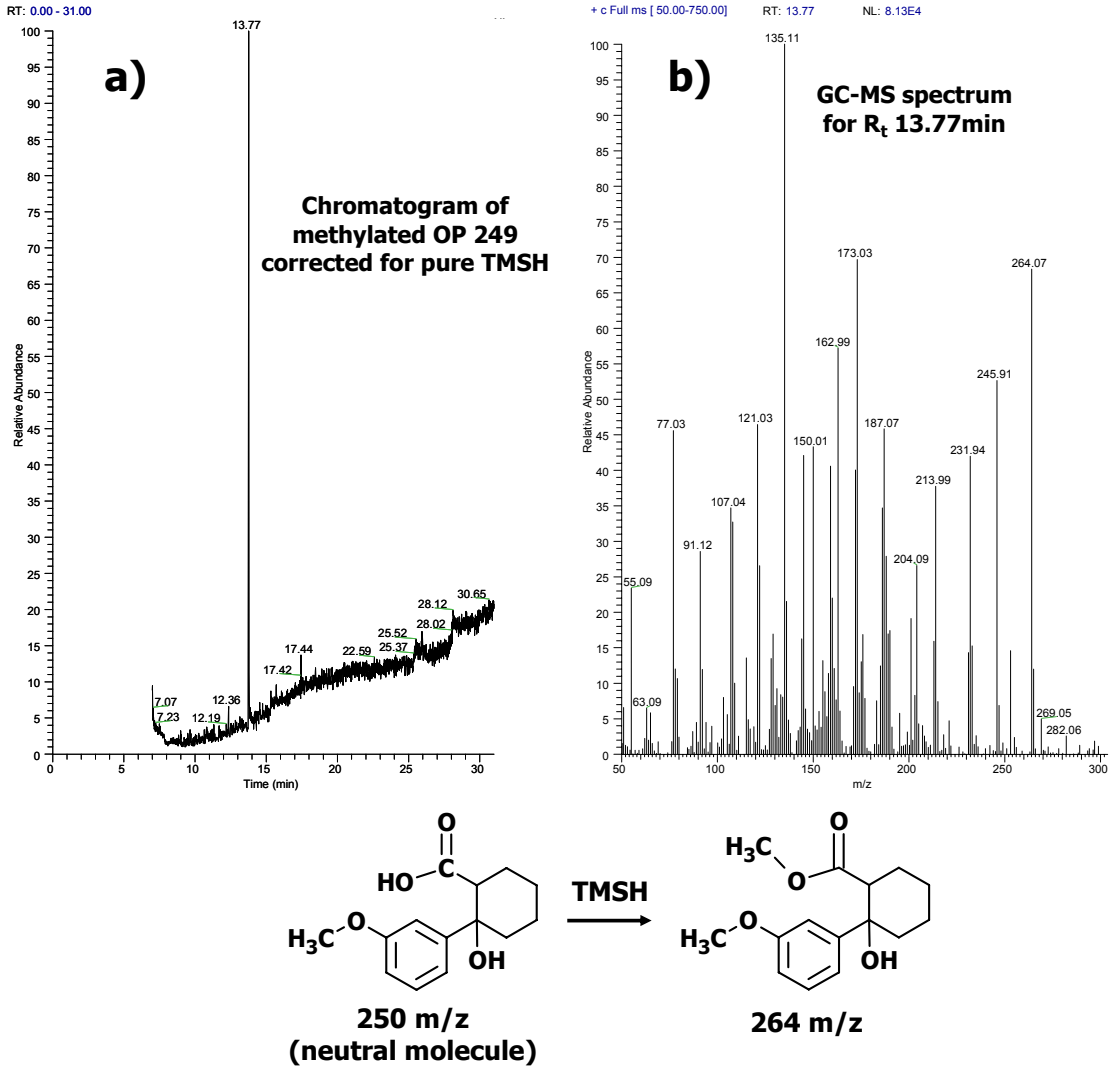

Figure S5.4. a) GC-MS chromatogram of methylated OP 249 and b) GC-MS spectrum at R_t 13.77 min. The methylating agent TMSH replaces acid protons such as in carboxylic groups but not protons of amines.

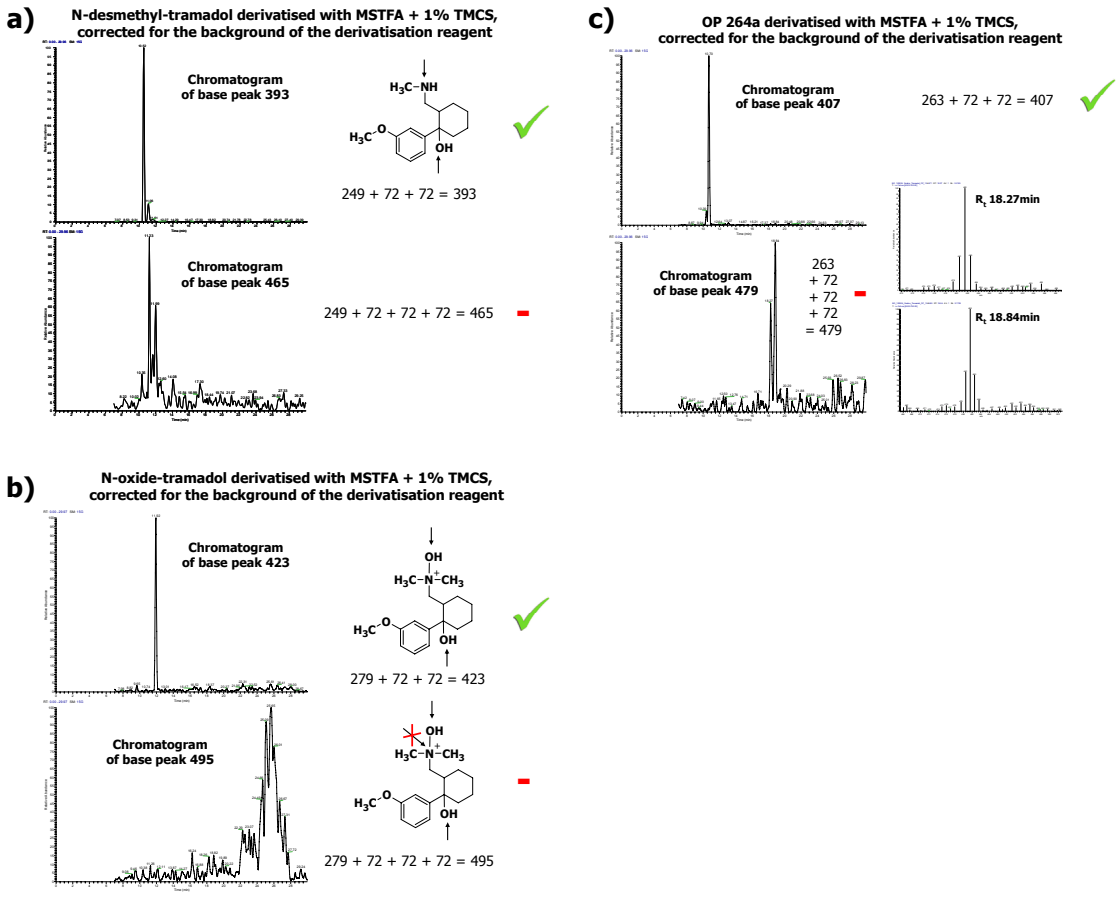

Figure S5.5. GC-MS chromatograms of indicated base peaks of silylated a) N-DES, b) N-OXID and c) OP 264a using MSTFA + 1 % TMCS. This silylation agent replaces labile hydrogen atoms on a wide range of functional groups (including hydroxyl groups and secondary amines) with a -Si(CH_3)$_3$ group (+72 m/z). As a proof of concept, N-DES was silylated twice at its hydroxyl group and secondary amine, while N-OXID was also silylated twice at its two hydroxyl groups, but not at the nitrogen atom. Subsequently, OP 264a was found to be silylated only twice, suggesting that silylation at the nitrogen atom was blocked by a hydroxyl group.

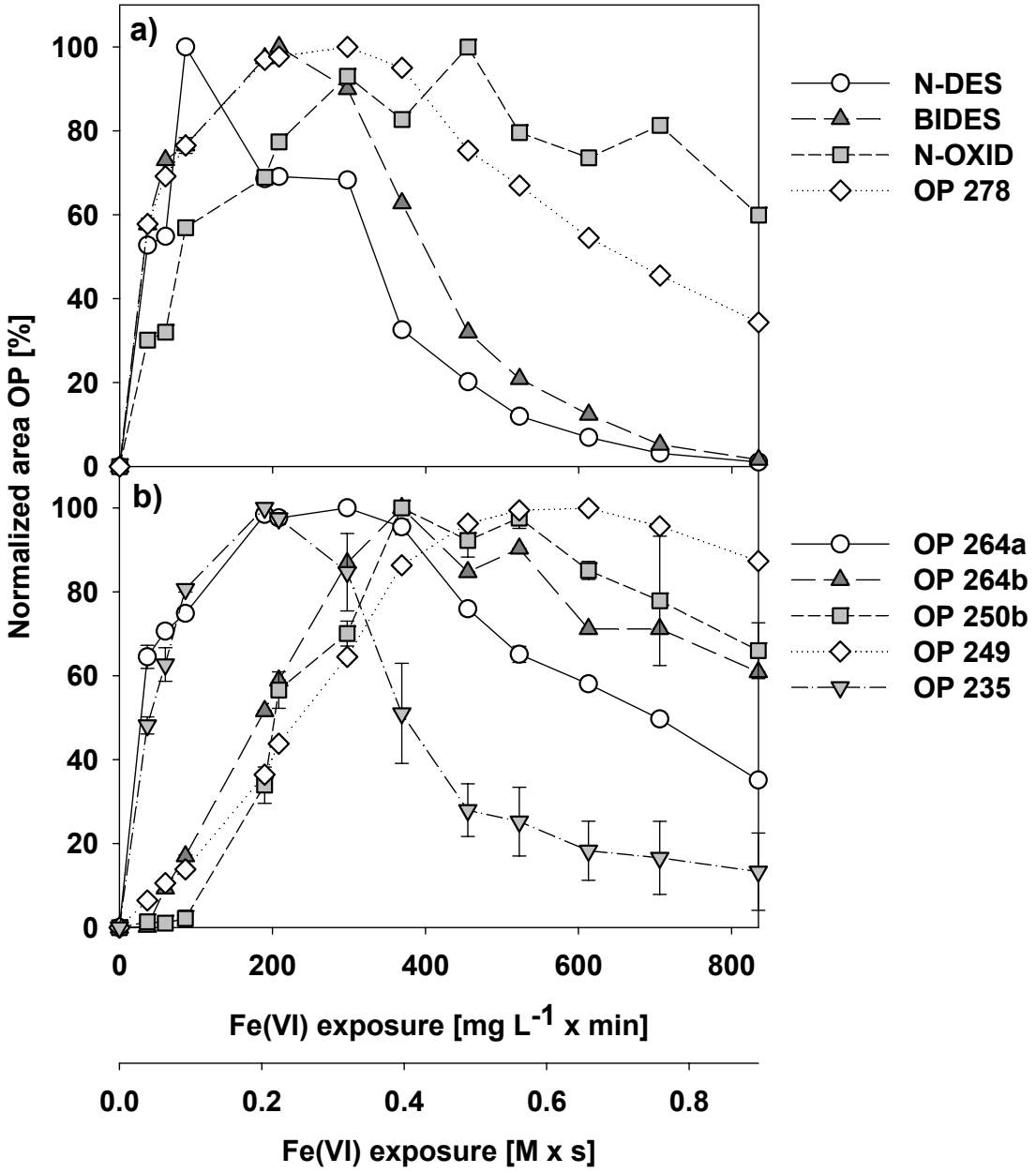

Figure S5.6. Formation of identified Fe(VI) OPs during the mass balance experiment, normalized to the highest peak area for each OP

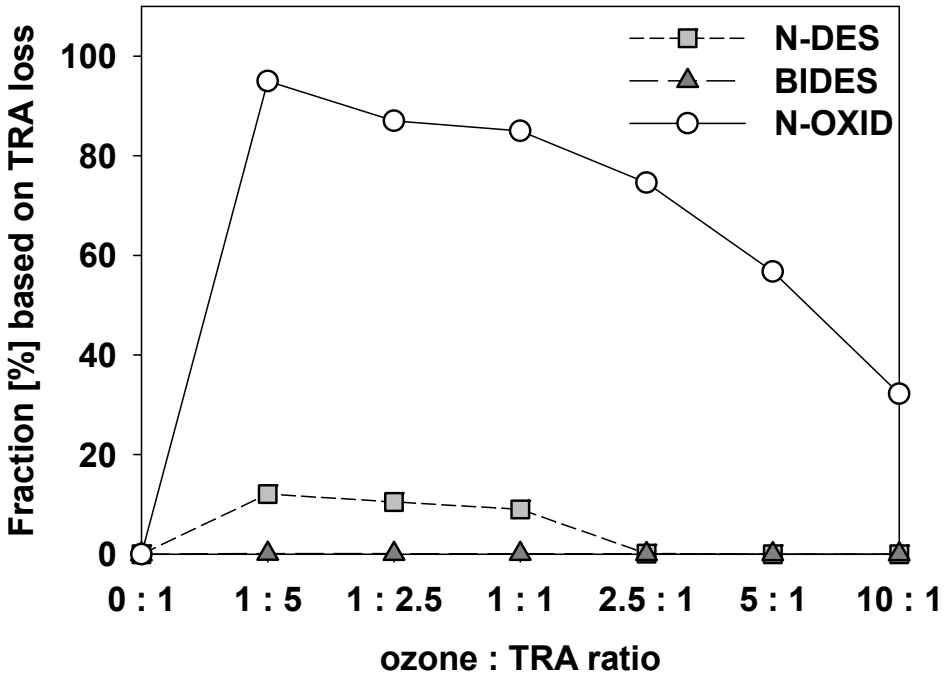

Figure S5.7. Formation and further oxidation of N-DES, BIDES and N-OXID during oxidative treatment of TRA by O_3 at pH 8, based on the TRA loss for each ozone:TRA ratio. $[TRA]_0$ = 50 µM. 5 mM tert-butanol was spiked as radical scavenger to prevent reactions with hydroxyl radicals.

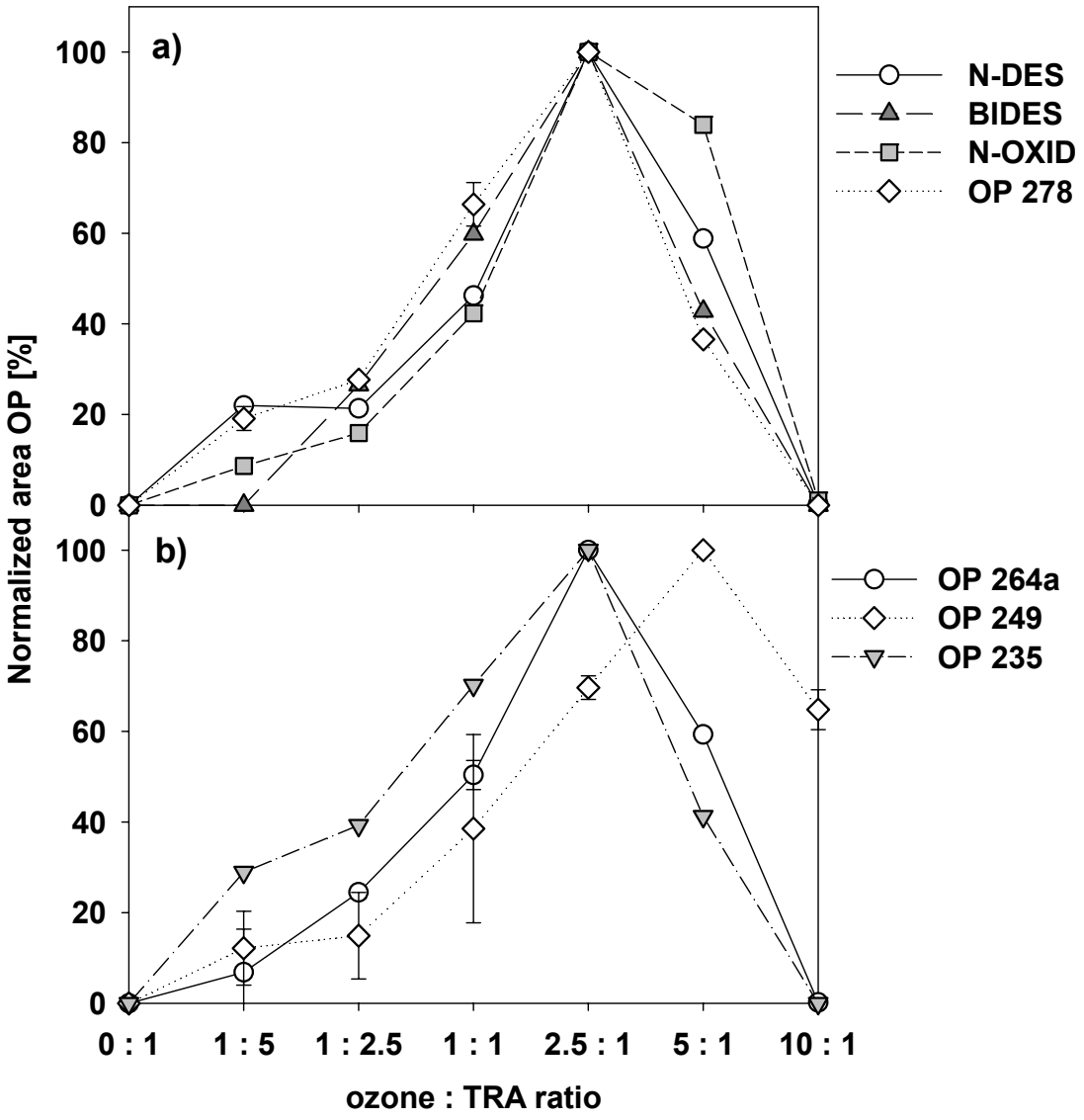

Figure S5.8. Formation of identified O_3 OPs during the mass balance experiment, normalized to the highest peak area for each OP

References

(1) Thompson, G. W.; Ockerman, L. T.; Schreyer, J. M. Preparation and Purification of Potassium Ferrate .6. *J. Am. Chem. Soc.* **1951**, *73*, 1379-1381.

(2) Lee, Y.; Zimmermann, S. G.; Kieu, A. T.; von Gunten, U. Ferrate (Fe(VI)) Application for Municipal Wastewater Treatment: A Novel Process for Simultaneous Micropollutant Oxidation and Phosphate Removal. *Environ. Sci. Technol.* **2009**, *43*, 3831-3838.

(3) Lee, Y.; Yoon, J.; von Gunten, U. Spectrophotometric determination of ferrate (Fe(Vl)) in water by ABTS. *Water Res.* **2005**, *39*, 1946-1953.

(4) Goff, H.; Murmann, R. K. Studies on Mechanism of Isotopic Oxygen Exchange and Reduction of Ferrate(Vi) Ion (Feo42-). *J. Am. Chem. Soc.* **1971**, *93*, 6058-6065.

(5) Bader, H.; Hoigné, J. Determination of ozone in water by the indigo method. *J Water Research* **1981**, *15*, 449-456.

(6) Sharma, V. K.; Burnett, C. R.; Millero, F. J. Dissociation constants of the monoprotic ferrate(VI) ion in NaCl media. *Physical Chemistry Chemical Physics* **2001**, *3*, 2059-2062.

(7) Yang, B.; Ying, G.; Zhao, J.-L.; Zhang, L.-J.; Fang, Y.-X.; Nghiem, L. D. Oxidation of triclosan by ferrate: Reaction kinetics, products identification and toxicity evaluation. *J. Hazard. Mater.* **2011**, *186*, 227-235.

(8) Hoigné, J.; Bader, H. Characterization of Water-Quality Criteria for Ozonation Processes. 2. Lifetime of Added Ozone. *Ozone-Sci. Eng.* **1994**, *16*, 121-134.

(9) Dodd, M. C.; Buffle, M. O.; von Gunten, U. Oxidation of antibacterial molecules by aqueous ozone: Moiety-specific reaction kinetics and application to ozone-based wastewater treatment. *Environ. Sci. Technol.* **2006**, *40*, 1969-1977.

(10) Takacs-Novak, K.; Box, K. J.; Avdeef, A. Potentiometric p*K*(a) determination of water-insoluble compounds: Validation study in methanol/water mixtures. *Int. J. Pharm.* **1997**, *151*, 235-248.

(11) Buxton, G. V.; Greenstock, C. L.; Helman, W. P.; Ross, A. B. Critical-Review of Rate Constants for Reactions of Hydrated Electrons, Hydrogen-Atoms and Hydroxyl Radicals (.Oh/.O-) in Aqueous-Solution. *J. Phys. Chem. Ref. Data* **1988**, *17*, 513-886.

(12) Canonica, S.; Jans, U.; Stemmler, K.; Hoigne, J. Transformation Kinetics of Phenols in Water - Photosensitization by Dissolved Natural Organic Material and Aromatic Ketones. *Environ. Sci. Technol.* **1995**, *29*, 1822-1831.

Chapter 6

General Conclusions

Ozonation of wastewater is currently considered one of the most promising options for the mitigation of micropollutants entering the aquatic environment via wastewater streams. It could be clearly shown for the ozonation step at wastewater treatment plant (WWTP) Wüeri in Regensdorf that a safe and reliable operation of a full-scale ozonation step is feasible. As outlined in Chapter 1, operation of ozone dosage at municipal WWTPs with a relatively low variability in dissolved organic carbon (DOC) concentrations can also be carried out in the flow-proportional mode. This circumvents problems with the signal stability of DOC analyzers necessary for DOC-load proportional dosing. Although the time needed for complete ozone decay is site-specific, a hydraulic retention time (HRT) within the sealed ozone reactor of 20 min for dry weather flow should be sufficient. During stormy weather conditions, the HRT should not be less than 5-10 minutes. In addition, a complete nitrification is recommended for the preceding biological treatment to prevent excessive ozone consumption since ozone reacts quickly with nitrite in a stoichiometric reaction. The energy consumption of the investigated ozone step was calculated to be approximately 0.06 kWh m^{-3}, corresponding to 15 -20 % of the energy consumption of a conventional WWTP.

In the present thesis, ozonation was shown to efficiently oxidize a broad range of 220 selected micropollutants with different reactivities in secondary wastewater effluent at the full-scale level. This confirmed results from previous laboratory and pilot-scale experiments and shows that up-scaling is possible in this case. The overall good performance even for micropollutants with lower reactivity towards ozone is explained by the combined attack of ozone and hydroxyl radicals which are formed in relatively high yields as secondary oxidants during wastewater ozonation. As a positive side effect, a good disinfection of the wastewater stream was also achieved. The receiving water of WWTP Wüeri even exhibited a microbiological water quality suitable for bathing, according to the amended bathing water directive of the European Union.

Two modeling approaches slightly overestimated the measured micropollutants oxidation in the real full-scale system. This overestimation was attributed to a certain protection of micropollutants from ozone attack by the interaction with aquatic colloids or sludge particles in the real wastewater system. The protection may be due to an ozone mass transfer limitation across the boundary layer of the sludge particles, as estimated based on film theory by a former study in wastewater ozonation. In contrast to micropollutant oxidation, predictions of *Escherichia coli (E. coli)* inactivation strongly overestimated full-scale measurements. This was attributed to the shielding of *E. coli* bacteria by activated sludge flocs, and not only to ozone mass transfer limitations. Since these hypotheses have not been experimentally confirmed yet, further research is needed to understand these processes in wastewater - ozone systems. Nevertheless, ozonation had an excellent performance with regard to the oxidation of a broad range of micropollutants as well as disinfection of wastewater in a full-scale system.

Adverse side effects such as the possible formation of ozonation by-products were also considered. Known by-products such as bromate, a potential human carcinogen, the carcinogenic *N*-nitrosodimethylamine (NDMA) or assimilable organic carbon (AOC) were formed during wastewater ozonation but either to only unproblematic levels, or decreased to unproblematic levels during post-sand filtration. These findings highlight the necessity of a biological post treatment step such as sand filtration after ozonation.

Ecotoxicological investigations were run in parallel at WWTP Wüeri by other researchers within the project “Strategy MicroPoll”. Their results from an *in-vitro* test battery indicate that the specific and unspecific toxicity of the wastewater (as tested by different toxicological endpoints such as baseline toxicity, algae inhibition and endocrine disruption) was significantly decreased during ozonation. However, *in-vivo* experiments exposing fish eggs to the differently treated wastewaters showed an increased toxicity after ozonation that was reduced to the level of the secondary wastewater effluent after post sand filtration. These results again highlight the necessity of a biological post treatment step after ozonation for the removal of subtle ecotoxicological effects of ozonation by-products. Still, ozonation without sand filtration

already decreased the specific and unspecific toxicity attributed to micropollutants considerably.

This thesis demonstrated for the first time that Fe(VI) is a powerful oxidant to eliminate various micropollutants containing electron-rich moieties as well as to remove phosphate during enhanced treatment of secondary wastewater effluents. Fe(VI) doses needed for micropollutants control were lower than those needed to remove phosphate to the regulatory limit in Switzerland. Therefore, a combined use of Fe(VI) and Fe(III) as an additional coagulant could be an option, since Fe(VI) is (up to now) significantly more expensive than Fe(III). Application of Fe(VI) to primary effluents or activated sludge suspension was less effective with regard to micropollutant oxidation due to the considerably lower Fe(VI) stability. Technologies for Fe(VI) production on the full-scale level are not available yet but much focus has been put on the development of electrochemical methods producing Fe(VI) *in situ*. This would be of advantage since off-site production as stable salts requires careful handling due to Fe(VI) instability in contact with water or humidity.

In conclusion, both oxidants are suitable for enhanced wastewater treatment with ozonation having the advantage of extensive operation experience from drinking water treatment and from the first full-scale ozonation plant for wastewater treatment in Switzerland. For an overall assessment, it is necessary to also consider oxidation products (OPs) formed during the respective treatment. A kinetic and mechanistic study focusing on tramadol oxidation by both Fe(VI) and ozone revealed that both oxidants lead initially to the same OPs for this amine-containing micropollutant; however, with significantly different yields. Under realistic treatment conditions, the identified ozone OPs will be further transformed into unknown OPs whereas the identified OPs will persist for realistic Fe(VI) doses. Whether these tramadol OPs exhibit adverse effects compared to tramadol could not be assessed in this thesis.

Curriculum Vitae

Saskia Gisela Zimmermann

Born on November 12, 1979 in Limburg a.d. Lahn, Germany

Citizen of Germany

1999	Abitur, Gymnasium Tilemannschule Limburg a.d. Lahn, Germany
1999 - 2006	Diploma studies in Applied Environmental Sciences University of Trier, Germany
	Diploma thesis title: "Sorption of sulfonamides to compost and manure" realized at Eawag, Department of Environmental Chemistry, Switzerland
2003 – 2004	ERASMUS student University of Lund, Sweden
2006 - 2007	PhD student Eawag, Department of Environmental Chemistry, Switzerland ETH Zürich, Institute of Biogeochemistry and Pollutant Dynamics, Switzerland
2007 - 2011	PhD student Eawag, Department of Water Resources and Drinking Water, Switzerland ETH Zürich, Institute of Biogeochemistry and Pollutant Dynamics, Switzerland